Márcio Milton Nunes Temtem

Development of biocompatible and "smart" porous structures using CO_2-assisted processes

Lisboa

2009

Márcio Milton Nunes Temtem

Development of biocompatible and "smart" porous structures using CO_2-assisted processes

Dissertação apresentada para a obtenção do grau de Doutor em Engenharia Química, especialidade Engenharia da Reacção Química, pela Universidade Nova de Lisboa, Faculdade de Ciências e Tecnologia.

Lisboa

2009

“Imagination is more important than knowledge”

by Albert Einstein

Agradecimentos

Ainda me lembro do dia em que a "grande chefe" me chamou ao seu gabinete para me apresentar um plano de doutoramento ambicioso para o qual nem ela nem eu fazíamos a mínima ideia do que se poderia tornar. Simplesmente tínhamos um sonho, de criar uma área nova no grupo, de aplicar os conhecimentos acumulados durante muitos anos de estudo na área de fluidos supercríticos. Esse sonho é agora uma realidade. O meu primeiro muito obrigado vai para a Ana Isabel. Para a amiga, para a professora, para a orientadora, para a minha "mãe do continente" como por vezes lhe chamo. Este trabalho não poderia ter sido efectuado sem o seu empenho e orientação, sem as suas palavras de apoio nos momentos mais difíceis, sem os seus incentivos e até mesmo sem os seus "puxões de orelhas". Qualquer que seja o desafio é a pessoa certa para termos ao nosso lado.

Gostava também de agradecer aos meus co-orientadores. Ao Prof. João Mano por toda a ajuda e orientação com os polímeros inteligentes, por me ter apresentado um mundo novo onde a imaginação é o limite, pela amizade e pelo carinho com que sempre me tratou. Ao Prof. Pedro Simões, por ter tido sempre a porta aberta quando alguma dúvida surgia, pela amizade, pelos grandes momentos e pelas longas conversas que tivemos ao longo deste período. Aprendi e cresci muito consigo!

Ao "grande chefe", Prof. Manuel Nunes da Ponte por me ter recebido no seu grupo, por toda a ajuda com o financiamento, pelas experiências únicas que tornou possível (Socrates, MIT, Iguaçu), pelos seus sábios ensinamentos científicos, humanos e desportivos. É com saudade que recordo as nossas longas conversas, o seu desafio constante e o seu sentido prático das coisas…"para que é que isso serve?".

À Teresa Casimiro antes de mais pela amizade, por ter estado sempre presente nos bons e nos maus momentos e pelas brilhantes discussões científicas. Foi com ela que aprendi o maravilhoso mundo dos fluidos supercríticos.

Ao Prof. João Sotomayor, ao Prof. Eurico Cabrita, à Prof. Isabel Fonseca, à Prof. Ana Botelho Rego, ao Prof. João Paulo Crespo e ao Dr. José Catita) pela ajuda nas mais variadas técnicas (ângulo de contacto, RMN, ASAP, MIP, XPS, permeabilidades, GPC/HPLC) e discussões científicas. Sem o seu esforço este seria com certeza um trabalho muito mais pobre.

Ao Prof. Michael Tatoulian, à Prof. Paula Hammond, ao Prof. Eckard Weidner e ao Prof. Marcus Peterman thanks for making me feel at home during the stay at your labs and for making possible so great experiences.

Ao Prof. Joaquim Sampaio Cabral, à Cláudia Lobato da Silva e ao Pedro Z. Andrade por todo o trabalho com as células estaminais.

Ao apoio financeiro prestado pela Fundação para a Ciência e Tecnologia através da bolsa de Doutoramento (SFRH/BD/16908/2004) e do projecto PTDC/CTM/70513/2006. Queria também agradecer todo o apoio financeiro prestado pela Fundação Calouste Gulbenkian e pelo MIT-Portugal Program, Bioengineering Systems Focus Area.

A todos os meus colegas do grupo de "Polymer Synthesis and Processing" um obrigado por terem feito deste o melhor grupo onde se pode trabalhar. Um especial agradecimento ao Mindu (Daniel), à Ti Té (Telma), à Mara à Gigi (Lígia) e à Silvia Mihaila por toda a ajuda com o trabalho experimental. Sem o vosso esforço e dedicação este trabalho não seria o mesmo.

À D. Joaquina, D. Palminha, D. Maria José, D. Conceição, D. Idalina, Isabel Rodrigues, Carla Rodrigues, Drª Rosário Caras Altas e ao Srº Ramalho (Air liquide) um muito obrigado por todo o vosso apoio e ajuda durante todo este percurso.

Ao Srº Luís da Graça e Paulo Graça pela sábia ajuda na construção e reparação das células de alta pressão.

Aos gnus João "Caloiro", João "Évora", Ricardo, Rita, Sofiazinha que me acompanharam neste percurso, um muito obrigado pelos momentos de boa disposição, pela vossa amizade e pelo vosso apoio incondicional ao longo destes anos. Um agradecimento especial ao "Évora" por todas as discussões filosóficas, por todos os momentos brilhantes de discussão científica e finalmente por toda a ajuda na parte da modelação.

Aos meus pais e aos meus irmãos, ao meu tio Dinis, à minha família pelos minutos, pelas horas, pelos dias pelo tempo que não puderam estar comigo, pelo vosso apoio, pela vossa compreensão. Foram quase 10 anos afastados, mas nas alegrias e nas tristezas estiveram e estão sempre no meu coração.

Finalmente, à pessoa que me iluminou o caminho quando eu estava perdido, que me incentivou e ajudou desde o primeiro ao último minuto, ao meu porto de abrigo quando tudo o resto era tempestade, à pessoa que partilhou comigo as alegrias e as tristezas, à amiga, à confidente, à namorada, à "esposa"… à Lili. Obrigado por fazeres parte da minha vida!

List of contents

List of Figures

List of contents

List of Tables

Resumo

Nas últimas três décadas a utilização de dióxido de carbono supercrítico ($scCO_2$) tornou-se uma alternativa atractiva para a produção e processamento de polímeros. O objectivo principal desta tese foi o desenvolvimento de estruturas porosas inteligentes utilizando tecnologia supercrítica.

Esta tese está organizada em quatro capítulos principais. O primeiro revê e destaca algumas potencialidades da tecnologia supercrítica e os seguintes compilam o trabalho experimental e os resultados obtidos. O trabalho desenvolvido encontra-se dividido em três partes principais: na primeira (2º capítulo) é aplicado um processo de inversão de fases para a produção de estruturas porosas, nomeadamente membranas, em que o não solvente é o dióxido de carbono supercrítico; na segunda parte (3º capítulo) aborda-se a síntese de polímeros inteligentes, em especial polímeros sensíveis à temperatura e/ou pH; finalmente estas duas áreas são conjugadas (4º capítulo) com vista à produção de estruturas porosas inteligentes com propriedades físicas e químicas definidas. Todos os trabalhos têm em comum a preparação e o processamento de materiais biodegradáveis e/ou biocompatíveis para a obtenção de matrizes porosas, nomeadamente membranas e *scaffolds*, com morfologia controlada.

Para a preparação das membranas foi desenvolvida, no laboratório, uma nova instalação e uma nova célula de alta pressão. O primeiro estudo consistiu na preparação de membranas de polisulfona, um polímero biocompatível com largas aplicações na medicina, em especial em membranas de hemodiálise. Neste trabalho foi estudada a influência de dois parâmetros: a velocidade de despressurização no final do processo e a afinidade entre solvente e não solvente (CO_2). A incorporação de um agente de expansão (policaprolactona) capaz de originar estruturas porosas quando despressurizado foi também testada. O processo baseia-se no facto deste polímero possuir uma grande capacidade para incorporar CO_2 o que faz com que seja possível

liquefazê-lo a temperaturas relativamente baixas. Durante o processo de descompressão a libertação rápida do gás dá origem à formação de uma espuma que ao solidificar leva à formação de uma estrutura porosa.

Finalmente foram preparadas membranas e partículas de quitosano, um polímero derivado do 2º polímero natural mais abundante na Terra, a quitina. Estes dispositivos foram produzidos utilizando três dos mais promissores solventes amigos do ambiente (etanol, água e CO_2). A sua morfologia e a estrutura tridimensional foram controladas através da alteração da composição do co-solvente (etanol) no não solvente (CO_2) durante o processo de inversão de fases. A análise por microscopia electrónica permitiu verificar que a forma como o co-solvente é introduzido (modo isocrático ou modo gradiente) era relevante para a estrutura obtida. Uma das vantagens apresentadas por estes dispositivos é a sua baixa solubilidade em condições neutras de pH, mesmo sem se proceder a processos adicionais de tratamento, como seja a reticulação, o que permite aumentar a biocompatibilidade das estruturas preparadas. Por esta razão, as membranas foram testadas em termos de citotoxicidade e capacidade de adesão e proliferação de célula estaminais humanas do mesenquima. Após duas semanas de cultura verificou-se um aumento de 9 vezes no crescimento das células nas membranas de quitosano contra um aumento de 6 vezes no meio de controlo, preservando a sua capacidade de diferenciação.

Demonstrou-se ainda que o método de preparação em causa era capaz de preparar, num único passo, membranas para libertação controlada, apenas por co-dissolução de uma molécula modelo (gentamicina) na solução de quitosano utilizada para preparar a membrana.

O próximo objectivo desta tese consistiu na preparação de polímeros inteligentes. No capítulo 3 é apresentada a síntese em $scCO_2$ de um dos polímeros sensíveis à temperatura mais estudados, o poli N-isopropilacrilamida (PNIPAAm). Desenvolveu-se também uma nova técnica para a impregnação/revestimento de estruturas porosas com este tipo de polímeros de forma a produzir

estruturas porosas inteligentes. Para provar este conceito foram utilizados *"scaffolds"* de quitosano.

A temperatura baixa de transição crítica, denominada LCST, que para o PNIPAAm se encontra perto dos 32ºC foi também ajustada através da copolimerização ou *grafting* do NIPAAm com outros monómeros. A copolimerização com hidroxietilmetacrilato (HEMA) permitiu diminuir o LCST de 32.2 para aproximadamente 27.7ºC. A medição de pontos de nuvem a 40 ºC, 50 ºC e 65 ºC conjuntamente com a modelação efectuada utilizando a equação de estado Soave-Redlich-Kwong com a regra de mistura Mathias-Klotz-Prausnitz permitiu optimizar as condições para a reacção de polimerização.

Para aumentar o LCST, produziram-se polímeros de PNIPAAm por *grafting* com poli(óxido de etileno). Foram ainda preparados polímeros sensíveis a dois estímulos (temperatura e pH) através da copolimerização do PNIPAAm com ácido metacrílico. Através dos estudos de impregnação e libertação de drogas modelo testaram-se as capacidades destes hidrogéis para serem aplicados em libertação controlada de moléculas bioactivas.

Finalmente no capítulo 4 combinaram-se os trabalhos descritos nos capítulos 2 e 3 referentes à preparação de estruturas porosas e à síntese de polímeros inteligentes para produzir estruturas porosas inteligentes, com propriedades físico-químicas bem definidas: i) *scaffolds* de quitosano; ii) membranas de polisulfona termosensíveis e iii) membranas de polimetilmetacrilato.

Os s*caffolds* de quitosano (sensível ao pH) foram impregnados/revestidos com uma camada de polímero sensível à temperatura (PNIPAAm). A análise por microscopia electrónica e por porosimetria de mercúrio permitiu verificar que o processo de revestimento era eficaz e que não provocava uma perda significativa na porosidade da matriz de quitosano. Verificou-se que este tipo de estruturas continuava a manter as mesmas capacidades dos polímeros isolados (cadeias

livres) nomeadamente, a capacidade de incharem na presença de água em diferentes proporções consoante as condições de pH e temperatura do meio.

Estas estruturas foram ainda impregnadas com drogas/ proteínas modelo (ibuprofeno e bovine serum albumin), utilizando duas estratégias distintas: impregnação com fluídos supercríticos e incorporação na solução de preparação dos *scaffolds*. A libertação de ambos os compostos ocorreu após vários dias e prolongou-se durante várias semanas, revelando um padrão de acordo com as condições de pH e temperatura.

Esta mesma metodologia foi utilizada na preparação de membranas de polisulfona sensíveis à temperatura. Estas membranas foram preparadas segundo a técnica e o procedimento desenvolvidos no capítulo 2 em que o CO_2 é utilizado como não solvente. A medida do fluxo de água através destas membranas a várias temperaturas diferentes demonstrou que estas apresentam uma resposta rápida de abertura e fecho dos poros quando a temperatura ultrapassa o LCST.

O mecanismo de abertura e fecho dos poros devido a variações de temperatura foi testado utilizando uma proteína modelo (BSA). Foi possível verificar que com mudanças de temperatura era possível controlar a difusão da proteína através da estrutura porosa. Desenvolveu-se um modelo de difusão baseado na lei de Fick e na adsorção de Langmuir para descrever o mecanismo de libertação através da membrana.

Finalmente foram preparadas membranas de poli(metilmetacrilato) contendo hidroxipropil-β-ciclodextrinas (HP-β-CDs) para aplicação em sistemas de libertação controlada. As membranas foram preparadas com HP-β-CD numa gama de 0 a 33.4% (p/p) através da incorporação destas na solução utilizada para preparar as membranas. A impregnação com um fármaco modelo (ibubrofeno), através de utilização de CO_2 como solvente permitiu a preparação de membranas para libertação controlada. Verificou-se que a libertação deste fármaco podia ser controlada

através da quantidade de ciclodextrina incorporada na membrana, representando uma alternativa para a preparação de estruturas porosas inteligentes.

Os materiais e os processos desenvolvidos nesta tese demonstram que o CO_2 supercrítico pode desempenhar um papel importante na síntese e na preparação de uma vasta gama de estruturas porosas de morfologia controlada e bem definida. Demonstra ainda como é possível transportar monómeros, moléculas activas e fármacos para o interior de estruturas porosas de uma forma extremamente eficiente e como preparar estruturas porosas prontas a utilizar sem processos adicionais de esterilização ou eliminação de solventes.

Abstract

Over the past three decades the use of supercritical carbon dioxide ($scCO_2$) has received much attention as a green alternative in the synthesis and processing of polymers. The scope of this thesis is the development of biocompatible and "smart" porous structures using CO_2-assisted processes.

This thesis is organized in four main chapters. The first one reviews and highlights some potentialities of supercritical fluid technology and the following ones compile the experimental work developed. The work is divided in three main parts: in the first part (2nd chapter) a CO_2-assisted phase inversion method was developed in order to prepare porous structures, namely membranes. In the second part (3rd chapter) the focus was the synthesis of "smart" polymers, especially thermo and pH sensitive polymers. Finally, these two areas were combined (4th chapter) for the preparation of "smart" porous structures. The common guide line was the preparation or processing of biodegradable and/or biocompatible materials with special emphasis on the preparation of porous matrices, namely membranes and scaffolds, with controlled morphology.

For membrane preparation a new high pressure apparatus and a new high pressure cell were developed. Polysulfone membranes (a biocompatible polymer with numerous applications in the medical field) were prepared and the effect of the solvent affinity and depressurization rate in the morphology and in the performance in terms of pure water flux of the membranes was investigated. The incorporation of a foaming agent was also analyzed and the high pressure CO_2 capability to swell and melt polycaprolactone (PCL) was used to produce and control the porosity and the properties of the membranes. Finally, a natural and water soluble polymer (chitosan) was processed. The presence of water in the casting solution introduced extraordinary difficulties due

to the low affinity between water and CO_2. To induce the phase inversion a co-solvent (ethanol) was introduced in the CO_2 stream. The obtained devices (membranes and beads) were fabricated using moderate temperatures and "green" solvents (ethanol, water and CO_2). The morphology and the three dimensional (3D) structures were controlled by altering the co-solvent (ethanol) composition in the CO_2 non-solvent stream during the demixing induced process. Microarchitectural analysis by scanning electron microscopy identified the formation of particulate agglomerates when 10% of ethanol in the $scCO_2$ stream was used and detected the development of porous membranes with different morphologies and mechanical properties depending on the programmed gradient mode and the entrainer percentage (2.5-5%) added to the $scCO_2$ stream. These chitosan matrices exhibited low solubility at neutral pH conditions, with no further modifications, demonstrating their applicability in bioreactors as static (membranes) or stirred (beads) culture devices. It was also demonstrated that the current method is able to prepare, in a single-step, an implantable antibiotic release system by co-dissolving gentamicin with chitosan and the solvent. In addition, the cytotoxicity as well as the ability of these structures to support the adhesion and proliferation of human mesenchymal stem cells (hMSC) in vitro were also addressed. After 2 weeks in culture, a 9-fold increase was obtained (versus 6 of the control). More importantly, cells maintained their clonogenic potential and immunophenotype (>95% CD 105+ Cells after 7 days of culture). In this chapter, a hypothetical schematic ternary diagram for the systems polymer–solvent–CO_2 is used to discuss and explain the results.

Another goal of this thesis was the synthesis of "smart" polymers. Chapter 3, addresses the precipitation polymerization of a thermoresponsive hydrogel, poly(N-isopropylacrylamide) (PNIPAAm), in $scCO_2$. This hydrogel has a transition temperature, hereinafter called low critical solution temperature (LCST), around 32 ºC in an aqueous solution, close to body temperature. A strategy of solvent-free impregnation/coating of polymeric surfaces with PNIPAAm was

suggested, in order to further extend the applications of membranes or porous bulky systems. The *in situ* synthesis of PNIPAAm within a chitosan scaffold was tested as a proof of concept, in order to produce smart partially-biodegradable scaffolds for tissue engineering applications.

The LCST was tuned by copolymerization or graft polymerization of NIPAAm with other monomers. Copolymerization with hydroxyethyl methacrylate (HEMA) was used to decrease the LCST temperature from 32.2 ºC to approximately 27.7 ºC. Cloud point measurements of CO_2 + HEMA system were used to optimize the polymerization temperature. Experimental data were obtained at 40 ºC, 50 ºC and 65 ºC and pressures up to 21.1 MPa. Soave-Redlich-Kwong equation of state with Mathias-Klotz-Prausnitz mixing rule was used to model experimental results and a good correlation was achieved.

To increase the LCST, polyethylene oxide (an hydrophilic polymer) was grafted to PNIPPAAm. Dual stimulus (thermo and pH responsive) hydrogels were also prepared by copolymerizing methacrylic acid with PNIPAAm. As a proof of concept fluorouracil was incorporated in the hydrogels network and their release was controlled by temperature and pH stimulus.

In chapter 4 the concepts of the previous chapters were put together envisaging the preparation of "smart" functional polymeric devices with targeted physical and chemical properties namely: (i) chitosan-based dual stimulus scaffolds (temperature and pH responsive); (ii) polysulfone-based thermoresponsive membranes and (iii) polymethylmethacrylate-based membranes.

The chitosan scaffolds (pH sensitive) were coated/impregnated with a thermoresponsive polymer, poly(N-isopropylacrylamide) (PNIPAAm), using $scCO_2$ as a carrier to homogeneously distribute the hydrogels monomer within the chitosan scaffolds and as a solvent to perform the polymerization reaction.

Abstract

Microarchitectural analysis by scanning electron microscopy and mercury intrusion porosimetry proved that the coating of the inner pore structure was efficiently achieved without a considerable loss of porosity. Two different strategies were used to upload the porous structures with target molecules: supercritical fluid impregnation to impregnate with a low molecular weight model drug (ibuprofen) and bulk loading for a model protein (bovine serum albumin, BSA). Both for ibuprofen and BSA the release appeared after several days and prolonged for several weeks. The release profiles showed a specific pattern accordingly to the parameters (pH and temperature).

The same methodology was used to prepare thermoresponsive polysulfone (PS) membranes. PS membranes were prepared using the CO_2-assisted phase inversion method using the procedure described in the previous chapters. Their pores were coated/impregnated with a thermoresponsive polymer - poly(N-isopropylacrylamide) using the same approach that was applied for the chitosan scaffolds. The on/off mechanism was tested using a model protein (BSA) as a proof of concept for the ability to control pore aperture by temperature stimulus. A diffusion model based on Fick`s law and Langmuir adsorption was developed.

The last application was the preparation of cyclodextrins-containing polymers that have proved themselves to be useful for controlled release. For that, poly(methylmethacrylate) (PMMA) membranes were prepared containing hydroxypropyl-β-cyclodextrins (HP-β-CDs) for potential application as drug delivery devices. The polymeric membranes were obtained with HP-β-CD contents ranging from 0 to 33.4 wt%, by changing the composition of the casting solution, and were further impregnated with ibuprofen using $scCO_2$ in batch mode. The influence of the membrane functionalization in the controlled release of ibuprofen was studied by performing *in vitro* experiments in buffer solution pH at 7.4. The release of the anti-inflammatory drug could be tuned by varying the cyclodextrin content on the membranes.

The materials and processes developed in the present work demonstrate that supercritical CO_2 can play a major role for the synthesis and preparation of a range of well defined porous polymeric structures that could have applicability in both biomedical and biotechnological fields. It demonstrates that it is possible to transport monomers, active molecules and drugs with high efficiency and at the same time to prepare new structures that could be utilized as a platform for different applications.

Chapter 1

INTRODUCTION

1. Introduction

The emergent demand in medicine and in the biomaterial field for materials with a more efficient therapeutic activity and without any contaminants has driven research to find new molecules and new synthetic approaches to produce and process polymers. Supercritical fluids (SCF) have assumed an important role, during the last two decades, as an efficient alternative not only by the environmental aspect, but also due to a number of specific physical, chemical and toxicological advantages that offer the opportunity to manipulate the outcome of reactions, including the polymer structure [1].

A supercritical fluid is any substance at a temperature and pressure above its thermodynamic critical point (pressure and temperature) but below the pressure at which the fluid will solidify (Figure 1.1) [2].

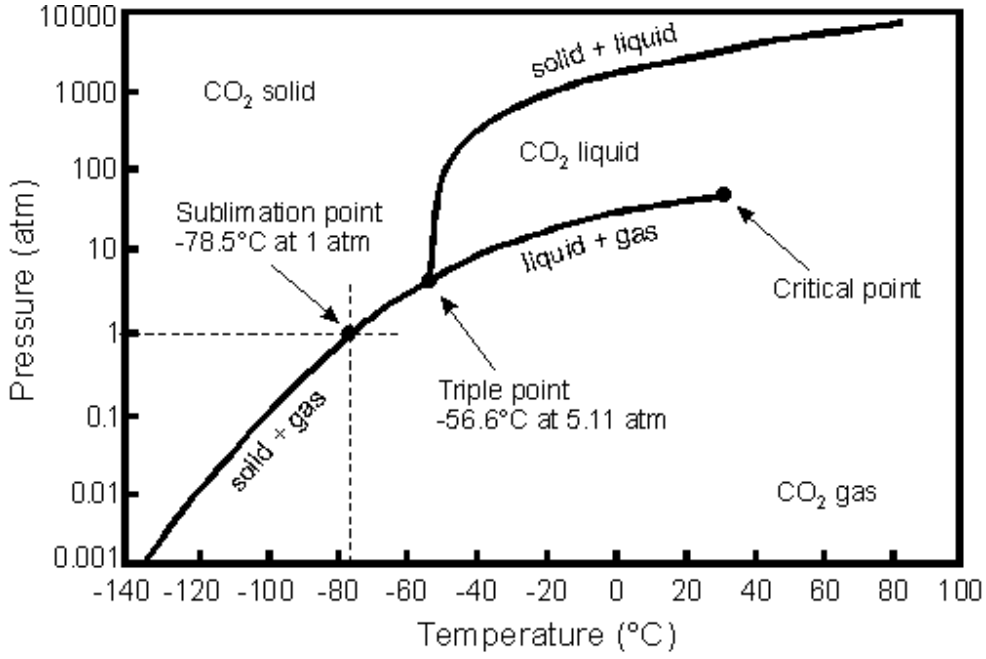

Figure 1.1 – Carbon dioxide phase diagram

In general terms, supercritical fluids have properties (viscosity, diffusivity and density) between those of a gas and a liquid, tuneable through the control of pressure and temperature (Table 1.1) [3].

Table 1.1 – Comparison of physical properties of gases, supercritical fluids and liquids

	Density (Kg/m^3)	Viscosity (cP)	Diffusivity (mm^2/s
Gases	1	0.01	1-10
Supercritical	100-1000	0.05-0.1	0.01-0.1
Liquids	1000	0.5-1.0	0.001

Several substances can be used as supercritical fluids. In Table 1.2 it is presented some of the critical properties of the most commonly used fluids.

Table 1.2 - Critical properties of various solvents [3].

Solvent	Critical temperature (K)	Critical pressure (MPa)
Carbon dioxide	304.1	7.38
Water	647.3	22.12
Ethane	305.3	4.87
Ethylene	282.4	5.04
Propane	369.8	4.25
Methanol	512.6	8.09
Acetone	508.1	4.70

In SCF technology, carbon dioxide is the most commonly used fluid because it is non-toxic, non-flammable, chemically inert, and inexpensive. The supercritical conditions are easily achieved (Tc = 304.1 K and Pc = 7.38 MPa) and since it is a gas the solvent may be removed by simple depressurization obtaining clean and dry products.

Supercritical fluids and specially supercritical carbon dioxide ($scCO_2$) have found applications in a broad range of areas [4]: extraction [5], polymerization [6, 7], particle design [8, 9], chemical reactions [10], drug impregnation [11], formation of porous structures [12, 13], dry cleaning [14], etc. In this thesis special attention will by given for polymer synthesis and processing, particularly the formation of porous structures and synthesis of "smart" polymers in $scCO_2$.

1.1 Porous structures

There are several reasons to consider SCF an alternative medium for the synthesis and processing of porous materials. Besides its environmental advantages, $scCO_2$ allows the production of a dry polymeric product (CO_2 is a gas under ambient conditions) [15, 16], introduces additional parameters (pressure, temperature, depressurization) to control membranes morphology, improves mass transfer (much lower viscosities than organic liquids, and easily adjusted with variations in pressure and temperature) [17] and reduces the solvent recovery costs. Surface modification of porous materials can be facilitated because SCF and in particular CO_2 are extremely versatile wetting agents due to their low surface tension (e.g.., liquid CO_2 will wet Teflon) and pore collapse can also be avoided because SCF do not give rise to a liquid-vapour interface.

During the years several techniques have been applied for the preparation of porous structures using SCF technology but the main processes are: foaming, emulsion templating and CO_2 assisted phase inversion method [12].

1.1.1 Foaming

Foaming of glassy polymers with carbon dioxide as a physical-blowing agent was first described by Martini and co-workers [18] and during the last three decades several works have been reported [13, 19, 20, 21, 22]. This method takes advantage of the large depression in glass

transition temperature (*Tg*) found for many polymers in the presence of CO_2 [21, 22, 23, 24] which means that the polymer may be kept in the liquid state at relatively low temperatures. Polymer foams are formed when a polymer, plasticized by saturation in the supercritical fluid is rapidly depressurized at a constant temperature. As pressure is released pockets of gas nucleate and grow in the polymer. As the supercritical fluid leaves the polymer, the *Tg* increases, generating nuclei due to supersaturation, which will grow to form the cellular structure until vitrification occurs. Figure 1.2 gives a schematic representation of the foaming process.

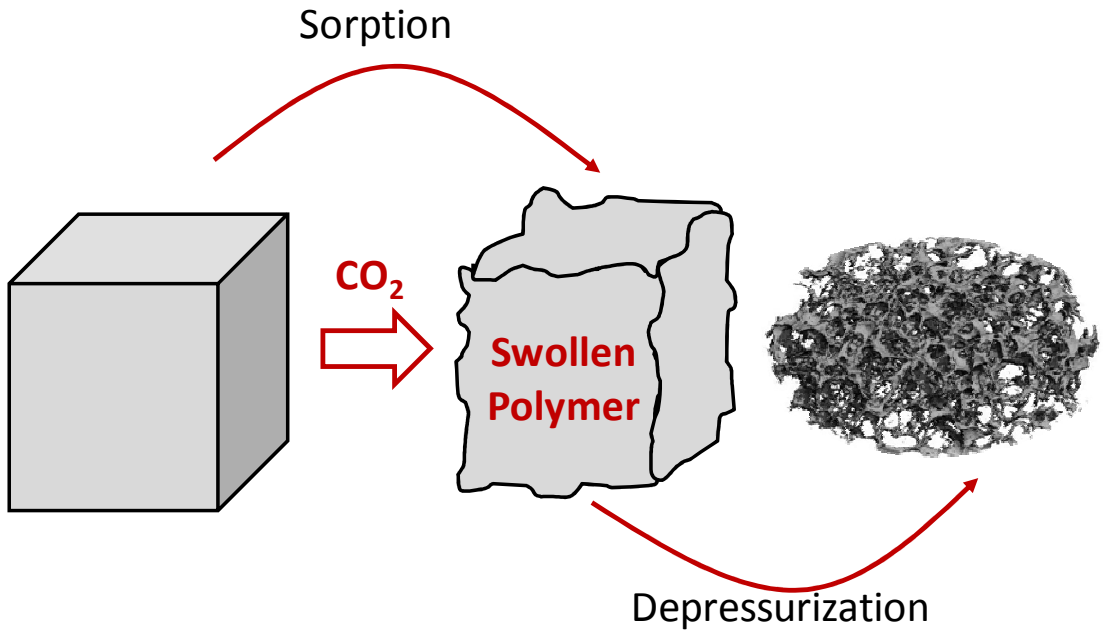

Figure 1.2 - Schematic representation of the foaming process using $scCO_2$.

A broad range of materials have been processed using this technology: Poly(methyl methacrylate) [21] Poly L-lactic acid and copolymers of D,L-lactide and glycolide [25], Polystyrene [26], Polysulfone [27, 28] and Poly(ether sulfone) [27], Poly(ether imide) [28], poly(vinylidene fluoride) [29], Poly(ethylene terephthalate) [30], polycarbonate [30], etc.

1.1.2 Emulsion templating

Emulsion templating is a versatile method for the preparation of well-defined porous polymers [31, 32] and inorganic materials [33]. The technique involves two steps: formation of a high internal phase emulsion and locking the structure of the external phase, usually by reaction induced phase separation (e.g., sol-gel chemistry, free-radical polymerization). Subsequent removal of the internal phase (i.e., the emulsion droplets) gives rise to a skeletal replica of the emulsion. This final step is very critical due to the fact that the internal oil phase (often an organic solvent) must be removed from the porous structures. Cooper and co-workers [34, 35] have developed a process for emulsion templating without volatile organic solvents, using only water and CO_2. CO_2 being a gas under normal pressure/conditions can be removed easily by depressurization.

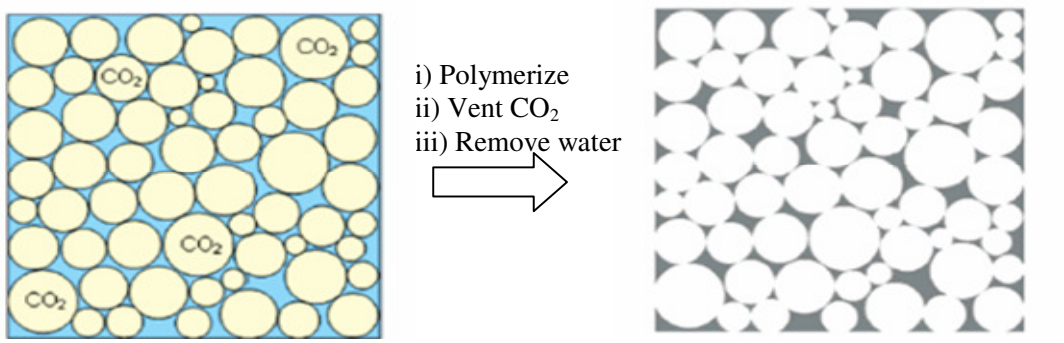

Figure 1.3– Schematic representation of the CO_2/Water emulsion templating process. Adapted from [35]

Several organic and inorganic porous matrixes were obtained using this technique: polyacrylamide [35], calcium Alginate hydrogels [36], silica [37], poly(vinyl alcohol) and naturally derived chitosan [38], dextran [39], etc.

1.1.3 CO_2 assisted phase inversion

A number of different techniques are available to prepare porous polymeric films, such as sintering, stretching, track etching, phase separation, sol-gel process, vapour deposition and solution coating. However, the majority of porous flat membranes are prepared from a homogenous polymer solution by the wet-phase inversion method in which a polymer solution (polymer plus solvent) is cast on a suitable support and immersed in a coagulation bath containing a non-solvent. Since the precipitation occurs due to the exchange of solvent and non-solvent, the correct choice of the pairs of solvents is a very important parameter to control the morphology of the membrane. Other important preparation parameters are: polymer concentration, temperature, humidity, evaporation time, and the composition of the casting solution (e.g. additives) [40].

Unfortunately many organic solvents used in membrane preparation are volatile, flammable and may pose a risk to health and the environment. Alternative approaches are being developed, and one with growing areas of application is the use of supercritical fluids, namely carbon dioxide. Figure 1.4 schematically represents this process.

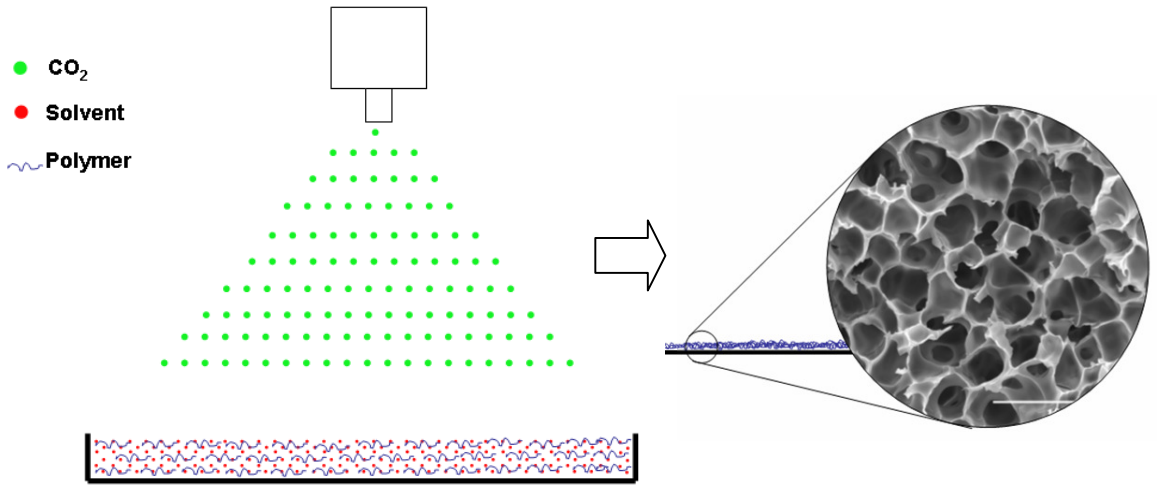

Figure 1.4 - Schematic description of the CO_2 induced phase inversion method

Kho *et al.* [41] were the first ones to report the preparation of membranes of a semicrystalline polyamide, Nylon 6, by exposing a 2,2,2-trifluoroethanol solution to $scCO_2$ to induce the phase separation of the polymer solution. Since then many authors have been applied to produce membranes of different materials as presented in Table 1.3.

Table 1.3- Resume of the materials that were processed by CO_2 induced phase inversion method

Authors	Polymer	Analysed effect
Kho *et. al* [41]	Polyamide (Nylon 6)	Polymer concentration, temperature and pressure.
Matsuyama *et. al* [42]	Polystyrene	Polymer concentration, temperature and pressure.
Matsuyama *et. al* [43]	Cellulose acetate	Solvent - nonsolvent affinity
E. Reverchon and S. Cardea [44]	Cellulose acetate	Polymer concentration, temperature and pressure.

E. Reverchon and S. Cardea [45]	Polysulfone	Polymer concentration, temperature and pressure.
E. Reverchon *et. al* [46]	Poly (methyl methacrylate)	Polymer concentration, temperature and pressure.
E. Reverchon and S. Cardea [47]	Poly(vinylidene fluoride)-co-hexafluoropropylene	Polymer concentration, temperature and pressure.
Reverchon *et. al* [48]	Poly(vinyl alcohol)	Polymer concentration, temperature, pressure, addition of an entrainer to the solvent.
Reverchon *et. al* [49]	Poly(vinyl alcohol)	Polymer concentration, temperature, pressure and different ethanol:CO_2 ratios for the Phase inversion,
Tsivintzelis *et. al* [50]	Poly(l-lactic acid)	Polymer concentration, temperature and pressure.
Xu *et. al* [51]	Polylactide	Polymer concentration, solvent affinity, depressurization rate and non-solvent composition.
Huang *et. al* [52]	Poly(vinylidene fluoride)	Polymer concentration, temperature, pressure and addition of poly(methyl methacrylate) in the casting solution.
Li *et. al* [53]	Poly(vinyl butyral)	Polymer concentration, temperature, pressure and depressurization.
Temtem *et. al* [54]	Polysulfone	Solvent - nonsolvent affinity, depressurization rate

Temtem *et. al* [55]	Blends of polysulfone-polycaprolactone	Foaming vs phase inversion.
Temtem *et. al* [56]	Chitosan	Entrainer effect.

When the solution of polymer is first immersed as a film into a coagulation bath rapid changes occur and usually a skin forms at the interface. As time proceeds, changes in the concentration occur in the layers further away from the interface, but these occur less rapidly than the interfacial changes. The rate at which the changes occur in the sub-layers has a profound effect on the structure. The 'tuneable' solvent power of the supercritical fluid, owing to its variable (with pressure or temperature) solvent density and viscosity is a serious advantage when compared with the traditional solvents.

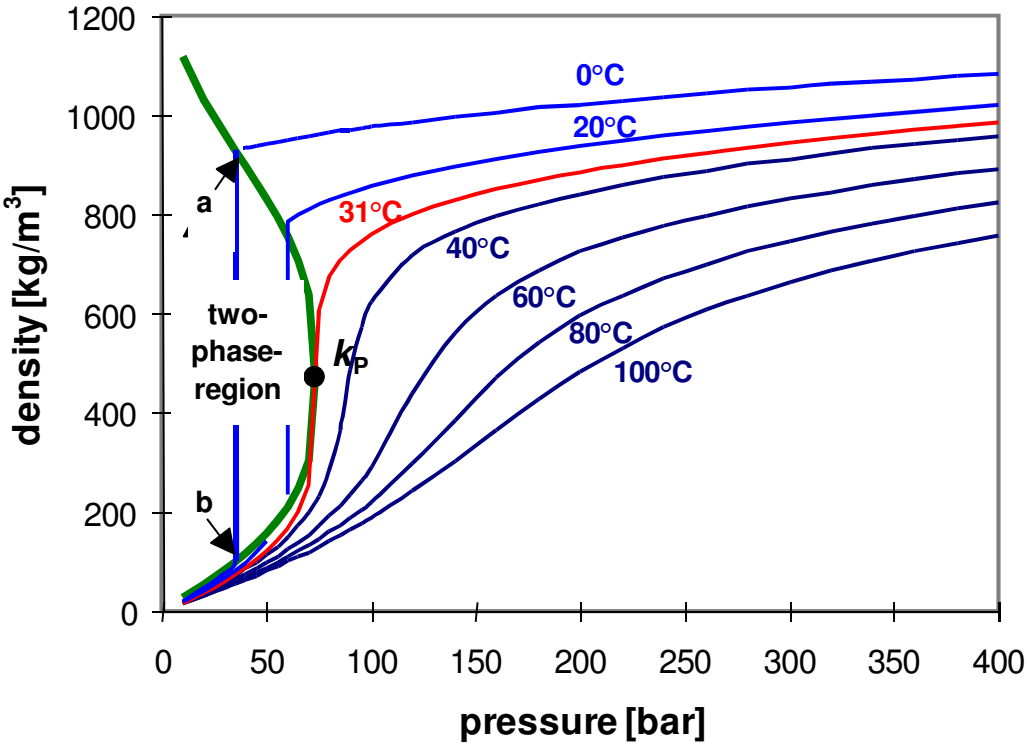

Figure 1.5– Carbon dioxide density *vs* temperature and pressure

Figure 1.5 shows the density-pressure phase diagram for carbon dioxide. One of the particularities of the critical point is that close to it a small increase in pressure or temperature causes a large increase in the density. This property is very important for the phase inversion process because it is closely related with the nonsolvent (CO_2) strength and it is known that the manipulation of the strengths of the solvent and nonsolvent is one of the primary means to control the properties of membranes formed by this process. Many authors have analysed the influence of these two parameters in membrane morphology (Table 1.3) and they all observed that the average pore size and membrane porosity decreased by increasing the pressure or decreasing the temperature [41, 42, 44, 45, 46, 47, 48, 49, 50, 52, 53].

A change in these two parameters will modify the phase diagram of the ternary system polymer/solvent/non-solvent, pressure and temperature dependent. In the analyses of these diagrams it is usually assumed a hypothetic diagram due to the inexistence of experimental data (vapour-liquid, liquid-liquid and solid-fluid). In this thesis a similar analysis will be performed on Chapter 2. Typically, a simple rule, is that higher CO_2 densities (high strength) will induce the formation of a large number of nucleation points, inducing the formation of small pores in a large quantity. In opposition smaller densities will produce very few nucleation points that will be responsible for the formation of large pores in small quantity.

CO_2-assisted phase inversion also guides with the same rules of the conventional process which means that the casting solution concentration is another key parameter to control membrane morphology. A simple rule is that an increase in the concentration will result in a decrease in the pore size diameter. Reverchon and co-workers have been developing an extensive work to explore this parameter [44, 45, 46, 47, 48, 49]. In Figure 1.6 it is represented a general phase diagram for the system polymer/solvent/non-solvent with different concentration paths.

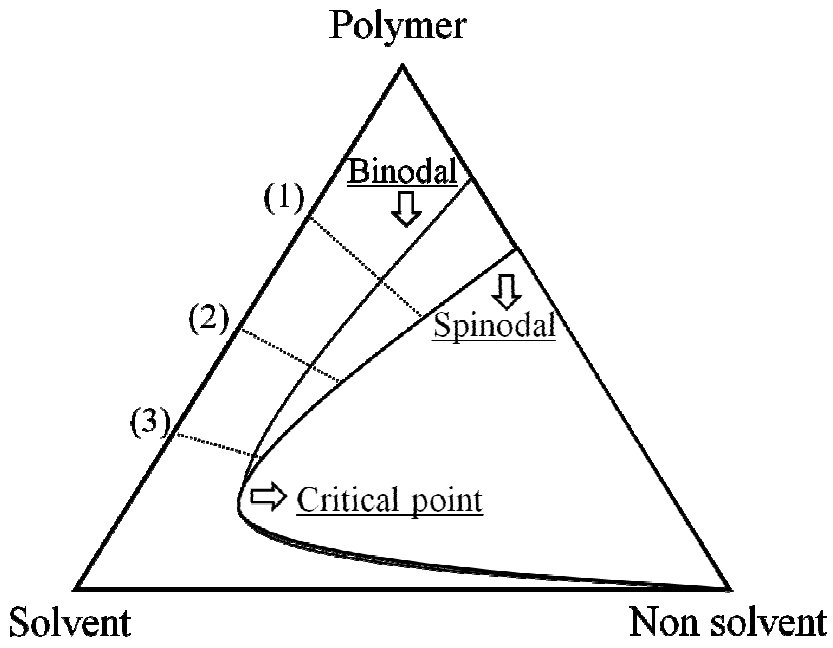

Figure 1.6– General phase diagram for the system polymer/solvent/non-solvent with different concentration paths.

Increasing the polymer concentration in the starting solution, i.e., passing from point 3 to 1 the operative point (the intersection between the tie-line and the composition path) shifts towards the polymer rich phase. Therefore, using the lever rule, we can observe that the polymer-lean phase decreases. As a consequence membranes will be produced with a larger number of pores but with a small diameter.

Other parameters, such as the depressurization rate or the ability of CO_2 to liquefy polymers have been used to modify the morphology of porous structures by phase-inversion. They will be discussed further in this thesis, especially in chapter 2.

1.2 "Smart" hydrogels

Another main research area explored in this work was the preparation and processing of smart polymers, particularly thermoresponsive and pH-sensitive hydrogels.

The last two to three decades have witnessed explosive growth in the synthesis and processing of smart polymers. They were widely used in the biomedical field due to their tuneable chemical and three-dimensional physical structure, biocompatibility properties and possibility to respond external *stimulus*, such as pH , temperature, ionic strength, and electric field [57]. Table 1.4 it is presents some examples of stimuli-responsive hydrogels used in drug delivery.

Table 1.4 – Examples of stimuli-responsive hydrogels in drug delivery

Stimuli	Polymer	Drug	Ref
Magnetic field	Ethylene-co-vinyl acetate	Insulin	[58]
Electric Field	Poly(2-hydroxyethyl methacrylate)	Propranol	[59]
Glucose	Ethylene-co-vinyl acetate	Insulin	[60]
Urea	Methyl vinyl ether-co-maleic anhydride	Hydrocortisone	[61]
Morphine	Methyl vinyl ether-co-maleic anhydride	Naltrexone	22 [62]
pH	Chitosan-poly(ethylene oxide)	Amoxicilin, metronidazole	[63]
pH	Poly(acrylic acid)-poly(ethylene oxide)	Salicylamide, nicotinamide, clonidine	[64]

		hydrochloride	
pH	Poly(acrylamide-co-maleic acid)	Terbinafine, hydrochloride	[65]
pH	N-vinyl pyrrolidone, polyethylene, glycol diacrylate, chitosan	Theophylline, 5-Fluoroacil	[66]
Temperature	Poly(N-isopropyl acrylamide)	Heparin	[67]
Temperature and pH	Poly(N-isopropyl acrylamide-co-butyl methacrylate-co-acrylic acid)	Calcitonin	[68]

1.2.1 Temperature responsive polymers

Temperature is the most widely used stimulus in environmentally responsive polymer systems not only because they are relatively easy to control, but also easily applicable both *in vitro* and *in vivo*.

Some hydrogels exhibit a separation from solution and solidification above a certain temperature. This threshold is defined as the lower critical solution temperature (LCST). Below the LCST, the polymers are soluble. Above the LCST, they become increasingly hydrophobic and insoluble, leading to gel formation. In contrast, hydrogels that are formed upon cooling of a polymer solution have an upper critical solution temperature (UCST). However, most applications are related to LCST based polymer systems [69,70].

For polymers exhibiting a lower critical solution temperature (LCST), temperature increase results in a negative free energy of the system which makes water– polymer association unfavorable, facilitating the other two types of interactions. This negative free energy (ΔG) is

attributed to the higher entropy term (ΔS) with respect to the increase in the enthalpy term (ΔH) in the thermodynamic relation $\Delta G = \Delta H - T\Delta S$. The entropy increases due to water–water associations which are the governing interactions in the system. In Table 1.5 it is presented some examples of thermoresponsive polymers.

Table 1.5- Examples of thermoresponsive polymers

Thermoresponsive polymer	Obs.
Poly(N-isopropylacrylamide)	It is the most studied thermoresponsive polymer.
Methylcellulose [71]	It gells at temperatures in the range of 60–80 ºC and turns into a solution upon cooling.
Poly(N-vinylisobutylamide) [72]	-
Poly(vinyl methyl ether)[73]	It has a LCST at moderate temperature ~35 °C.
Poly(N-vinylcaprolactam) [74]	Shows a dissolution/precipitation transition in water at temperatures close to physiological temperatures (30±40 ºC)
Gelatin [75]	By cooling the temperature the chains transform their conformation from random coil to triple-helix, during which physical junctions are promoted and gel networks occur.
Gellan benzyl ester [76]	Double helix conformations via hydrogen bonding in aqueous systems
Elastin-like polypeptides	Composed of Val-Pro-Gly-Xaa-Gly amino acid repeat units (Xaa is a ‘guest residue’ except proline)

Poly(N-isopropylacrylamide), PNIPAAm, is probably the most studied thermoresponsive hydrogel. It has low critical solution temperature (LCST), around 32 ºC in an aqueous solution [77, 78], close to body temperature and dissolves in water below the LCST; precipitates from the aqueous solution above the LCST due to the disruption of hydrogen bonding with water and the increasing hydrophobic interactions among isopropyl groups (Figure 1.7). Due to this unique property, PNIPAAm gels have been widely used in biomedical fields, for example, as matrices in protein-ligand recognition, in drug controlled release, in enzyme and cell immobilization and in artificial organs / cell sheet technology [79, 80, 81, 82, 83, 84] .

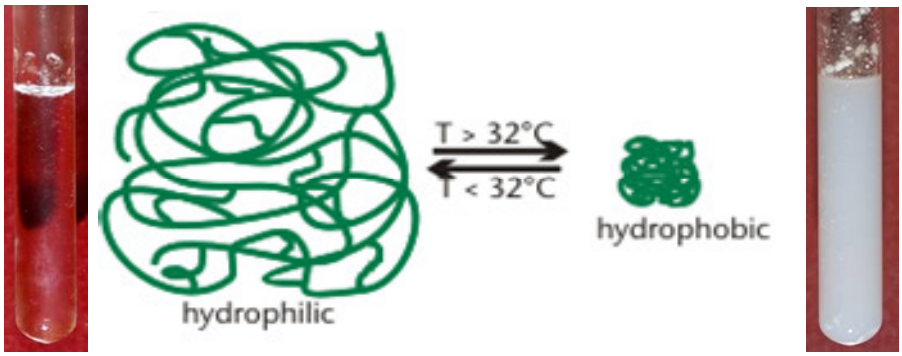

Figure 1.7– Typical behaviour of a thermoresponsive polymer. PNIPAAm case: soluble in a aqueous solution below the LCST and insoluble above this temperature

During the last years several thermoresponsive polymers were developed most of them copolymers of PNIPAAm (Figure 1.8) in order to optimize some of the properties such as faster shrinking rates when heated through the LCST or for instance sensitivity to additional stimuli to combine two or more stimuli-responsive mechanisms into one polymer system. In chapter 3 some examples will be studied.

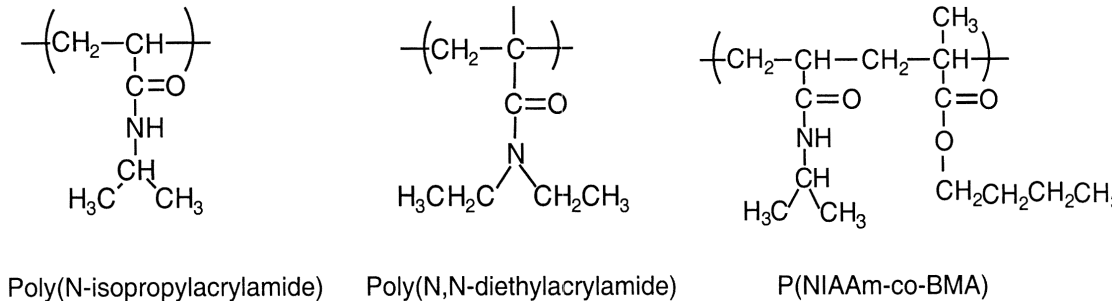

Figure 1.8 - Examples of thermoresponsive polymers based of PNIPAAm

In general, as the polymer chain contains more hydrophobic constituents the LCST becomes lower. Copolymerization of NIPAAm with a more hydrophilic monomer increases the overall hydrophilicity of the polymer, and the stronger polymer–water interactions lead to an increase in the LCST. Likewise, copolymerization with a more hydrophobic monomer results in a lower LCST than PNIPAAm [85]. Moreover, the phase transition temperature is influenced by the presence of salts [86] and pH to a certain extent [87].

A good review about the functional copolymers of NIPAAm for bioengineering applications can be found in the literature [88].

1.2.2 pH-sensitive polymers

All the polymers containing pendant groups that either accept or release protons in response to changes in environmental are pH sensitive polymers. Such materials, called polyelectrolytes, swell or collapse depending on the pH of their environment.

There are two kinds of pH sensitive materials: one which have acidic group (-COOH, $-SO_3H$) and swell in basic pH (Figure 1.9), and others which have basic groups ($-NH_2$) and swell in acidic pH. In this work these two types of polymers were applied.

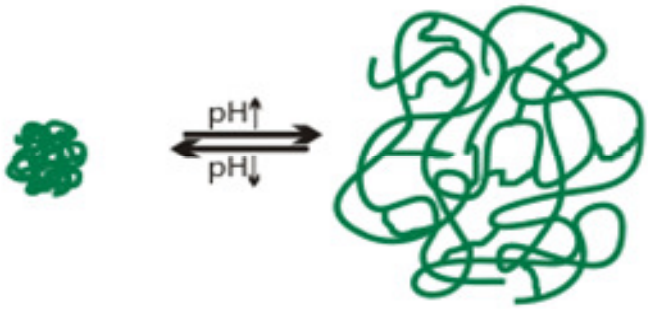

Figure 1.9– Typical behaviour of a pH sensitive polymer acidic groups

The response is triggered due to the presence of ionisable functional groups (like -COOH, -NH_2) which get ionized and acquire a charge (+/-) in a certain pH. As the environmental pH changes, the degree of ionization in a polymer bearing weakly ionizable groups is dramatically altered at a specific pH that is called pKa. This rapid change in net charge of pendant groups causes an alternation of the hydrodynamic volume of the polymer chains. The transition from collapsed state to expanded state is explained by the osmotic pressure exerted by mobile counterions neutralizing the network charges. There are two types of pH-responsive polyelectrolytes; weak polyacids and weak polybases.

Examples of pH sensitive polymers that are polyacids and polybases are represented in Figure 1.10 and in Figure 1.11.

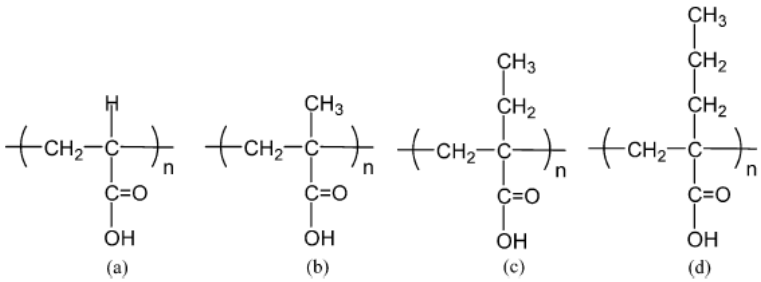

Figure 1.10 - Representative pH-responsive polyacids; (a) poly(acrylic acid) (PAAc), (b) poly(methacrylic acid) (PMAAc), (c) poly(2-ethyl acrylic acid) (PEAAc), (d) poly(2-propyl acrylic acid) (PPAAc).

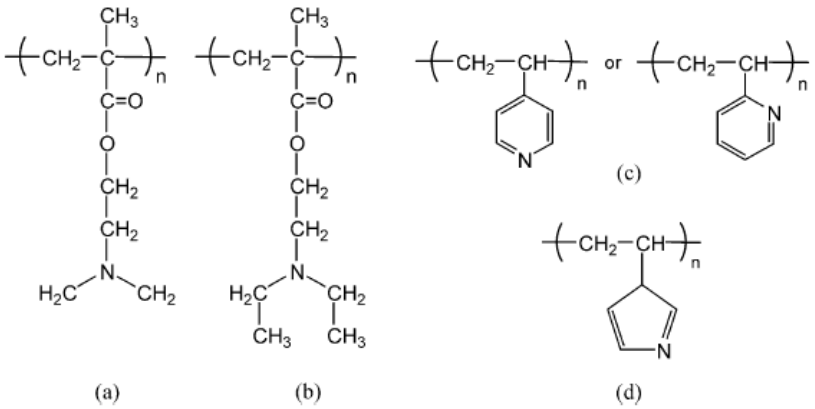

Figure 1.11 - Representative pH-responsive polybases. (a) Poly(N,N-dimethyl aminoethyl methacrylate) (PDMAEMA), (b) poly(N,N-diethyl aminoethyl methacrylate) (PDEAEMA), (c) poly(4 or 2-vinylpyridine) (PVP), (d) poly(vinyl imidazole).

In this thesis special attention will be given to polymethacrylic acid as an example of polyacid and to chitosan as a polybase. The preparation of dual stimulus hydrogels will also be attempted.

1.3 "Smart" drug/biomolecule delivery devices

The field of drug delivery is developing rapidly and is gaining the attention of scientists, pharmaceutical makers and industry.

The final aim of pharmacy and medicine is the delivery of any drug at the right time in a safe and reproducible manner to a specific target at the required level [89]. With traditional tablets or injections, the drug level in the blood follows the profile shown in Figure 1.12. a), in which the level rises after each administration of the drug and then decreases until the next administration. The problem consists in the fact that the blood level of the agent should remain between maximum values, which may represent a toxic level, and a minimum value, below which the drug is no longer effective. In controlled drug delivery systems designed for long-term administration, the drug level in the blood follows the profile shown in Figure 1.12. b), remaining constant, between the desired maximum and minimum, for an extended period of time.

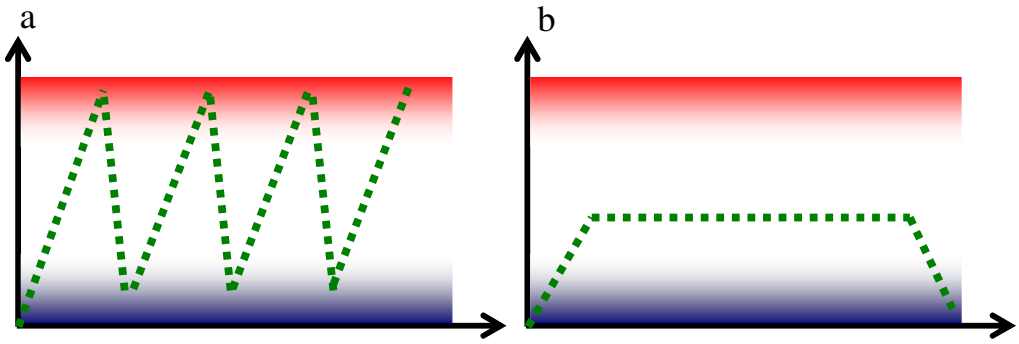

Figure 1.12 – Drug levels in the blood with (a) traditional drug dosing and (b) controlled-delivery dosing.

Another issue is the fact that patients do not always follow the doctor's orders, so there is a concern about patients' compliance.

In the last decades several systems were developed in order to overcome these issues.

Table 1.6 resumes some of the approaches that were used.

Table 1.6 – Resume of new technologies for controlled drug delivery

Technology	Application	Description
Drug polymer conjugates [90]	Prepare a form of insulin that can be given orally.	Low molecular weight polymers (PEG) are attached to specific sites on drug molecules to create drug–polymer conjugates
Usage of absorption enhancers [91]	Pulmonary drug delivery	Chitosan powder was tested for the nasal administration of insulin and morphine
Iontophoresis and Ultrasound [92]	Transdermal drug delivery	Administration of iontocaine for local dermal anesthesis
Micelles and liposomes [93]	Encapsulation of therapeutic active molecules	Transport molecules unto the interior of cells
Drug releasing chambers [94]	Diabetes, cancer and for a range of target sites (i.e. eye, brain)	Delivery of potent drugs for extended periods.
Nanoparticles [95]		Nanoparticles that can become nanopills taking drugs through diminutive capillaries into the cell's internal machinery

Herein it is reported the development of a new strategy that could be applied in the preparation of smart porous structures with application as controlled delivery devices.

The work developed in this thesis will focus at combining: (i) production of porous structures by clean processes with $scCO_2$; (ii) the potential of CO_2 to be used in the in situ polymerization of

hydrogels inside the porous structures; (iii) the possibility to impregnate the smart devices with a non-residue technology; (iv) the potential of these smart devices to be used in controlled drug release.

1.4 References

[1] E.J. Beckman, Supercritical and near-critical CO_2 in green chemical synthesis and processing. *J. Supercrit. Fluids* 28 (**2004**) 121-191.

[2] P. Jessop, W. Leitner, Chemical Synthesis using supercritical fluids, Wiley-VCH, New York, **1999**.

[3] R.C. Reid, J.M. Prausnitz, B.E. Poling, The properties of gases and liquids. **1987**: Mc-Graw-Hill.

[4] M. Perrut, Supercritical Fluid Applications: Industrial Developments and Economic Issues, *Ind. Eng. Chem. Res.* 39 (**2000**) 4531-4535.

[5] P. C. Simões, P. J. Carmelo, P. J. Pereira, J. A. Lopes, M. Nunes da Ponte, G. Brunner, Quality assessment of refined olive oils by gas extraction. *J. Supercrit. Fluids* 13 (**1998**) 337-341.

[6] P. Christian, M.R. Giles, R.M.T. Griffiths, D.J. Irvine, R.C. Major, S.M. Howdle, Free Radical Polymerization of Methyl Methacrylate in Supercritical Carbon Dioxide Using a Pseudo-Graft Stabilizer: Effect of Monomer, Initiator, and Stabilizer Concentrations. *Macromolecules*, 33 (**2000**) 9222–9227.

[7] J. M. DeSimone, E. E. Maury, Y. Z. Menceloglu, J. B. McClain, T. J. Romack, and J. R. Combes, Dispersion Polymerizations in Supercritical Carbon Dioxide. *Science* 265 (**1994**) 356-359.

[8] J. Jung, M. Perrut, Particle design using supercritical fluids: Literature and patent survey. *J. Supercrit. Fluids* 20 (**2001**) 179-219.

[9] Z. Knez, E. Weidner, Particles formation and particle design using supercritical fluids. *Current Opinion in Solid State and Materials Science* 7 (**2003**) 353–361.

[10] E. Bogel-ukasik, I. Fonseca, R. Bogel-ukasik, Y. A. Tarasenko, M. Nunes da Ponte, A. Paiva and G. Brunner Phase, equilibrium-driven selective hydrogenation of limonene in high-pressure carbon dioxide. *Green Chem*. 9 (**2007**) 427 – 430.

[11] A.R.C. Duarte, M. S. Costa, A. L. Simplício, M. M. Cardoso and C. M.M. Duarte, Preparation of controlled release microspheres using supercritical fluid technology for delivery of anti-inflammatory drugs. *Int. J. Pharm*. 308 (**2006**) 168-174.

[12] A.I. Cooper, Porous Materials and Supercritical Fluids. *Adv. Mater*. 15 (**2003**) 1049-1059.

[13] J.J.A. Barry, H.S. Gidda, C.A. Scotchford, S.M. Howdle, Porous methacrylate scaffolds: supercritical fluid fabrication and in vitro chondrocyte responses. *Biomaterials* 25 (**2004**) 3559-3568.

[14] M. Sousa, M. João Melo, T. Casimiro and A. Aguiar-Ricardo, The art of CO_2 for art conservation: a green approach to antique textile cleaning. *Green Chem*. 9 (**2007**) 943- 947.

[15] T. Casimiro, A.M. Banet-Osuna, A.M. Ramos, M. Nunes da Ponte and A. Aguiar-Ricardo, Synthesis of highly cross-linked poly(diethylene glycol dimethacrylate) microparticles in supercritical carbon dioxide, *Eur. Polym. J*., 41 (**2005**) 1947-1953.

[16] M.R. Giles, R.M.T. Griffiths, A. Aguiar-Ricardo, M.M.C.G. Silva and S.M. Howdle, Fluorinated graft stabilizers for polymerization in supercritical carbon dioxide: the effect of stabilizer architecture. *Macromolecules*, 34 (**2001**) 20-25.

[17] R. Ruivo, M.J. Cebola, P.C. Simões and M. Nunes da Ponte, Fractionation of edible oil model mixtures by supercritical carbon dioxide in a packed column Part II: a mass transfer study, *Ind. Eng. Chem. Res*., 41 (**2002**) 2305–2315.

[18] J. E. Martini, The Production and Analysis of Microcellular Foam. Ph.D. Thesis, Massachusetts Institute of Engineering, **1981**.

[19] S.K. Goel, E.J. Beckman, Generation of microcellular polymers using supercritical CO_2. *Cellular Polymers* 12 (**1993**) 251 -274.

[20] D.J. Mooney, D.F. Baldwin, N.P. Suh, L.P. Vacanti, R. Langer, Novel approach to fabricate porous sponges of poly(D,L-lactic-co-glycolic acid) without the use of organic solvents. *Biomaterials* 17 (**1996**) 1417-1422.

[21] S.K. Goel, E.J. Beckman, Generation of microcellular polymeric foams using supercritical carbon dioxide. Cell-growth and skin formation. *Polym. Eng. Sci*. 34 (**1994**) 1148–1156.

[22] S.K. Goel, E.J. Beckman, Generation of microcellular polymeric foams using supercritical carbon-dioxide.1. Effect of pressure and temperature on nucleation. *Polym. Eng. Sci*. 34 (**1994**) 1137–1147.

[23] P.D. Condo, K. P. Johnston, In situ measurement of the glass transition temperature of polymers with compressed fluid diluents. *J. Poly. Sci., Part B, Poly. Phys*. 32 (**1994**) 523-533.

[24] P. D. Condo, I. C. Sanchez, C. G. Panayiotou, K. P. Johnston, In situ measurement of the glass transition temperature of polymers with compressed fluid diluents. *Macromolecules* 25 (**1992**) 6119-6127.

[25] M.H. Sheridan, L.D. Shea, M.C. Peters; D.J. Mooney, Bioabsorbable polymer scaffolds for tissue engineering capable of sustained growth factor delivery. *J. Control. Release* 64 (**2000**) 91–102.

[26] K.A. Arora, A.J. Lesser, T.J. McCarthy, Preparation and characterization of microcellular polystyrene foams processed in supercritical carbon dioxide. *Macromolecules* 31 (**1998**) 4614-4620.

[27] B. Krause, R. Mettinkhof, N.F.A. van der Vegt, M. Wessling, Microcellular Foaming of Amorphous High-Tg Polymers Using Carbon Dioxide. *Macromolecules* 34 (**2001**) 874-884.

[28] B. Krause, H. J. P. Sijbesma, P. Münüklü, N. F. A. van der Vegt, M. Wessling Bicontinuous Nanoporous Polymers by Carbon Dioxide Foaming. *Macromolecules* 34 (**2001**) 8792 -8801.

[29] S. Siripurapu, Y.J. Gay, J.R. Royer, J.M. DeSimone, R.J. Spontak, S.A. Khan, Generation of microcellular foams of PVDF and its blends using supercritical carbon dioxide in a continuous process. *Polymer* 43 (**2002**) 5511-5520.

[30] M.T. Liang, C.M. Wang, Production of engineering plastics foams by supercritical CO_2. *Ind. Eng. Chem. Res*. 39 (**2000**) 4622-4626.

[31] P. Hainey, I. M. Huxham, B. Rowatt, D. C. Sherrington, L. Tetley, Synthesis and Ultrastructural Studies, of Styrene-Divinylbenzene Polyhipe Polymers. *Macromolecules* 24 (**1991**) 117-121.

[32] A. Barbetta, N. R. Cameron, S. J. Cooper, High internal phase emulsions (HIPEs) containing divinylbenzene and 4-vinylbenzyl chloride and the morphology of the resulting PolyHIPE materials. *Chem. Commun*. 3 (**2000**) 221-222.

[33] A. Imhof, D. J. Pine, Uniform Macroporous Ceramics and Plastics by Emulsion Templating. *Adv. Mater*. 10 (**1998**) 697-700.

[34] R. Butler, C. M. Davies, A. I. Cooper, Emulsion Templating Using High Internal Phase Supercritical Fluid Emulsions. *Adv. Mater*. 13 (**2001**) 1459-1463.

[35] R. Butler, I. Hopkinson, A. I. Cooper, Synthesis of Porous Emulsion-Templated Polymers Using High Internal Phase CO_2-in-Water Emulsions. *J. Am. Chem. Soc*. 125 (**2003**) 14473-14481.

[36] S. Partap, I. Rehman, J. R. Jones, and J. A. Darr, "Supercritical carbon dioxide in water" emulsion-templated synthesis of porous calcium alginate hydrogels. *Adv. Mater*. 18 (**2006**) 501–504.

[37] J. Wang, Y. Xia, W. Wang, R. Mokaya and M. Poliakoff, Synthesis of siliceous hollow spheres with large mesopore wall structure by supercritical CO2-in-water interface templating. *Chem. Commun*. 2 (**2005**) 210–212.

[38] J.-Y. Lee, B. Tan, and A. I. Cooper, CO_2-in-Water Emulsion-Templated Poly(vinyl alcohol) Hydrogels Using Poly(vinyl acetate)-Based Surfactants. *Macromolecules* 40 (**2007**) 1955-1961.

[39] C. Palocci, A. Barbetta, A.L. Grotta, and M. Dentini, Porous Biomaterials Obtained Using Supercritical CO_2-Water Emulsions. *Langmuir* 23 (**2007**) 8243-8251.

[40] M. Mulder, Basic Principles of Membrane Technology, Kluwer Academic Publisher, Netherlands, **1997**.

[41] Y.W. Kho, D.S. Kalika, B.L. Knutson, Precipitation of Nylon 6 membranes using compressed carbon dioxide. *Polymer* 42 (**2001**) 6119-6127.

[42] H. Matsuyama, H. Yano, T. Maki, M. Teramoto, K. Mishima, K. Matsuyama, Formation of porous flat membrane by phase separation with supercritical CO_2. *J. Membrane Sci*., 194 (**2001**) 157-163.

[43] H. Matsuyamaa, A. Yamamoto, H. Yano, T. Maki, M. Teramoto, K. Mishima, K. Matsuyama, Effect of organic solvents on membrane formation by phase separation with supercritical CO_2. *J. Membrane Sci*. 204 (**2002**) 81–87.

[44] E. Reverchon, S. Cardea, Formation of cellulose acetate membranes using a supercritical fluid assisted process. *J. Membrane Sci*. 240 (**2004**) 187-195.

[45] E. Reverchon, S. Cardea, Formation of polysulfone membranes by supercritical CO_2. *J. Supercrit. Fluids* 35 (**2005**) 140-146.

[46] E. Reverchon, S. Cardea, E.S. Rappo, Production of loaded PMMA structures using the supercritical CO_2 phase inversion process. *J. Membrane Sci*. 273 (**2006**) 97-105.

[47] E. Reverchon, S. Cardea, PVDF-HFP Membrane Formation by Supercritical CO_2 Processing: Elucidation of Formation Mechanisms. *Ind. Eng. Chem. Res*. 45 (**2006**) 8939-8945.

[48] E. Reverchon, S. Cardea, C. Rapuan, Formation of Poly-Vinyl-Alcohol Structures by Supercritical CO_2. *J. Appl. Polym. Sci*. 104 (**2007**) 3151-3160.

[49] E. Reverchon, S. Cardea, C. Rapuan, Membranes formation of a hydrosoluble biopolymer (PVA) using a supercritical CO_2-expanded liquid. *J. Supercrit. Fluids* 45 (**2008**) 356–364.

[50] I. Tsivintzelis, E. Pavlidou, C. Panayiotou, Porous scaffolds prepared by phase inversion using supercritical CO_2 as antisolvent. *J. Supercrit. Fluids* 40 (**2007**) 317-322.

[51] Q. Xu, M. Pang, Q. Peng, Y. Jiang, J. Li, H. Wang, M. Zhu, Effect of different experimental conditions on biodegradable polylactide membranes prepared with supercritical CO_2 as nonsolvent. *J. Appl. Polym. Sci*. 98 (**2005**) 831-837.

[52] S.R. Huang, G.Z. Wu, S.M. Chen, Preparation of microporous poly(vinylidene fluoride) membranes via phase inversion in supercritical CO_2. *J. Membrane Sci*. 293 (**2007**) 100-110.

[53] Z. Li, H. Tang, X. Liu, Y. Xia and J. Jiang, Preparation and characterization of microporous poly(vinyl butyral) membranes by supercritical CO_2-induced phase separation. *J. Membrane Sci*. 312 (**2008**) 115–124

[54] M. Temtem, T. Casimiro, A. Aguiar-Ricardo, Solvent power and depressurization rate effects in the formation of polysulfone membranes with CO_2-assisted phase inversion method. *J. Membrane Sci*. 283 (**2006**) 244-252.

[55] M. Temtem, T. Casimiro, J.F. Mano and A. Aguiar-Ricardo, Preparation of membranes with polysulfone/polycaprolactone blends using a high pressure cell specially designed for a CO_2-assisted phase inversion. *J. Supercrit. Fluids* 43 (**2008**) 542-548.

[56] M. Temtem, L. Silva, P. Andrade, F. Santos, C. Lobato da Silva, J.M.S. Cabral, M.M. Abecasis and A. Aguiar-Ricardo, Supercritical CO_2 Generating Chitosan Devices with Controlled Morphology. Potential Application for Drug Delivery and Mesenchymal Stem Cell Culture. *In press J. Supercrit. Fluids doi:10.1016/j.supflu.2008.10.020*

[57] W.-F. Lee, C.-H. Shieh, pH-Thermoreversible Hydrogels. I. Synthesis and Swelling Behaviors of the (N-isopropylacrylamide-co-acrylamide-co-2-hydroxyethyl methacrylate) Copolymeric Hydrogels. *J. Appl. Polym. Sci*. 71 (**1999**) 221–231.

[58] H.M. Creque, R. Langer, J. Folkman One month of sustained release of insulin from a polymer implant. *Diabetes* 29 (**1980**) 37–40.

[59] A. D'Emanuele, J.N. Staniforth, An electrically modulated drug delivery device: I. *Pharm. Res*. 8 (**1991**) 913–918

[60] L.R. Brown, E.R. Edelman, X.F. Fischel-Ghodsian, R. Langer, Characterization of glucose-mediated insulin release from implantable polymers. *J. Pharm. Sci*. 85 (**1996**) 1341–1345

[61] J. Heller, R. W. Baker, R. M. Gale, J. O. Rodin, Controlled drug release by polymer dissolution. I. Partial esters of maleic anhydride copolymers – properties and theory. *J. Appl. Polym. Sci*. 22 (**1978**) 1991–2009

[62] K.V. Roskos, J.A. Tefft, B.K. Fritzinger, J. Heller, Development of a morphine-triggered naltrexone delivery system. *J. Control. Release* 19 (**1992**) 145–160.

[63] V.R. Patel, M.M. Amiji, Preparation and characterization of freeze-dried chitosan-poly(ethylene oxide) hydrogels for site-specific antibiotic delivery in the stomach. *Pharm. Res.* 13 (**1996**) 588–593.

[64] A. Bilia, V. Carelli, G. Di Colo, E. Nannipieri, In vitro evaluation of a pH-sensitive hydrogel for control of GI drug delivery from silicone-based matrices. *Int. J. Pharm*. 130 (**1996**) 83–92.

[65] M. Sen, C. Uzun, O. Güven Controlled release of terbinafine hydrochloride from pH sensitive poly(acrylamide/maleic acid) hydrogels. *Int. J. Pharm*. 203 (**2000**) 149–157.

[66] K.L. Shantha, D.R.K. Harding, Preparation and in vitro evaluation of poly(N-vinyl-2-pyrrolidone-polyethylene glycol diacrylate)-chitosan interpolymeric pH-responsive hydrogels for oral drug delivery. *Int. J. Pharm*. 207 (**2000**) 65–70.

[67] A. Gutowska, Y.H. Bae, J. Feijen, S.W. Kim, Heparin release from thermosensitive hydrogels. *J. Control. Release* 22 (**1992**) 95–104.

[68] A. Serres, M. Baudy, S.W. Kim, Temperature and pH sensitive polymers for human calcitonin delivery. *Pharm. Res*. 13 (**1996**) 196–201.

[69] S. Fujishige, K.K.I. Ando. Phase transition of aqueous solutions of poly(N-isopropylacrylamide) and poly(N-isopropylmethacrylamide). *J. Phys. Chem*. 93 (**1989**) 3311-3313.

[70] E. S. Gil, S. M. Hudson, Stimuli-reponsive polymers and their bioconjugates, *Prog. Polym. Sci*. 29 (**2004**) 1173-1222.

[71] M. Takahashi, M. Shimazaki, J. Yamamoto, Thermoreversible gelation and phase separation in aqueous methyl cellulose solutions, *J. Polym. Sci. B* 39 (**2001**) 91-100.

[72] K. Suwa, K. Yamamoto, M. Akashi, K. Takano, N. Tanaka, S. Kunugi. Effects of salt on the temperature and pressure responsive properties of poly(N-vinylisobutyramide) aqueous solutions. *Colloid Polym Sci*. 276 (**1998**) 529-33.

[73] Y. Maeda, IR spectroscopic study on the hydration and the phase transition of poly(vinyl methyl ether) in water. *Langmuir* 17 (**2001**) 1737-42.

[74] T. Inoue, G.Chen, K. Nakamae, A.S. Hoffman, Temperature sensitivity of a hydrogel network containing different LCST oligomers grafted to the hydrogel backbone. *Polym. Gels Netw*. 5 (**1997**) 561-575.

[75] A.J. Kuijpers, G.H.M. Engbers, J. Feijen, S.C. De Smedt, T.K.L. Meyvis, J. Demeester, J. Krijgsveld, S.A.J. Zaat, J. Dankert. Characterization of the network structure of carbodiimide cross-linked gelatin gels. *Macromolecules* 32 (**1999**) 3325-3333.

[76] M. Dentini, P. Desideri, V. Crescenzi, Y. Yuguchi, H. Urakawa, K. Kajiwara, Solution and gelling properties of gellan benzyl esters. *Macromolecules* 32 (**1999**) 7109–7115.

[77] H.G. Schild, Poly(iV-isopropylacrylamide): experimental and. application. *Prog. Polymer Sci*. 17 (**1992**) 163-249.

[78] V. V. A. Fernandez, N. Tepale, J. C. Sanchez-Diaz, E. Mendizabal, J. E. Puig and J. F. A. Soltero, Thermoresponsive nanostructured poly(N -isopropylacrylamide) hydrogels made via inverse microemulsion polymerization *Colloid Polym. Sci*. 284 (**2006**) 387-395.

[79] T. Okano, N. Yamada, H. Sakai, Y. Sakurai, A novel recovery system for cultured cells using plasma-treated polystyrene dishes grafted with poly(N-isopropylacrylamide) *J. Biomd. Mat. Res.* 27 (**1993**) 1243-1251.

[80] P.S. Stayton, T. Shimoboji, C. Long, A. Chilkoti, G. Chen, J. M. Harris and A. S. Hoffman, Control of protein-ligand recognition using a stimuli-responsive polymer, *Nature* 378 (**1995**) 472-474;

[81] Y. Qiu and K. Park, Environment-sensitive hydrogels for drug delivery, *Adv. Drug Delivery Rev*. 53 (**2001**) 321-339.

[82] L. C. Dong and A. S. Hoffman, Thermally reversible hydrogels: III. Immobilization of enzymes for feedback reaction control, *J. Control. Release* 4 (**1986**) 223-227.

[83] R.A. Stile, W. R. Burghardt and K. E. Healy, Synthesis and Characterization of Injectable Poly(N-isopropylacrylamide)-Based Hydrogels That Support Tissue Formation in Vitro, *Macromolecules* 32 (**1999**) 7370-7379.

[84] K.-H. Park and Y. H. Bae, Phenotype of hepatocyte spheroids in Arg-GLY-Asp (RGD) containing a thermo-reversible extracellular matrix, *Biosci. Biotechnol. Biocehm*. 66 (**2002**) 1473-1478.

[85] H.G. Schild, Poly(N-isopropylacrylamide): experiment, theory and application, *Prog. Polym. Sci*. 17 (**1992**) 163– 249.

[86] X.M. Liu, L.S. Wang, L. Wang, J. Huang, C. He, The effect of salt and pH on the phase-transition behaviors of temperature-sensitive copolymers based on N-isopropylacrylamide, *Biomaterials* 25 (**2004**) 5659–5666.

[87] Y. Pei, J. Chen, L. Yang, L. Shi, Q. Tao, B. Hui, J. Li, The effect of pH on the LCST of poly(N-isopropylacrylamide) and poly (N-isopropylacrylamide-co-acrylic acid), *J. Biomater. Sci. Polym*. Ed. 15 (**2004**) 585–594.

[88] Z. M. O. Rzaev, S. Dinçer, Erhan Piskin,Functional copolymers of N-isopropylacrylamide for bioengineering applications, *Prog. Polym. Sci*. 32 (**2007**) 534–595

[89] G. Orive, R.M. Hernández, A.R. Gascón, A. Domínguez-Gil and J.L. Pedraz, Drug delivery in biotechnology: Present and future, *Current Opinion in Biotechnology*, 14 (**2003**) 659-664.

[90] F.M. Veronese, J.M. Harris, Introduction and overview of peptide and protein PEGylation. *Adv. Drug Deliv. Rev*. 54 (**2002**) 453-456.

[91] L. Illum, I. Jabbal-Gill, M. Hinchcliffe, A.N. Fisher, S.S. Davis, Chitosan as a novel system for vaccines. *Adv. Drug Deliv. Rev*. 51 (**2001**) 81-96.

[92] R. Langer, Where a pill won't reach. *Sci. Am*. 288 (**2003**) 50-57.

[93] R. Savic, L. Luo, A. Eisenberg, D. Maysinger, Micellar nanocontainers distribute to defined cytoplasmic organelles. *Science* 300 (**2003**) 615-618.

[94] D. LaVan, T. McGuire and R. Langer, Small-scale systems for *in vivo* drug delivery, *Nature Biotechnology*, 21 (**2003**) 1184-1191.

[95] T.C, Yih; M. Al-Fandi, Engineered nanoparticles as precise drug delivery systems. *J Cell. Biochem*. 97 (**2006**) 1184-90.

Chapter 2

PRODUCTION OF POROUS STRUCTURES

2. Production of porous structures with a CO_2-assisted phase inversion method

One the goals in this work, was the development of a CO_2-assisted phase inversion method able to prepare porous structures, namely membranes. The work here presented will focus in the processing of a biocompatible polymer with large applications in the haemodialysis area (polysulfone) and in the preparation of membranes and beads of a water soluble biodegradable and biocompatible polymer (chitosan).

2.1 Polysulfone membranes

Polysulfone is a polymer, with high chemical and mechanical stability and excellent thermal and electrical properties over a wide temperature range. Due to its durability to hot water, steam, and alcohol, and because it is not noxious, PS is widely used in the manufacture of medical devices [1], particularly in the preparation of membranes. In Figure 2.1 it is presented the chemical structure of the PS used in this work.

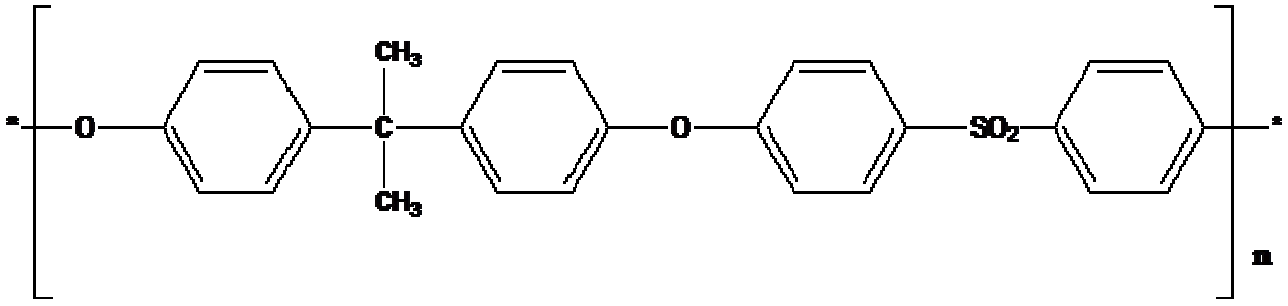

Figure 2.1 – Chemical structure of the polysulfone used in this work

The application of a CO_2 – assisted phase inversion method in the preparation of PS membranes is of great interest since $scCO_2$ is a clean and versatile solvent. Reverchon and co-workers [2] have prepared this type of structures using this technique. They analyzed the effect of pressure,

temperature and polymer concentration in the pore size, using two different casting solutions: PS/N-methylpyrrolidone and PS/chloroform and observed that the pore size decreases at higher pressures, lower temperatures and using casting polymer solutions with higher concentrations.

The main goal of this work was to study the solvent affinity and depressurization rate on the morphology of PS membranes. It is known that the mutual affinity between solvent and non solvent is a key point to obtain the desired membrane structure [3]. Matsuyama *et al.* [4] studied the preparation of porous cellulose acetate membranes using four organic solvents in the preparation of the casting solution and noted that as the mutual affinity between the solvent and supercritical CO_2 decreased, the membrane porosity and the average pore size increased. More recently, Reverchon *et al.* [5] studied the production of poly(methyl methacrylate) membranes and evidenced similar results. In addition, the depressurization rate may influence the membrane formation. It is reported in the literature the influence of depressurization rate in particle formation with supercritical fluids [6, 7] and in the preparation of polylactide membranes when $scCO_2$ is used as non solvent [8].

In this work, six organic solvents and two depressurization rates were tested in the formation of PS membranes using a supercritical CO_2 to induce the phase inversion.

2.1.1 Experimental

2.1.1.1 Materials

Polysulfone (molecular weight 67,000) was obtained from Sigma-Aldrich in pellet form. N-methylpyrrolidone (purity ≥ 99.5 %), N,N-dimethylpropionamide (purity ≥ 98 %), N, N-dimethylacetamide (purity ≥ 98 %) and dimethylsulfoxide (purity ≥ 99 %) were purchased from Sigma-Aldrich and N,N-dimethylformamide (purity ≥ 95 %) from May & Baker. Carbon dioxide was obtained from Air Liquide with 99.998 % purity.

All reagents were used without any further purification.

2.1.1.2 Membrane production

The membrane production was undertaken in a high-pressure apparatus schematically presented in Figure 2.2.

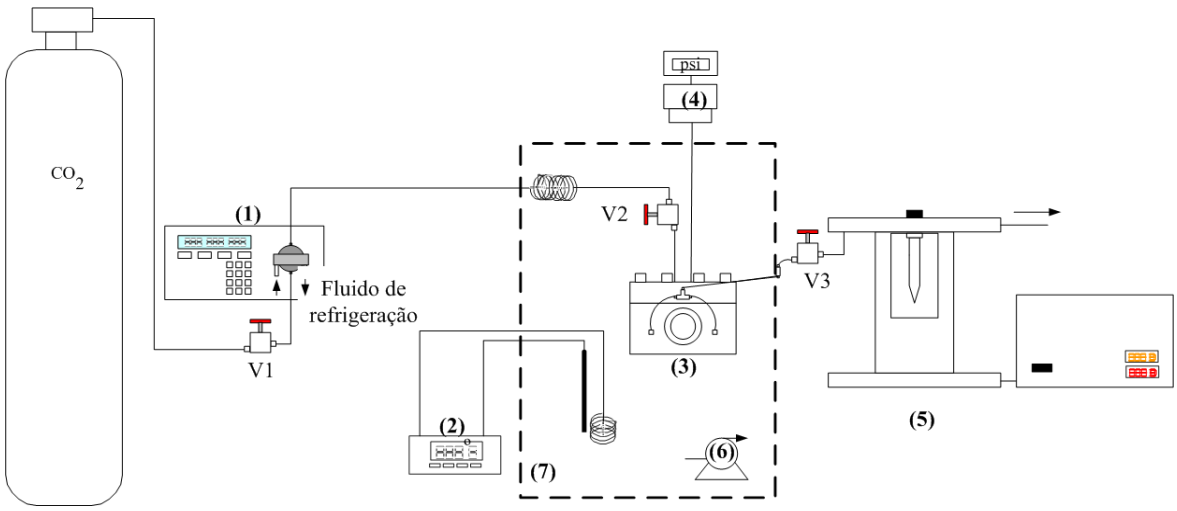

Figure 2.2 - Layout of the high-pressure apparatus for the membrane formation: (1) Gilson 305 piston pump; (2) temperature controller; (3) high-pressure cell; (4) pressure transducer (5) back Pressure Regulator

A new high pressure cell, schematically represented in Figure 2.3, was developed in order to increase membrane area and allow visual inspection of all production process. This cell was fabricated in 316 stainless steel using standard machining techniques. In the core it has a porous structure that supports a bed of Raschig rings, which allows the homogeneous dispersion of CO_2 in the top of the casting solution. All the equipment was tested with pressures up to 30MPa and no signs of failure were observed. The stainless steel cover of the cell contains openings for the inlet valve of CO_2 admission and pressure transducer. The cell is immersed in a visual

thermostated water bath, heated by means of a controller (Hart Scientific, Model 2200) that maintained the temperature within ±0.01 °C. The pressure is monitored with a pressure transducer (Setra Systems Inc., Model 204) with a precision of ± 100 Pa.

In a typical procedure, the casting solution is loaded into the high-pressure vessel which is then placed in the thermostated water bath. Approximately 400 mg of solution was spread over the sapphire window (with a diameter of 2.4 cm) in order to produce membranes with thickness ranging from 450 to 550 μm. CO_2 is added until the desired pressure, with an exact flow, using a Gilson 305 piston pump. After reaching the normal operational pressure, the supercritical solution passes through a back pressure regulator (Jasco 880-81) which separates the CO_2 from the solvent.

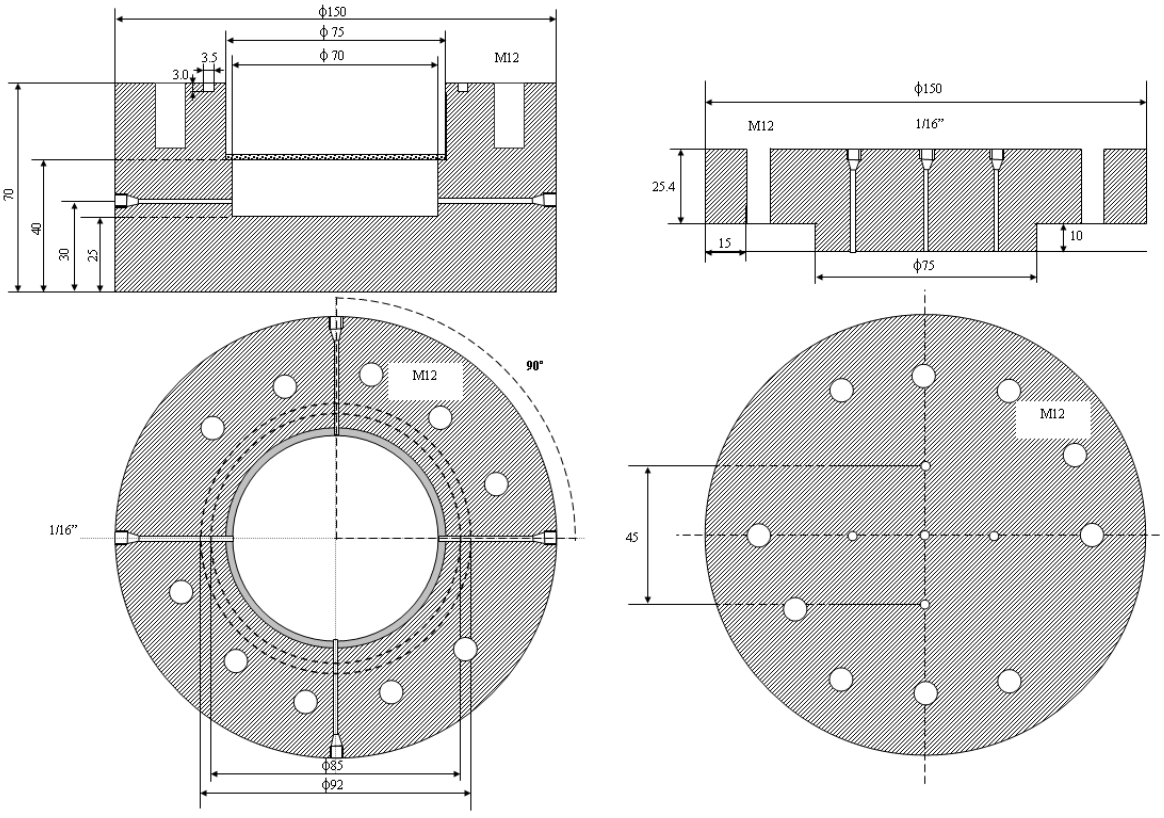

Figure 2.3 - Schematic representation of the new high pressure cell used for membrane preparation.

All the experiments were realized at 18.6 ± 0.7 MPa with a CO_2 flow of 9.8 g/min during 2 hours. At the end the system is depressurized and a thin homogeneous membrane is obtained (Figure 2.4).

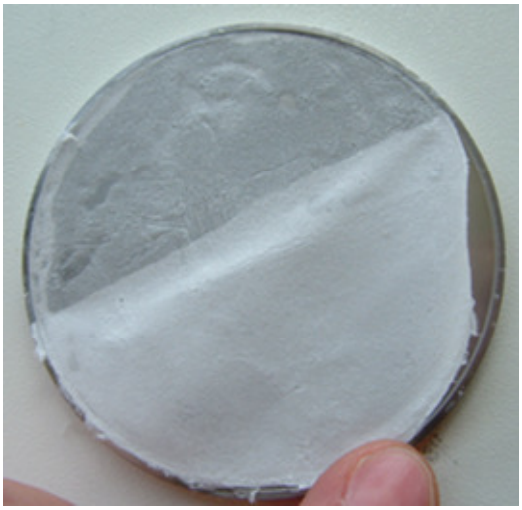

Figure 2.4 – Polysulfone membrane obtained with the $scCO_2$-assisted phase inversion method

2.1.1.3 Membranes characterization

Membranes were characterized using Scanning Electron Microscopy (SEM) in a Hitachi S-2400, with an accelerating voltage set to 15 kV. For cross-section analysis the membrane samples were frozen and fractured in liquid nitrogen. All samples were coated with gold before analysis.

Pore size diameters and porosity were obtained by image analysis using SigmaScan Pro (Systat Software Inc.). EasyFit (MathWave Technologies) was used to fit statistical distributions to our data (Weibull, Lognormal) and to perform the Kolmogorov –Smirnov [9] and Anderson-Darling [10] tests to select the more adequate distribution function to each system under study.

The permeability to pure water was determined by measuring the water flux trough the membranes using a 10 ml filtration unit (Amicon Corp., model 8010) with an effective area of 4.1

cm^2. All the experiments were carried out varying the applied hydrostatic pressure from 0 to 0.24 MPa. At least three clean water flux measurements were performed for each membrane.

2.1.2 Results and discussion

In this study, all the process parameters were fixed: temperature, pressure and polymer solution concentration (45 ºC, 18.6 MPa and 15% w/w, respectively). Different casting solutions were prepared using the following solvents: N-methylpyrrolidone, N,N-dimethylformamide, N, N-dimethylacetamide, chloroform, dimethylsulfoxide and N,N-dimethylpropionamide. The effect of depressurization rate was studied comparing membrane morphologies obtained in experiments performed with fast (less than one minute) and slow (approximately one hour) depressurization rates.

2.1.2.1 Influence of the casting solution

Observing the SEM images presented in Figure 2.5 it is possible to note a strong dependence of membranes morphology with the solvent used in the casting solution.

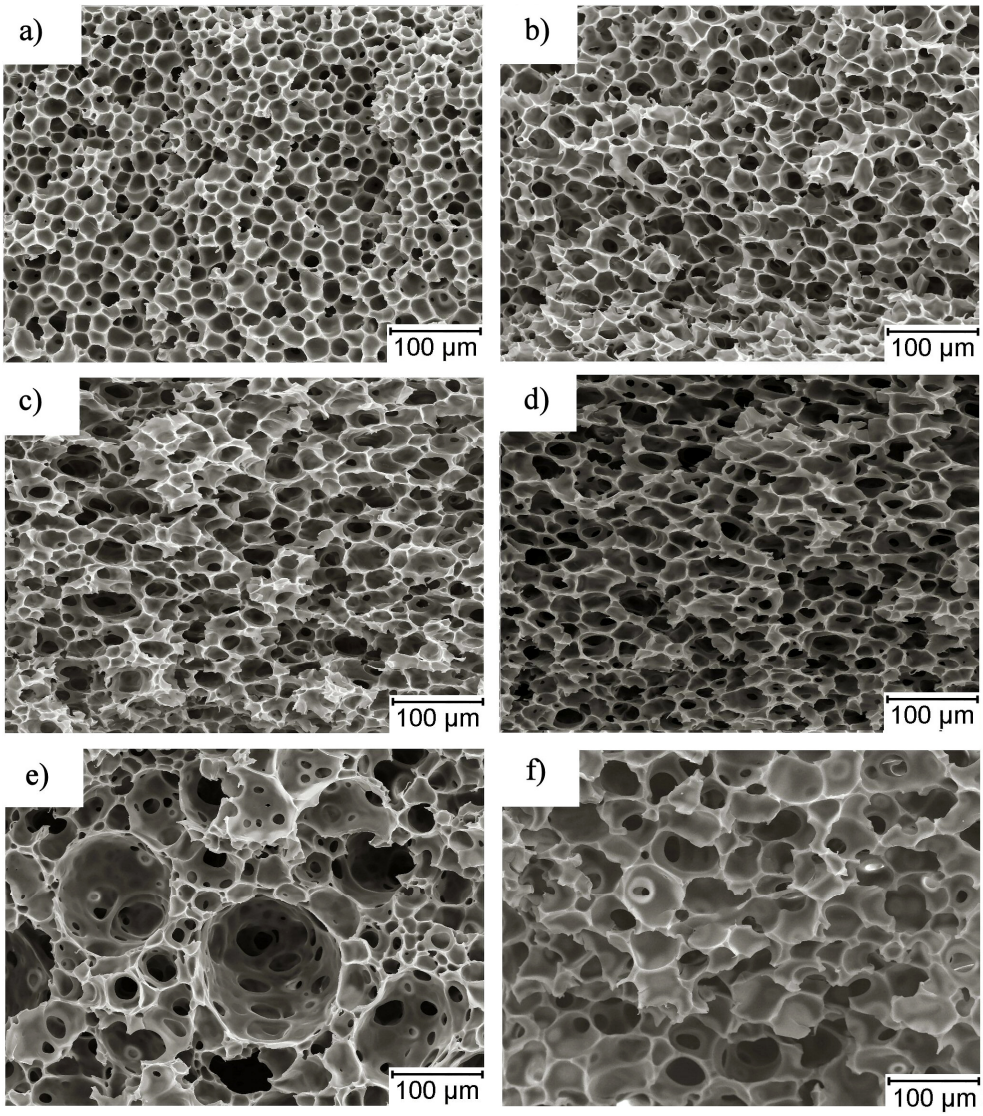

Figure 2.5 - Scanning electron micrographs of membranes cross sections obtained with fast depressurization. Solvents: a) chloroform; b) N,N-dimethylformamide; c) N, N-dimethylacetamide; d) N,N-dimethylpropionamide; e) dimethylsulfoxide; f) N-methylpyrrolidone.

The same conclusion can be attempted by the analyses of the pore size distributions presented in Figure 2.6 for the six solvents. These profiles were obtained using EasyFit software. A histogram

with the percentage of pores having a given diameter is drawn and a statistical function is fitted to obtain the distribution curves that are plotted in Figure 2.6.

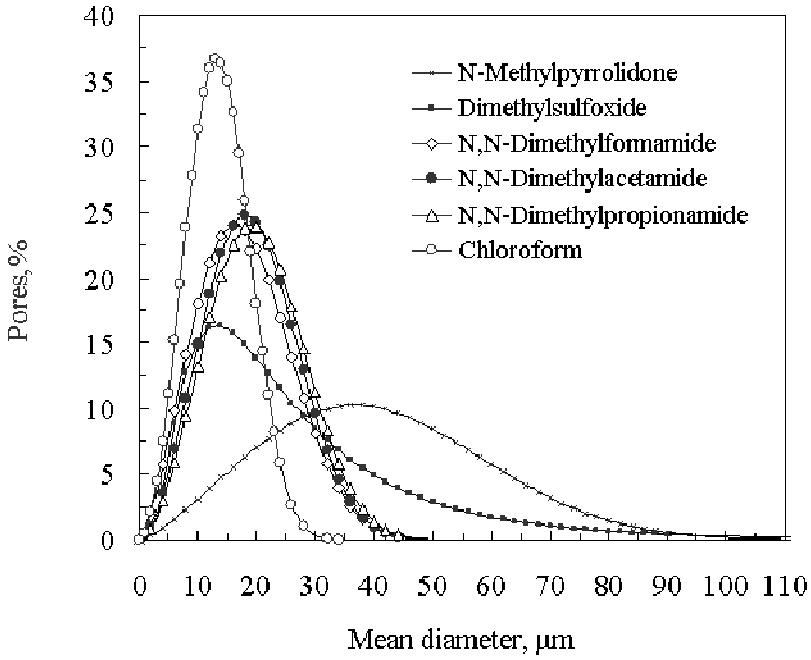

Figure 2.6 - Pore size distribution of PS membranes produced using different solvents with a depressurization in less than one minute.

Membranes produced with chloroform exhibit the smallest pore size diameter (around 13 µm), confined in a narrow range, and followed by the membranes produced with the amide solvents. Larger pores were obtained with dimethylsulfoxide and N-methylpyrrolidone (c.a. the 40 µm), with pore mean diameters restrained in a broad range. Similar trends were observed for the experiments performed with slower depressurization rate and by Reverchon and Cardea [2], for membranes produced with chloroform and N-methylpyrrolidone.

The application of similar solvents to produce de casting solution (N,N-dimethylformamide, N,N-dimethylacetamide and N,N-dimethylpropionamide) was the first attempt to correlate the pores of membrane and the molecular size of solvents. Despite the similar morphologies, the membranes obtained whit the amide solvents present a small variation in the pore size. With the

small increase of solvent molecular size (addition of one methyl group) it is observed an increase of (1.4 ± 1.0) μm in the pore size (Figure 2.7).

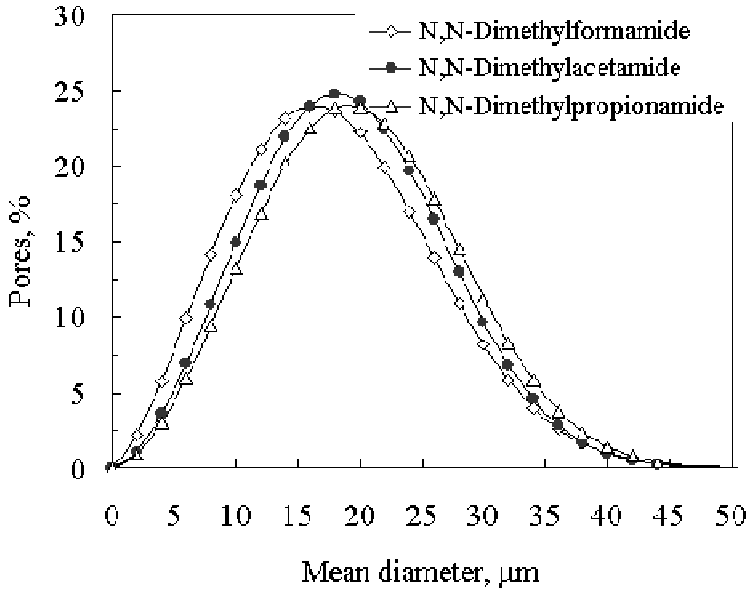

Figure 2.7 - Influence of the solvent molecular size in the pore size diameter.

The relative affinity of a polymer and solvent can be assessed invoking the solubility parameter concept which is a numerical value that indicates the relative solvency behaviour of a specific solvent. Table 2.1 reports the solubility parameter of pure components [11] together with their boiling points.

Table 2.1- Solubility parameters and boiling points of the pure solvents.

	$\delta(MPa)^{1/2}$	$T_{boiling}$ (C)
Carbon dioxide	13.5[a)]	-78
Chloroform	19.0	61
N,N-dimethylformamide	24.8	153
N, N-dimethylacetamide	22.7	166
N,N-dimethylpropionamide	22.5	175
Dimethylsulfoxide	26.7	189
N-methylpyrrolidone	22.9	202

a) Value at 318.15 K and 18.6 MPa.

According to Giddings *et al.*, the solubility parameter of the $scCO_2$ and $scCO_2$/solvent is calculated by equation 1 as [12, 13, 14]:

$$\delta = 1.25 P_c^{1/2} \left[\frac{\rho_r}{\rho_r(liq)} \right] \quad (1)$$

where δ is the solubility parameter of the supercritical fluid, P_c is the critical pressure of the supercritical fluid, ρ_r the reduced density of the supercritical fluid and $\rho_r(liq)$ is the typical reduced density of the supercritical fluid in the liquid state, assumed to be 2.66 [13].

Critical pressures of the binary mixtures were calculated based on experimental data available in literature for the mixtures CO_2 + Chloroform [15], CO_2 + N,N-dimethylformamide [16], CO_2 + N,N-dimethylacetamide [17] and CO_2 + dimethylsulfoxide [18]. Due to the inexistence of critical data for CO_2 + N,N-dimethylpropionamide and CO_2 + N-methylpyrrolidone, solubility parameters were not estimated to avoid large errors of these values.

Table 2.2 - Values of the critical temperatures (Tc), critical pressures (Pc) and acentric factors (ω) used in the PR-EOS.

Solvent	T_C (K)	P_C (MPa)	ω
Carbon dioxide	304.2	7.38	0.225
Chloroform	536.4	5.37	0.218
N,N-dimethylformamide	649.6	5.50	0.367
N, N-dimethylacetamide	617.2	3.60	0.299
Dimethylsulfoxide	726.0	5.71	0.294
N-methylpyrrolidone	723.6	4.78	0.358

Reduced densities were calculated based on Peng-Robinson equation of state with quadratic mixing rules for each mixture using the interaction parameters reported in literature (Table 2.2 and Table 2.3). PE program was applied in these calculations [19].

Table 2.3 - Binary interaction parameters used in PR-EOS.

Solvent	k_{ij}	l_{ij}
CO_2 + chloroform	0.0561	0.0000
CO_2 + N,N-dimethylformamide	0.0170	-0.0430
CO_2 + N, N-dimethylacetamide [a)]	0.0500	-0.0300
CO_2 + dimethylsulfoxide	0.0496	-0.0484
CO_2 + N-methylpyrrolidone	0.0198	-0.0352

[a)] Ajusted for PR-EOS [17]

Comparing the solubility parameters (δ) of the pure solvents, listed in Table 2.1 it is found that the δ values of solvents have the following order: chloroform < N,N-dimethylpropionamide < N,N-dimethylacetamide < N-methylpyrrolidone < N,N-dimethyl-formamide < dimethylsulfoxide. In Table 2.4, the δ values for mixtures solvent-scCO_2 have a similar order, except dimethylsulfoxide which presents a smaller solubility parameter than the amide solvents.

Table 2.4 - Solubility parameters for mixtures solvent–CO_2 (5% w/w), estimated for 318.15 K and 18.6 MPa.

	δ(MPa)1/2
CO_2 + chloroform	16.5
CO_2 + N,N-dimethylformamide	23.0
CO_2 + N, N-dimethylacetamide	21.4
CO_2 + dimethylsulfoxide	18.7

The difference between the solubility parameter of the solvent and non-solvents is related with the mutual affinity of both compounds. The increase of solubility parameter difference means the decrease of the mutual affinity [4]. When the mutual affinity is low, the outflow of solvent into the supercritical CO_2 phase decreases. This means that there is enough time for polymer-lean phase formed by the phase separation to grow, which leads to the formation of larger cells.

Another approach to relate the affinity between solvent and non-solvent is the solubility of the solvent into the non-solvent. Figure 2.8 shows the vapour-liquid equilibrium of three solvents: chloroform [15], N,N-dimethylformamide [20] and N-methylpyrrolidone [21] in scCO_2 obtained using Peng-Robinson equation of state (PR-EOS) with quadratic mixing rules. The interaction parameters and critical properties, used in the calculations are listed in the Table 2.2 and Table 2.3. Chloroform presents the highest solubility in scCO_2 followed by N,N-dimethylformamide and N-methylpyrrolidone. Higher solubility means higher affinity with scCO_2.

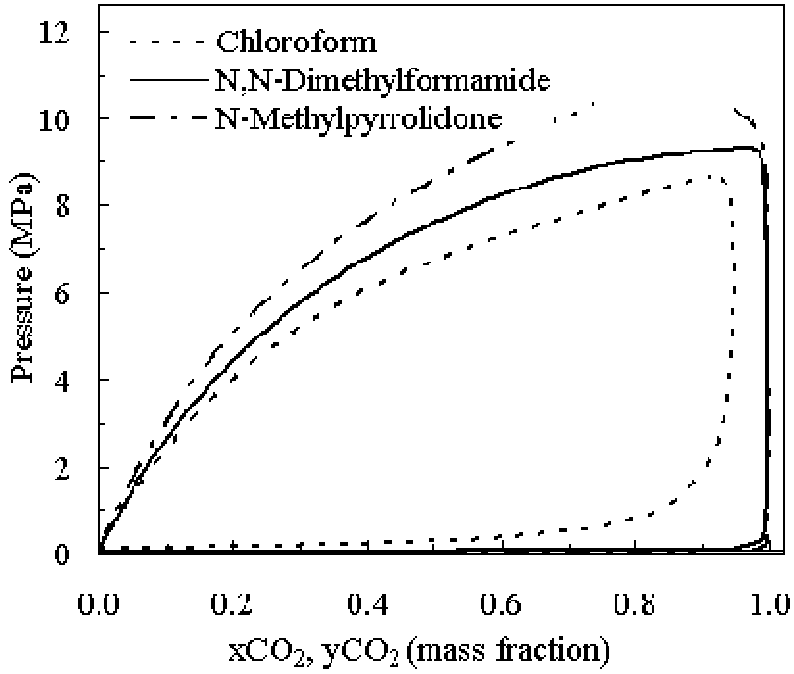

Figure 2.8 - Vapour liquid equilibrium of the mixtures carbon dioxide + chloroform, carbon dioxide + N,N-dimethylformamide and carbon dioxide + N-methylpyrrolidone at 318.15 K.

Relating these results with the cell size diameter, in Figure 2.6, it is possible to conclude that an increase in solvent affinity will decrease the cell size diameter.

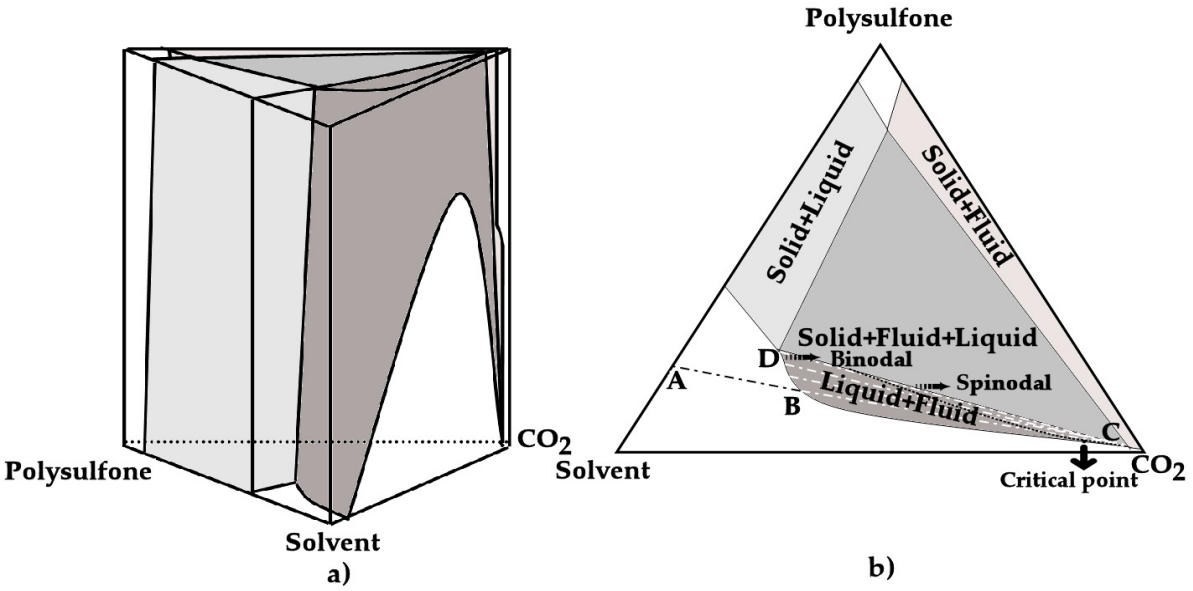

Figure 2.9 - a) Schematic representation of an isothermal phase diagram for the ternary system PS–solvent–CO_2. Diagram is not to scale. b) Cross section of the ternary diagram at pressures above the critical point of the binary mixture carbon dioxide + solvent.

To better explain these assumptions it is necessary to understand the mechanisms related to this process and take into account both thermodynamic and kinetic aspects. A possible schematic representation of the phase behaviour for such a ternary system is shown as an isothermal cut in Figure 2.9.a. The three sides of the prism are the *P-x* diagram for each binary pair. The Solvent-CO_2 pair takes the type of behaviour described in Figure 2.8. The following assumptions were made: both solvent and CO_2 are able to swell the polymer, the polymer presents a reduced solubility in scCO_2, much lower when compared to that in the liquid solvent, meaning that it is possible to extract the solvent without removing the polymer.

For easier visualization of our process an isobaric cut is presented in Figure 2.9. b with a possible operation line (white trace). Such isobaric cut presents five different regions: a Solid + Fluid, a Solid + Liquid, a Liquid + Fluid, a Solid + Fluid + Liquid and a homogeneous region. The Solid + Liquid region extends from the Solvent – Polysulfone edge and by addition of CO_2 it comes

into a three phase region. In this region, a solid phase that is essentially polysulfone with some solubilised solvent and CO_2, is in equilibrium with a liquid phase, that is a solvent rich liquid phase with polymer and CO_2, and a vapour phase, which is a $scCO_2$ phase saturated with solvent and negligible polymer. From the diagram, it is evident that as we add CO_2 to the binary system solvent + polysulfone, the solubility of polymer in the liquid decreases signifying the role of CO_2 as non-solvent. On the other side of the ternary diagram, the region marked as Solid + Fluid means that polysulfone, with some CO_2 incorporated, is in equilibrium with the gas phase (CO_2 with some solvent and negligible polymer). At the pressure of the isobaric cut the mixture CO_2 + solvent has become supercritical and so the Liquid + Fluid region no longer touches the solvent – CO_2 edge. The intersection of the three two-phases regions results in the solvent + fluid + liquid three phase region as described above.

The events that lead to the precipitation can be represented by the different mass transfer pathways on the ternary phase diagram. When the composition path directly enters into the solidification region, the polymer solidifies (gel type). When the path intersects the liquid-liquid phase separation region, the casting solution separates into polymer-rich and polymer-poor phases and results in porous structure [22] which is our case.

The membrane formation mechanism in this system is as follows. The polymer solution is placed inside the high pressure cell and at this moment some amounts of organic solvent will evaporate according to the vapour pressure (A). After the introduction of net CO_2 inside the cell the solvent will spread out into the supercritical phase (B). CO_2 is continuously fed and once achieved the desired pressure the back pressure regulator will open the outlet valve and allow the system to operate in a continuous mode extracting the organic solvent (C) from the membrane solution.

When it reaches point D it will enter in the three phases region promoting the formation of the solid.

The variations obtained with different casting solutions should be related with the difference in the ternary diagram of each system: polymer – solvent – CO_2.

If the solvent is highly soluble in $scCO_2$, the liquid-fluid area in Fig. 6b should be relatively smaller. This fact will restrain the metastable region limited by the spinodal and binodal curves. Smaller metastable regions should induce faster nucleation and growth of the droplets of the polymer lean phase with further solidification of the polymer rich phase which forms the membrane cellular structure.

2.1.2.2 Depressurization rate

SEM pictures of membranes produced using chloroform as the casting solution with different depressurization rates are shown in Figure 2.10.

Figure 2.11 presents the cell size distributions for membranes produced using two different casting solutions: chloroform and N,N-dimethylacetamide. As it is evident the depressurization rate influences the pore size: higher rates produce larger pores. Similar trends were obtained with other solvents used. This is divergent from the results obtained by Xu *et al.* [8] in the preparation of polylactide membranes. They observed an increase of the average pore size and a decrease in pore density with prolonged depressurization times, explaining these results with the ability of CO_2 to act as foaming agent. The main difference between their procedure and ours is in the fact that they do not operate the system in a continuous mode. The polymer solution is immersed in a vessel with CO_2 for a period of one hour and afterwards the cell is vented promoting the formation of the solid with the depressurization. In our procedure, when the depressurization is done, the polymer precipitation already occurred due to the continuous extraction of the solvent.

A homogeneous CO_2 concentration profile was established during the film formation which is confirmed by the homogeneity of the porosity of the membrane structures.

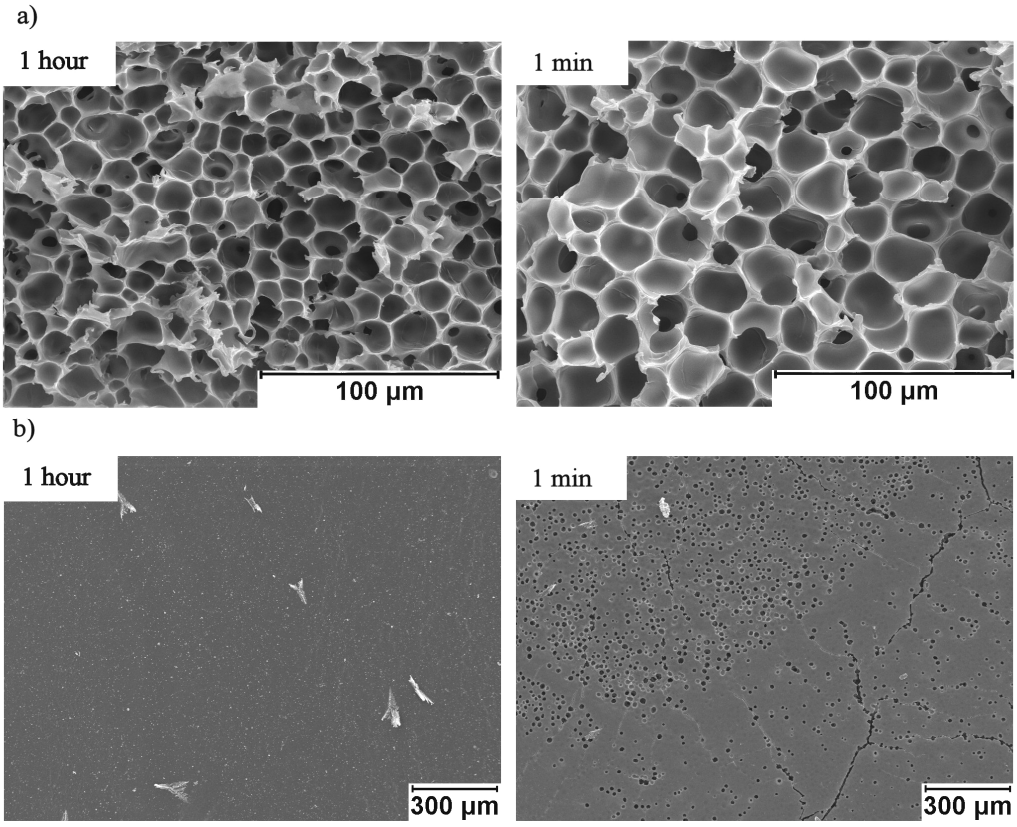

Figure 2.10 - Scanning electron micrographs of PS membranes produced using chloroform as the casting solution. Depressurization rate effect: a) cross section b) surface top view.

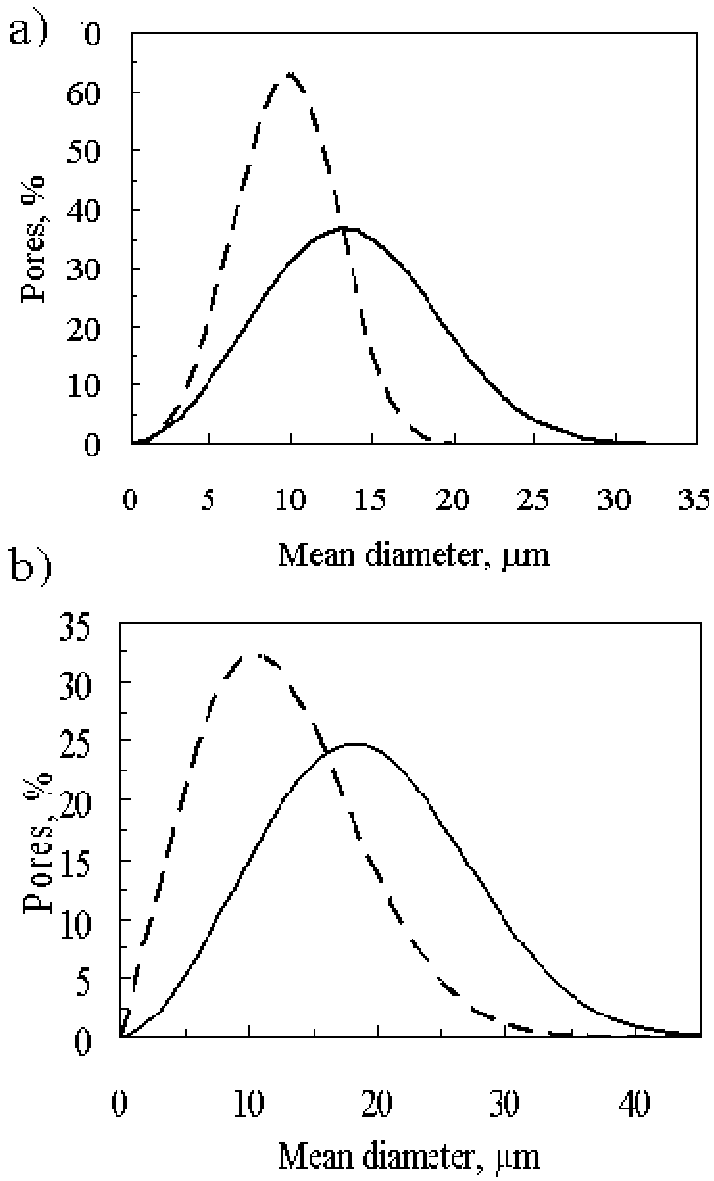

Figure 2.11 - Depressurization effect in the pore size distribution of PS membranes using two different solvents: a) chloroform b) N,N-dimethylacetamide. Doted line - slow depressurization; continuous line - fast depressurization

Tang *et al.* [23] studied the sorption and diffusion of $scCO_2$ into PS, as well as its plasticization effect. They observed that at similar temperature and pressure conditions CO_2 diffuses well into the PS with sorption amounts rounding 10% (w/w). CO_2 is able to plasticize the polymer but as

the temperature is bellow its glass transition temperature, T_g, the polymer/CO_2 mixture is in a glassy state and thus the mechanical properties avoid expansion (foaming) of the polymer, as it was possible to confirm by visual inspection of the cell during depressurization. Figure 2.10 b) shows the outer skin of a membrane subjected to a slow decompression (1 hour) and rapid decompression (1 min). In a slow depressurization the CO_2 diffuses slowly out of the polymer phase not affecting the polymer structure. A fast depressurization of the large CO_2 amount, dissolved in the polymer, should shrink the pores and consequently increase in the mean diameter. The blowing of some pores, in order to rapidly release the CO_2, explains the holes in the membrane skin. The analysis of SEM images of the membranes surface confirms the above suggested explanation: fast depressurizations tend to increase surface porosity and promote the appearance of fissures in the membrane top layer.

Table 2.5 - Water fluxes of PS membranes produced using different solvents with low and fast depressurization rate.

Solvent	Depressurization	Water flux (x 10^{-3} L/(m^2.h.bar))
Chloroform	low	none
	fast	0.004
N,N-dimethylformamide	low	0.010
	fast	0.16
N, N-dimethylacetamide	low	0.66
	fast	0.72
N,N-dimethylpropionamide	low	1.07
	fast	1. 89
Dimethylsulfoxide	low	8.18
	fast	8.34
N-methylpyrrolidone	low	11.1
	fast	45.1

The information on clean water flux for the all set of porous membranes prepared in this work are summarized in Table 2.5. The pure water flux which is defined as the volumetric flow rate divided by the membrane area and the pressure difference was determined for all the membranes varying the applied hydrostatic pressure from 0 to 2.4 bar. It can be concluded that both depressurization rate and the mutual affinity between solvent and CO_2 influence the water permeability. Water flux through the membranes augments by increasing the rate of the depressurization. This trend was expected since as it was discussed previously higher rates

produce larger pores which may enhance membrane permeability. Moreover fast depressurizations tend to increase the surface porosity and promote the appearance of surface fissures.

The influence of the solvent affinity in the performance of membranes in terms of water flux can be discussed by analyzing the results described in Table 2.5 and the pore size distribution curves shown in Figure 2.6. The lowest water flux was obtained for PS membrane prepared using chloroform in the casting solution, this membrane also presents the smallest mean pore size and the narrower pore size distribution curve. As expected, the higher water fluxes were obtained with PS membranes prepared in N-methylpyrrolidone and dimethylsulfoxide which are the membranes with higher mean pore sizes and broader pore size distribution curves. Moreover, a large variation of pore sizes can favor the interconnectivity between the pores and subsequent increase in the water permeability of the membranes. This can be confirmed by comparison of the SEM images for chloroform and methylpyrrolidone (Figure 2.5 a and f, respectively) which present the smallest and highest water permeabilities and, respectively, also the smaller and the larger pores. As it can be observed the majority of the pores are closed and do not show any interconnectivity holes which explains the low water flux obtained. In contrast the SEM of the membrane obtained with methylpyrrolidone shows larger pores where is possible to observe large interconnectivities between the pores of the membrane thus explaining the high water flux obtained.

Water permeabilities of membranes produced using dimethylformamide, dimethylacetamide and dimethylpropionamide show intermediate values and increase with the molecular size of the solvents. This can be explained with the increase of the mean pore size of the membranes (pore

diameters: dimethylformamide < dimethylacetamide < dimethylpropionamide) that correlates well with the variation of the water flux obtained respectively for those membranes.

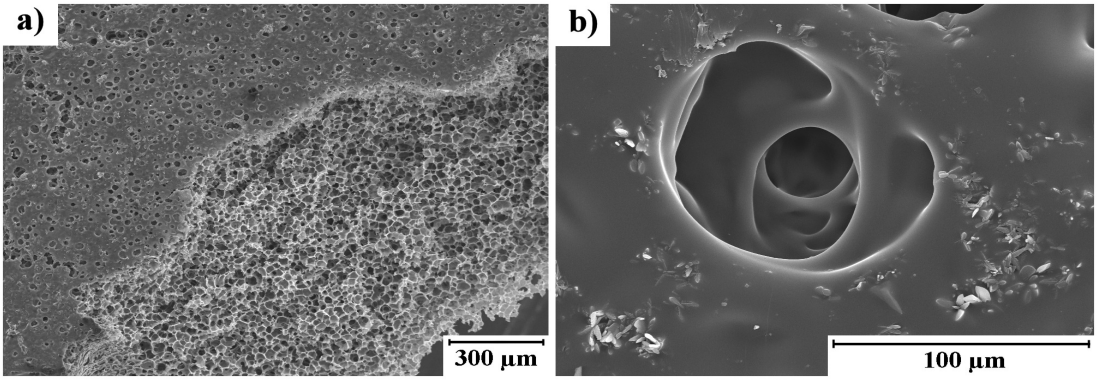

Figure 2.12 - Surface details of PS membranes. a) 45º cut (N,N-dimethylformamide and fast depressurization) b) SEM picture of a pore in the surface (N,N-dimethylacetamide and slow depressurization).

CO_2 – assisted phase inversion method is capable to produce homogenous membranes as shown in Figure 2.12 with highly regular structures and with good interconnectivity between different pores.

The broad range of water fluxes exhibited by the different PS membranes prepared with different casting solutions and the CO_2 – assisted phase inversion method proves the versatility of the process and its ability to produce membranes for a large number of applications.

2.1.3 Conclusions

Most of the works reported in the literature analyse the influence of pressure, temperature and polymer concentration and only few works analyse the influence of other important parameters in the formation of the structures of membranes, such as solvent affinity and rate of depressurization. It was shown that these could be additional parameters in CO_2 – assisted phase inversion method, to control membrane morphology.

In the next section a foaming agent- Polycaprolactone- will be incorporated in the casting solution. The high pressure CO_2 capability to swell and melt polycaprolactone (PCL) will be used to produce and control the porosity and the properties of the membranes.

2.2 Polysulfone-Polycaprolactone membranes

During this work we have also developed a new strategy to manipulate the properties of the membranes combining two techniques – foaming with a blowing agent and membrane preparation with polymer blends, which opens a new dimension in the control of membranes morphology and properties [24].

Polymer foaming using environmentally friendly physical blowing agents in their supercritical or nonsupercritical state has become significant interest in the past decades [25] especially for membrane preparation [26]. In this process the samples are saturated with supercritical CO_2 ($scCO_2$) reducing the glass transition temperature (T_g) and/or the melting temperature (T_m) of the mixture, liquefying the polymer. Upon depressurization the CO_2 rapidly expands, causing voids and precipitation of the polymer matrix.

Polycaprolactone (PCL) is a biocompatible and biodegradable aliphatic polyester that is bioresorbable and non-toxic for living organisms. Because of its unique combination of biocompatibility, permeability, and biodegradability, PCL, has been widely applied in medicine as artificial skin, artificial bone, and containers for sustained drug release.

The CO_2 capability to swell PCL, and decrease the T_m [27, 28] was used to produce and control the porosity and the properties of the membranes.

The membranes produced were analysed in terms of morphology, hydrophilicity, transport properties and mechanical performance. Membrane hydrophilicity is an important parameter because it can significantly contribute to enhance blood compatibility and reduce fouling [29, 30]. One of the primary factors enhancing the adsorption of a protein is hydrophobic interactions between membrane surfaces and protein molecules [31, 32]. Information about the mechanical performance of membranes is important in many applications, where the systems are required to support mechanical loads. Dynamic mechanical analysis (DMA) is a popular technique that

enables to decouple the elastic and viscous components of the viscoelastic properties of materials. In this work, DMA will be used to detect the influence of the PCL content in the viscoelastic features of the porous membranes.

2.2.1 Experimental

2.2.1.1 Materials

Polysulfone (molecular weight 67,000) and polycaprolactone (molecular weight 65,000) were obtained from Sigma-Aldrich in pellet form. Chloroform was also purchased from Sigma-Aldrich (purity ≥ 99.8 %) and used without any further purification. Carbon dioxide was obtained from Air Liquide with 99.998 % purity.

2.2.1.2 Membrane preparation

The experimental apparatus used in this section was the same as reported in the previous section 2.1.

2.2.1.3 Membrane characterization

Membranes were characterized using Scanning Electron Microscopy (SEM) and the pore size distribution was obtained by image analysis following the methodology described in section 2.1. Water flux permeability to pure water was also performed following the same procedure.

Membrane hydrophobicity was evaluated through the measurement of the contact angle of water droplets Goniometer Ramé – Hart Inc. NRL C.A., Model 100-00-230.

Differential scanning calorimetry (DSC) measurements were carried out at the REQUIMTE associated laboratory using a Setaram (Model DSC 131) equipment. The analyses were performed from -125ºC to 220ºC at 5ºC/min under a dry nitrogen atmosphere.

The dynamic mechanical analysis experiments were performed in a TRITEC2000B equipment, from Triton Technology Ltd. (Nottinghamshire, UK) using the tensile mode. The frequency was scanned in the range 0.05 to 100 Hz, at room temperature. The dynamic modulus, *E**, was measured for a constant strain amplitude of 50 μm in membranes samples with ca. 4 mm width and 15 mm length.

2.2.2 Results and discussion

In this study, the process parameters that were able to influence membrane formation - temperature (40ºC), pressure (20 MPa), casting solution concentration (15% w/w) and depressurization rate (30 minutes) - were fixed. All the experiments were performed using a CO_2 flow of 9.8 g/min for 2 hours. Different blends of PS and PCL were produced and their properties were analyzed in terms of water flux measurements, contact angles with water, scanning electron microscopy (SEM), pore size diameter and dynamic mechanical analysis (DMA).

Table 2.6 presents a summary of the blends compositions prepared as well as their permeabilities and contact angles

Table 2.6 - Effect of the different amounts of PCL in the water flux measurements and contact angles.

Entry	% (w/w) PCL	Permeability ($L/(m^2.h.bar)$)	Contact angle (º)
1	0.0	0*	57
2	10.3	0.05	72
3	24.4	9	73
4	40.4	20000	93
5	51.6	Too high to be measured	101

* With an applied pressure of 5 bar

Observing the results it is possible to notice a clear dependence from the contact angles and water flux measurements with the amount of PCL in the blend.

It must be noted that contact angle measurements are dependent on both the hydrophilicity of the surface as well as the roughness and porosity of the surface. The contact angles that were measured are relatively smaller than the ones that were expected for these kind of membranes. Wavhal and Fisher [32] performed several experiments in which they used carbon dioxide plasmas to modify hydrophobic polysulfone ultrafiltration membranes into hydrophilic. In their measurements they have detected a contact angle of 94º for the untreated membranes. In our case a contact angle of 57º was observed for the membranes prepared with pure PS and a slightly increase was obtained with increasing amounts of PCL. This is probably related with the higher porosity and roughness of the surfaces as it can be confirmed in Figure 2d and 2e. According to these results the CO_2-assisted phase inversion method is able to produce membranes with more homogeneous surfaces than the traditional methods, leading to membranes with improved hydrophobic properties.

The pure water flux which is defined as the volumetric flow rate divided by the membrane area and the pressure difference was determined for all the membranes varying the applied hydrostatic pressure from 0 to 0.5 MPa. The membranes that were exclusively produced from PS tend to have an insignificant water flux that was lower than our detection limit. By increasing the PCL content the water flux significantly increased. It turned to be impossible to measure the water flux for the membrane with the highest PCL content (entry 5 of Table 2.6).

The broad range of water flux obtained proves that the water permeability of the produced membranes has a straight correlation and can be tuned by changing the PCL content of the blend.

These results can be explained with the analysis of Figure 2.13 and Figure 2.14. Observing the SEM images presented in Figure 2.13 it is possible to note a strong dependence of membranes morphology and pore size diameter with the amount of PCL in the blend. Increasing the amount of PCL in the blend produces membranes with larger pores.

The roughness of the membranes is also influenced by the amount of PCL due to the damage of the surface during the process of foaming.

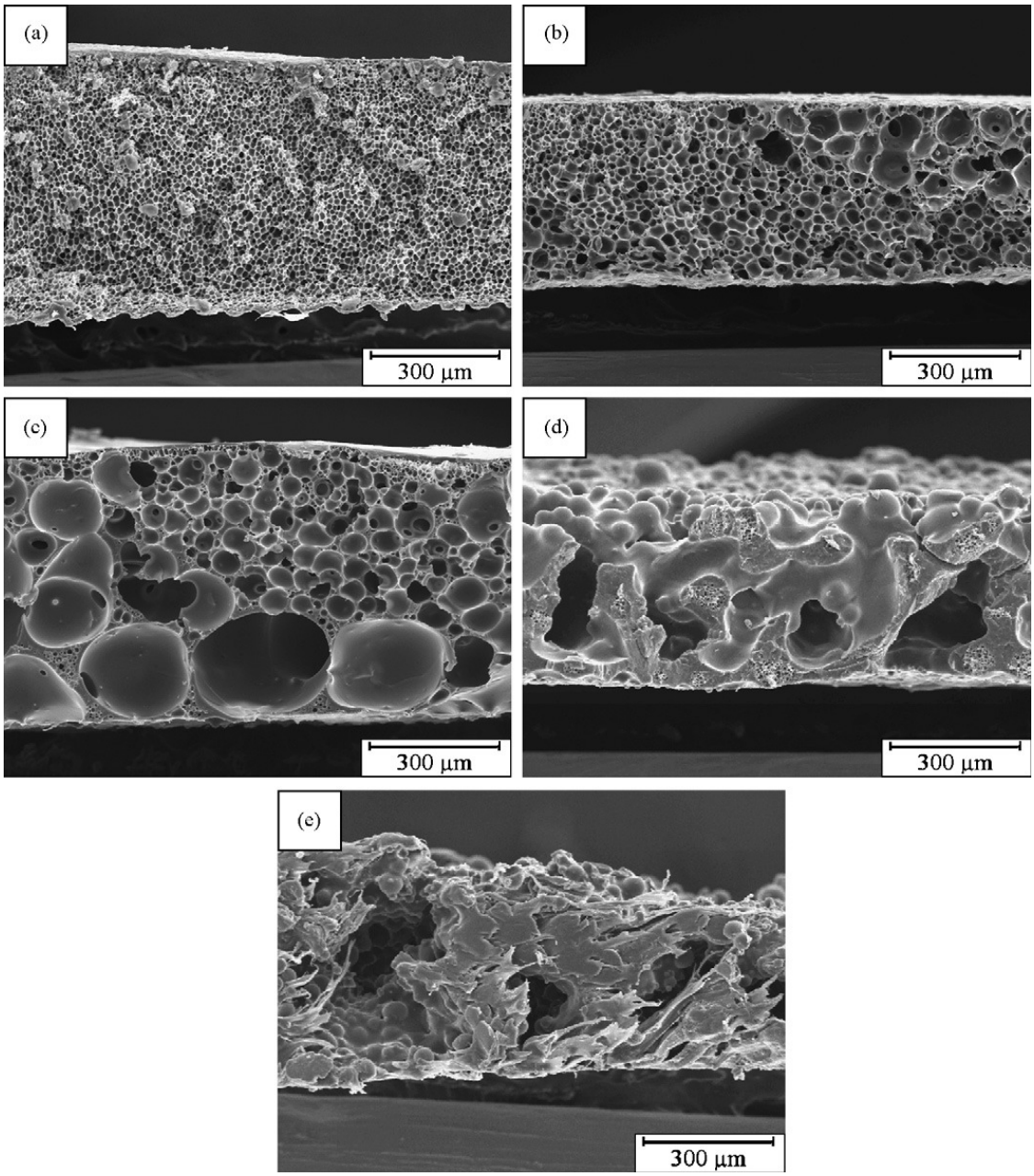

Figure 2.13 - Scanning electron micrographs of the cross section of the membranes with different PCL weight percentage: (a) 0 wt.%; (b) 10.3 wt.%; (c) 24.4 wt.%; (d) 40.4 wt.%; (e) 51.6 wt.%.

The same conclusion can be attempted by the analysis of the cumulative distribution functions presented in Figure 2.14. These profiles were obtained using EasyFit software and applying a Weibull distribution.

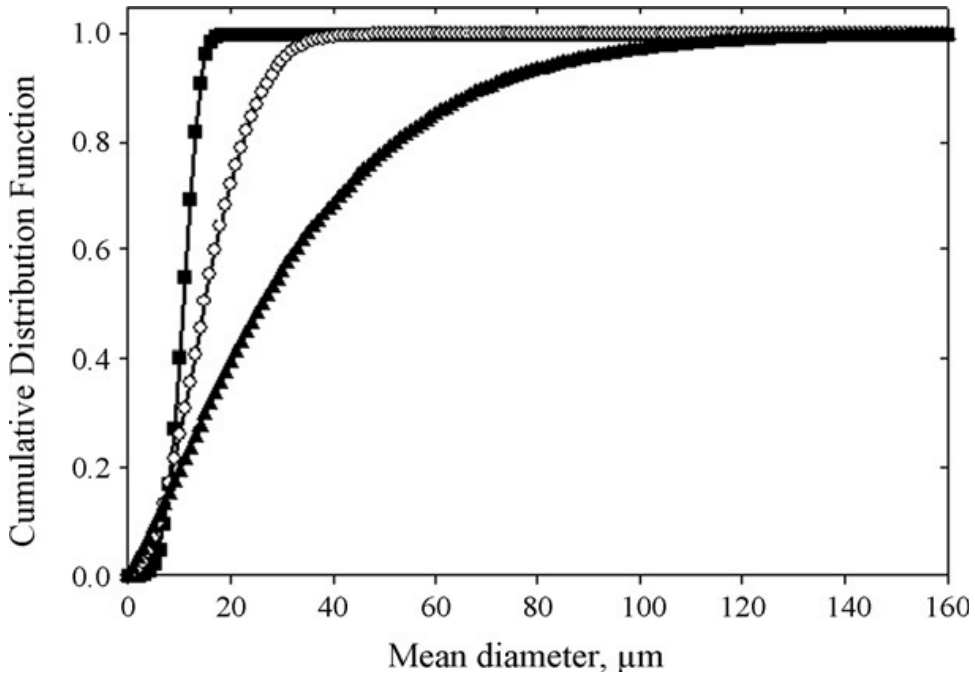

Figure 2.14 - Pore size cumulative distribution curves. (■) – 0 wt.%; (○) – 10.3 wt.%; (▲)– 24.4 wt.%.

In the previous section 2.1 we have proposed a mechanism for the membrane formation with the CO_2-assisted phase inversion method that can explain the morphology of membranes when only pure PS was used. In the case of the membranes that were produced with polymer blends we have the combination of the same mechanism, which relates the pore size diameter with the nucleation time, with a different effect induced by the fact that CO_2 can act as a blowing agent for PCL. As CO_2 is highly soluble in PCL [33] it reduces the intermolecular interactions and increases chain separation, inducing the melting [28]. In the meantime the nucleation and growth of the PS droplets start with the extraction of the solvent promoting the appearing of the polymer lean

phase (internal part of the pores) and polymer rich phase (membrane cellular structure). At the end of the process when depressurization occurs, CO_2 acts as a blowing agent for the PCL in the mixture increasing the pores that were previously formed.

The steps involved in the membrane formation and foaming process: 1) dissolution of gas in the polymer and formation of a polymer/gas solution, in this case, dissolution of CO_2 in the PS+PCL+chloroform solution); 2) in the continuous extraction process the solvent is removed and the PS solid phase starts to form but mixed in the molten PCL; 3) after the complete extraction of chloroform we have a polymer blend; during depressurization a second cell nucleation is induced by thermodynamic instability as a result of decrease in pressure; 4) cell nuclei are formed by phase separation between CO_2 and polymer phase; 5) cell growth by a combination of mass and heat transfer; and 6) cell stabilization when the cell growth process is stopped by the end of gas release.

As PCL is a crystalline polymer it is much more difficult to control the cellular structure during foaming compared to amorphous polymers like PS, because gases do not dissolve in the crystalline regions and the polymer-gas solution formed during the foaming process is non-uniform which explains the different morphologies obtained for neat PS and blend membranes.

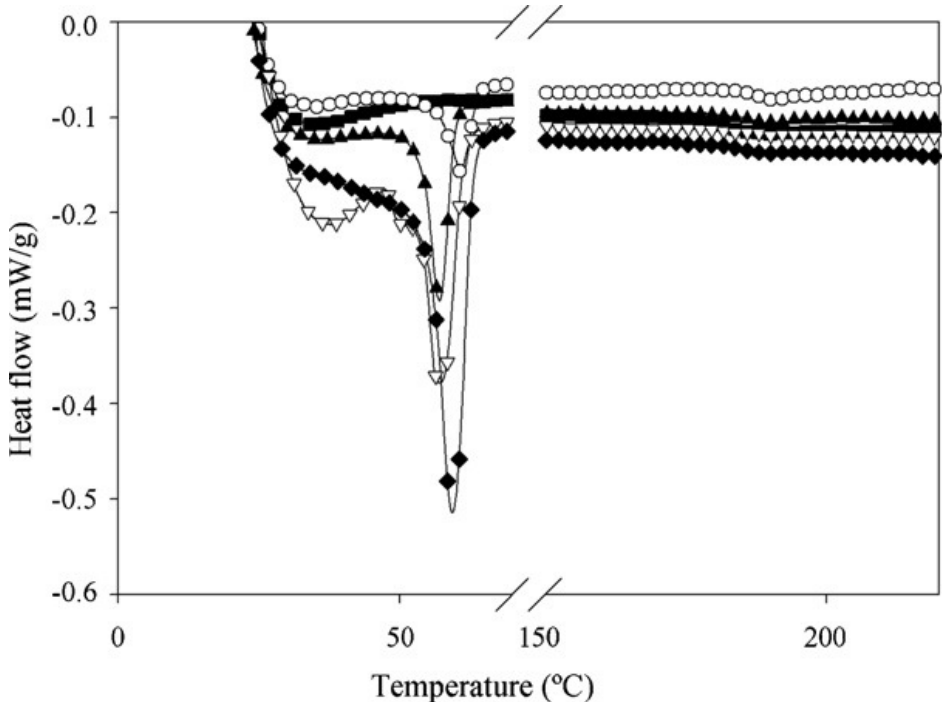

Figure 2.15 – DSC analysis of the blend membranes with different PCL weight percentage. (■) – 0 wt.%; (○) – 10.3 wt.%; ▲– 24.4 wt.%.; (▽) 40.4 wt.%; (◆) 51.6 wt.%.

In order to investigate miscibility and phase behaviour of polymer blends, differential scanning calorimetry (DSC) was used. Determination of the miscibility between two amorphous polymers is based on the observation of a single glass transition temperature (*Tg)*, between those of pure components, indicative of state of dispersion while the appearance of both *Tg's* suggests the occurrence of phase separation [34].

In this case we have a blend of an amorphous polymer with a crystalline polymer that does not present *Tg*.

Table 2.7 - Enthalpy of melting of PCL phase, glass transition temperatures and melting point of PS/PCL blends

% PCL (w/w)	Tg (ºC)	Melting Point (ºC)	Enthalpy (J/g)
0	183.14	-	-
10.3	188.97	61.19	5.24
24.4	186.29	57.19	9.9499
40.4	188.14	57.11	17.3718
51.6	184.20	59.46	32.5677

Polycaprolactone is a crystalline polymer which is characterized by an endothermic melting peak at about 58-60ºC. DSC results on non processed polycaprolactone show this pronounced peak as well as a minor *Tg* around -60ºC which maybe due to a small portion of amorphous PCL. PS is a completely amorphous polymer which could be confirmed by the absence of melting point and *Tg* around 183ºC. The DSC data of the blends show both the melting point peak of the PCL and the *Tg* of the PS. *Tg* values of the blends scatter around 187ºC showing no compositional dependence, suggesting that the phase interactions between polymers are merely physical and not chemical. The compositional independence of the T_m of PCL and the T_g of PS indicate a substantial immiscibility of the two polymers [35].

Despite the lack of chemical interaction between the polymers in the blend, and for that reason the name immiscible blend is often used, the resulting material can have interesting morphological and mechanical properties and hence different applications according to the blend composition. Particularly, in this case we demonstrate that by increasing the PCL content in the blend and taking advantage of the particular behaviour of PCL under $scCO_2$ it is possible to

change drastically the morphology of the prepared membranes increasing their permeability in spite of their lower surface hydrophilicity. In future work compatibilizers, such as block or graft copolymers, could be used to increase the polymer miscibility.

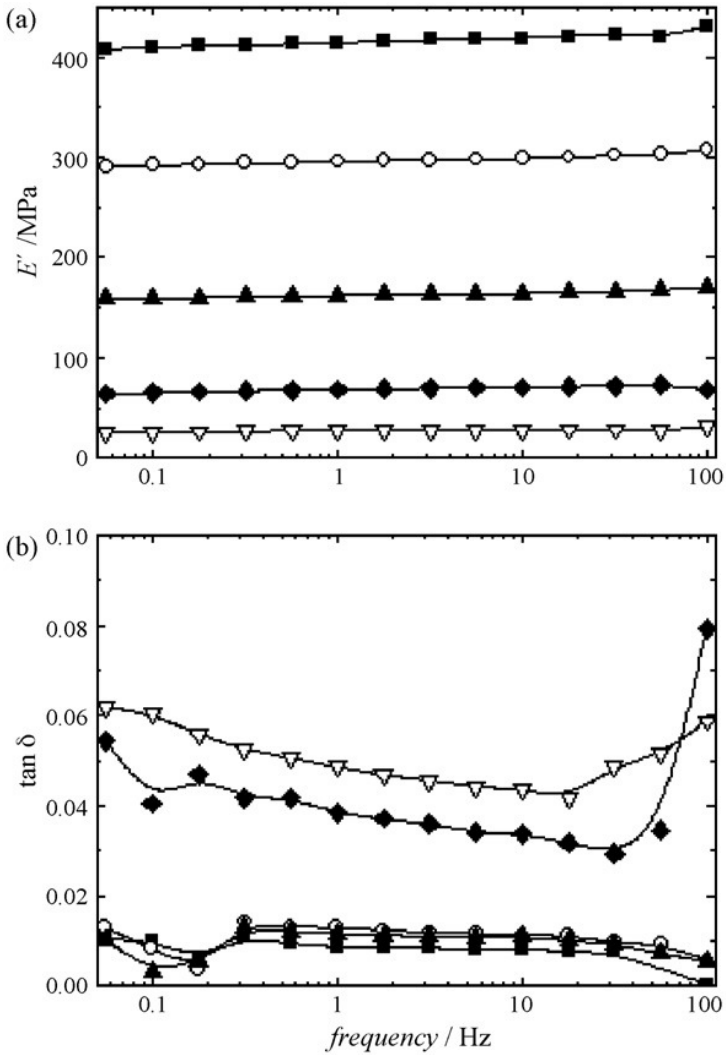

Figure 2.16 - DMA spectra of the prepared porous matrixes with different PCL compositions (see legend). Tensile frequency scan experiments at room temperature where the storage modulus (a) and the loss factor (b) were recorded: (■) – 0 wt.%; (○) – 10.3 wt.%; ▲– 24.4 wt.%.; (∇) 40.4 wt.%; (◆) 51.6 wt.%.

Finally, DMA was used to characterize the viscoelastic properties of the membranes developed in this work. This technique allows us to obtain, for example, the dependence of the complex

moduli as a function of temperature or frequency, $E^*=E'+\mathbf{i}E''$, where $\mathbf{i}=\sqrt{(-1)}$. The storage modulus, E', is the elastic, or the real component of E^*, which is in phase with the stress, σ, and is related to the stiffness of the material. The loss modulus, E'', is the viscous (also called imaginary) component of E^* which is $\pi/2$ out of phase in relation to σ. E'' is associated with the dissipation of energy, as heat, due to internal friction at the molecular level. The ratio $E''/E' = \tan\delta$, the loss factor, is a measure of the damping capability of a material. Figure 2.16 presents the frequency dependency, at room temperature, of the storage modulus and the loss factor. In the frequency range studied, corresponding to more than 3 decades, E' did not show any significant dependency on frequency, for all formulations analyzed. Such steady behaviour is related to the fact that no relaxation process occurs at room temperature around the time scale of the experiments. The results in Figure 2.16a) suggest that E' tends to decrease as the quantity of PCL increases. This trend is basically a consequence of the increase of porosity of the membranes when more PCL is incorporated; moreover PCL is less stiff than polysulfone. The values of $\tan\delta$ of the membranes with low PCL content are quite small (~0.01) indicating that the materials exhibit essentially an elastic behaviour (see Figure 2.16b). However, for the highest PCL contents the damping properties of the membranes increase significantly. This should be related to the fact that PCL have a much higher viscous nature than polysulfone. The loss factors obtained for the membranes with 40 and 50% PCL are, in fact, similar to the ones observed in pure PCL: for examples, $\tan\delta=0.05$, at 1 Hz and 37 ºC was reported before for injected moulded PCL [36].

2.2.3 Conclusions

This study has shown that CO_2-assisted phase inversion method combined with the capability of CO_2 to act as a blowing agent can be used to produce PS/PCL membranes. By adjusting the

PS/PCL ratio it was possible to vary the morphology, the hydrophilicity and the mechanical performance of the membranes. SEMs analysis showed that significant changes in the morphological characteristics were obtained upon the addition of PCL. Higher weight percentage of PCL in the blend resulted in phase separation and non-homogeneous membranes were produced. It is estimated that the mean pore radius of the PS/PCL membranes increased from 11 to 26 μm, when the concentration of PCL increased from 0 to 25 wt %. The PCL addition increased significantly the damping properties of the membranes and decreased the elastic behaviour.

Since one of the goals in this chapter is the development of porous structures for biomedical applications, the next work will focus the preparation of biocompatible membranes using a water soluble polymer with application in drug delivery and cell expansion.

2.3 Chitosan membranes

Biocompatible and biodegradable polymers have various important applications in the biomedical field particularly in the development of supports for tissue repair and regeneration [37]. These structures have a high level of porosity, with a good interconnectivity among the pore network system together with significant mechanical strength and flexibility. Membranes are the most widely studied scaffolds for guided bone regeneration. They are useful for repair in sites where limited mechanical loading exists, for example, in some cranial or maxillofacial areas, in dental applications [38] and as 3D matrices in perfusion bioreactors [39]. Another important area of application of such materials is in drug delivery. $scCO_2$ technology potentially allows the production of sterile, ready to use devices, due to the high pressure features of this technique. In fact, reports in the literature suggest that $scCO_2$ can be potentially used for sterilization of biomedical devices, being effective against bacteria [40], viruses [41] and spores [42], although additives are required in order to achieve terminal sterilization, namely hydrogen peroxide [42] or peracetic acid [43]. A complete review concerning the potentialities of supercritical fluids in the processing of polymer systems for drug delivery, as well as tissue engineering/regenerative medicine can be found in the literature [44].

In this work, chitosan, a well-known biodegradable, biocompatible and non-toxic natural polymer with possible applications in the biomedical field [45] (*e.g.* dialysis membranes, contact lenses, antitumor uses, drug delivery controlled-release systems and tissue engineering) was processed using a CO_2-assisted phase inversion method. In particular, chitosan-based membranes have been used for medical applications, such as suture thread and artificial skin [46]. Recently, chitosan was used as starting material elected to fabricate biodegradable stents that can deliver drugs locally [47]. The administration of drugs by a device delivery system has advantages over

conventional drug therapies. Depending on the appropriate clinical application, a rational design of the system namely concerning the selection of the support material, its morphology and the technique to incorporate the therapeutic molecules is decisive. In this work, we attempted to produce a low cost chitosan porous implantable material that would allow the release of an antibiotic in an affected region. Gentamicin is a widely used antibiotic in the treatment of gram negative infections and its incorporation in a chitosan controlled release device could be useful in the prevention or treatment of wound infections thereby facilitating wound healing [48]. In the present study, gentamicin was used as a model molecule to be incorporated into chitosan membranes by mixing it with the polymeric casting solution.

Chitosan has also been proposed as a scaffold to sustain cell adhesion and proliferation for application in tissue engineering [49]. In this context, human mesenchymal stem cells (MSC) from the bone marrow (BM) are a potential source of osteoblasts and chondrocytes for bone and cartilage repair, respectively. Many efforts have been performed to design suitable biomaterials to support MSC adhesion/proliferation, by attempting to mimic the BM *in vivo* microenvironment and maintaining cell multipotency. However, most of the ongoing research is more focused on the controlled differentiation of MSC [50, 51, 52], rather than the *ex-vivo* expansion/maintenance of these multipotent stem cells. Due to the very low number of MSC present in the BM, a rapid *ex-vivo* expansion method is needed to meet the highly demanding dose of MSC for clinical application in terms of cellular therapy (*e.g.* 1-2 million MSC/kg in the settings of hematopoietic stem cell transplantation, enhancing the engraftment and/or preventing/treating graft-versus-host disease) [53, 54, 55]. Therefore, the successful expansion of MSC under strictly controlled conditions would clearly facilitate their potential clinical uses. Here, chitosan membranes produced by $scCO_2$ technology were evaluated in terms of cytotoxicity following International Standard guidelines, as well as their ability to support MSC

adhesion/proliferation *in vitro* under static conditions, envisaging the future use of these devices as scaffolds to sustain stem cell function and proliferation *in vitro* in a highly controlled culture system for application in clinical settings [56, 57].

2.3.1 Experimental

2.3.1.1 Materials

Chitosan (75-85% deacetylated, M_w = (190 – 310) kg mol^{-1}), absolute ethanol, glacial acetic acid (purity ≥ 99%), gentamicin sulphate (UPS testing specifications), o-phthalaldehyde (purity≥97%), sodium 1-heptanesulfonate, thioglycolic acid (purity≥98%), phenol (purity≥95%), crystal violet, phosphate buffered saline (PBS), accutase^{TM}, methanol and acetonitriline (HPLC grade) were purchased from Sigma-Aldrich. Isopropanol alcohol (purity ≥ 99%) was purchased from Pronalab and sodium hydroxide (purity ≥ 99%) from Riedel-De-Haën. RPMI-1640 (a Roswell Park Memorial Institute medium), Dulbecco's modified essential medium low glucose (DMEM-LG), anti human CD105, trypan blue and fetal bovine serum (FBS) used in cell culture were purchased from Invitrogen. L929 cells were obtained from DSMZ, Germany and WST-1 Proliferation Kit from Roche. Carbon dioxide was obtained from Air Liquide with 99.998% purity. All materials and solvents were used as received without any further purification.

2.3.1.2 Membrane preparation

Membranes were prepared in the apparatus previously presented in Figure 2.2. In a typical procedure, the casting solution, normally 4% (w/w$_t$) of polymer in acidified water (1% acetic acid) is loaded into a stainless steel cap (with a diameter of 68 mm and 1.5 mm height) and placed inside the high pressure vessel. The cell is then immersed in a visual thermostated water bath, heated by means of a controller (Hart Scientific, Model 2200) that maintains the

temperature within ±0.01 °C and a non-solvent flow is added until the desired pressure is reached, with an exact flow, using two Gilson piston pumps model 305 and 306. The non-solvent is a binary mixture of ethanol and CO_2 with different compositions from 2.5% to 10% of ethanol. The ethanol addition mode to the non-solvent stream is a key parameter to control membrane morphology. Figure 2.17 presents two variants that were tested in this work: introduction of a co-solvent (ethanol) in the non-solvent with variable composition (gradient mode) and with a constant composition (isocratic mode).

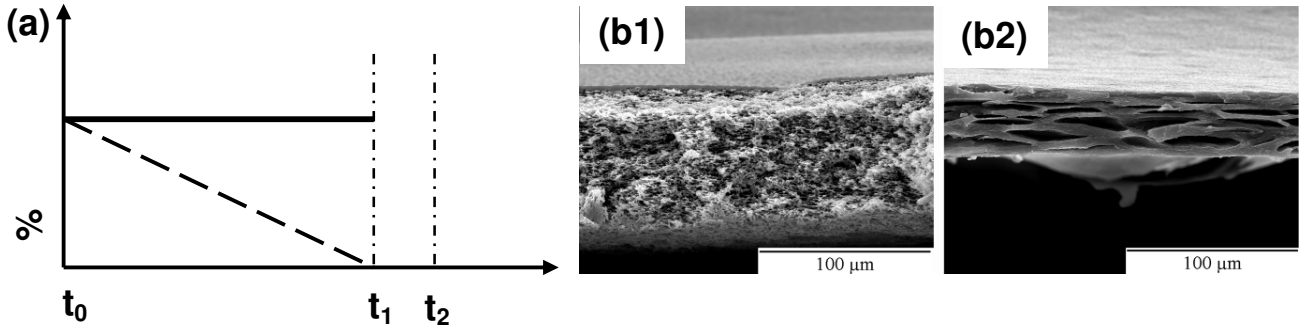

Figure 2.17 - (a) Different operational modes that can be used to introduce the co-solvent (ethanol) in the non-solvent (CO_2) stream. Hatched line-gradient mode; SEM pictures of chitosan membranes prepared (b1) isocratic mode and (b2) gradient mode.

After reaching the normal operational pressure (20 MPa), the supercritical solution passes through a back pressure regulator (Jasco 880-81) which separates the CO_2 from the acidified water used in the casting solution. The pressure inside the system is monitored with a pressure transducer (Setra Systems Inc., Model 204) with a precision of ± 100 Pa.

All the experiments were performed at 20 MPa and 60ºC with a non-solvent (CO_2+ Ethanol) flow of 4.9 g/min during 6 hours. After this time period, a pure CO_2 flow is passed through the high pressure cell to remove the ethanol. At the end, the system is slowly depressurized during 10 minutes and a thin homogeneous membrane is obtained.

2.3.1.3 Membrane characterization

Membranes were characterized using scanning electron microscopy (SEM) in a Hitachi S-2400, with an accelerating voltage set to 15 kV. Then membrane samples were frozen and fractured in liquid nitrogen for cross-section analysis. All samples were coated with gold before analysis. The tensile properties of the membranes were tested with a tensile testing machine (MINIMAT firm-ware v.3.1) at room temperature. The samples were cut into strips with 2x15 mm^2. The length between the clamps was set at 5 mm and the speed of testing set to 0.1 mm/min. A full scale load of 20 N and maximum extension of 90 mm were used. Measurements were performed with dried membranes, as well as membranes soaked in PBS solution for 1 hour before testing. Load extension graphs were obtained during testing and converted to stress strain curves applying the following equations:

$$\text{Stress} = \sigma = F/A \quad (1)$$

$$\text{Strain} = \varepsilon = \Delta l/L \quad (2)$$

where F - applied force; A - cross sectional area; Δl - change in length; L - length between clamps.

The permeability to pure water was determined by measuring the water flux through the membranes using a 10 ml filtration unit (Amicon Corp., model 8010) with an effective area of 4.1 cm^2. All the experiments were carried out varying the applied hydrostatic pressure from 0 to 0.5 MPa. At least three clean water flux measurements were performed for each membrane.

The porosity of the membrane was determined by mercury porosimetry (micromeritics, autopore IV).

2.3.1.4 Membrane degradation studies

The biodegradability of chitosan films *in vitro* was studied by degrading chitosan structures in lysozyme solution (Lys) [58] and PBS (pH=7.4). After specific time intervals, the films were taken out from the solutions, washed with distilled water and freeze-dried. The weight was measured before and after lyophilization.

2.3.1.5 Drug loading

Gentamicin was loaded into the chitosan membranes by co-dissolving it with the polymer in acidified water. Different amounts of drug, 40, 80 and 160 $mg_{gentamicin}/g_{chitosan}$ were used. The membranes were prepared using 2.5 % (w/w) ethanol isocratic mode in the non-solvent.

For the controlled release studies, a membrane portion, with approximately 3 cm^2, was immersed in 25 ml of PBS solution (pH = 7.4), at 37ºC and 1 ml aliquots were withdrawn at predetermined time intervals. The samples were analysed by HPLC (Knauer Smartline Pump 1000 combined with a Low Pressure Gradient, autosampler and UV/Vis SmartLine 2500). To determine the amount of gentamicin, a derivatization procedure was applied according to the USP reference standards. Briefly, the o-phthalaldehyde (OPA) reagent was prepared by adding 1g of OPA to 5 ml of methanol, and 95 ml of boric acid solution 0.4 mol/L, previously adjusted with 8 N sodium hydroxide to a pH of 10.4, and 2 ml of thioglycolic acid. The resulting solution was adjusted with 8 N sodium hydroxide to a pH of 10.4. Samples were prepared by adding 1 ml of gentamicin solution, 0.5 ml of isopropyl alcohol and 0.4 ml of OPA reagent, mixing and adding isopropyl alcohol to obtain 2.5 ml of solution. The mixture was heated at 60ºC for 15 minutes. The mobile phase was prepared adding 700 ml of methanol, 250 ml of water, 50 ml of glacial acetic acid, 5 g of sodium 1-heptanesulfonate. A C18 column (Knauer) was used in isocratic conditions with a flow rate of 1.4 ml/min and a volume of injection 20 µl. Quantification was performed at 330 nm. The total mass of released drug was calculated taking into account the aliquots taken.

2.3.1.6 Cytotoxicity assay

Chitosan membranes were tested for cytotoxicity following the ISO 10993-5 guidelines. Briefly, triplicates of 1 cm^2 membranes were placed in polystyrene tubes containing 3 ml of RPMI – 1640 with 10% (v/v) of FBS and kept in an incubator (37ºC, 5% CO_2, fully humidified) for 3 days. The liquid extracts were used to culture L929 mouse fibroblasts (initial density $80x10^3$ cells/cm^2) in 24-well plates for 2 days. The cell metabolic activity was determined by analyzing the conversion of WST-1 (light red) to its formazan derivative (dark red – absorbance at 450 nm after a 2.5 hour incubation at 37ºC) using a WST-1 Cell proliferation kit. The results were normalized to the negative control for cytotoxicity (fresh RPMI medium) and compared to the positive control (0.01 M Phenol).

In order to evaluate the effect of the direct interaction between chitosan membranes and L929 cells, membranes were conditioned with RPMI medium (2 cm^2/ml) overnight before cell seeding in 24 well-plates (6000 cells per well). At day 3 of culture, cells cultured on the membranes were stained with crystal violet and then observed under an inverted light-phase microscope (Olympus) in order to qualitatively evaluate the morphology, cell-to-cell contact and attachment. Briefly, cells were washed with PBS solution and then stained with crystal violet (0.5% (w/v) in methanol) for 30 minutes, washed three times with PBS solution and then observed.

2.3.1.7 Mesenchymal stem cell cultures

Heparinized human bone marrow (BM) was obtained from healthy donors after informed consent. BM mesenchymal stem cells (MSC) were isolated as previously described [59] and kept cryopreserved in liquid nitrogen until further use. Passage 3 MSC (negative for the hematopoietic markers CD14, CD34, CD45 and over 90% positive for CD73, CD90 and CD105, assessed by flow cytometry) were seeded on top of chitosan membranes (2.5% ethanol, isocratic mode Figure

2.18–a), previously conditioned overnight at 37ºC with DMEM-LG supplemented with 10% FBS (MSC qualified), at a cell density of 3000 cells/cm^2 using 24-well plates (in triplicate). Medium was replaced twice a week within the 2-week culture period. At days 7 and 15, cells were harvested with 0.5 ml accutase^{TM}, counted and characterized in terms of cell viability using the trypan blue exclusion dye test under the inverted light-phase microscope. A control condition without membranes was also performed by culturing cells on traditionally used tissue culture wells made of polystyrene.

In order to evaluate the phenotype of the cells cultured on the chitosan membranes, an anti-human CD105 monoclonal antibody was used, with an appropriate anti-IgG isotype control. At each time point, cells were stained with anti-CD105 and analyzed in a FACScalibur equipment (Becton Dickinson). In addition, cells were characterized in terms of clonogenic ability by performing colony forming-unit fibroblast (CFU-F) assays. At day 0 and 7, cells were plated at a density of 10 cells/cm^2 in T-25 flasks (250 cells per flask) and cultured for 2 weeks, without medium replenishment. They were then stained with crystal violet (0.5% w/v in methanol) for 30 minutes, washed three times with PBS solution and observed under the microscope. Only colonies with more than 50 cells were considered.

2.3.2 Results and Discussion

2.3.2.1 Beads/membranes production

In this study a new strategy was proposed to produce porous chitosan structures (membranes and particles) using supercritical carbon dioxide ($scCO_2$) processing. The production of porous structures using a CO_2-assisted phase inversion method has some requirements. The first one is the solubilization of the polymer in a solvent and secondly the solubility of this solvent in $scCO_2$ that will act has a non-solvent and will induce the precipitation of the polymer. The widespread

use of $scCO_2$ to process non-modified chitosan is limited due to the fact that this polymer is only soluble in acidified water which is a solvent with very little affinity/solubility in $scCO_2$. To overcome this limitation it was necessary to use an entrainer (ethanol) in the supercritical fluid to increase the mutual affinity between solvent and non-solvent. The group of solvents used in this work (carbon dioxide, water and ethanol) are three of a short (and ever-diminishing) group of solvents that may be used without restrictions and for this reason ideal for the generation of porous structures. Reverchon and co-workers have used a similar approach, ethanol expanded by $scCO_2$, to prepare poly (vinyl alcohol) membranes [60]. In this work the amount of ethanol was minimized in order to maximize the advantages of using supercritical fluid technology.

In a previous section focusing membrane production using $scCO_2$ processing we observed that the affinity between solvent and non-solvent was a key-parameter to modulate the morphology of the membrane in terms of pore size distribution and also interconnectivity. As the mutual affinity between solvent and $scCO_2$ decreases, the membrane porosity and the average pore size increases. The 'tunable' solvent power of the supercritical fluid, owing to its variable solvent density (dependent on pressure and temperature) and viscosity, is an important advantage when compared to traditional solvents. In this particular case, the mutual affinity between the solvent and non-solvent is very low since water and CO_2 are from two completely different natures. To overcome this drawback, a co-solvent or entrainer was added to the non-solvent following an isocratic or a gradient mode (Figure 2.14 a). The introduction of the co-solvent is crucial to control the morphology, as it is shown in Figure 2.14 (b1 and b2), where the comparison of the two SEM images clearly shows the differences observed when changing from gradient to isocratic mode. When the gradient mode was used (Figure 2.17 - b2) starting from 5% ethanol at t = 0 min and ending with 0% ethanol at t = 300 min, membranes with large pores were obtained;

however, when the co-solvent composition remained constant the pore size diameter decreased. Similar results were observed by changing the ethanol composition from 2.5% to 10% (Figure 2.18). When the ethanol ratio reaches a certain level, particle agglomerates were obtained (Figure 2.18b), highlighting the broad potential of this technology.

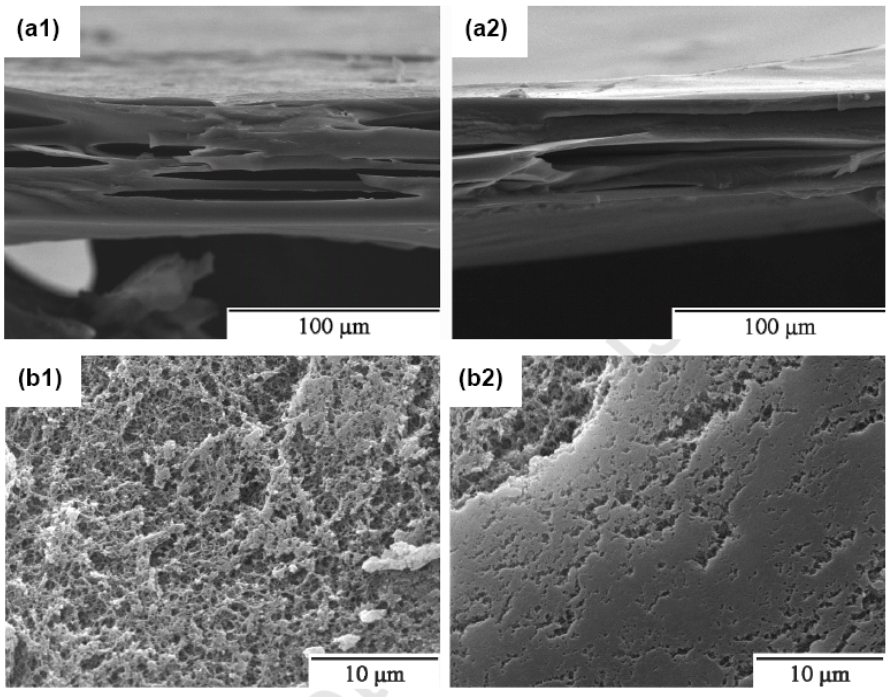

Figure 2.18 - SEM pictures of the membranes cross section prepared with different co-solvent compositions: a1) – 2.5% isocratic; a2) – 2.5% gradient; b1) – 10% isocratic; b2) – 10 % gradient.

Overall, the CO_2 induced phase inversion technique can create porous structures in a membrane shape, but also particle agglomerates or beads with interesting potential applications. Membranes produced by isocratic and gradient mode exhibited structures with low porosity, 40 to 30% respectively, while particle agglomerates present higher levels of porosity around 65-50%. The decrease in porosity from isocratic *versus* gradient mode can be attributed to the different morphologies that were obtained. The ethanol composition in the non-solvent stream and

operational mode used, isocratic or gradient, and the resulting morphology and water permeability of different chitosan structures are summarized in Table 2.8.

Table 2.8 - Influence of nonsolvent composition in devices morphology and water permeability.

% ($wt_{ethanol}$/ wt_{Total})	Mode	Morphology	Water flux ($L/(m^2.h.bar)$)
2.5	Isocratic	Porous membrane	1.02 ± 0.19
2.5	Linear gradient	Porous membrane	0.18 ± 0.01
5	Isocratic	Porous membrane	0.42 ± 0.03
5	Linear gradient	Porous membrane	0.39 ± 0.05
10	Isocratic	Particle agglomerates	N/A
10	Linear gradient	Particle agglomerates	N/A

Clearly, permeability through a porous material is an important parameter for its function, particularly considering the operation of a polymeric membrane under dynamic conditions. Fluid flow through the membranes decreased when the addition mode of ethanol changed from isocratic to gradient, in agreement with the relative membrane porosities. These structural differences are related with the thermodynamics and kinetics of the phase-inversion process. The richness of the solvent-non-solvent interactions and operational conditions that can be selected to control for the solubilization or precipitation of polymer structures is represented in a simplified hypothetical quasi-ternary phase diagram for the system Polymer – Solvent – Non-solvent (see Figure 2.19 and its caption). All possible composition combinations of the components can be plotted in a triangle. The corners represent each intervenient: i) the polymer – chitosan; ii) the solvent – acidified water and iii) the non-solvent – ($scCO_2$ + ethanol); the axes represent the three pseudo-binary systems and a point in the triangle is the overall mixture. In the liquid + fluid region a primary envelope (binodal curve) and a secondary envelope (spinodal curve) enclose

demixing boundary. Both curves coincide at the critical point and the region between them corresponds to a metastable state. The phase diagram is pressure and temperature dependent.

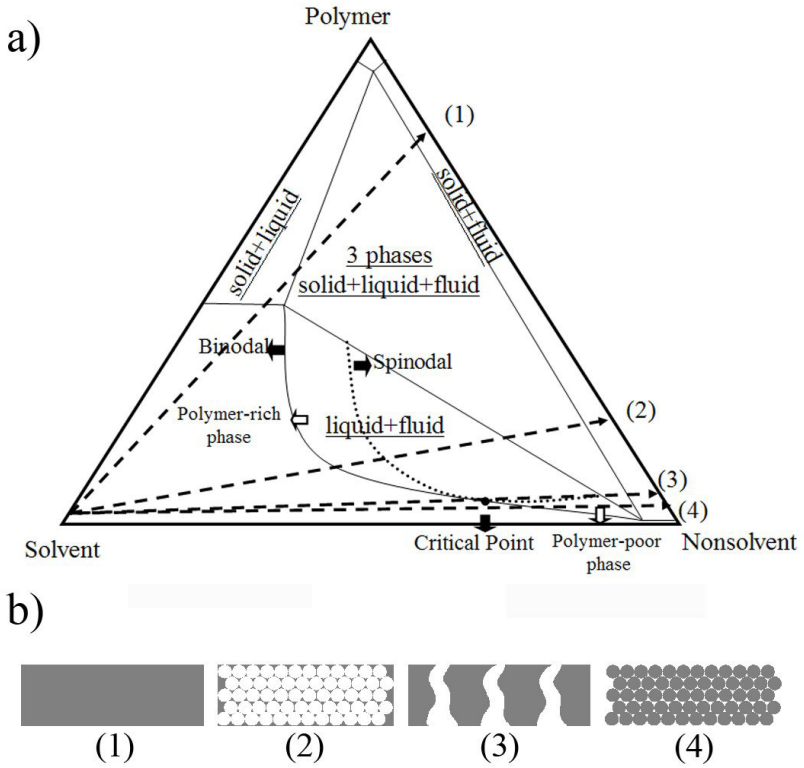

Figure 2.19 - Hypothetical ternary phase diagram for the system Polymer – Solvent – Non-solvent. a) Composition paths that can occur during membrane formation; b) Possible structure formation in the different paths of the gelation/vitrification region and liquid-liquid demixing gap: dense structure formation (1), nucleation and growth of droplets of the polymer lean phase with further solidification of the polymer-rich phase, leading to a cellular structure (2), bicontinuous morphology due to spinodal decomposition (3) microparticles due to nucleation and growth of droplets of the polymer-rich phase, followed by solidification of the polymer-rich phase (4).

As far as liquid – liquid demixing of polymer solutions is concerned, two different mechanisms have to be considered: nucleation/growth and spinodal decomposition [61]. The type of structures obtained and pore dimension depend on the path followed through the ternary diagram [62, 63]. Nucleation and growth (usually a slow process) is the expected mechanism when a system leaves

the thermodynamically stable condition and slowly enters the metastable region (region between the spinodal and the binodal) and can be represented in the ternary diagrams by the two distinguished paths (4 and 2) (please refer to Figure 2.19. Path (4) – when demixing is started somewhere below the gas-liquid critical point – nucleation and growth of concentrated phase (polymer-rich phase) occurs followed by solidification of the polymer-rich phase. Therefore, low-integrity powdery agglomerates (beads like structure) would be produced as it is exemplified in Figure 2.18b where chitosan powder agglomerates can be observed.

Considering Path (2) – ternary polymer solution becomes metastable; nucleation and growth of droplets of the polymer lean phase occurs with further solidification of the polymer-rich phase, leading to a cellular structure. The former pathway originates porous structures while the latter one results in a porous solid matrix as it is exemplified in Figure 2.18a.

The second mechanism, much less considered in literature, is spinodal decomposition that takes place in a fast quench into the two phase region limited by the spinodal curve or even in a slower transition crossing the metastable region near the critical point. In this case, phase separation initiates with concentration fluctuations of increasing amplitude, giving rise to two continuous phases (Path 3). An example of this type of membranes was presented by Reverchon and co-workers [64] who prepared cellulose acetate membranes using a supercritical fluid assisted process. Finally, it is also possible to obtain a membrane when polymer molecules solidify by gelation or crystallization giving rise to the formation of dense structures (Path 1).

Chitosan devices were characterized in terms of mechanical properties and biodegradability. Tensile tests provide an indication of the strength and elasticity of the membranes which are important considering their potential applications; for instance, it is suggested that films suitable

for wound dressing should be preferably strong, though flexible [65]. Figure 2.20 presents the stress-strain curves under dry and wet conditions.

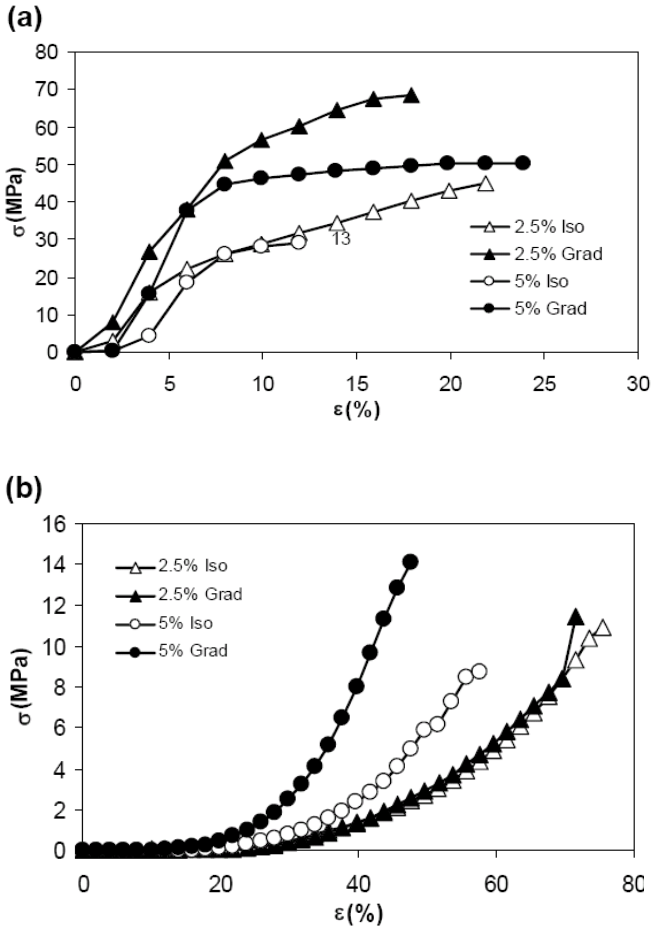

Figure 2.20 - Stress-strain curves for chitosan membranes under a) dry conditions and b) wet conditions (soaked in PBS for 1 h).

Under dry conditions (Figure 2.20a) films revealed an elastic behavior for 8% strain and after this value the stress exceeds a critical value, undergoing plastic, or irreversible, deformation. Membranes prepared with gradient mode exhibited a very high stress break (50-70MPa, for 2.5% and 5% ethanol respectively) in accordance with literature values [66, 67] while the ones that were produced with isocratic mode 2.5% and 5% revealed the ability to undergo a longer elongation at the break, probably due to their higher porosity. Under wet conditions (Figure

2.20b) membranes revealed an exclusive elastic behavior with appreciably different stress-strain behavior relative to the dry samples with higher elongation values (50-75%) and a lower break stresses (8-16 MPa) also in agreement with the data from literature [66, 67]. The different mechanical properties allow us to conclude that CO_2-assisted phase inversion is able to prepare membranes with a wide range of tensile properties.

In the human body, chitosan is mainly degraded by lysozyme and its *in vitro* biodegradability is generally investigated by using a lysozyme containing PBS solution (LysS) [58]. Our results in Figure 2.21 show that the supercritical processed devices have different degradation profiles when immersed in LysS or in PBS solution.

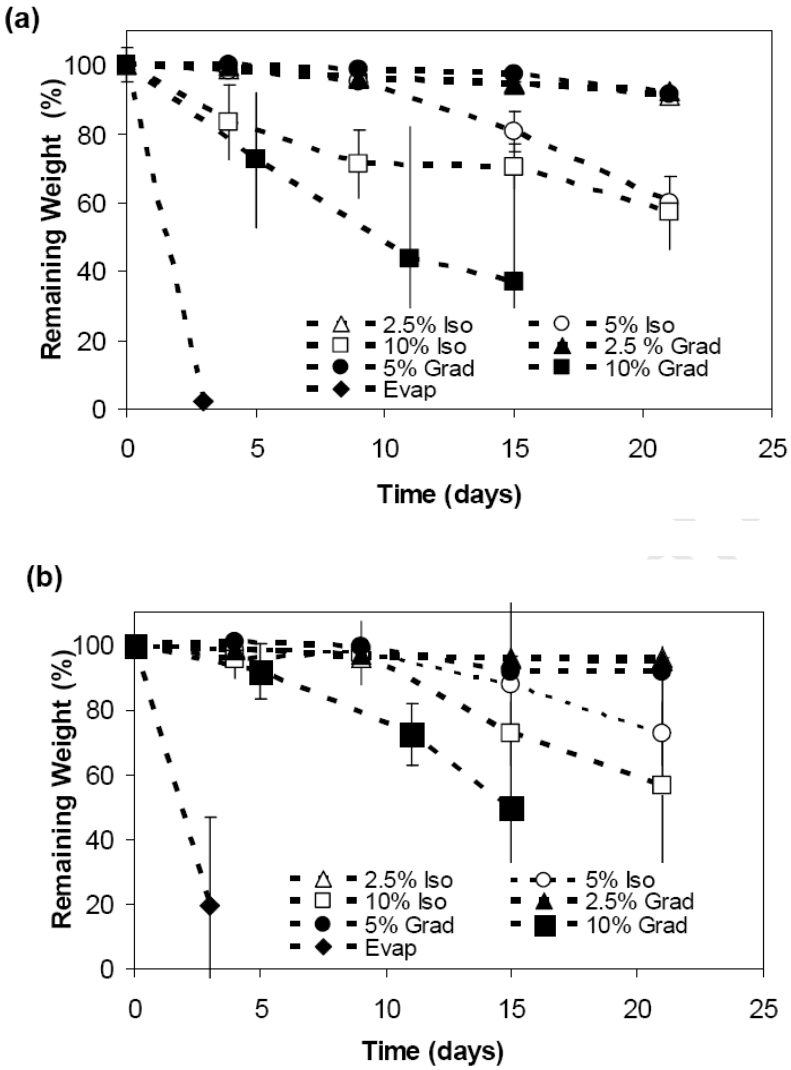

Figure 2.21 - Degradation of the different chitosan porous structures. (a) Lysozyme solution and (b) Phosphate buffer solution.

Analyzing Figure 2.21a we can observe that after 10 days membranes kept 95% of its initial weight, while for the particle agglomerates there was a loss of 30%. The higher porosity of the latter structures facilitates enzyme access to chitosan. Longer immersion periods lead to faster degradation rate of membranes prepared with 5% ethanol (isocratic mode) and 10% ethanol (either isocratic or gradient mode), and after 20 days of immersion, all these devices had lost

approximately 50% of its initial weight. However, the ones produced with 2.5% ethanol kept more than 90% of their initial weight. In terms of immersion in PBS (Figure 2.21b), after a 10 days period, it is possible to observe a negligible loss of weight for the structures that were prepared by the CO_2 assisted phase inversion method contrary to the membrane that was prepared by evaporation, that shows a completely loss of weight after a 3 days immersion. Chitosan membranes prepared with 2.5% ethanol, either following isocratic or gradient mode kept more than 95% of their weight even after a 20 days immersion period but other chitosan structures degraded faster, loosing 30 to 50% of its weight after the same time period. Usually chitosan dissolution of scaffolds or membranes is prevented by rehydrating samples in either diluted NaOH, or in an ethanol series. In our methodology, $scCO_2$ is able to remove the acetic acid vestiges and prepare structures without additional post-treatment processes avoiding some of the disadvantages of the post-treatments: for instance, scaffolds hydrated in NaOH exhibited some shrinkage and distortion, probably caused by base-induced changes in crystallinity and associated structural stresses [68]. Another possibility is the use of reticulation procedures, but since crosslinking agents are usually toxic compounds that might detrimentally affect bioactive substances or cells attached to the surface of the material [69], therefore these were avoided in this work.

2.3.2.2 Drug release devices

Apart from their biological activity, one of the more important properties of polysaccharides, in general, is their ability to form hydrogels and their application as drug release devices. $ScCO_2$ has the potential to be an excellent environment to form controlled release systems [70]. In this work, gentamicin was used as a model drug, being incorporated into the membrane by bulk loading in the casting solution. The membrane prepared with 2.5% ethanol isocratic mode was selected for

these particular studies due to the relative high porosity and water permeability. The mechanical properties, specially the high elasticity of this particular membrane type, were also an important feature for this particular choice.

Figure 2.22 shows the release profiles exhibited by membranes loaded with different amounts of gentamicin. Three different loadings were introduced in the casting solution. After membrane preparation the release profiles were determined using membrane areas of approximately 3 cm^2. The total amount of drug released was proportional to the amount of drug initially dissolved with the polymer into the casting solution which allows us to confirm that the amount of drug released can be easily controlled by the amount of drug that it is loaded.

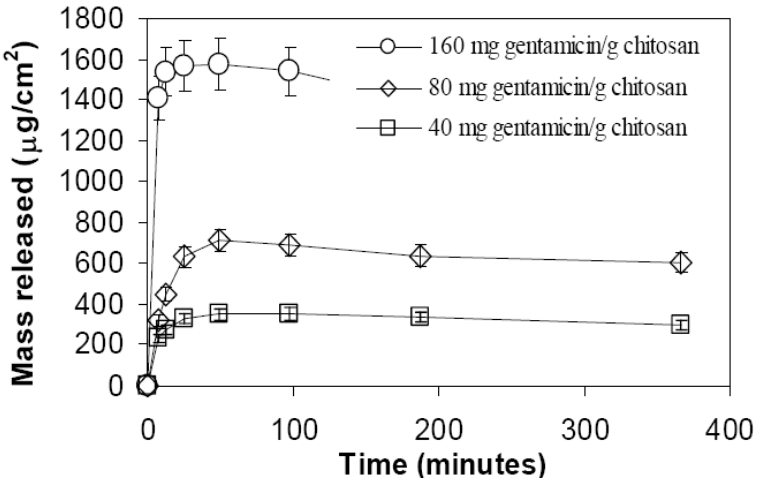

Figure 2.22 - In vitro drug release profiles for chitosan membranes loaded with 40, 80 and 160 mg gentamicin /gchitosan

Membranes prepared with 40 and 80 $mg_{gentamicin}/g_{chitosan}$ released 90% of its gentamicin in PBS at 37ºC in 25 min with a total dosage of 329 and 630 $\mu g/cm^2$ respectively, while the membrane loaded with 160 $mg_{gentamicin}/g_{chitosan}$ displayed the 90% release in only 7 minutes. These profile features are due to the nonexistence of a crosslinking procedure with a reticulation agent (*e.g.* glutaraldehyde). Indeed, when Thacharodi and co-workers [71] reported the preparation of

chitosan membranes and their use has as transdermal delivery system for nifedipine, they observed higher rates in the membranes that were not crosslinked and attributed this to the higher permeability of this type of membranes. These results might be explained by the inexistence of chemical bonds between the drug and the polymer and the prevalence physical interactions as reported by Reverchon and co-workers [72]. Another possible explanation is the high swelling degree of these membranes, around 260% ((weight after 24 hour immersion– dried weight) / dried weight*100) in aqueous physiological conditions which makes the drug highly accessible and fasten released. $ScCO_2$ process was able to efficiently prepare an implantable membrane incorporating a small antibiotic molecule, gentamicin, with a broad dosage range (up to 160 $mg_{gentamicin}/g_{\ chitosan}$) within a 3D stable and controlled morphologic matrix. However, 160 $mg_{gentamicin}/g_{\ chitosan}$ is by no means an upper limit, as incorporation in the bulk solution is only limited by the chitosan and gentamicin solubilities in the acidified water.

2.3.2.3 Cytotoxicity Assay

The use of biomaterials in the settings of tissue engineering and regenerative medicine requires a cytotoxicity evaluation to test cell responses when interacting with the material. Chitosan membranes prepared using different ethanol concentrations - isocratic mode (2.5, 5 and 10% - Figure 2.17b2, 2.16a1 and 2.16b1) were tested.

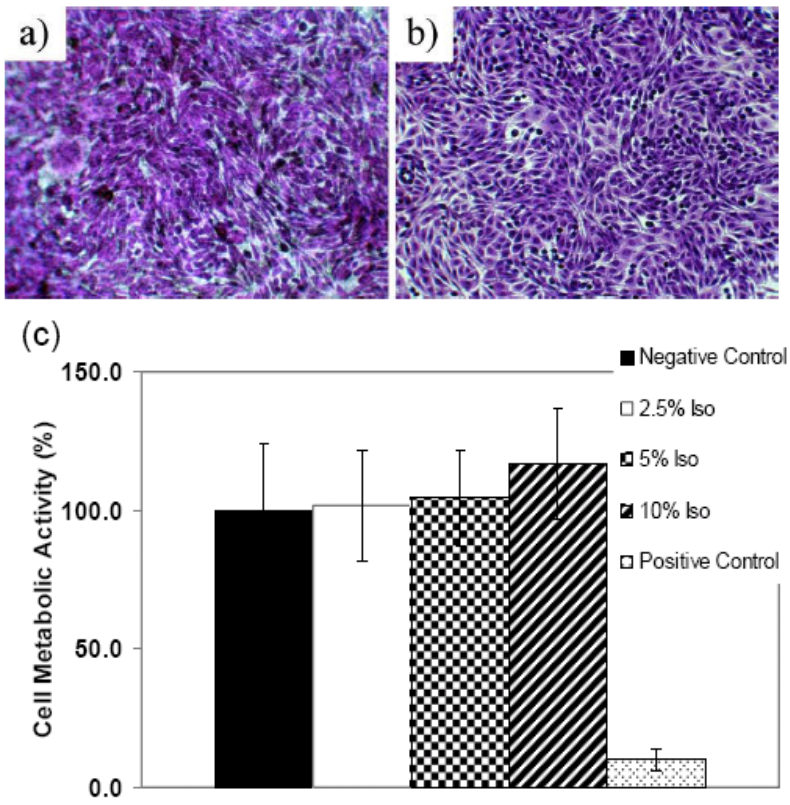

Figure 2.23 - Representative images of L929 fibroblast cells cultured on chitosan membranes (2.5% isocratic) (a) and polystyrene control (b) after 3 days in culture, presenting their characteristic morphology. (c) Cytotoxicity tests of the chitosan membranes following the ISO standards for biomaterials. Negative control: tissue culture plate control (polystyrene); Positive control: 0.01 M phenol.

In Figure 2.23a and b it is possible to observe that cells cultured on chitosan membranes presented their characteristic fibroblastic morphology. Figure 2.23c presents the metabolic activity of the L929 cells (normalized to control) after 48 hours of culture with medium extracts of the different structures. No cytotoxic effect was observed for any of the chitosan membranes prepared, when compared to commonly used tissue culture grade polystyrene (negative control). These results are in agreement with previously reported data attesting the non cytotoxicity of chitosan-based materials [73]. Therefore, the non-cytotoxicity of chitosan membranes enables their potential use as scaffolds to sustain human stem cell adhesion and proliferation *in vitro*.

2.3.2.4 MSC adhesion and proliferation

Although MSC have been studied for more than 20 years, only recently their true potential for clinical use is being explored. The use of MSC in Cellular Therapy, taking advantage of their trophic and immunoregulatory activities is now considered a practical procedure in the clinical field with promising results, whereas tissue engineering approaches using MSC as starting cell source for their controlled differentiation to form bone and cartilage stands at a research level [74]. Therefore, it is of great interest to have a suitable material that would allow successful MSC expansion *in vitro* to obtain clinically relevant numbers.

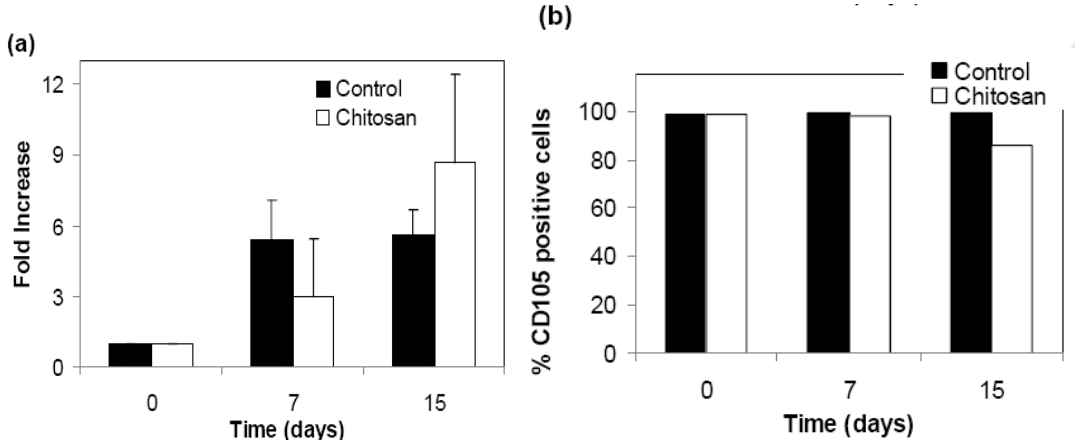

Figure 2.24 - Output of MSC culture on chitosan membranes (2.5% isocratic) in terms of fold increase in total cell number (a) and CD105 expression (%) (b) in comparison to cells cultured on tissue culture plate control (polystyrene).

Results presented in Figure 2.24a) indicate that 2.5% ethanol (isocratic mode) chitosan membranes allowed successful MSC adhesion and proliferation, similar to the control condition during the 2-week culture period (9 *versus*. 6-fold increase at day 15). Due to limited cell numbers, immunophenotypic analyses at day 7 and 15 were performed only for CD105

expression. Expanded cells maintained their characteristic immunophenotype, with over 85% positive cells for CD105. CD105 (endoglin) is typically expressed by endothelial and hematopoietic cells [75] but also by MSC, which are consistently negative for endothelial and hematopoietic markers [74]. Endoglin contains the three peptide motif Arg-Gly-Asp (RGD) in its extracellular domain which is associated with the extracellular matrix protein fibronectin. The slight decrease observed in the expression of CD105 by cells cultured on chitosan membranes compared to control condition (86 *versus* 98%) might be due to the need to expose cells attached to the membranes to a longer period with the enzymatic agent (accutase) in order to harvest the cells (2 cycles of 10 minutes incubation at 37ºC were needed). It was previously reported that a prolonged exposure of cells to proteases is potentially harmful and/or might damage surface cell receptors, namely by decreasing the number of functional integrins available [76]. Ongoing studies testing a range of different scaffolds impregnated/coated with chemomechanical polymers, *e.g.* poly(N-isopropylacrylamide), to acquire direct response to pH levels or temperature changes are being performed. In particular, the incorporation of a thermoresponsive polymer in the scaffold should provide other possibilities such as controlling cell adhesion/detachment, facilitating cell harvesting upon cell expansion *in vitro* [77].

The clonogenic potential of the cultured cells as assessed by the CFU-F assay at day 7 showed 37 and 43 colonies respectively for the chitosan expanded cells and control expanded cells.

Overall, it is envisaged that chitosan membranes might represent suitable structures to support MSC expansion *in vitro*.

2.3.3 Conclusions

In summary, we were able to make stable and sterile chitosan porous devices with controlled morphology using the more sustainable supercritical carbon dioxide induced phase-inversion process. The results here obtained showed that by changing process conditions we can modulate

cell size and membranes morphology from porous membranes to highly porous microparticles and decrease degradation rates of chitosan-based structures *in vitro* physiological conditions by processing them with $scCO_2$. We also used the new process to incorporate therapeutic quantities of gentamicin into the 3D structures. The methodology described in these studies provide a starting point for the design and production of polymeric molded scaffolds, that will be able to incorporate other biologically active molecules such as adhesion molecules and growth factors.

We have demonstrated that the supercritical CO_2-induced phase inversion technique can be harnessed in the field of solid-state porous biomedical materials to make different chitosan devices with a potential to be used as drug delivery systems and scaffolds to sustain *in vitro* cell adhesion and proliferation for possible applications in tissue engineering and regenerative medicine. In particular, we envisage the future use of these stable and sterile, ready-to-use, porous chitosan devices, with defined morphology and pore size, as scaffolds for expansion of human stem cells *in vitro* under highly controlled culture conditions [56, 57].

2.4 References

[1] F. Chen, G.S. Luo, Y.J. Wang, Preparation of polysulfone-coated chitosan beads by emulsion phase-inversion method. *J. Appl. Polym. Sci*., 91 (**2004**) 3542 - 3548.

[2] E. Reverchon, S. Cardea, Formation of polysulfone membranes by supercritical CO_2. *J. Supercrit. Fluids*, 35 (**2005**) 140 -146.

[3] M. Mulder, Basic Principles of Membrane Technology, Kluwer Academic Publisher, Netherlands, **1997**.

[4] H. Matsuyama, A. Yamamoto, H. Yano, T. Maki, M. Teramoto, K. Mishima, K. Matsuyama, Effect of organic solvents on membrane formation by phase separation with supercritical CO_2. *J. Membrane Sci*., 204 (**2002**) 81-87.

[5] E. Reverchon, E. Schiavo Rappo, S. Cardea Flexible supercritical CO_2- assisted process for Poly(methyl methacrylate) structure formation. *Polym. Eng. Sci*., 46 (**2006**) 188-197.

[6] R. Sui, A.S. Rizkalla, P.A. Charpentier, Synthesis and formation of silica aerogel particles by a novel sol-gel route in supercritical carbon dioxide. *J. Phys. Chem. B*, 108 (**2004**) 11886-11892.

[7] B. Harjo, K.M. Ng, C. Wibowo, Synthesis of supercritical crystallization processes. *Ind. Eng. Chem. Res*., 44 (**2005**) 8248-8259.

[8] Q. Xu, M.Pang, Q. Peng,Y. Jiang, J. Li, H. Wang, M. Zhu, Effect of different experimental conditions on biodegradable polylactide membranes prepared with supercritical CO2 as nonsolvent, *J. Appl. Polym. Sci*. 98 (**2005**) 831-837.

[9] I.M Chakravarti, R.G Laha, J. Roy, Handbook of Methods of Applied Statistics, Volume I, John Wiley and Sons, **1967**.

[10] M.A. Stephens, EDF Statistics for Goodness of Fit and Some Comparisons, *J. Amer. Stat. Assoc*. 69 (**1974**) 730-737.

[11] A.F.M. Barton, Handbook of Solubility Parameters and Other Cohesion Parameters, CRC Press, Boca Raton, **1991**.

[12] J.C. Giddings, M.N. Myers, L. Mclaren and R.A. Keller, High pressure gas chromatography of nonvolatile species, *Science* 62 (**1968**) 67-73.

[13] J.W. King, Z. Zhang, Selective extraction of pesticides from lipid-containing matrixes using supercritical binary gas mixtures, *Anal. Chem.*, 70 (**1998**) 1431-1436.

[14] K. Hirogaki, I. Tabata, K. Hisada, T. Hori, An investigation of the interaction of supercritical carbon dioxide with poly(ethylene terephthalate) and the effects of some additive modifiers on the interaction. *J. Supercrit. Fluids*, 36 (**2005**) 166-172.

[15] A.M. Scurto, C.M. Lubbers, G. Xu, J.F. Brennecke, Experimental measurement and modeling of the vapor–liquid equilibrium of carbon dioxide + chloroform. *Fluid Phase equilibria*, 190 (**2001**) 135-147.

[16] H.-S. Byun, N.-H. Kimb, C. Kwak, Measurements and modeling of high-pressure phase behavior of binary CO_2–amides systems. *Fluid Phase Equilibria*, 208 (**2003**) 53-68.

[17] H.-S. Byun and N.-S. Jeon, Phase behavior measurement of the binary carbon dioxide–N,N-dimethylacetamide and carbon dioxide–N,N-diethylacetamide systems at high pressure, *Fluid Phase Equilibria*, 167 (**2000**) 113-122.

[18] A.V. Gonzalez, R. Tufeu, P. Subra, High-pressure vapor-liquid equilibrium for the binary systems carbon dioxide + dimethyl sulfoxide and carbon dioxide + dichloromethane, *J. Chem. Eng. Data*, 47 (**2002**) 492-495.

[19] O. Pfohl, S. Petkov, G. Brunner, Usage of PE - A program to calculate phase equilibria, Herbert Utz Verlag, München, **1998**.

[20] A. Kordikowski, A.P. Schenk, R.M. Van Nielen, C.J. Peters, Volume expansions and vapor-liquid equilibria of binary mixtures of a variety of polar solvents and certain near-critical solvents. *J. Supercrit. Fluids*, 8 (**1995**) 205-216.

[21] R. Rajasingam, L. Lioe, Q.T. Pham, F.P. Lucien. Solubility of carbon dioxide in dimethylsulfoxide and N-methyl-2-pyrrolidone at elevated pressure. *J. Supercrit. Fluids*, 31 (**2004**) 227-234.

[22] J.-M. Cheng, D.-M. Wang, F.-C. Lin and J.-Y. Lai, Formation and gas flux of asymmetric PMMA membranes. *J. Membrane Sci*., 109 (**1996**) 93-107.

[23] M. Tang, Y.-C. Huang, Y.-P. Chen, Sorption and diffusion of supercritical carbon dioxide into polysulfone. *J. Appl. Polym. Sci*., 94 (**2004**) 474-482.

[24] D.-J. Lin, C.-L. Chang, C.-K. Lee, L.-P. Cheng, Preparation and characterization of microporous PVDF/PMMA composite membranes by phase inversion in water/DMSO solutions. *Eur. Polym. J*., 42 (**2006**) 2407-2418.

[25] B. Krause, H. J. P. Sijbesma, P. Mu1nu1 klu1 , N. F. A. van der Vegt, M. Wessling, Bicontinuous Nanoporous Polymers by Carbon Dioxide Foaming. *Macromolecules*, 34 (**2001**) 8792-8801.

[26] B. Krause, N.F.A. van der Vegt, M. Wessling, New ways to produce porous polymeric membranes by carbon dioxide foaming. *Desalination*, 144 (**2002**) 5-7.

[27] Y.-T. Shieh, H.-S. Yang, Morphological changes of polycaprolactone with high-pressure CO_2 treatment. *J. Supercrit. Fluids*, 33 (**2005**) 183-192.

[28] Z. Lian, S.A. Epstein, C. W. Blenk, A. D. Shine, Carbon dioxide-induced melting point depression of biodegradable semicrystalline polymers. *J. Supercrit. Fluids*, 39 (**2006**) 107–117.

[29] D. Pospiech, K. Eckstein, L Haüßler, H. Komber, D. Jehnichen, K. Grundke, F. Simon, Hydrophilic modification of polysulfone via incorporation of poly(oxy-1,4-butanediyl) segments. *Macromol. Chem. Phys*., 200 (**1999**) 1311-1325.

[30] M. Diamantoglou, J. Vienken, Strategies for the development of haemocompatible dialysis membranes. *Macromol. Symp*., 103 (**1996**) 31-42.

[31] A.D. Marshall, P.A. Munro, G. Trägadh, The effect of protein fouling in microfiltration and ultrafiltration on permeate flux, protein retention and selectivity: A literature review. *Desalination*, 91 (**1993**) 65-108.

[32] D. S. Wavhal, E. R. Fisher, Modification of polysulfone ultrafiltration membranes by CO_2 plasma treatment. *Desalination*, 172 (**2005**) 189-205.

[33] G.A. Leeke, J. Cai, M. Jenkins, Solubility of supercritical carbon dioxide in polycaprolactone (CAPA 6800) at 313 and 333K, *J. Chem. Eng. Data*, 51 (**2006**) 1877-1879.

[34] G. Qipeng, Liu Zhenhai, Phase Behavior of Polymer Blends. *J. Therm. Anal. Calorim*., 59 (**2000**) 101-120.

[35] V. Thirtha, R.Lehman, T. Nosker, Morphological effects on glass transition behavior in selected immiscible blends of amorphous and semicrystalline polymers. *Polymer*, 47 (**2006**) 5392-5401.

[36] Y. Wang, M.A. Rodruiguez-Perez, R.L. Reis, J.F. Mano, Thermal and Thermomechanical Behaviour of Polycaprolactone and Starch/Polycaprolactone Blends for Biomedical Applications. *Macromol. Mat. Eng*.,290 (**2005**) 792-801.

[37] D. W. Hutmacher, Scaffolds in tissue engineering bone and cartilage. *Biomaterials*, 21 (**2000**) 2529-2543.

[38] M. Kellomaki, H.Niiranen, K. Puumanen, N. Ashammakhi, T. Waris, P. Tormala, Bioabsorbable scaffolds for guided bone regeneration and generation. *Biomaterials*, 21 (**2000**) 2495-2505.

[39] A. C. A. Wan, B. C. U. Tai, K. M. Schumacher, A. Schumacher, S. Y. Chin, J. Y. Ying, Polyelectrolyte Complex Membranes for Specific Cell Adhesion. *Langmuir*, 24 (**2008**) 2611-2617.

[40] A. K. Dillow, F. Dehghani, J. S. Hrkach, N. R. Foster, R. Langer, Bacterial inactivation by using near- and supercritical carbon dioxide, *Proc. Nat. Am. Soc*., 96 (**1999**) 10344-10348.

[41] J. Fages, B. Poirier, Y. Barbier, P. Frayssinet, M. L. Joffret, W. Majewski, G. Bonel, D. Larzul, Viral inactivation of human bone tissue using supercritical fluid extraction, *ASAIO J*., 44 (**1998**) 289-293.

[42] J. Zhang, S. Burrows, C. Gleason, M. A. Matthews, M. J. Drews, M. Laberge, Y. H. An, Sterilizing Bacillus pumilus spores using supercritical carbon dioxide, *J. Microbiol*. *Methods*, 66 (**2006**) 479-485.

[43] A. White, D. Burns, T. W. Christensen, Effective terminal sterilization using supercritical carbon dioxide. *J. Biotechnol*., 123 (**2006**) 504-515.

[44] O. R. Davies, A. L. Lewis, M. J. Whitaker, H. Tai, K. M. Shakesheff, S. M. Howdle, Applications of supercritical CO_2 in the fabrication of polymer systems for drug delivery and tissue engineering. *Adv. Drug Deliver. Rev*., 60 (**2008**) 373–387.

[45] J. L. Drury, D. J. Mooney, Hydrogels for tissue engineering: scaffold design variables and applications. *Biomaterials*, 24 (**2003**) 4337–4351

[46] J.-K. F. Suh, H. W. T. Matthew, Application of chitosan-based polysaccharide biomaterials in cartilage tissue engineering: a review. *Biomaterials* 21 (**2000**) 2589-2598.

[47] M.-C. Chen, H.-W. Tsai, Y. Chang, W.-Y. Lai, F.-L. Mi, C.-T. Liu, H.-S. Wong, H.-W. Sung, Rapidly Self-Expandable Polymeric Stents with a Shape-Memory Property. *Biomacromolecules* 8 (**2007**) 2774-2780.

[48] H. Ueno, T. Mori, T. Fujinaga, Topical formulations and wound healing applications of chitosan. Adv. Drug Deliver. Rev. 52 (**2001**) 105–115.

[49] M. Mochizuki, Y. Kadoya, Y. Wakabayashi, K. Kato, I. Okazaki, M.Yamada, T. Sato, N. Sakairi, N. Nishi, M. Nomizu, Laminin-1 peptide-conjugated chitosan membranes as a novel approach for cell engineering. *FASEB J.* , 17 (**2003**) 875–877.

[50] D. W. Hutmacher, J. T. Schantz, C. X. Lam, K. C. Tan, T. Lim, State of the art and future directions of scaffold-based bone engineering from a biomaterials perspective. *J. Tissue Eng. Regen. Med*. 1 (**2007**) 245-260.

[51] N. Zaidi, J. A. Nixon, Stem Cell Therapy in Bone Repair and Regeneration. *Ann. N. Y. Acad. Sci.* 1117 (**2007**) 62-72.

[52] C.J. Xian, B.K. Foster, Repair of Injured Articular and Growth Plate Cartilage Using Mesenchymal Stem Cells and Chondrogenic Gene Therapy. *Curr. Stem Cell. Res. Ther*. 1 (**2006**) 213-229.

[53] K. Le Blanc, I. Rasmusson, B. Sundberg, C. Götherström, M. Hassan, M. Uzunel, O. Ringdén, Treatment of severe acute graft-versus-host disease with third party haploidentical mesenchymal stem cells. *Lancet*, 363 (**2004**) 1439-1441.

[54] X. Chen, H. Xu, C. Wan, M. McCaigue, G. Li, Bioreactor Expansion of Human Adult Bone Marrow-Derived Mesenchymal Stem Cells. *Stem Cells*, 24 (**2006**) 2052-2059.

[55] A.I. Caplan, Adult mesenchymal stem cells for tissue engineering versus regenerative medicine. *J. Cell. Physiol*. 213 (**2007**) 341-347.

[56] F. Zhao, T. Ma, Perfusion bioreactor system for human mesenchymal stem cell tissue engineering: dynamic cell seeding and construct development. *Biotechnol. Bioeng*., 91 (**2005**) 482-493.

[57] L. Meinel, V. Karageorgiou, R. Fajardo, B. Snyder, V. Shinde-Patil, L. Zichner, D. Kaplan, R. Langer, G. Vunjak-Novakovic, Bone Tissue Engineering Using Human Mesenchymal Stem Cells: Effects of Scaffold Material and Medium Flow. *Ann. Biomed. Eng*., 32 (**2004**) 112-122.

[58] K. Tomihata, Y. Ikada, *In vitro* and *in vivo* degradation of films of chitin and its deacetylated derivatives. *Biomaterials*, 18 (**1997**) 567-575.

[59] D.P. Lennon, A.I. Caplan, Isolation of human marrow-derived mesenchymal stem cells. *Exp. Hematol*., 34 (**2006**) 1604-1605.

[60] E. Reverchon, S. Cardea, E. Schiavo Rappo, Membranes formation of a hydrosoluble biopolymer (PVA) using a supercritical CO_2-expanded liquid. *J. Supercrit. Fluids*, 45 (**2008**) 356–364.

[61] S. P. Nunes, T. Inoue, Evidence for spinodal decomposition and nucleation and growth mechanisms during membrane formation. *J. Membrane Sci*., 111 (**1996**) 93-103.

[62] E. Reverchon, S. Cardea, C. Rapuano, Formation of poly-vinyl-alcohol structures by supercritical CO_2. *J. Appl. Polym. Sci*. 104 (**2007**) 3151–3160.

[63] A. F. Ismail, L. P. Yean, Review on the development of defect-free and ultrathin-skinned asymmetric membranes for gas separation through manipulation of phase inversion and rheological factors. *J. Appl. Polym. Sci*., 88 (**2003**) 442-451.

[64] E. Reverchon, S. Cardea, Formation of cellulose acetate membranes using a supercritical fluid assisted process. *J. Membr. Sci.* 240 (**2004**) 187–195.

[65] T. A. Khan, K.K. Peh, H. S. Ch`ng, Mechanical, bioadhesive strength and biological evaluations of chitosan films for wound dressing. *J. Pharm. Pharmaceut. Sci*., 3 (**2000**) 303-311.

[66] A. Sarasam, S.V. Madihally, Characterization of chitosan–polycaprolactone blends for tissue engineering applications. *Biomaterials*, 26 (**2005**) 5500-5508.

[67] M. Cheng, J. Deng, F. Yang, Y. Gong, N. Zhao, X. Zhang, Study on physical properties and nerve cell affinity of composite films from chitosan and gelatin solutions. *Biomaterials* 24 (**2003**) 2871-2880.

[68] S. V. Madihally, H.W.T. Matthew, Porous chitosan scaffolds for tissue engineering. *Biomaterials*, 20 (**1999**) 1133-1142.

[69] W. E. Hennink, C. F. van Nostrum, Novel crosslinking methods to design hydrogels. *Adv. Drug Deliver. Rev*. 54 (**2002**) 13-36.

[70] B. Subramaniam, R.A. Rajewski, K. Snavely, Pharmaceutical processing with supercritical carbon dioxide. *J. Pharm. Sci*., 86 (**1997**) 885-890.

[71] D. Thacharodi, K. Panduranga Rao, Rate-controlling biopolymer membranes as transdermal delivery systems for nifedipine: Development and *in vitro* evaluations, *Biomaterials* 17 (**1996**) 1307-1312.

[72] E. Reverchon, S. Cardea, E. Schiavo Rappo, Production of loaded PMMA structures using the supercritical CO_2 phase inversion process. *J. Membr. Sci*., 273 (**2006**) 97-105.

[73] T. Koyano, N. Minoura, M. Nagura, K.-. Kobayashi, Attachment and growth of cultured fibroblast cells on PVA/chitosan-blended hydrogels. *J. Biomed. Mater. Res*, 39 (**1998**) 486-490.

[74] A.I. Caplan, Adult mesenchymal stem cells for tissue engineering versus regenerative medicine. *J. Cell. Physiol.,* 213 (**2007**) 341-347.

[75] Y.Q. Liu, B. Jovanovic, M. Pins, C. Lee, R.C. Bergan, Over expression of endoglin in human prostate cancer suppresses cell detachment, migration and invasion. *Oncogene*, 21 (**2002**) 8272-8281.

[76] M.A. Brown, C.S. Wallace, C.C. Anamelechi, E. Clermont, W.M. Reichert, G.A. Truskey, The use of mild trypsinization conditions in the detachment of endothelial cells to promote subsequent endothelialization on synthetic surfaces. *Biomaterials*. 28 (**2007**) 3928-3935.

[77] M. Yamato, M. Utsumi, A. Kushida, C. Konno, A. Kikuchi, T. Okano. Thermo-responsive culture dishes allow the intact harvest of multilayered keratinocyte sheets without dispase by reducing temperature. *Tissue Eng*. 7 (**2001**) 473-480.

Chapter 3

“GREEN” PREPARATION OF SMART POLYMERS

3. "Green" preparation of smart polymers

In this chapter one of the most studied polymer families were hydrogels, widely used in the biomedical field due to their tuneable chemical and three-dimensional physical structure, biocompatibility properties and possibility to respond to changes in surrounding conditions, such as pH, temperature, ionic strength, and electric field. Special emphasis was applied to temperature and pH sensitive polymers.

3.1 Poly(N-Isopropylacrylamide)

Poly(N-isopropylacrylamide), PNIPAAm, is a thermoresponsive hydrogel that has a low critical solution temperature (LCST), around 32 ºC in an aqueous solution [1, 2], close to body temperature. It dissolves in water below the LCST and precipitates from the aqueous solution above the LCST due to the disruption of hydrogen bonding with water and the increasing hydrophobic interactions among isopropyl groups. Due to this unique property, PNIPAAm gels have been widely used in biomedical fields, for example, as matrices in protein-ligand recognition, in drug controlled release, in enzyme and cell immobilization and in artificial organs / cell sheet technology [3, 4, 5, 6, 7, 8].

The preparation of hydrogels from soluble polymers requires typically a cross-linking procedure that will allow the system to swell water without compromising the integrity of the material. N,N-methylenebisacrylamide (MBAM) is the cross-linking agent normally used to prepare PNIPAAm-based hydrogels. The synthesis of PolyNIPAM using this cross-linker was first reported by Pelton and Chibante in 1986 [9] and since then many publications describing the preparation, characterization and application of temperature-sensitive hydrogels have been reported in literature [10, 11, 12, 13, 14].

During the last years, an effort has been made to modify and improve the properties of PNIPAAm hydrogels. In many attempts the strategies involve the use of organic solvents or toxic additives, which should be then recovered and recycled [15, 16]. In this section we report the precipitation polymerization of PNIPAAm in supercritical carbon dioxide ($scCO_2$). Our $scCO_2$-assisted method to produce PNIPAAm hydrogels present an enormous advantage when compared with conventional polymerization since there is no need of an intensive drying action before further processing or characterization steps.

The use of $scCO_2$ as a polymerization medium offers many advantages over conventional solvents: CO_2 is nontoxic, non-flammable, inexpensive and readily available in high purity from a variety of sources [17, 18]. Since it is a gas at normal pressure by simply reducing the pressure of the system, it is possible to easily separate the solvent from the polymer, leading to highly pure materials [19] ideal for medical applications.

The synthesis of other acrylamides in $scCO_2$ is already reported in literature [20]. These polymer syntheses are normally performed in the presence of highly expensive surfactants to emulsify the insoluble monomer in $scCO_2$. In our case as the monomer is highly soluble in $scCO_2$ the polymerization could be realized without any surfactants.

Chitosan, as mentioned in the previous chapter, is a well known natural polymer that is biodegradable, biocompatible and non-toxic [21, 22, 23] with possible applications in the medical field, including dialysis membranes, contact lenses, antitumor uses, drug delivery controlled-release systems and tissue engineering.

The production of smart partially-biodegradable scaffolds for tissue engineering applications combining the thermoresponsive properties of PNIPAAm, the biocompatible properties of chitosan with the green aspects of polymerizations in $scCO_2$ is a desired goal.

In this work it is presented a new strategy for the polymerization of PNIPAAm that provides new possibilities for the impregnation/coating of these hydrogel in porous structures (membranes and scaffolds).

3.1.1 Experimental

3.1.1.1 Materials

N-isopropylacrylamide (NIPAAm, 97% purity), N,N-methylenebisacrylamide (MBAm, purity ≥ 98 %), chitosan (~85% deacetylated, medium molecular weight) and 2,2`-azobis (isobutyronitrile) (AIBN, 98% purity) were purchased from Sigma-Aldrich and used without further purification.

Carbon dioxide was obtained from Air Liquide with 99.998 % purity.

3.1.1.2 Preparation of PNIPAAm hydrogels

Polymerisation reactions were carried out in a high-pressure apparatus already described elsewhere [19] and schematically presented in Figure 3.1.

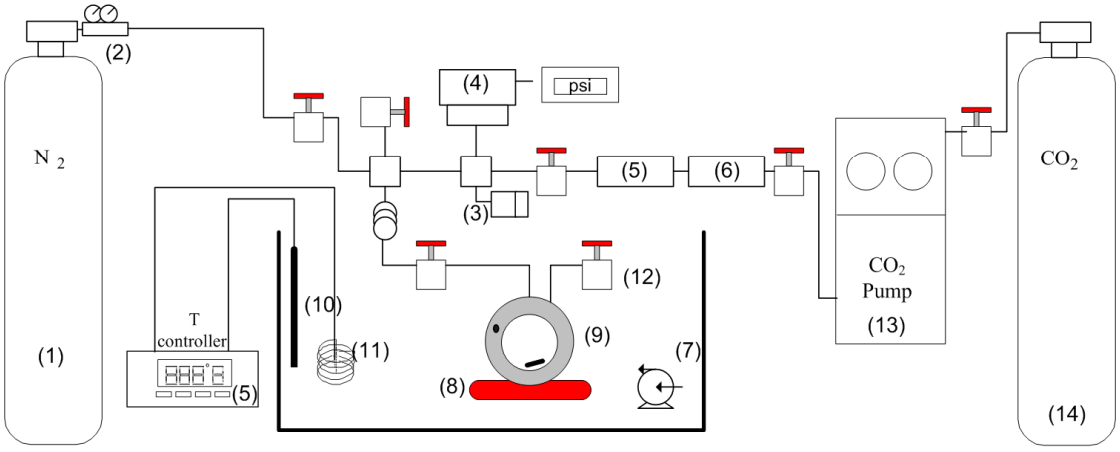

Figure 3.1 - Schematic representation of the apparatus used in the polymerisation reactions. 1- nitrogen cylinder; 2-gas regulator; 3-rupture disc; 4- high-pressure manometer; 5- check-valve; 6- line filter; 7-water bath; 8-immersible stirrer; 9-high pressure cell

In a typical procedure monomer, cross-linking agent (if included), and initiator (2 wt%) are loaded into the high-pressure cell then sealed and nitrogen is added to purge the cell and test leaks. The nitrogen is slowly released and liquid carbon dioxide is loaded into the cell using a high-pressure compressor. The cell is immersed in the water bath and temperature and pressure are allowed to rise to the required experimental conditions. Additional CO_2 may be added to reach the exact desired pressure. The reaction was allowed to proceed for 24 hours under stirring.

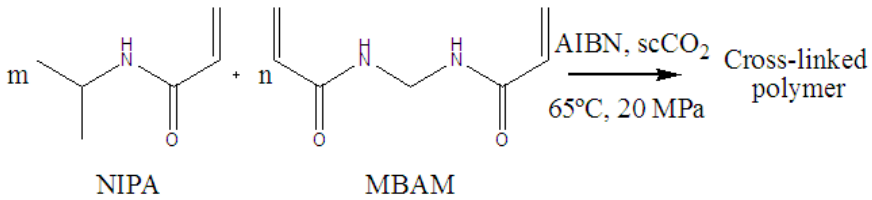

Scheme 1

Table 3.1 - Effect of cross-linker ratio on the PNIPAAm polymerization in $scCO_2$.

Entry	wt% MBAM [a]	Yield (%)	LCST (ºC)	ΔH ($J.g^{-1}$)	Surface area m^2/g	Polymer morphology
1	0.0	74.7	33.3	51	6.1	Highly
2	1.2	89.6	31.7	37	10.6	Defined particles
3	2.4	86.9	30.5	16	14.3	Defined particles
4	4.5	94.6	30.7	10.3	17.3	Defined particles

[a] weight of MBAM/Total weight (NIPAAm, AIBN, MBAM)

The reactions were performed at 65ºC and 20 MPa, according to scheme 1. At these experimental conditions we have a homogeneous phase with all the reactants completely soluble in the supercritical medium. Different concentrations of cross-linker were tested as summarized in Table 3.1. Two hours after the beginning of the reaction the mixture turned yellow, then soft orange (Tyndall effect) and within few minutes white particles of polymer started to precipitate. The reaction was then stopped and the resulting polymer was washed with fresh high-pressure CO_2 (65ºC, 20 MPa for one hour) in order to extract the remaining residues of unreacted monomer and cross-linker. When cross-linker was added the polymers were conformed closely to the interior of the reaction vessel as a dry, white polymer with a soft consistence. No significant shrinkage was observed upon venting the CO_2. When no cross-linker was used the polymer precipitated at the bottom of the cell as a fluffy, dry, white, free flowing powder.

3.1.1.3 Structural/Morphological Analysis

The synthesized polymers were analysed by Nuclear Magnetic Resonance (NMR) and Matrix Assisted Laser Desorption /Ionization- Time Of Flight Mass Spectrometry (MALDI-TOF MS). NMR spectra were performed in a Bruker equipment (ARX 400 MHz), using deuterated

chloroform ($CDCl_3$) as solvent and internal reference. MALDI-TOF MS was used to obtain the molecular weight and it was performed in a AUTOFLEX Bruker using Dithranol (1,8,9-anthracenetriol) as matrix. Polymer yield was determined gravimetrically.

Differential scanning calorimetry (DSC) was applied to investigate the thermal features. The LCST of the hydrogel samples was determined in a PerkinElmer DSC 7. The thermal analyses were performed from 15 to 40 °C at 3 ^{o}C/min under a dry nitrogen atmosphere (flow rate = 20 ml/min). Calibration for the temperature and energy scale was carried out using a pure indium standard.

Specific surface areas of the networks were determined by adsorption of N_2 according to the BET method. An accelerated surface area and porosimetry system (ASAP 2010 MICROMERITICS) was used under nitrogen flow.

The morphology of hydrogel particles was also evaluated using Scanning Electron Microscopy (SEM) in a Hitachi S-2400, with an accelerating voltage set to 15 kV. Particles size diameters and porosity were obtained by image analysis using SigmaScan Pro (Systat Software Inc.). EasyFit (MathWave Technologies) software was used to fit statistical distributions to our data (Weibull, Lognormal) and perform the Kolmogorov – Smirnov and Anderson – Darling tests to select the more adequate distribution function to each system under study24.

3.1.1.4 Swelling measurements

Equilibrium hydration or swelling degree (W,%) of synthesized samples was determined as defined by equation 1:

$$\text{Water content (W,\%)} = \frac{W_t - W_d}{W_d} \times 100 \qquad (1)$$

where W_d is the weight of the dried polymer sample and W_t is the weight after 24 hours of immersion.

3.1.1.5 In situ polymerization inside Chitosan Scaffolds

PNIPAAm was synthesized inside chitosan scaffolds using $scCO_2$ assisted polymerizations in order to investigate the feasibility of this technology to produce smart partially-biodegradable matrices for tissue engineering applications.

Chitosan scaffolds were previously prepared by dissolving medium molecular weight chitosan in 0.2 M acetic acid solution at a concentration of 3 wt%. The solution was then placed in cylindrical silicon moulds, freezed at -80 ºC and lyophilized (Telstar-Cryodos-80, Spain) up to 4 days to complete remove the frozen solvent. Then, the scaffolds were neutralized using a 0.1 M NaOH solution and freeze-dried again.

For the in situ polymerization of PNIPAAm, scaffolds and reactants were placed inside the high pressure vessel and $scCO_2$ was used as carrier of the monomer/initiator/cross-linker into the porous structures as well as reaction medium. The reaction was performed in the same conditions that were tested in the preparation of PNIPPAAm hydrogels.

3.1.2 Results and discussion

In the absence of cross-linking agent, the precipitation polymerization of PNIPAAm in $scCO_2$ resulted in a low molecular weight polymers (Mw = 660) with 75% yield (entry 1 in Table 3.1). Figure 3.2 shows the NMR and MALDI-TOF MS spectra of PNIPAAm synthesised without cross-linker.

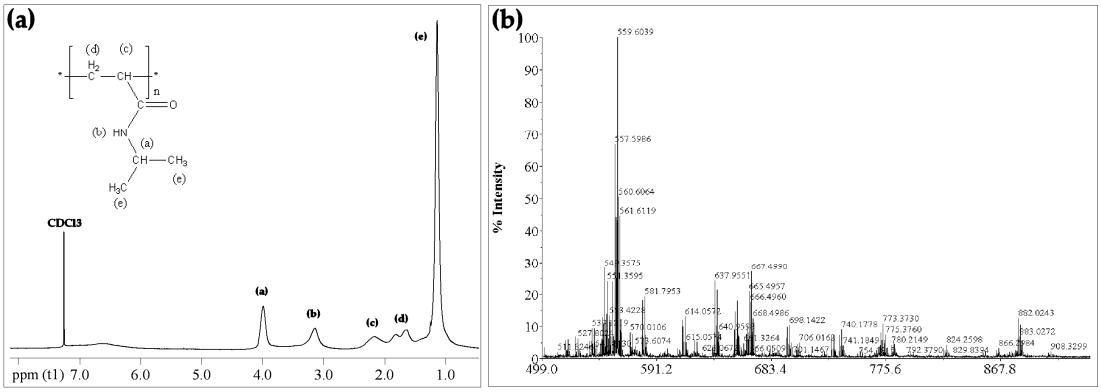

Figure 3.2- Characterization of the PNIPAAm hydrogel polymerized without cross-linker a) ^{1}H NMR in $CDCl_3$ b) MALDI-TOF MS spectrum.

NMR spectrum confirms the structure of PNIPAAm as well as its high purity after the efficient high-pressure CO_2 washing step at the end of the reaction. The NMR and MALDI-TOF MS spectra of the cross-linked synthesized polymers were not used in the discussion due to the low solubility of these hydrogels in the solvents generally used in these techniques, such as chloroform, hexane, acetone and water. By increasing the cross-linker concentration from 1 to 5 %, the yield increased up to 95 % (entries 2 to 4 in Table 3.1). This trend might be due to the ability of the cross-linker MBAM to enhance the solubility of the growing polymer in $scCO_2$ leading to higher yields. Cooper *et al.* observed a similar behavior in the synthesis of cross-linked polystyrene in $scCO_2$ [25].

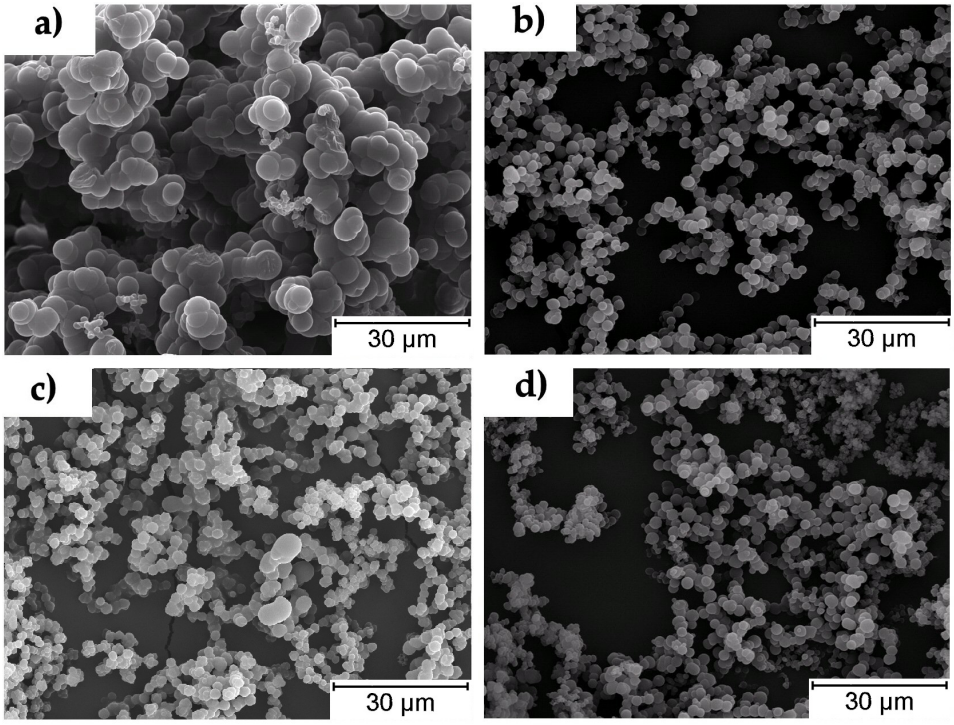

Figure 3.3- Scanning electron microscopy images of the hydrogels prepared in different conditions. Samples: a) 0 wt% MBAM, b) 1.2 wt% MBAM, c) 2.4 wt% MBAM, d) 4.5 wt% MBAM.

In precipitation polymerization, [26,26,27] both monomer and initiator are soluble in the continuous phase but as the polymer grows the insoluble polymer chains precipitate and the particles tend to group forming an undefined, agglomerated powder. By increasing the concentration of cross-linker the number of nuclei generated in the reaction increases thus reducing the particle size diameter. Even a small increase of cross-linker (from 1 to 5%) leads to a significant decrease of the particle diameters (from 2.7 to 2.1 µm). PNIPAAm synthesized without cross-linker showed larger particles (5.4 µm), although quite agglomerated (Figure 3.3a), while when cross-linker was added the particle diameters were significantly reduced (2.1 µm). This trend can be clearly observed by comparing SEM images from Figure 3.3 and particle size distributions from Figure 3.6. The small variation in cross-linker concentration explains the

visual similarity between Figure 3.3 b, c and d. All samples show some agglomeration which is typical in a precipitation polymerization without the use of a stabiliser. Usually higher cross-linking degree results in less agglomerated polymers since particles are stabilised against coagulation by their cross-linked surfaces rather than by added stabilizers [26]. This trend is also easily observed in our work. As it can be seen in Figure 3.3 the sample synthesised in absence of cross-linker shows a higher degree of agglomeration when compared with the cross-linked samples. It is expected that the morphology of the materials, and their corresponding properties, could be tailored by changing the processing conditions, which makes this strategy a versatile way for preparing thermoresponsive gels.

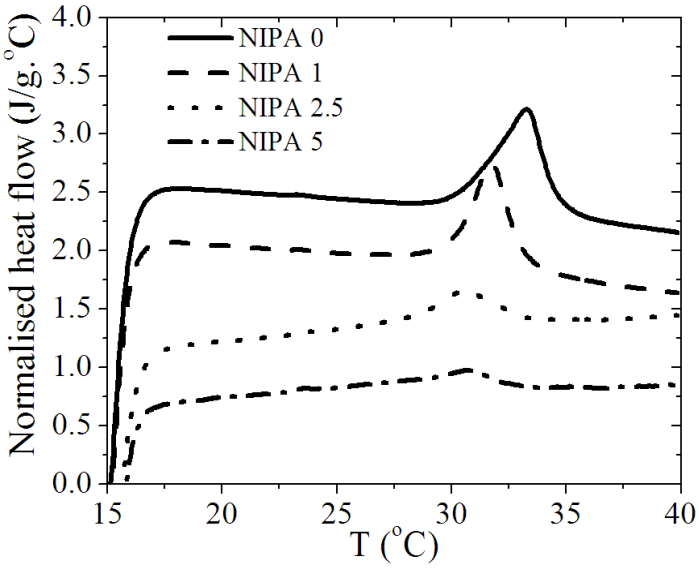

Figure 3.4- DSC thermograms of the hydrogels prepared. 1- 0 wt% MBAM; 2- 1.2 wt% MBAM; 3- 2.4 wt% MBAM; 4- 4.5 wt% MBAM.

Figure 3.4 shows the DSC thermograms of each sample, which were previously soaked in distilled water for 24 h. An endothermic peak is clearly observed around 32 ºC, resulting from the cleavage of the hydrogen bonds between –NH and –C=O groups of PNIPAAm chains and the

surrounding water molecules. The values of the peak temperature (defined as LCST) and endothermic enthalpies (ΔH) are shown in Table 3.1. For the first three formulations a continuous decreasing in the LCST is observed. We can then conclude that the cross-linking influences the phase behaviour of PNIPAAm. The strong variation in the enthalpy clearly suggests that cross-linking highly suppress the thermoresponsive intensity of such hydrogels, as the cross-linking regions will not participate in this event, and may even repress its occurrence. It should be remarked that for linear polymers (without cross-linker) the enthalpy obtained is of the same order of previously results [1], where values of 6.3 kJ/mol (55.8 J/g) were reported for PNIPPAm with different molecular weight distributions, and recognized to be typical for hydrogen bond interactions.

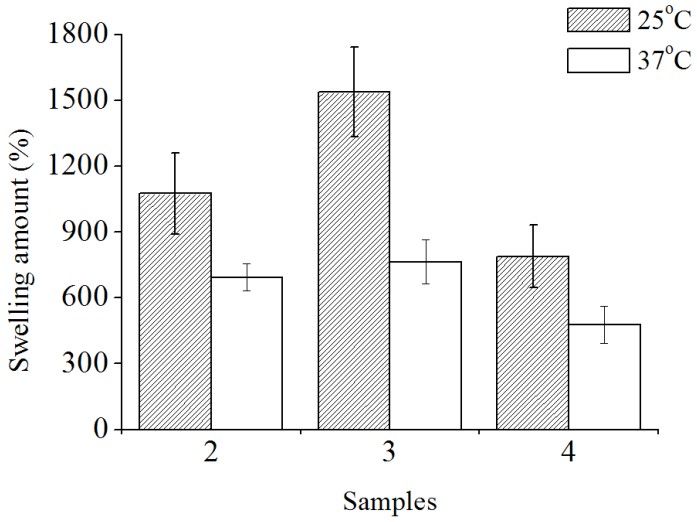

Figure 3.5- Equilibrium swelling at 37ºC and 25ºC for PNIPAAm hydrogels. 2- 1.2 wt% MBAM; 3- 2.4 wt% MBAM; 4- 4.5 wt% MBAM

The swelling degree of a thermoresponsive hydrogel is an important property to be characterised because it will determine properties such as the absorption and diffusion of solutes through the

hydrogel, mechanical properties under wet conditions and water uptake capability. Figure 3.5 shows the swelling behaviour, at 25ºC and 37ºC, of the PNIPAAm samples produced in $scCO_2$.

In the swelling process, the water molecules penetrate the dry hydrogel, wetting the polymer chains. They are weakly adsorbed on the hydrophilic polymer chains or are connected with hydrogen bonds to each other, being trapped in the hydrophilic polymer matrices. All of these interactions lead the hydrogel to swell well at a temperature lower than the LCST. In temperatures above the LCST, this balance is disturbed, and the interactions among the hydrophobic groups begin to play a dominant role, and so the polymer chains aggregate together. As a result, the entrapped water is squeezed out. In our case 300-700% w/w differences were observed which indicates that water is entrapped inside the gel network via hydrogen bonds and influenced by the LCST. In all samples the differences in swelling for the two temperatures analysed are statistically significant with 95% confidence. The differences observed for the different samples are due to the influence of the cross-linker in the morphology of the hydrogels. As suggested by the DSC results, with increasing of the cross-linking degree, the effect of temperature in the water up-take should be smaller, being consistent with the data of Figure 3.5.

The average particle size, the particle size distribution, and the porosity are also important factors in solute permeation into and out of a hydrogel. The porosity of all the hydrogels produced in this work where essentially the same, around 40% even though they present quite different particles diameters and surface areas.

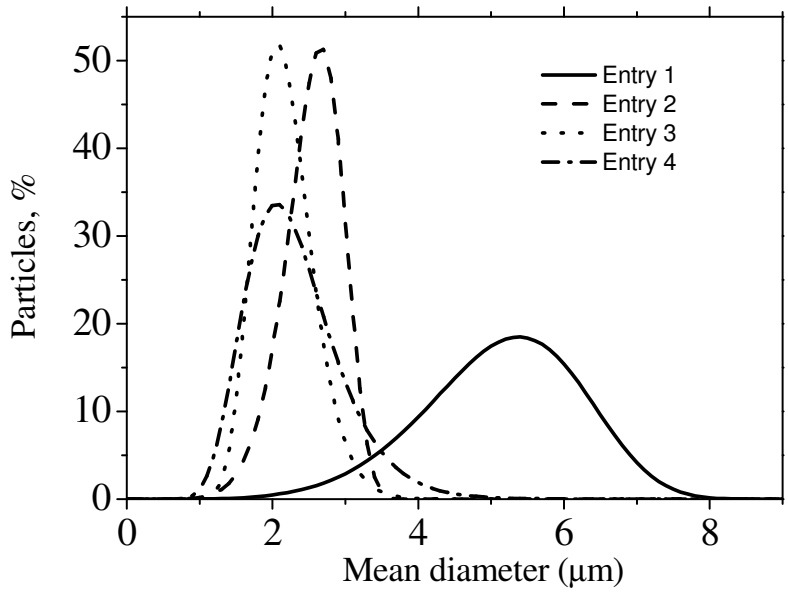

Figure 3.6- Particle size distributions of the different samples.

The surface areas obtained by multipoint BET method (type II) are collected on Table 3.1. According to the isotherms analysis there is an hysteresis (H3 type) confirming an agglomerated material with slit-pores. These areas are in agreement with the particle size distribution presented in Figure 3.6. The hydrogel synthesized without cross-linker has the highest mean diameter (entry 1 in Table 3.1), and presents the smallest surface area per gram. The particles of the hydrogels produced with different amounts of cross-linker show smaller mean diameters. There is a clear trend between the hydrogels cross-linking and surface area/particles sizes. By increasing the cross-linker concentration a decrease of particles size diameters, as well as an increase of their specific surface areas are observed. This behaviour was already observed by other authors in conventional polymerization [28].

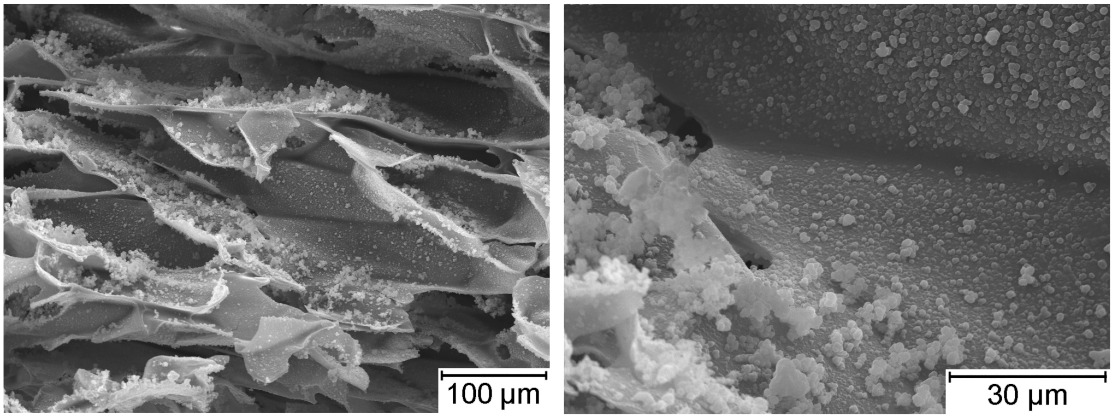

Figure 3.7- SEM pictures of PNIPAAm hydrogel impregnated in a chitosan scaffold.

This work demonstrates the feasibility for synthesizing thermoresponsive polymers and hydrogels in a $scCO_2$ environment. It would be interesting to extend this strategy towards the surface modification or impregnation of previously prepared polymeric systems with a thermoresponsive polymer. This could help in preparing novel smart films, membranes or porous bulky devices with surface properties that could change with temperature. The implementation of such strategy was tested in this work, where PNIPAAm was impregnated in situ within a biodegradable porous structure, made of chitosan, using supercritical fluid technology. Biodegradable foams can be used, for example, in tissue engineering applications where it is required an adequate non-permanent support for cell adhesion and proliferation prior implantation in a regenerative medicine context [29, 30, 31]; porous biocompatible and biodegradable polymers have been widely used for this purpose. The incorporation of a fraction (mainly in the surface) of a thermoresponsive polymer could provide to the scaffold other possibilities, including improved or switchable release control of bioactive agent, such as growth factors, or to control cell adhesion/detachment. Porous structures of chitosan can be easily prepared by freeze-drying, where the final structure may be controlled by the processing conditions [32]. PNIPAAm was synthesized within a previously prepared chitosan scaffold.

Figure 3.7 presents two SEM images of the materials prepared. Such preliminary results clearly show that the hydrogel is uniformly distributed in large amounts inside the pores of the scaffolds.

3.1.3 Conclusion

In summary, we have developed a novel, simple and green method to synthesize PNIPAAm hydrogels without using organic solvents or any other additives (e.g. surfactants). In addition a chitosan scaffold was used as a matrix for the in situ polymerisation of NIPA in $scCO_2$. This would allow producing matrices with thermoresponsive capability that could be used as porous membranes for advanced purification/separation applications, systems for switchable release of molecules or scaffolds for tissue engineering applications. An application of this work will be presented on chapter 4.

3.2 Decreasing the LCST

An important and useful feature of thermosensitive polymers is the possibility of controlling their LCST by various means. It has been shown that the LCST of PNIPAAm-solutions can be changed by adding cosolvents [33], salts [34], surfactants [35], polyelectrolytes [36] or by copolymerization with other polymers [37] especially with others hydrogels. In this work only this last strategy will be presented. Copolymerization of NIPAAm with a more hydrophilic monomer increases the overall hydrophilicity of the polymer, and the stronger polymer–water interactions lead to an increase in the LCST. Likewise, copolymerization with a more hydrophobic monomer results in a lower LCST than PNIPAAm [38].

Poly(2-hydroxyethyl methacrylate) (PHEMA) is one of the hydrogels that presents more interest due to it biocompatibility[39, 40]. It was used as a soft contact lens material due to its high water content at equilibrium, rubbery behavior and good biocompatibility, resembling natural tissues more closely than other synthetic materials [41]. Several authors have reported the synthesis of copolymers of PNIPAAm and PHEMA [42, 43, 44].

The polymerization of PHEMA was already performed in $scCO_2$ by Shiho and DeSimone [45]. In that work the dispersion polymerization took place in a carbon dioxide continuous phase with a diblock copolymer of polystyrene and poly(1,1-dihydroperfluorooctyl acrylate) as the stabilizer.

In the present, the polymerisation of a thermosensitive random copolymer of NIPAAm and 2-hydroxyethylmethacrylate (HEMA) was performed in supercritical CO_2.

3.2.1 Experimental

3.2.1.1 Materials

N-isopropylacrylamide (NIPAAm, 97% purity, Sigma-Aldrich), 2-hydroxyethyl methacrylate (HEMA, > 99% purity, Sigma-Aldrich) and 2,2`-azobis (isobutyronitrile) (AIBN, 98% purity,

Sigma-Aldrich) were used as received. Carbon dioxide and nitrogen were obtained from Air Liquide with 99.998 % and 99.995% purity respectively.

3.2.1.2 Phase-behaviour studies

Phase behaviour studies were performed for the HEMA+CO_2 system in order to verify the solubility of the monomer in the supercritical medium. As one of the most usual polymerization temperatures is 65ºC, cloud points were measured for several mixtures of CO_2 + HEMA at 40ºC, 50ºC, and 65ºC and pressures up to 21.1 MPa.

The cloud point apparatus used in this work is similar to the one described in our earlier publications [46, 47] and is schematically represented in

Figure 3.8. The cloud-point measurements were undertaken in a high-pressure variable volume steel cell with a front sapphire window and a bottom screw-tap connected to a teflon piston that can be moved with water under pressure. Pressure was generated via a hand pump (High Pressure Equipment Co., Model 37-6-30) and monitored with a pressure transducer (Setra Systems Inc., Model 204) with a precision of ±0.0001 MPa. The high-pressure cell was immersed in a 40 L thermostated water bath, heated by means of a PID controller (Hart Scientific, Model 2000) that maintained the temperature within ±0.01 ºC. Carbon dioxide was introduced in the high pressure and added to the monomers using a high-pressure compressor (NWA PM-101). The mixtures were prepared in the cell and the composition was determined by weighing the cylinder in a balance (Precisa, 1212 M) to within ± 0.001 g.

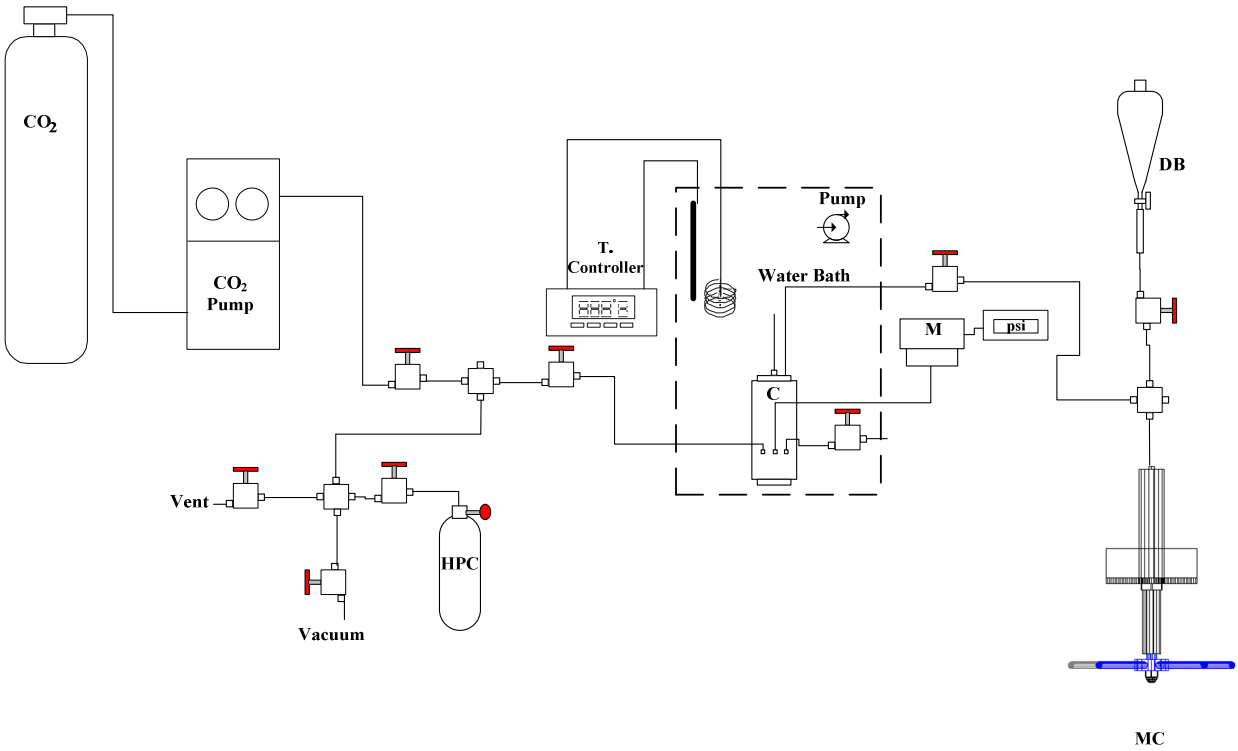

Figure 3.8 - Cloud point measurements apparatus scheme. HPC, high-pressure cylinder; MC, manual controller; C, cell; M, manometer; DB, decantation blister.

The pressure was increased with the hand pump and the system was allowed to equilibrate for 15 minutes at the desired temperature to guarantee that a homogeneous phase was present. A good mixing was provided by means of a magnetic bar. The measurements were undertaken at constant temperature and the pressure was slowly decreased until two phases were observed. The cloud point pressure recorded was the pressure at which the cell became completely cloudy (white opaque). Cloud points were measured and reproduced at least three times to within ± 0.3 MPa.

Using a non-commercially program for high-pressure phase equilibria, PE [51], experimental data were correlated using Soave-Redlich-Kwong (SRK) equation of state [48] (EOS) with the Mathias-Klotz-Prausnitz (MKP) mixing rule [49,50]. The Soave-Redlich-Kwong EOS is a

modification of the simple Redlich-Kwong EOS where the parameter *a* was made temperature dependent. This equation is given by:

$$P = \frac{RT}{v-b} - \frac{a(T)}{v(v+b)} \quad (1)$$

$$a(T) = a(T_c)\alpha(T,\omega) \quad (2)$$

$$a(T_c) = 0.42747 \times \frac{R^2 T_c^2}{P_c} \quad (3)$$

$$\alpha(T,\omega) = \left[1 + m\left(1 - \sqrt{\frac{T}{T_c}}\right)\right]^2 \quad (4)$$

$$m = 0.48 + 1.574\omega - 0.176\omega^2 \quad (5)$$

$$b = 0.08664\frac{RT_c}{P_c} \quad (6)$$

The Mathias-Klotz-Prausnitz mixing rule, includes three adjustable interaction parameters, k_{ij}, λ_{ij} and l_{ij}:

$$a = \sum_{i=1}^{N}\sum_{j=1}^{N} x_i x_j \sqrt{a_i a_j}\left(1 - k_{ij}\right) + \sum_{i=1}^{N} x_i \left[\sum_{j=1}^{N} x_j \left(\sqrt{a_i a_j}\,\lambda_{ij}\right)^{1/3}\right]^3 \quad (7)$$

with $k_{ij} = k_{ji}$ and $\lambda_{ij} = -\lambda_{ji}$

$$b_{ij} = \frac{b_i + b_j}{2}\left(1 - l_{ij}\right) \quad (8)$$

with $l_{ij} = l_{ji}$

The Soave-Redlich-Kwong equation requires three input parameters per pure compound: critical temperature, T_c, critical pressure, P_c and accentric factor, ω [51]. The critical properties of carbon dioxide are available in the literature, yet, for hydroxyethyl methacrylate, however, no information was available. Therefore estimated data had to be used. Using Chem Draw program

it was possible to obtain the required values. In Table 3.2 it is presented the critical constants and accentric factors used in the modelling experiments.

Table 3.2 - Critical constants and accentric factor for CO_2 and HEMA

Component	T_c/ºC	P_c/ MPa	ω
CO_2	31.0	7.38	0.225
HEMA	368.73	3.673	0.986

The minimum difference between experimental and calculated values was obtained for kij equal to - 0.0085, λij equal to 0.004 and lij equal to - 0.003. Many other parameter values were tested but the best fit was achieved with this optimized set.

3.2.1.3 Polymers preparation

Polymerization reactions were carried out using an apparatus already described previously for the polymerization of PNIPAAm. In a typical procedure the cell is loaded with monomer(s) and initiator (2%wt), sealed and nitrogen is added to purge and test leaks. The nitrogen is slowly released and liquid carbon dioxide is loaded into the cell using a high-pressure compressor. The cell is immersed in the thermostatted water bath at 65ºC and temperature and pressure are allowed to rise to the required experimental conditions. Additional CO_2 may be added to reach the exact desired pressure. The reaction is allowed to proceed for 24h under stirring. Different proportions of HEMA and NIPAAm were tested as described in Table 3.4.

3.2.1.4 Polymer characterization

Nuclear magnetic resonance (NMR) analysis was used to confirm the structure and purity of the polymer. NMR spectra were performed in a Bruker equipment (ARX 400 MHz), using deuterated chloroform ($CDCl_3$) as solvent and internal reference.

Differential scanning calorimetry (DSC) was applied to investigate the thermal features. Analyses were performed from 0 to 40 °C at 3 °C/min under a dry nitrogen atmosphere (flow rate = 20 ml/min). Calibration for the temperature and energy scale was carried out using a pure indium standard.

Specific surface areas of the networks were determined by adsorption of N_2 according to the BET method. An accelerated surface area and porosimetry system (ASAP 2010 MICROMERITICS) was used under nitrogen flow.

The morphology of hydrogel particles was also evaluated using Scanning Electron Microscopy (SEM) in a Hitachi S-2400, with an accelerating voltage set to 15 kV.

3.2.2 Results and Discussion

3.2.2.1 Phase behaviour studies

Experimental data for CO_2 + HEMA system at 40ºC, 50ºC and 65ºC are shown in Table 3.3 and are graphically presented in Figure 3.9.

Table 3.3 - Experimental data for the CO_2 + HEMA system. BP-bubble point, CP-critical point. DP-dew point

T/ºC	x_{HEMA}	x_{CO2}	P/MPa	Transition
40	0.579	0.421	5.30	BP
	0.466	0.534	6.80	BP
	0.387	0.613	7.59	BP
	0.323	0.677	8.48	BP
	0.215	0.715	9.95	BP
	0.180	0.820	11.29	BP
	0.154	0.846	12.55	BP
	0.122	0.878	13.87	BP
	0.093	0.907	14.26	CP
	0.055	0.945	14.00	DP
	0.042	0.958	12.98	DP
	0.035	0.965	12.09	DP
	0.030	0.970	11.48	DP
	0.026	0.974	10.99	DP

T/ºC	x_{HEMA}	x_{CO2}	P/MPa	Transition
			0.00	
50	0.851	0.149	2.88	BP
	0.579	0.421	5.83	BP
	0.466	0.534	7.45	BP
	0.387	0.613	8.81	BP
	0.323	0.677	10.61	BP
	0.215	0.715	11.92	BP
	0.18	0.820	13.64	BP
	0.154	0.846	15.06	BP
	0.122	0.878	16.30	BP
	0.093	0.907	16.65	CP
	0.055	0.945	16.32	DP
	0.042	0.958	15.33	DP
	0.035	0.965	14.63	DP
	0.030	0.970	13.87	DP
	0.026	0.974	13.43	DP
			0.00	
65	0.851	0.149	2.75	BP
	0.579	0.421	7.00	BP
	0.466	0.534	8.89	BP
	0.387	0.613	10.71	BP
	0.323	0.677	14.12	BP
	0.215	0.715	16.90	BP
	0.18	0.820	17.25	BP
	0.154	0.846	18.27	BP
	0.122	0.878	19.42	BP
	0.093	0.907	21.04	CP
	0.055	0.945	19.39	DP
	0.042	0.958	18.35	DP
	0.035	0.965	17.76	DP
	0.030	0.970	16.89	DP
	0.026	0.974	16.41	DP

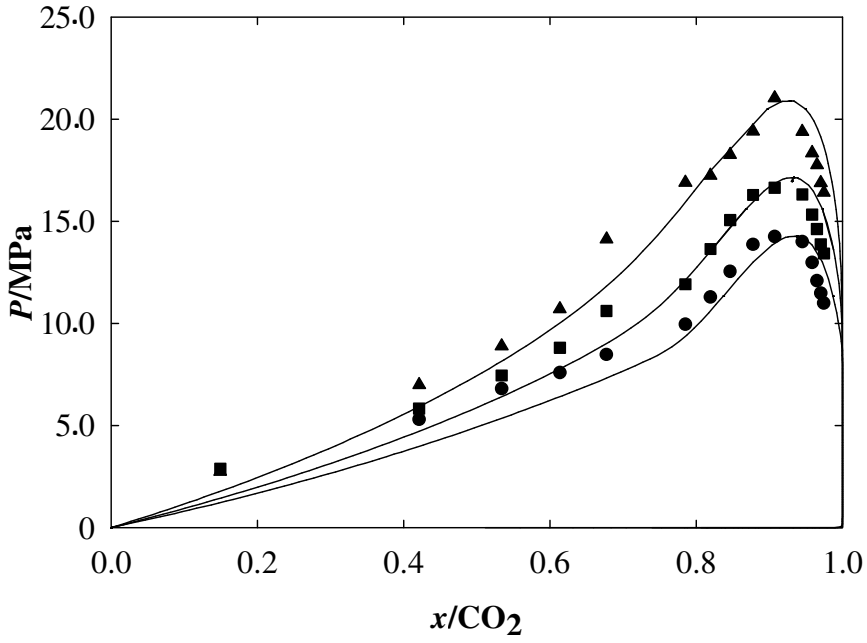

Figure 3.9 - Comparison of experimental data (symbols) for the CO_2 + HEMA system with calculated data (solid lines) obtained with the Soave-Redlich-Kwong equation of state with kij = - 0.0085, λij = 0.004 and lij = - 0.003. The black symbols (●, ■ and ▲) represent experimental data obtained in this study at 40ºC, 50ºC and 65ºC, respectively.

Solubility dependence with temperature is a well known phenomenon [52]. In general, for systems with a supercritical fluid as a component, temperature increase yields to solubility decrease. As expected, as the temperature increased the critical pressure of the mixture also increased. In fact as the temperature increased, a higher pressure was needed to obtain a single-phase solution from a two-phase solution. This means that the solubility decreases with the temperature increase.

3.2.2.2 Polymerizations reactions

A series of copolymers of HEMA and NIPAAm were prepared using $scCO_2$ as solvent. All the process parameters were fixed except the composition of the monomers that were used according to Table 3.4.

Table 3.4 - Experimental results obtained in the polymerization of HEMA and NIPAAm and copolymerization of HEMA with NIPAAm.

Entry	w (monomer)		Yield [2] (%)
	w (HEMA) (g)	w (NIPAAm) (g)	
PHEMA 0 [1]	-	0.9604	75
PHEMA 20	0.2184	0.7765	42
PHEMA 40	0.4559	0.5122	68
PHEMA 60	0.6203	0.3570	73
PHEMA 80	0.8058	0.1734	73
PHEMA 100 [1]	0.9861	-	82

[1] These entries correspond to PNIPAAm and PHEMA homopolymers respectively

[2] (collected material/(monomers +initiator weight))x100

With the addition of some HEMA proportions to the copolymerization, it was observed a decreased in the yield (75 to 42%) followed by an increase, which can be explained probably due to the loss of efficiency during copolymerization.

To confirm this supposition, NMR spectra for all the prepared polymers were obtained (Figure 3.11).

Figure 3.10 shows the ^{1}H NMR spectrum of PHEMA, which is consistent with the work presented by Ruckenstein and Zhang [53]. The NMR spectra also confirmed the structure, as well as its high purity after the efficient high-pressure CO_2 washing step at the end of the reaction.

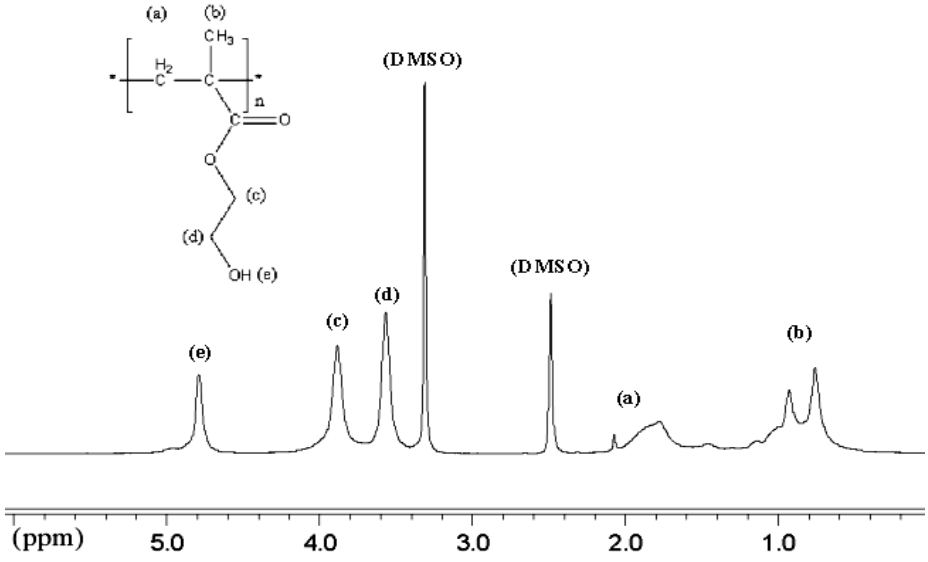

Figure 3.10 - ^{1}H NMR spectrum for PHEMA

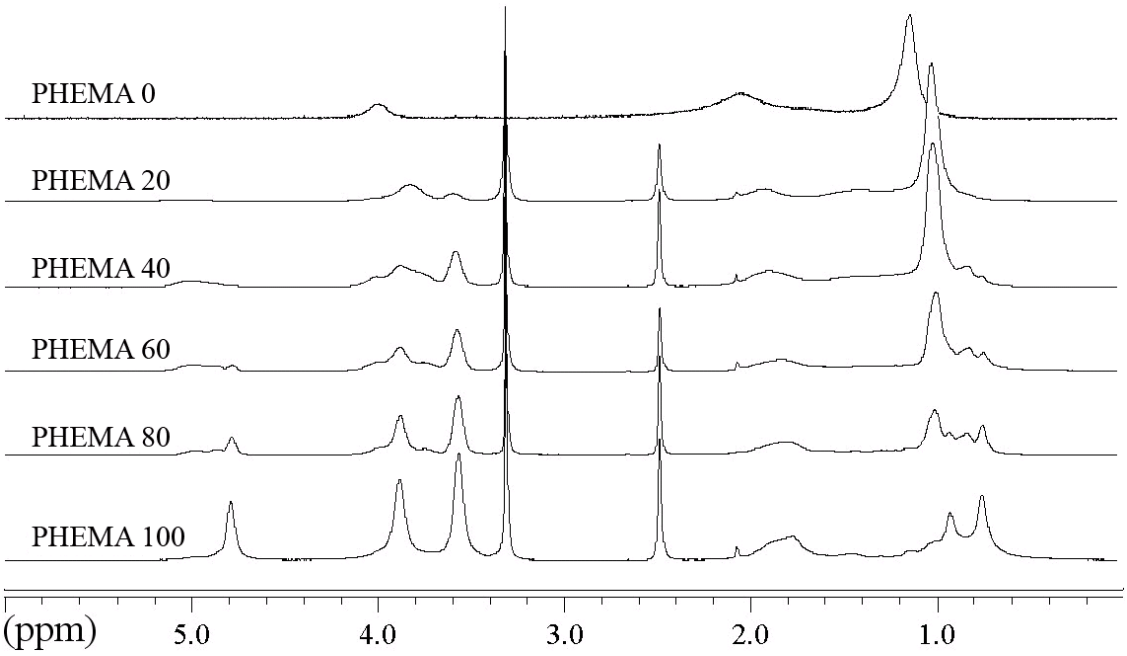

Figure 3.11 - NMR for the different HEMA-NIPAAm copolymers. Labelling according to Table 3.4

In Figure 3.11 is presented the ^{1}H NMR spectra of the entries in Table 3.4. As expected an increase in the amount of monomer promotes the insertion in the random copolymers, which is particularly evident for the peak corresponding to the hydroxyl group (peak (e) from Figure 3.10).

The morphology of the polymers is also an important parameter to characterize. Figure 3.12 presents the typical morphology of the hydrogels produced, where it can be seen that these polymeric materials are formed by agglomerates of small and discrete particles. Particle size tends to decrease with the addition of the thermoresponsive polymer.

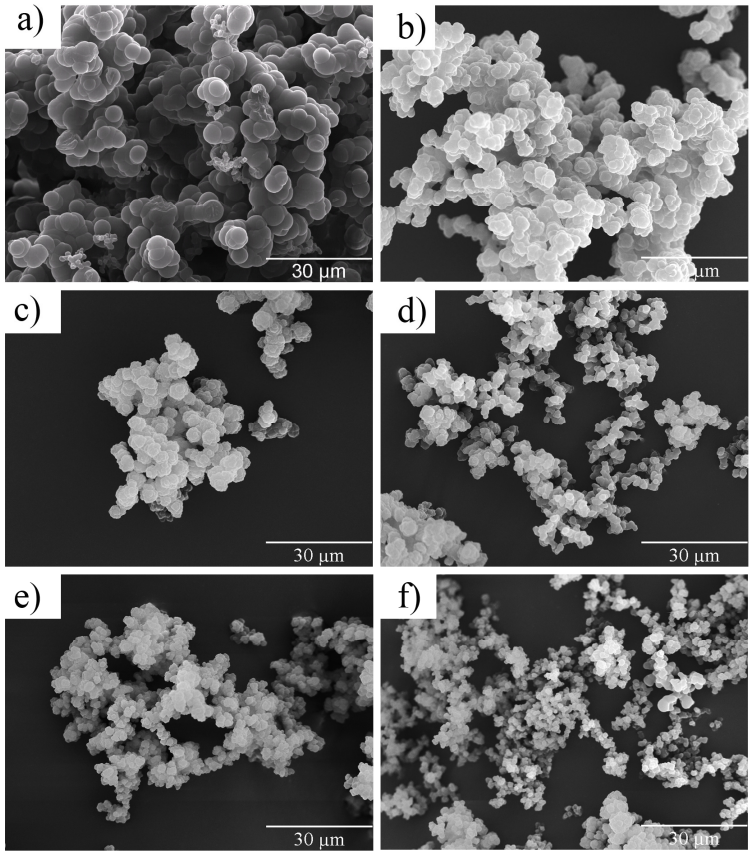

Figure 3.12 – Scanning electron microscopy images of the hydrogels prepared in different conditions. Samples: a) PHEMA 0; b) PHEMA 20; c) PHEMA 40; d) PHEMA 60; e) PHEMA 80; f) PHEMA 100.

In precipitation polymerization [54] both monomer and initiator are soluble in the continuous phase but as the polymer grows the insoluble polymer chains precipitate and the particles tend to group forming an undefined, agglomerated powder.

Spherical particles would be obtained if a stabilizer was added to the initial mixture of monomer(s) and initiator [55].

Finally to confirm the influence of HEMA in the LCST several DSC runs were performed (Figure 3.13). In these tests the polymers were mixed with a small amount of water in order to observe the first order transition that is characteristic of a LCST.

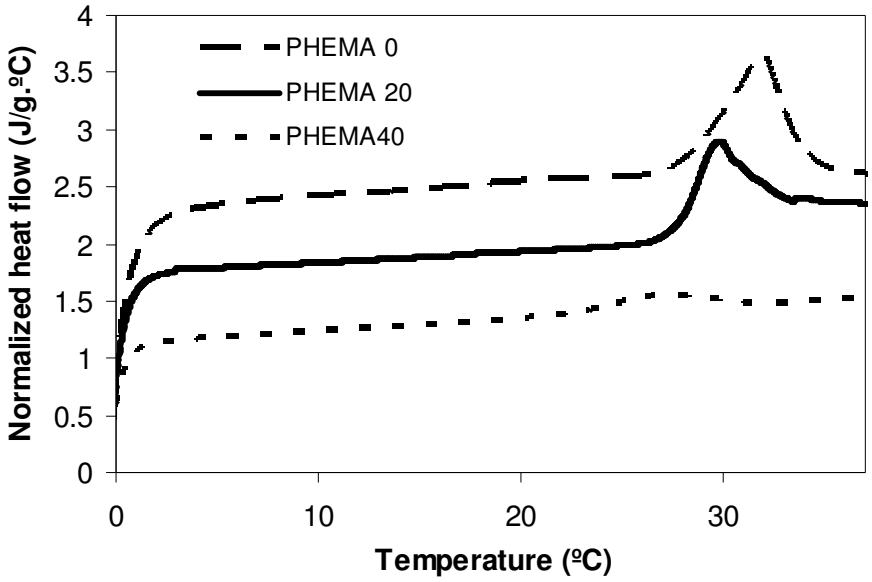

Figure 3.13 – DSC thermograms of the thermoresponsive hydrogels prepared

It was observed that hydrogels with less than 60-70 w/w % NIPAAm (PHEMA 60, PHEMA 80 and PHEMA 100) do not present any thermoresponsive behavior which is in accordance with literature [56]. For the polymers labeled with the name PHEMA 20 and PHEMA 40 a decrease in the LCST from 32.2 ºC to 30.1 ºC and 27.7 ºC respectively was observed. This behavior is in accordance to what is reported in the literature [57]. Nevertheless there are also papers in the literature that report an increase in the LCST with the copolymerization of NIPAAm with HEMA [58, 59, 60]. A possible explanation to the contradictions is the influence of molecular weight in the LCST transitions. In the case of $scCO_2$, without any surfactants, only low molecular weight polymers should be produced.

3.2.3 Conclusions

Phase behavior studies for the system CO_2 + HEMA were performed in order to optimize the operational conditions for the HEMA polymerization. The SEM images showed that the synthesized polymeric materials are formed by agglomerates of small and discrete particles and an efficient decrease in the LCST was possible to attain with the copolymerization of NIPAAm with HEMA.

3.3 Increasing the LCST

In this section it was investigated the polymerisation of NIPAAM with a more hydrophilic monomer in $scCO_2$ medium in order to produce a polymer with higher gelation temperature. PEO also known as poly(ethylene glycol) (PEG), is a good example of an hydrophilic polymer. It is also one of the most commercially important type of polyether and one the polymers with more applications in the medical field.

Several works have been published reporting the graft, block or the copolymerization of Polyethylene oxide with PNIPAAm [61, 62, 63, 64, 65, 66]. In this work it is presented the graft polymerization of NIPAAm with varying amounts of ethylene oxide olygomers in scO_2. The effect of copolymer composition on swelling and thermal behaviour was evaluated.

3.3.1 Experimental

3.3.1.1 Materials

N-isopropylacrylamide (97% purity), poly(ethylene glycol) methyl ether acrylate (Mn ~454 g/mol) and 2,2`-azobis (isobutyronitrile) (AIBN, 98% purity, Sigma-Aldrich) were used as received. Carbon dioxide and nitrogen were obtained from Air Liquide with 99.998 % and 99.995% purity respectively.

3.3.1.2 Polymers preparation

Poly N-isoprpylacrylamide-graft-poly(ethylene oxide) (PAN-g-PEO) was synthesized by free radical polymerization following a the previous procedure.

The polymerization procedure and the operational conditions 65ºC and 25 MPa were similar to the ones that were used in previous chapters (2% w/w initiator). The reaction started in a homogeneous phase. In Table 3.4 it is summarized the conditions that were used.

Table 3.5 – Details of feed composition, sample designation for grafted polymers prepared and experimental results obtained in the graft polymerization of EO and NIPAAm

Entry	w (monomer)		Yield [1] (%)
	w (PEO) (g)	w (NIPAAm) (g)	
PNIPAAm-g-PEO 10	0.100	0.885	77%
PNIPAAm-g-PEO 20	0.200	0.791	63 %
PNIPAAm-g-PEO 30	0.300	0.707	62 %

[1] (collected material/(monomers +initiator weight))x100

3.3.2 Results and discussion

Thermal characterization of the gels was done using DSC. Fully swollen gels were taken for recording DSC scans in the temperature range of 0 to 80 ºC at a heating rate of 3 ºC/min.

The DSC thermograms for the prepared hydrogels are shown in Figure 3.14.

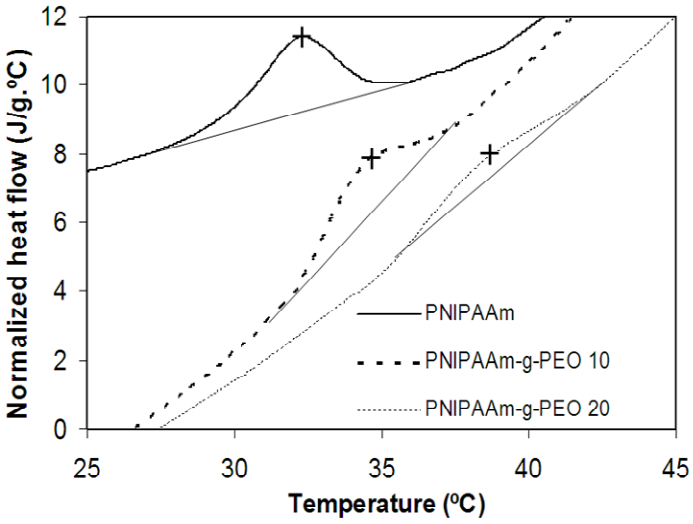

Figure 3.14 – DSC thermograms of the PNIPAAm-PEO hydrogels

With the introduction of the PEO chains the phase transition temperature shifted from the usual value of 32 ºC to 34.3 ºC and 37.7 ºC for PNIPAAm-g-PEO 10 and 20 respectively. Hydrogels with 30% w/w did not presented any temperature responsive behaviour.

Incorporation of hydrophilic comonomers reduces the ratio of hydrophobic groups allowing more water and hydrophilic group interactions to be established. As the temperature is increased, hydrophobic domains aggregate to minimize the hydrophobic surface area contacting the bulk water, reducing the amount of structured water surrounding the hydrophobic domains and maximizing the solvent entropy. The temperature at which gelation occurs depends on concentration of the polymer, the length of the hydrophobic block, and the chemical structure of the polymer: the more hydrophilic the segment, the smaller the entropic cost of water structuring, the lower driving force for hydrophobic aggregation and therefore the higher the gelation temperature [67, 68].

3.3.3 Conclusion

On the basis of the present investigations it can be concluded that it is possible to prepare graft thermoresponsive polymers in supercritical medium and that it is possible to increase the gelation transition temperature (LCST) by copolymerizing PNIPAAm with other hydrophilic monomers.

3.4 Dual stimulus – pH/Thermoresponsive polymers

Recently, a much great attention has been drawn to the development of dual-stimuli-responsive hydrogels, especially for the delivery vehicles that respond to localized conditions of pH and temperature in the human body. These hydrogels may be prepared by combining PNIPAAm with other monomers containing weakly acidic groups, such as acrylic acid [69]. Poly (methacylic acid) (PMAA) is a hydrophilic polymer that exhibits a greatly pH-dependent swelling behaviour due to the ionization / deionization of the carboxylic acid groups, swelling to high degrees in basic solutions (pH >7) and collapsing in acidic pHs. Due to their drastic swelling in response to pH changes, these polymeric hydrogels have been studied for many biomedical applications [70] such as intelligent matrices in the controlled or targeted drug release.

This section reports the copolymerization of NIPAAm and MAA, in different proportions, in $scCO_2$, using AIBN (2% wt/wt) as initiator at 65 ºC and pressures up to 22 MPa. A model drug (5-Fluorouracil) was used to access the ability to control drug release by external stimulus – pH and temperature.

3.4.1 Experimental

3.4.1.1 Materials

Methacrylic acid (MAA), N-isopropylacrylamide (NIPAAm, 97% purity), N,N-methylenebisacrylamide (MBAm, purity ≥85%), 2,2´-azobis(isobutyronitrile) (AIBN, 98%

purity), ethylene glycol dimethacrylate (EGDMA), 5-Fluorouracil (5-FU) were purchased from Sigma Aldrich and used without further modifications. Carbon dioxide was obtained from Air Liquide with 99.998% purity.

3.4.1.2 Synthesis of poly (NIPAAm-co-MAA)

Polymerization reactions were carried out in the high-pressure apparatus previously described (Chapter 3.1, Figure 3.1). As a typical procedure, the monomers (NIPAAm and MAA) the cross-linking agent (MBAm or EGDMA, 1%) and initiator (AIBN, 2 wt%) are loaded into the high pressure cell, which is then sealed and nitrogen is added to purge the cell and test leaks. The nitrogen is slowly released and liquid carbon dioxide is loaded into the cell using a high-pressure compressor. The cell is immersed in a water bath (65ºC) and the pressure is allowed to increase slowly at the required experimental conditions (22 MPa). At these conditions all the monomers are soluble what can be confirmed by the existence of a single phase inside the high pressure cell. Reactions were allowed to proceed for 24 hours, under continuous magnetic stirring.

After polymerization a continuous flow of high pressure CO_2 was passed through the cell, during 1 hour, in order to remove / wash the unreacted monomers, the cross-linker and the initiator (65ºC and 22MPa). After this time, the cell was slowly depressurized for 10 minutes. Different concentrations of MAA were tested as summarized in Table 3.6.

Table 3.6 - Formulations used for the synthesis, sample designations and experimental results obtained in the copolymerisation of NIPAAm and MAA

Formulations	Crosslinker (1%)[1]	MAA (mg)	NIPAAm (mg)	Yield (%)	LCST ºC
MAA 0	MBAm	0	978	95	32.2
MAA 20	MBAm	160	839	89	29.3
MAA 40	MBAm	337	662	90	-
MAA 90	MBAm	890	103	88	-
MAA 100	EGDMA	1000	0	83	-

[1]Weight of cross-linker / total weight (NIPAAm, MAA, AIBN, cross-linker)

3.4.1.3 Structural/Morphological Analysis

The morphology of hydrogel particles was also evaluated using Scanning Electron Microscopy (SEM) in a Hitachi S-2400, with an accelerating voltage set to 15 kV.

Because these hydrogels were crosslinked during polymerization it was possible to study the swelling degree (W,%) of synthesised the hydrogels impregnated/coated with PNIPAAm was determined as defined in chapter 3.1.

The measurements were performed with 3 replicas in order to verify the reproducibility of the experimental data. Phosphate-buffered solution (pH 7.4) and acetate-buffered solution (pH 5.5) with the same ionic strength were used. The oscillatory swelling experiments were conducted to investigate whether the hydrogels present any response to the environmental pH and temperature changes and if this changes were reversible and to examine how fast the hydrogels could respond to the stimuli.

3.4.1.4 Drug loading

The dried hydrogels were immersed in 1mg 5-FU / ml distillated water solution (100 ml) at 20ºC, for at least 24 hours to reach the equilibrated state. During this period, the drug diffused into the hydrogel network with the water. After this, the solutions were filtered using filter paper and washed with fresh distilled water. The hydrogel was collected from the filter paper and then lyophilized for 24 hours (Telstar cryodos-50).

3.4.1.5 In vitro drug release study

5-FU release experiments were monitored under pulsatile conditions into pH buffered solutions (pH 2 and 7.4). The pH was adjusted by adding HCl 4M to obtain acid media (pH = 2), or by adding NaOH 8M to obtain basic media (pH = 7.4). The experiments were conducted by immersing the drug loaded hydrogels into buffer solutions (100 ml). Temperature was varied between 20 ºC and 37 ºC. At a series of different time points, 1 ml of sample was removed without reposition of additional solution. The release period was extended over several cycles until no further drug was released. Samples were frozenat − 20 °C until analyzed. The 5-FU released was monitored at 266 nm, using the UV spectrophotometer (Helios Alpha Double-Beam UV / VIS Spectrophotometer). Calibration curve was obtained by using 5-FU standard samples with concentrations between 0.001 and 0.05 mg/ml in the same buffer. Before measuring the absorvance, samples were centrifuged (Sigma Santorius 1-15K, 10.000 rpm, for 30 min at 5ºC).

3.4.2 Results and discussion

The morphology of the hydrogels is very similar to the previous results (Figure 3.15) with particles with undefined shape agglomerated. The decrease in the particle size is also observed with the addition of the pH sensitive monomer.

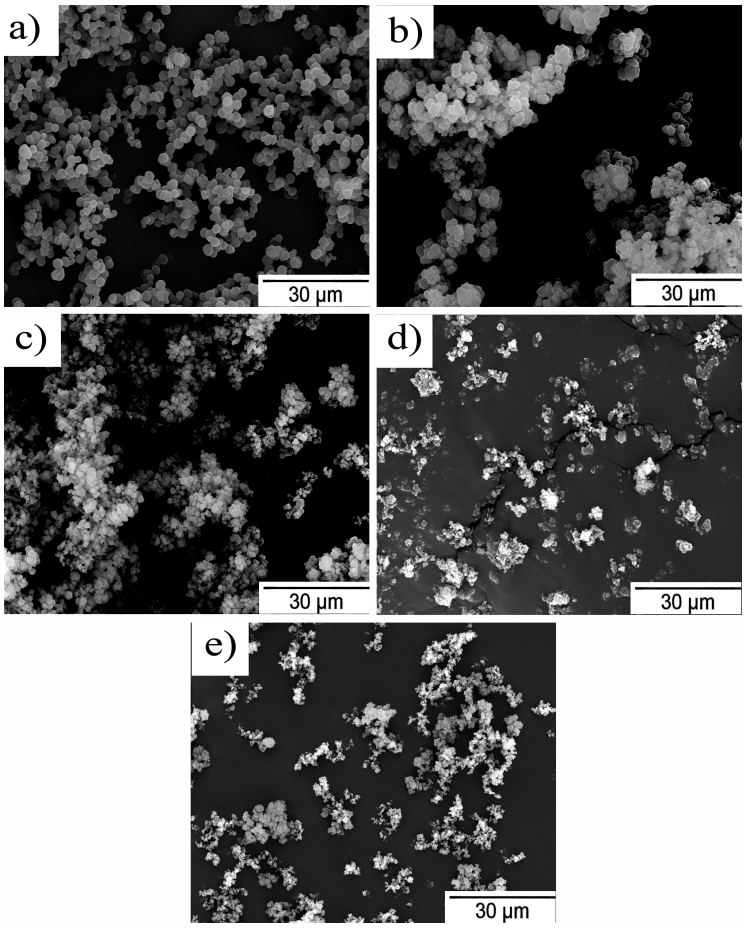

Figure 3.15 – Scanning electron microscopy images of the hydrogels prepared with different monomer proportions. a) MAA 0; b) MAA 20; c) MAA 40; d) MAA 90; e) MAA 100

In relation to the LCST, it is reported in the literature that in the case of copolymerization of PNIPAAm with acid monomers, the effect on the LCST behavior of PNIPAAm by random copolymerization is very delicate and depends not only on copolymer composition but also on ionization degree and especially on the chemical identity of the comonomer [71]. For the particular case of copolymerization with methacrylic acid a decrease in the LCST should be expected [72] as it is presented in table Table 3.6.

In order to analyze their applicability as drug delivery vehicles, these hydrogels were crosslinked. With the exception of MAA 100 (Figure 3.15 e) that was crosslinked with EGDMA all the other

reacted with MBA. This was due to the loss of efficiency in the reticulation procedure of the homopolymerization of methacrylic acid polymerization.

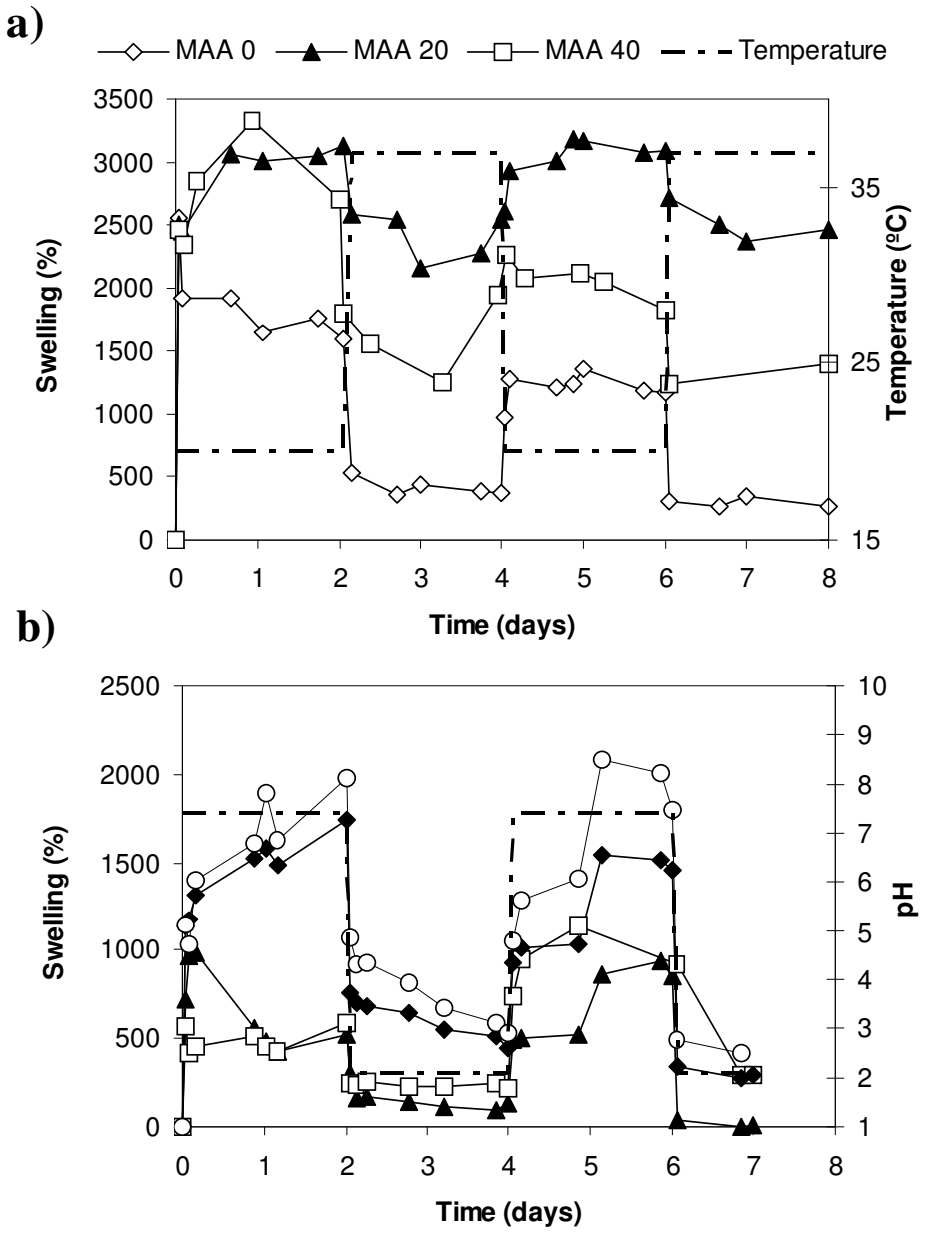

Figure 3.16 – Equilibrium volume swelling ratio of a) thermoresponsive hydrogels (MAA0, MAA20 and MAA40) in a PBS solution at 37 °C as function of temperature and b) Pulsatile swelling behavior in response to a stepwise pH change between 2.1 and 7.4 at 37°C.

The swelling degree of a drug delivery hydrogel is an important property to be characterized, since it will determine properties such as the absorption/ diffusion of solutes through the hydrogel and the ability to respond to external stimulus. In Figure 3.16 it is presented the swelling under different pH and temperature conditions.

As reported before in the previous sections, we should not expect that the hydrogels, with lower contents of PNIPAAm, possess any response to temperature changes. This was observed with the swelling (Figure 3.16 a) and DSC measurements that confirmed the thermoresponsive behavior only in the hydrogels MAA0, MAA20 and MAA40. A small decrease in the LCST was also observed. The introduction of MAA groups allowed higher swelling without compromising the ability to respond to temperature. This phenomenon is due to the desprotonation of the methacrylic acid groups at the swelling conditions (pH=7.4). To compensate the negative charges the hydrogel incorporates more water in its structure. This is confirmed with the results of Figure 3.16 b) that presents the swelling vs pH. The hydrogels with higher MAA content present intense pulse effect as expected due to the presence of a higher content of carboxylic acid groups.

As proof of concept, that the swelling could be used to control the release of drugs, Flurouacil was incorporated in the hydrogel network and the controlled released was performed with temperature and pH pulse.

In Figure 3.17a) it is shown the release profiles for the three thermoresponsive hydrogels MAA0, MAA20 and MAA40. The initial drug release (first time point) was subtracted to eliminate the effect of burst release directly related with the drug that it is not present in the hydrogel structure but it is directly available in its surface [73].

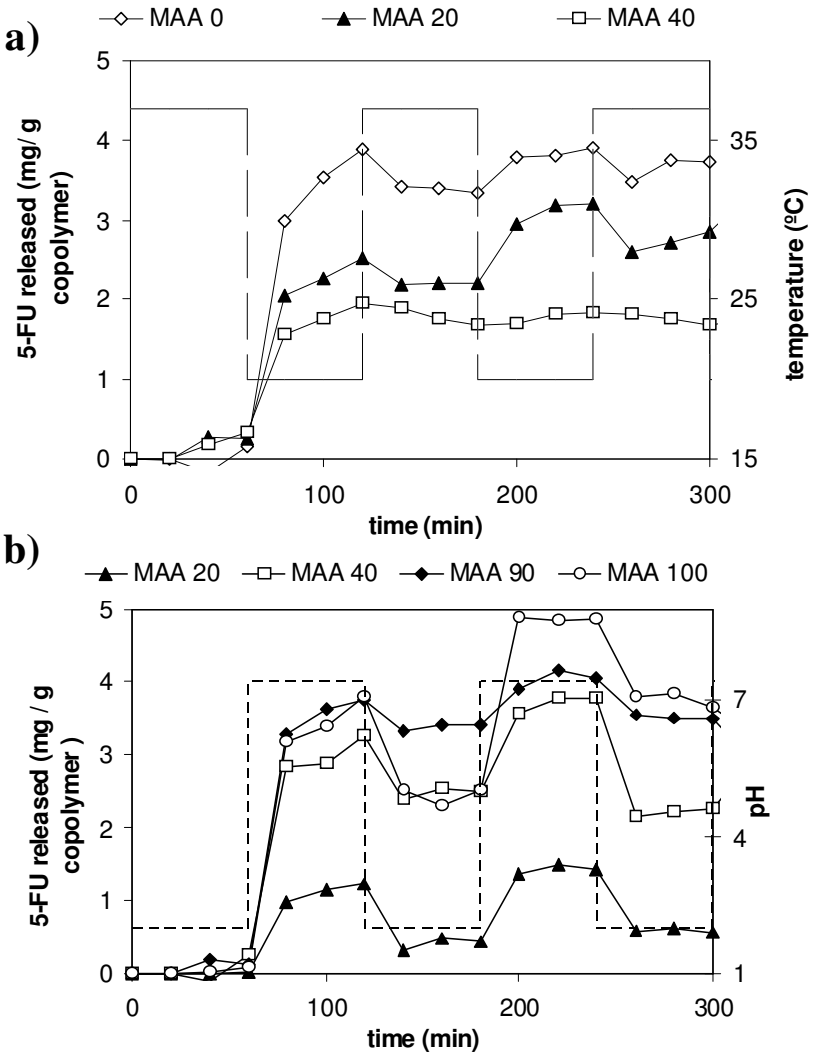

Figure 3.17 – Fluorouacil release profiles for the PNIPAAm-co-MAA hydrogels at different pH and temperature conditions. a) Temperature pulse effect at pH 7.4; b) pH pulse effect at 37ºC.

It is interesting to observe the temperature pulse. At 37ºC only a small amount of drug is released to the phosphate buffer solution. This is explained due to the shrunken state of the hydrogel that does not allow the release of the drug. In opposition when the temperature is decreased and the transition from the shrunken state to a swelled state occur almost all the drug is released immediately. The differences between the amount of drug released (~2 mg 5-FU/ g hydrogel in

MAA 40 and ~4 mg 5-FU/ g hydrogel in MAA 0) can be explained due to the different electrostatic charges of the drug and hydrogel. The in vitro drug release with a pH *stimulus* (Figure 3.17b) confirmed that this stimulus could be used to control the drug release. Even the hydrogel with the lowest amount of metacrylic acid (MAA20) presented a pulse effect.

3.4.3 Conclusion

The hydrogels investigated in this work were shown to display both temperature and pH-sensitivity. The transitions from the collapsed to the swollen state influenced drug released. Fluorouacil was used as proof of concept in order to investigate the influence of temperature and pH pulses in the release of drugs.

3.5 References

[1] H.G. Schild, Poly(N-isopropylacrylamide): experiment, theory and application, *Prog. Polym. Sci*. 17 (**1992**) 163-249.

[2] V. V. A. Fernandez, N. Tepale, J. C. Sanchez-Diaz, E. Mendizabal, J. E. Puig and J. F. A. Soltero, Thermoresponsive nanostructured poly(N -isopropylacrylamide) hydrogels made via inverse microemulsion polymerization *Colloid Polym. Sci*. 284 (**2006**) 387-395.

[3] T. Okano, N. Yamada, H. Sakai, Y. Sakurai, A novel recovery system for cultured cells using plasma-treated polystyrene dishes grafted with poly(N-isopropylacrylamide) *J. Biomd. Mat. Res*. 27 (**1993**) 1243-1251.

[4] P. S. Stayton, T. Shimoboji, C. Long, A. Chilkoti, G. Chen, J. M. Harris and A. S. Hoffman, Control of protein-ligand recognition using a stimuli-responsive polymer,*Nature* 378 (**1995**) 472-474

[5] Y. Qiu and K. Park, Environment-sensitive hydrogels for drug delivery, *Adv. Drug Delivery Rev*., 53 (**2001**) 321-339.

[6] L. C. Dong and A. S. Hoffman, Thermally reversible hydrogels: III. Immobilization of enzymes for feedback reaction control, *J. Control. Release* 4 (**1986**) 223-227.

[7] R.A. Stile, W. R. Burghardt and K. E. Healy, Synthesis and Characterization of Injectable Poly(N-isopropylacrylamide)-Based Hydrogels That Support Tissue Formation in Vitro, *Macromolecules* 32 (**1999**) 7370-7379.

[8] K.-H. Park and Y. H. Bae, Phenotype of hepatocyte spheroids in Arg-GLY-Asp (RGD) containing a thermo-reversible extracellular matrix, *Biosci. Biotechnol. Biocehm*. 66 (**2002**) 1473-1478.

[9] R.H. Pelton and P. Chibante, Preparation of aqueous latices with N-isopropylacrylamide, *Colloids Surf*. 20 (**1986**) 247-256.

[10] S.-X. Cheng, J.-T. Zhang and R.-X. Zhuo, Macroporous poly(N-isopropylacrylamide) hydrogels with fast response rates and improved protein release properties, *J. Biomed. Mater. Res*. 67A (**2003**) 96-103.

[11] X. Zhang, Y. Yang, T. Chung and K. Ma, Preparation and Characterization of Fast Response Macroporous Poly(N-isopropylacrylamide) Hydrogels, *Langmuir*,17 (**2001**) 6094-6099.

[12] R.-X Zhuo and W. Li, Preparation and characterization of macroporous poly(N-isopropylacrylamide) hydrogels for the controlled release of proteins, *J. Polym. Sci. A Polym. Chem*. 41 (**2003**) 152-159.

[13] J.-T Zhang, S.-W Huang and R.-X Zhuo, Preparation and Characterization of Novel Temperature Sensitive Poly(N-isopropylacrylamide-co-acryloyl beta-cyclodextrin) Hydrogels with Fast Shrinking Kinetics, *Macromol. Chem. Phys*. 205 (**2004**) 107-113.

[14] X.-Z Zhang and R.-X Zhuo, Preparation of fast responsive, thermally sensitive poly(N-isopropylacrylamide) gel, *Eur. Polym. J*. 36 (**2000**) 2301-2303.

[15] X.-Z. Zhang and C.-C. Chu, Synthesis of temperature sensitive PNIPAAm cryogels in organic solvent with improved properties, *J. Mater. Chem*., 13 (**2003**) 2457-2464.

[16] D. Kuckling, C. D. Vo, H.-J. P. Adler, A. Völkel and H. Cölfen, Preparation and Characterization of Photo-Cross-Linked Thermosensitive PNIPAAm Nanogels, *Macromolecules*, 39 (**2006**) 1585-1591.

[17] A. I. Cooper, Polymer synthesis and processing using supercritical carbon dioxide, *J. Mater. Chem*., 10 (**2000**) 207-234.

[18] J. L. Kendall, D. A. Canelas, J. L. Young and J. M. DeSimone, Polymerizations in Supercritical Carbon Dioxide, *Chem. Rev*. 99 (**1999**) 543-564.

[19] T. Casimiro, A. M. Banet-Osuna, A. M. Ramos, M. Nunes da Ponte and A. Aguiar-Ricardo, Synthesis of highly cross-linked poly(diethylene glycol dimethacrylate) microparticles in supercritical carbon dioxide, *Eur. Polym. J*, 41 (**2005**) 1947-.1953

[20] F. A. Adamsky and E. J. Beckman, Inverse emulsion polymerization of acrylamide in supercritical carbon dioxide, Macromolecules, 27 (1994) 312-314; (b) W. Ye and J. M. DeSimone, Emulsion Polymerization of N-Ethylacrylamide in Supercritical Carbon Dioxide, *Macromolecules*, 38 (**2005**) 2180-2190.

[21] P. J. VandeVord, H.W. T. Matthew, S. P. DeSilva, L. Mayton, B. Wu and P. H. Wooley, Evaluation of the biocompatibility of a chitosan scaffold in mice, *J. Biomed. Mater. Res*. 59 (**2002**) 585-590.

[22] K. Tuzlakoglu, C. M. Alves, J. F. Mano and R. L. Reis, Production and Characterization of Chitosan Fibers and 3-D Fiber Mesh Scaffolds for Tissue Engineering Applications, *Macromol. Biosci*. 4 (**2004**) 811-819

[23] A. Di Martino, M. Sittinger, M.V. Risbud, Chitosan: A versatile biopolymer for orthopaedic tissue-engineering, *Biomaterials* 26 (**2005**) 5983-5990.

[24] M. Temtem, T. Casimiro and A. Aguiar-Ricardo, Solvent power and depressurization rate effects in the formation of polysulfone membranes with CO2-assisted phase inversion method, *J. Membr. Sci*., 283 (**2006**) 244-252.

[25] A. I. Cooper, W. P. Hems and A. B. Holmes, Synthesis of Highly Cross-Linked Polymers in Supercritical Carbon Dioxide by Heterogeneous Polymerization, *Macromolecules*, 32 (**1999**) 2156-2166;

[26] R. Arshady, Suspension, emulsion, and dispersion polymerization: A methodological survey, *Colloid Polym. Sci*., 270 (**1992**) 717-732.

[27] W. Wang, R. M. T. Griffiths, A. Naylor, M. R. Giles, D. J. Irvine and S. M. Howdle, Preparation of cross-linked microparticles of poly(glycidyl methacrylate) by dispersion polymerization of glycidyl methacrylate using a PDMS macromonomer as stabilizer in supercritical carbon dioxide, *Polymer* 43 (**2002**) 6653-6659.

[28] C. Sayil and O. Okay, Macroporous poly(N-isopropylacrylamide) networks, *Polymer Bulletin*, 48 (**2002**) 499-506.

[29] M. Chapekar, Tissue engineering: Challenges and opportunities, *J. Biomed. Mater. Res*. 53 (**2000**) 617-620.

[30] X. Liu and P.X. Ma, Polymeric scaffolds for bone tissue engineering *Annals Biomed. Eng*. 32 (**2004**) 477-486.

[31] V. Karageorgiou and D. Kaplan, Porosity of 3D biomaterial scaffolds and osteogenesis, *Biomaterials*, 26 (**2005**) 5474-5491.

[32] S.V. Madihally and H.W.T. Matthew, Porous chitosan scaffolds for tissue engineering, *Biomaterials*, 20 (**1999**) 1133-1142.

[33] F.M. Winnik, M.F. Ottavianni, S.H. Bossnann, M. Garcia-Garibay, N.J. Turro, Cosolvency of poly(N-isopropylacrylamide) in mixed water–methanol solutions: a look at spin labeled polymers. *Macromolecules* 25 (**1992**) 6007–6017.

[34] H.G. Schild, D.A. Tirrell. Microcalorimetric detection of lower critical solution temperatures in aqueous polymer solutions. *J. Phys. Chem*. 94 (**1990**) 4352–4356.

[35] H.G. Schild, D.A. Tirrell, Interaction of poly(N-isopropylacrylamide) with sodium n-alkylsulfates in aqueous solution. *Langmuir* 7 (**1991**) 665–71.

[36] M.K. Yoo, Y.K. Sung, C.S. Cho, Y.M. Lee. Effect of polymer complex formation on the cloud-point of poly(N-isopropylacrylamide) (PNIPAAm) in the poly(NIPAAm-coacrylic acid): polyelectrolyte complex between poly(acrylic acid) and poly(allylamine). *Polymer* 38 (**1997**) 2759–2765.

[37] H. Feil, Y. H. Bae, J. Feijen, S. W. Kim. Effect of Comonomer Hydrophilicity and Ionization on the Lower Critical Solution Temperature of N-Isopropylacrylamide Copolymers. *Macromolecules*, 26 (**1993**) 2496-2500.

[38] H.G. Schild, Poly(N-isopropylacrylamide): experiment, theory and application, *Prog. Polym. Sci*. 17 (**1992**) 163– 249.

[39] R.W. Korsmeyer, E.W. Meerwall, N.A. Peppas. Solute and penetrant diffusion in swellable polymers. II. Verification of theoretical models, *J Polym Sci Polym Phys*. 24 (**1986**) 409-434.

[40] N. M. Franson, N. A. Peppas, Influence of copolymer composition on non-fickian water transport through glassy copolymers. *J Appl Polym Sci* 28 (**1983**) 1299-1310.

[41] N.A. Peppas, Y. Huang, M. Torres-Lugo, J. H. Ward, J. Zhang, Physicochemical Foundations and structural design of hydrogels in medicine and biology. *Annu. Rev. Biomed. Eng.* 2 (**2000**) 9-29.

[42]H. Cicek, A. Tuncel, Preparation and Characterization of Thermoresponsive Isopropylacrylamide–Hydroxyethylmethacrylate Copolymer Gels. *J Polym Sci Part A*: *Polym Chem*, 36 (**1998**) 527–541.

[43] Z. Shen, K. Terao, Y. Maki, T. Dobashi, G. Ma, T. Yamamoto, Synthesis and phase behavior of aqueous poly(N-isopropylacrylamide-co-acrylamide), poly(N-isopropylacrylamide-co-N,N-dimethylacrylamide) and poly(N-isopropylacrylamide-co-2-hydroxyethyl methacrylate). *Colloid Polym Sci*, 284 (**2006**) 1001–1007.

[44] Z. Cao,W. Liu, G Zhao, X Lin, X Gao, P Yao K. N-Isopropylacrylamide/2-Hydroxyethyl Methacrylate Star Diblock Copolymers: Synthesis and Thermoresponsive Behavior. *Macromol Chem Phys*, 207 (**2006**) 2329–2335

[45] H. Shiho, J. M. DeSimone, Dispersion Polymerization of 2-Hydroxyethyl Methacrylate in Supercritical Carbon Dioxide. *J Polym Sci Part A: Polym Chem*, 38 (**2000**) 3783–3790.

[46] N. Ribeiro, T. Casimiro, C. Duarte, M. Nunes da Ponte, A. Aguiar-Ricardo, Vapor-Liquid Equilibrium and Critical Line of the CO2 + Xe System. Critical behavior of CO_2 + Xe versus CO + n-Alkanes. *J. Phys. Chem.*, 104 (**2000**) 791-795.

[47] A. Aguiar-Ricardo, M. Temtem, T. Casimiro, N. Ribeiro,, A visual accoustic high-pressure cell for the study of critical behavior of nonsimple mixtures. *Rev. Sci. Instrum.*, 75 (2004) 3200-3202.

[48] G. Soave, Equilibrium constants from a modified Redlich-Kwong equation of state, *Chem. Eng. Sci.*, 27 (**1972**) 1197-1203.

[49] P.M. Mathias, H. C. Klotz, J. M. Prausnitz, Equation-of-state mixing rules for multicomponent mixtures: the problem of invariance. *Fluid Phase Equilibr.*, 67 (**1991**) 31-44.

[50] R. Ruivo, A. Paiva, P. Simões, Phase equilibria of the ternary system methyl oleate/squalene/carbon dioxide at high pressure conditions. *J. of Supercritical Fluids*, 29 (**2004**) 77-85.

[51] O. Pfohl, S. Petkov, G. Brunner, *Usage of PE – A Program to Calculate Phase Equilibria*, Herbert Utz Verlag: München, **1998**.

[52] L. A. Blanchard, Z. Gu, J. F. Brennecke, High-Pressure Phase Behavior of Ionic Liquid/CO_2 Systems, *J. Phys. Chem. B*, 105 (**2001**) 2437-2444.

[53] E. Ruckenstein, H. Zhang, Well-defined poly(2-hydroxyethyl methacrylate) and its amphiphilic block copolymers via acidolysis of anionically synthesized poly(2-vinyloxyethyl methacrylate), *Polymer Bulletin*, 47 (**2001**) 113-119.

[54] A. I. Cooper, W. P. Hems, A. B. Holmes, Synthesis of Highly Cross-Linked Polymers in Supercritical Carbon Dioxide by Heterogeneous Polymerization, *Macromolecules*, 32 (**1999**) 2156-2166.

[55] M. R. Giles, R.T.M Griffiths, A. Aguiar-Ricardo, M.M.C.G. Silva, S.M. Howdle, Fluorinated Graft Stabilizers for Polymerization in Supercritical Carbon Dioxide: The Effect of Stabilizer Architecture, *Macromolecules*, 34 (**2001**) 20-25.

[56] J. Zhang, N.A. Peppas, Synthesis and Characterization of pH- and Temperature-Sensitive Poly(methacrylic acid)/Poly(N-isopropylacrylamide) Interpenetrating Polymeric Networks. *Macromolecules* 33 (**2000**) 102 -107.

[57] Z. Shen, K. Terao, Y. Maki, T. Dobashi, G. Ma, T. Yamamoto, Synthesis and phase behavior of aqueous poly(N-isopropylacrylamide-co-acrylamide), poly(N-isopropylacrylamide-co-N, N-dimethylacrylamide) and poly (N-isopropylacrylamide-co-2-hydroxyethyl methacrylate), *Colloid. Polym. Sci*. 284 (**2006**) 1001–1007.

[58] A. Tuncel, An engineering analysis for the continuous reactor behavior of a-chymotrypsin-immobilized thermosensitive gel cylinders, *J. Biotechnol*. 63 (**1998**) 41-54

[59] M. Bayhan and A. Tuncel, Uniform poly(isopropylacrylamide) gel beads for immobilization of -chymotrypsin, *J Appl Polym Sci* 67 (**1998**) 1127-1139.

[60] C. Ni, Z. Wang, X.X. Zhu, Preparation and Characterization of Thermosensitive Beads with Macroporous Structures. *J. Appl. Polym. Sci*., 91 (**2004**) 1792–1797.

[61] K. K. Lee, J. C. Jung, M. S. Jhon, The synthesis and thermal phase transition behavior of poly(N-isopropylacrylamide)-b-poly(ethylene oxide) *Polymer Bulletin* 40 (**1998**) 455–460.

[62] S. Qin, Y. Geng, D. E. Discher, and S. Yang, Temperature-Controlled Assembly and Release from Polymer Vesicles of Poly(ethylene oxide)-block-poly(N-isopropylacrylamide), *Adv. Mater*. 18 (**2006**) 2905–2909

[63] C.-Y. Hong, Y.-Z. You, C.-Y. Pan, Synthesis and Characterization of Well-Defined Diblock and Triblock, Copolymers of Poly(N-isopropylacrylamide) and Poly(ethylene oxide), *Journal of Polymer Science. Part A. Polymer chemistry*, 42 (**2004**) 4873-4881.

[64] J. Virtanen, S. Holappa, H. Lemmetyinen, and H. Tenhu, Aggregation in Aqueous Poly(N-isopropylacrylamide)-block-poly(ethylene oxide) Solutions Studied by Fluorescence Spectroscopy and Light Scattering, *Macromolecules*, 35 (**2002**) 4763-4769.

[65] J. Virtanen, C. Baron, and H. Tenhu, Grafting of Poly(N-isopropylacrylamide) with Poly(ethylene oxide) under Various Reaction Conditions, *Macromolecules* 33 (**2000**) 336-341

[66] D. Singh, D. Kuckling, V. Koul, V. Choudhary, H.-J. Adler, A.K. Dinda, Studies on copolymerization of N-isopropylacrylamide with poly(ethylene glycol) methacrylate. *Eur. Polym. J*. 44 (**2008**) 2962–2970

[67] T. G. Park, A. S. Hoffman, Immobilization and characterization of -galactosidase in thermally reversible hydrogel beads, *J. Biomed. Res*. 24 (**1990**) 21-38.

[68] G. Chen, A. S. Hoffmann, Graft copolymers that exhibit temperature-induced phase transition over a wide range of pH, *Nature*, 373 (**1995**) 49-52.

[69] X. D Xu , X. Z. Zhang, S.X. Cheng, R.X. Zhuo , J. F. Kennedy, A strategy to introduce the pH sensitivity to temperature sensitive PNIPAAm hydrogels without weakening the thermosensitivity, *Carbohydrate Polymers* 68 (**2007**) 416–423

[70] T.L. Lowe, H. Tenhu, H.Tylli, Effect of hydrophobicity of a drug on its release from hydrogels with different topological structures, *Journal of Applied Polymer Science* 73, (**1999**) 1031–1039

[71] R. Salgado-Rodríguez, A. Licea-Clavería, K.F. Arndt, Random copolymers of N-isopropylacrylamide and methacrylic acid monomers with hydrophobic spacers: pH-tunable temperature sensitive materials. *European Polymer Journal* 40 (**2004**) 1931–1946.

[72] S. Zhou, B. Chu, Synthesis and volume phase transition of poly(methacrylic acid-co-N-isopropylacrylamide) microgel particles in water. *J. Phys. Chem.102* (**1998**) 1364–1371.

[73] X. Huang, C. S. Brazel , On the importance and mechanisms of burst release in matrix-controlled drug delivery systems *Journal of Controlled Release* 73 (**2001**) 121–136

Chapter 4

SMART POROUS STRUCTURES

4. Production of smart porous structures

4.1 Dual stimuli responsive scaffolds for drug release

Specific delivery of drugs to a target site is essential to increase their efficacy and decrease their side effects. The development of external regulated delivery systems designed to deliver drugs and/or active agents at a constant rate over a certain period of time results from this demand of better control and also from the need of prolonged drug administrations [1, 2]. During the last years several devices were presented as being able to control release of drugs with different stimulus: pH [3, 4, 5], temperature [6,7] , magnetic [8, 9] and electric field [10]. Particular interest has been given to pH or temperature sensitive materials because these two factors can be easily controlled and applicable both *in vitro* and *in vivo* conditions.

For biomedical applications it is important to circumvent, whenever possible, harmful solvents during polymer synthesis or processing and the accumulation of toxic low molecular weight compounds. In this chapter supercritical carbon dioxide ($scCO_2$) was used to prepare dual stimulus chitosan scaffolds by coating them with a thermoresponsive polymer, Poly(N-isopropylacrylamide) (PNIPAAm).

The application of $scCO_2$ as a carrier to homogeneously distribute the hydrogel monomer within the chitosan scaffolds and as solvent to perform the polymerization reaction was introduced in this chapter[11]. The developed procedure can extended the green aspects of polymerizations using $scCO_2$ (eliminating the use of toxic organic solvents) to the production of smart devices for controlled drug release by using the biocompatible chitosan scaffolds as microreactors for *in situ* PNIPAAm synthesis.

Chitosan (CHT) scaffolds impregnated/coated with the hydrogel were characterized with different techniques including FT-IR and SEM. Swelling data of the produced devices were

obtained as a function of time and temperature and pulsatile swelling profiles were obtained testifying the reversible changes of structure according to the switching of the external variables. The performance of the obtained structures as controlled releases devices was undertaken using a model drug, ibuprofen, and a model protein, bovine serum albumin (BSA). Two different strategies were tested to incorporate the model compounds into the scaffolds: (i) mixing the BSA to the polymeric solution (before freeze-drying), and (ii) supercritical fluid impregnation of the model low molecular weight drug. The release profiles were analysed to study the influence of pH and temperature.

4.1.1 Experimental

4.1.1.1 Materials

Chitosan (75~85% deacetylated, medium molecular weight), N-isopropylacrylamide (NIPAAm, purity > 97%), N,N-methylenebisacrylamide (MBAm, purity ≥85%), 2,2´-azobis(isobutyronitrile) (AIBN, purity > 98%), Bovine Serum Albumin (BSA, purity ≥98)%), ibuprofen (purity ≥ 98%), glutaraldehyde (GA, 50 wt.% in water), Ibuprofen and acetic acid (purity ≥ 99 %) were purchased from Sigma Aldrich. Carbon dioxide was obtained from Air Liquide with 99.998% purity. All materials and solvents were used as received without any further purification.

4.1.1.2 Scaffolds preparation

Scaffolds were prepared following the procedure described by Madihally and Matthew [12]. In a typical procedure 3% (w/w total) chitosan solutions were prepared by dissolving the polymer in diluted acetic acid aqueous solution (1% v/v). The solution was placed in glass tubes and freezing was accomplished by immersing the tubes, containing 3/5 ml of solution, in a freezing baths maintained at -20 ºC. The samples were then lyophilized (Telstar cryodos-50) until dry.

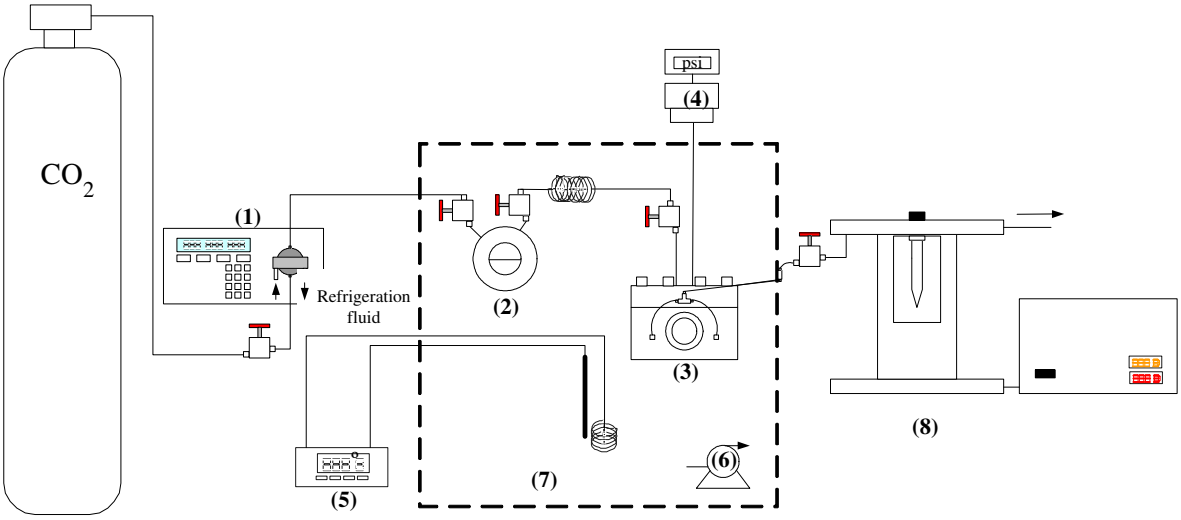

Figure 4.1- High-pressure apparatus for scaffold reticulation: (1) Gilson 305 piston pump; (2) high pressure cell with crosslinker; (3) high pressure cell with the scaffolds; (4) pressure transducer; (5) temperature controller; (6) recirculation pump; (7) thermostated water bath; (8) back pressure regulator

The 3D structures were reticulated using a CO_2 flow saturated with GA applying an apparatus schematically represented in Figure 4.1. Typically a GA solution 1% v/v in water is placed in a high pressure vessel (2) and the scaffolds are located in the second vessel (3). During 10 minutes, a constant CO_2 flow rate of 9.8 g/min (saturated with GA) passes through the vessel containing the scaffolds inducing the crosslinking. After this procedure, a pure CO_2 flow is passed through the vessel where the scaffolds are found during one hour to remove any traces of GA. The pressure in the apparatus is monitored using a pressure transducer (Setra Systems Inc., Model 204) and is controlled to 20MPa using a back pressure regulator (8) (Jasco 880-81). The temperature is also maintained constant (40ºC), by means of a controller (5) (Hart Scientific, Model 2200), during the whole process. At the end of operation, the system is slowly depressurized during 10 minutes.

4.1.1.3 Scaffolds Coating/impregnation with PNIPAAm

Coating/impregnation with the thermoresponsive polymer was undertaken in a high pressure apparatus already described in previous works (chapter 3) [11,13]. In a typical polymerization procedure, monomer, scaffolds, cross linking agent (MBAm, 1% w/w) and initiator (AIBN, 2% w/w) are loaded into the high pressure cell which is then sealed and nitrogen is added to purge the cell and test possible leaks. The nitrogen is slowly released and liquid carbon dioxide is loaded into the cell using a high-pressure compressor. The cell is immersed in the water bath and temperature and pressure are allowed to rise to the required experimental conditions. Additional CO_2 may be added to reach the exact desired pressure. The reactions were performed at 65ºC and 20 MPa. At these experimental conditions we have a homogeneous phase with all the reactants completely soluble in the supercritical medium. CO_2 is used as a carrier of the monomer / initiator / cross-linker into the porous structure as well as a reaction medium. The reaction was allowed to proceed for 24 hours under stirring. After this period, the reaction was stopped and the resulting PNIPAAm coated scaffolds were ´´washed´´ with fresh CO_2 (65°C, 20 MPa), during one hour, in order to extract the remaining residues of unreacted monomer and cross linking agent.

4.1.1.4 Scaffolds characterization

Scaffolds before and after coating were characterized using Scanning Electron Microscopy (SEM) in a Hitachi S-2400, with an accelerating voltage set to 20 kV. For cross-section analysis scaffolds samples were frozen and fractured in liquid nitrogen. All samples were coated with gold before analysis.

Fourier transform infrared (FTIR) was used to study the interactions between chitosan and PNIPAAm after impregnation. FTIR measurements were made using a Winfirst Lite equipment,

16 scans at a resolution of 1cm^{-1}. The samples were prepared by adding little portions of the sample to dried KBr.

Equilibrium hydration or swelling degree of PNIPAAm impregnated/coated scaffolds was determined using the procedure already described in Chapter 3. Equilibrium and oscillatory swelling studies were conducted on these devices as functions of environmental pH and temperature, to examine the behaviour of the scaffolds upon swelling in pH buffer solutions at 20 ºC and 37 ºC. Three 3 replicas were performed in order to verify the reproducibility of the experimental data. Phosphate-buffered solution (pH 7.4) and acetate-buffered solution (pH 5.5) with the same ionic strength were used.

Mercury intrusion porosimetry (micromeritics, autopore IV) was used to study the pore structure of the scaffolds before and after coating.

The *in vitro* biodegradability of the scaffolds was followed in 20 ml of 0.1 M PBS with pH 7.4 at 37 ºC containing 2µg / ml lysozyme. The initial weight of each sample was determined (W_i). After 3, 6, 12, 18 and 24 days, samples were removed from the medium, washed with distilled water, lyophilized for 4 hours and then weighted (W_f). The lysozyme solution was refreshed weakly to ensure the continuous enzyme activity over the scaffolds degradation. To differentiate between the enzymatic degradation and the dissolution of the porous structure, control samples were stored for 24 days under the same conditions as the previous ones, but without adding lysozyme [14].

The weight percentage of scaffold remaining was calculated using equation 1:

$$\text{Weight remaining } (W,\%)=100-\left(\frac{W_i - W_f}{W_i}\right) \quad (1)$$

where W_i is the dry weight of the sample before starting the degradation test, W_f is the dry weight of the sample after degradation at a certain moment of time since the starting of the degradation test. Values are expressed as the mean ± standard deviation.

4.1.1.5 Drug loading

Bulk drug loading

BSA was loaded into the chitosan scaffolds by co-dissolving it with the polymer in the solvent (acidified water) and the scaffolds were prepared in the same mode as reported previously. Due to the negligible solubility of the BSA in $scCO_2$ it was assumed that the initial amount of protein added to the solution remained unmodified in the smart "scaffolds" after the reticulation and impregnation/coating procedures.

Supercritical fluid impregnation

The impregnation was performed in a discontinuous apparatus using a modified version of the high pressure cell described by Sampaio *et al.*[15] with two sapphire windows on top and bottom and a Teflon O-ring to provide the seal at both ends. The polyacetal washer and the stainless-steel washer avoid damage to the window. The interior is divided in two parts with a porous structure in order to avoid any contact of scaffolds (in the superior part) with the drug inferior part. Impregnations were performed at 40 ºC and 20 MPa using an excess of ibuprofen. After 24 hours of continuous stirring the high pressure vessel was fasten depressurized.

4.1.1.6 Controlled release studies

A small portion of the scaffold (around 20 mg) was placed inside a 100 ml of buffer solution (pH 7.4- 5.5) and at different temperatures (37-20ºC). 1 ml aliquots were withdraw periodically from the solutions and collected in *Eppendorf* tubes.

Quantification of the released drug takes into account the portion of solution that was removed from the released solution. Ibuprofen was quantified by UV spectroscopy (Helios Alpha Double-Beam UV / VIS Spectrophotometer) at the maximum absorbance around 220 nm and BSA at 280 nm.

4.1.2 Results and Discussion

4.1.2.1 Scaffold preparation and morphological characterization

In this study, we have applied our group background in the synthesis of thermoresponsive polymers using supercritical fluid technology [11]. The incorporation of a fraction of a thermoresponsive polymer could provide other properties, to the scaffolds, including improved or switchable release control of impregnated bioactive agents, such as growth factors, or to control cell adhesion/detachment.

$ScCO_2$ was used as a carrier to homogeneously distribute the monomer, initiator and cross-linker within the micropores of a polymeric substrate and there act as reaction medium for the polymerization reaction using the pores as micro-reactors. Figure 4.2 presents SEM images of the materials prepared in this work before and after coating (Figure 4.2a vs Figure 4.2 b).

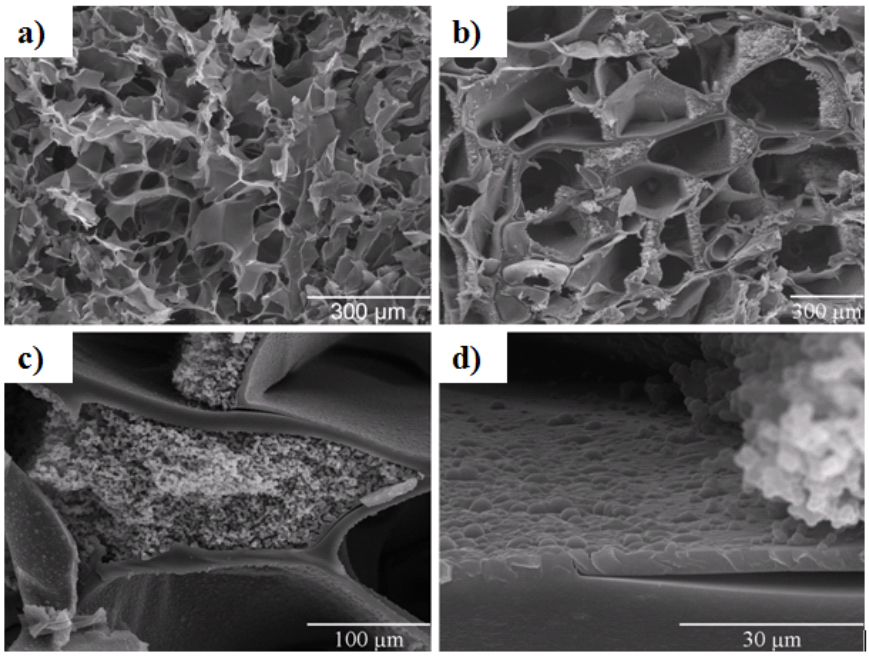

Figure 4.2 - SEM pictures of CHT scaffolds. a) previous to impregnation/ coating; b) after impregnation/coating c) detail of a pore d) pore surface coated with the thermoresponsive polymer.

These results show that large amounts of hydrogel (~300% weight increase) are uniformly distributed inside the pores of the scaffolds and that large empty volumes remain inside the pores. A very small number of pores were completely full with the hydrogel (Figure 4.2c) in opposition to a completely coating of the pores surface with the thermoresponsive polymer (Figure 4.2d) which is an important role since pore size diameter is a relevant parameter to enable cells adhesion to the materials. FTIR analysis confirmed that hydrogel and the scaffolds where physically but no chemically bound.

Mercury intrusion porosimetry (Figure 4.3) was used to characterize the microstructures. Before coating the raw scaffolds presented a median pore diameter of 17.9 µm while after reaction this value decreased to 16.3 µm. No significant differences were observed in terms of porosity that

was constant around a value of 85% confirming that the coating was efficient enough in the halls but the pores were not blocked.

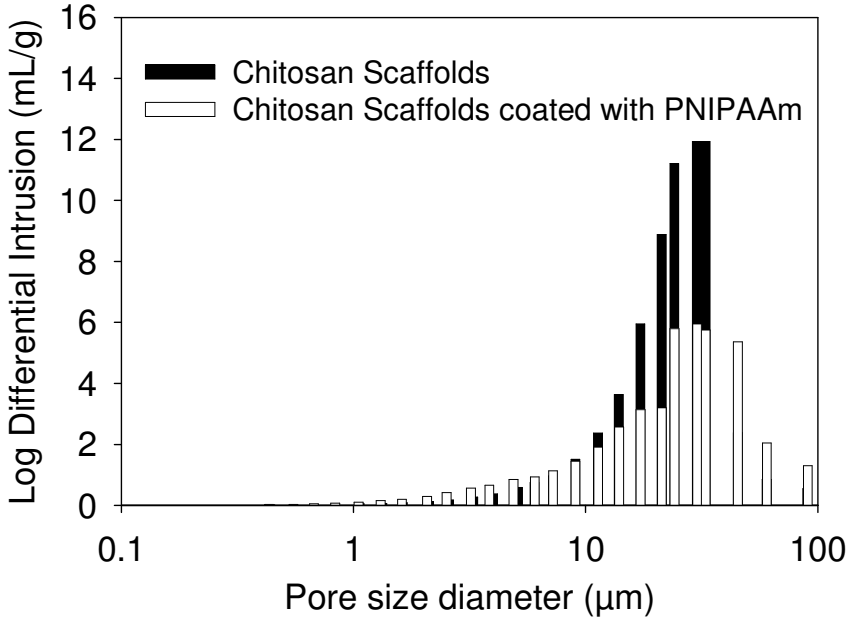

Figure 4.3 - Mercury porosimetry results of CHT scaffolds and PNIPAAm coated CHT scaffolds.

The swelling degree of the *dual stimulus* scaffolds is also an important property to be characterized because it will determine properties such as the absorption and diffusion of solutes, mechanical properties under wet conditions and water uptake capability.

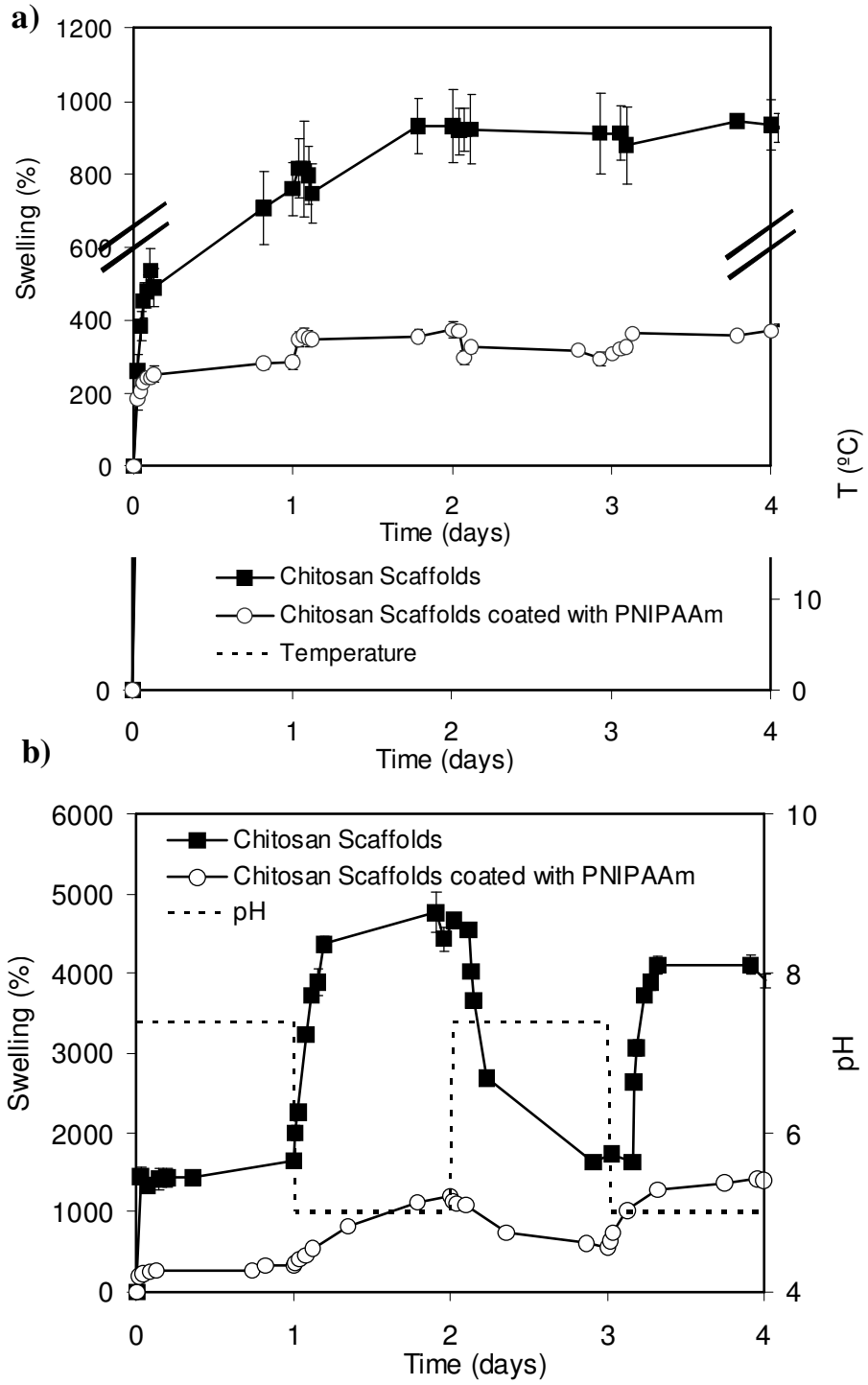

Figure 4.4- Equilibrium volume swelling ratio of CHT scaffolds and PNIPAAm coated scaffolds with a) temperature pulses between 20°C and 37°C in PBS (pH=7.4); b) pH pulses between 5.5 an 7.4 in a buffered solution at 37 °C.

Figure 4.4a) shows the swelling behaviour, at 20ºC and 37ºC, of the smart devices produced in $scCO_2$. As it was expected the swelling increased with a decrease in the temperature [11]. It is well known that the hydrophilic/hydrophobic balance of the PNIPAAm hydrogels is due to the existence of the amide hydrophilic groups and the isopropyl hydrophobic groups in the side chains [16]. When the temperature is above the LCST hydrophobic interactions among hydrophobic segments are strong and the hydrogen bond interaction with water is weak. When the temperature decreases, the hydrogen bonding between the hydrophilic segments of the polymer chain and water molecules are dominant, what leads to a swelling increase. This suggests that it should be possible to control the release of molecules by simply adjusting the temperature. No temperature sensitivity was observed in the chitosan scaffolds that were not coated.

It would also be a desirable characteristic to have pH-sensitive controlled-release scaffolds with controllable swelling ability. As it can be seen in Figure 4.4b) the results demonstrate that the impregnated and the non impregnated scaffolds change their ability to absorb solution when the environmental pH is altered. The Donnan theory states that the swelling ability is basically determined by the osmotic pressure gradient between the inside and outside of a gel [17]. Therefore, from a macroscopic point of view, the swelling phenomenon appears to be a balance of the osmotic pressure gradient or concentration gradient between the interior of the hydrogel and the external solution. At higher pH, the degree of ionization is reduced, due to the deprotonation of chitosan amino units [18, 19] and the samples swelling decrease as the osmotic pressure and charge repulsion decrease. As it was expected this behaviour is more pronounced in the scaffolds that were not coated.

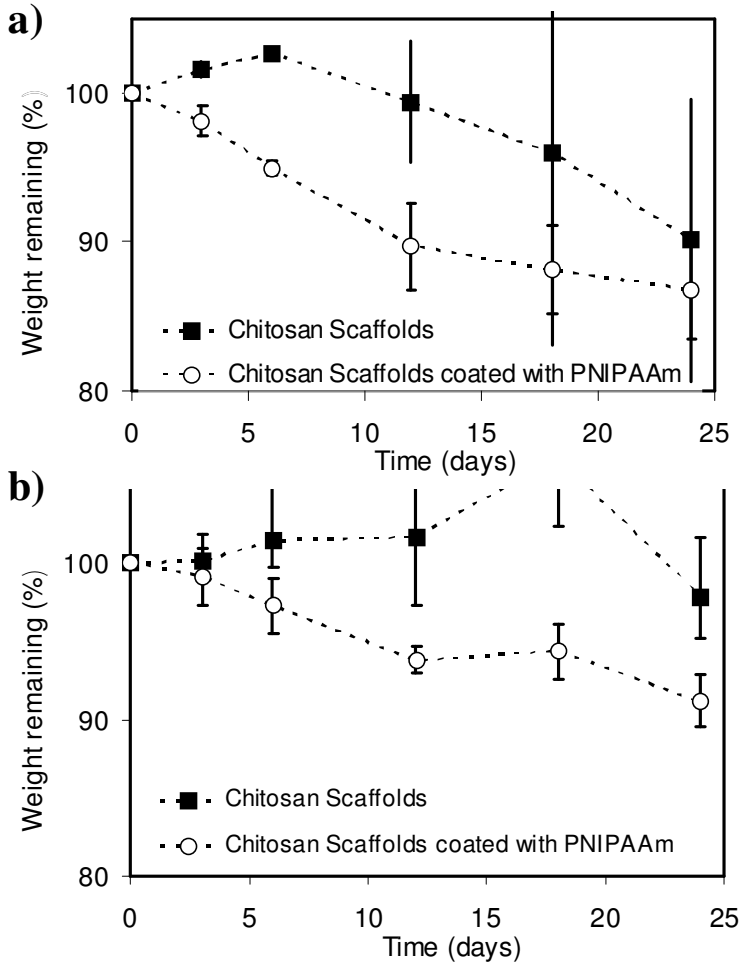

Figure 4.5 - Biodegradability of the CHT scaffolds coated and non coated with PNIPAAm (a)PBS with Lysozyme (b) PBS

To analyze the structures biodegradability they were immersed during 24 days in a phosphate buffer solution (PBS) containing lysozyme (Figure 4.5 a), the main enzyme responsible for chitosan degradation in the body [20]. An accelerated mass loss was observed for both types of scaffolds. This loss is higher in the coated scaffolds probably due to some losses of PNIPAAM that was not efficiently crosslinked. This was confirmed in the biodegradability tests performed in the absence of the enzyme (Figure 4.5 b) where only the coated scaffolds exhibited a weight loss.

4.1.2.2 Drug/protein release studies

From the point of view of the potential utility of PNIPAAm/chitosan matrixes as drug delivery systems, it is crucial to know the drug release kinetics under different physiological conditions and to analyze if they are capable of encapsulate and release of molecules when triggered by a small change in temperature or pH. First, it was tested the possibility of using $scCO_2$ as a solvent to perform the impregnation of a model drug (ibuprofen).

Supercritical mixing and impregnation is simple and highly more attractive as it avoids the use of organic solvents [21] According to the report of Kazarian *et al*. [22], there are two mechanisms of supercritical fluid impregnation of drugs into polymer matrixes, i.e. simple deposition and preferential partitioning. In this work ibuprofen was efficiently impregnated into the chitosan porous matrix due to the high solubility of the drug in the supercritical fluid and preferential deposition on the hydrogel structure although the high chitosan T_g. This could be a major advantage for drugs that are highly soluble in $scCO_2$ such as the case. In the tested conditions, approximately 160 mg of drug was loaded per gram of scaffold.

This was efficiently achieved due to the high solubility of the drug in the supercritical fluid [23]. This could be a major advantage for drugs that are highly soluble in $scCO_2$ such as the case. In the tested conditions, approximately 160 mg of drug was loaded per gram of scaffold.

Drug dissolution tests were conducted to investigate the drug release behaviours from the chitosan- ibuprofen impregnated-scaffolds.

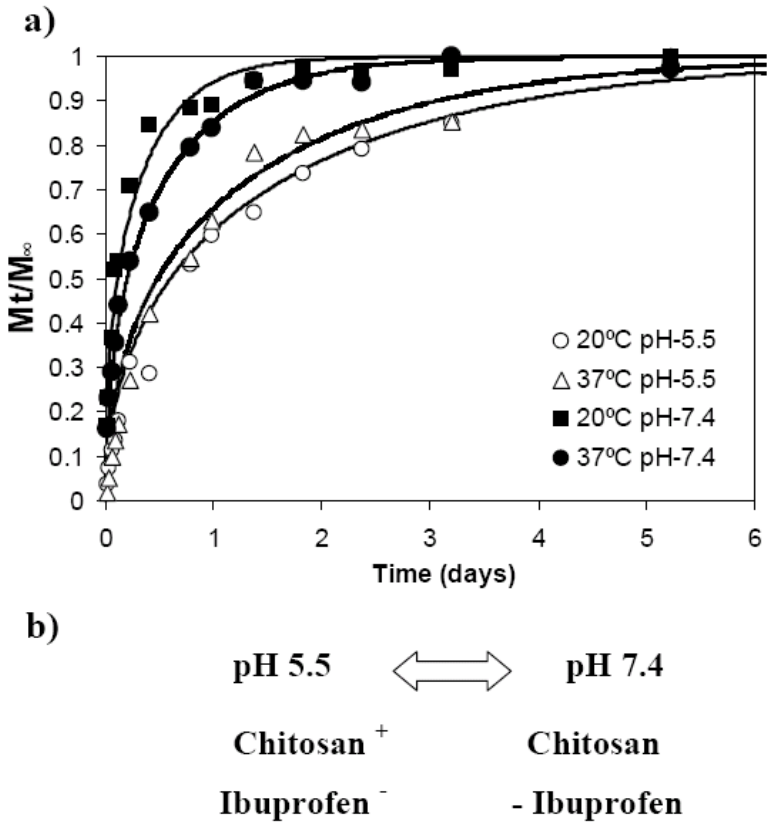

Figure 4.6 - a) Release of Ibuprofen from PNIPAAm coated CHT scaffolds; b) Different charges that are present in the scaffold and in the drug in the tested conditions.

In Figure 4.6 it is presented the overall drug release of this model drug at different pH (5.5 and 7.4) and temperature (20 ºC and 37 ºC) conditions. After 6 days all the drug was released from the scaffold. . Immediate drug release in the first few minutes is mainly governed by dissolution of the unimpregnated drug particles and/or the amorphous drug bonded or dispersed on the chitosan matrix surface. After the initial drug release stage, the swelling effect, resulting from different stimulus, become more important. To evaluate the influence of the different *stimulus* in the diffusion of the drug a simple model was developed.

The Fick's second law in cylindrical systems, considering axial and radial mass transfer, may be used to describe the drug transport. In the case of cylinders (considering axial as well as radial mass transport) [24, 25]:

$$\frac{M_t}{M_\infty} = 1 - \frac{32}{\pi^2}\sum_{n=1}^{\infty}\frac{1}{q_n^2}\exp\left(-\frac{q_n^2}{R^2}Dt\right)\sum_{p=0}^{\infty}\frac{1}{(2p+1)^2}\exp\left(-\frac{(2p+1)^2\pi^2}{H^2}Dt\right) \quad (3)$$

where Mt and M∞ denote the absolute cumulative amounts of drug released at time t and at infinite, respectively; n and p denote dummy variables; the q_n are the roots of the Bessel function of the first kind of zero order [$J0(q_n) = 0$], D is the diffusion coefficient and R and H denote the radius and height of the cylinder.

Table 4.1 - Parameters used to adjust Fick law of diffusion to ibuprofen and BSA release

		Ibuprofen	**BSA**
R (mm)		2.5	
H (mm)		5	
D (m^2/s)	20 ºC; pH 7.4	2×10^{-11}	1×10^{-12}
	37 ºC; pH 7.4	1.2×10^{-11}	4×10^{-14}
	20 ºC; pH 5.5	4×10^{-12}	2×10^{-14}
	37 ºC; pH 5.5	5×10^{-12}	5×10^{-15}

In Table 4.1 it is presented the diffusion coefficients (D) and the parameters (R and H) that were used to adjust the ibuprofen release in the different environments. A good fitting was achieved which suggest a Fick's behaviour for the release of the model drug. Confronting these results with ibuprofen experimental release profiles it is possible to observe that ibuprofen is released at a much slower rate at pH 5.5 ($D = 4 \times 10^{-12}$ and 5×10^{-12} for 20 ºC and 37 ºC respectively) than at pH 7.4 ($D = 2 \times 10^{-11}$ and 1.2×10^{-11} for 20 and 37 ºC respectively), contradicting what should be

the expected. If swelling was paramount higher diffusion coefficients should be obtained at lower pH. We believe that this may be caused by the different charges that are present in the scaffold and in the drug (Figure 4.6b). Under acidic conditions, pH below the pKa of chitosan (6.5), the amino groups are almost completely protonated, and thus the charge density of chitosan is positive in opposition to ibuprofen that has carboxylic acid groups with a pKa of 4.4 which indicates that in the experiments at pH 5.5 the negative charges predominate in the molecule. The ionic attraction between them prevails and withdraws the effect of swelling.

The results obtained with the studied temperatures are contradictory. For a pH of 7.4 as expected the drug release was mainly controlled by diffusion of the drug out of the swollen chitosan matrix with faster rate ($D = 2 \times 10^{-11}$ vs 1.2×10^{-11} for 20 ºC and 37 ºC, respectively). In contradiction at the lower pH, despite only a small variation being observed) the diffusion coefficient is bigger at the higher temperatures ($D=4 \times 10^{-12}$ *vs* 5×10^{-12} for 20 ºC and 37ºC respectively) which suggests that other effects should be influencing rate of ibuprofen dissolution.

With the impregnation of a model protein we intended to test a second approach for the impregnation of high molecular weight bioactive molecules. The loading of the bioactive molecules with this approach allow us to control with a high accuracy/ precision the amount of protein that remains in the scaffolds. For these tests it was used approximately 1 gram of protein per gram of scaffold. BSA was loaded previous to the supercritical coating/impregnation procedure with the thermoresponsive polymer which means that protein is only available in the chitosan walls of the scaffold. Release profiles at different pH and temperature are reported in Figure 4.7.

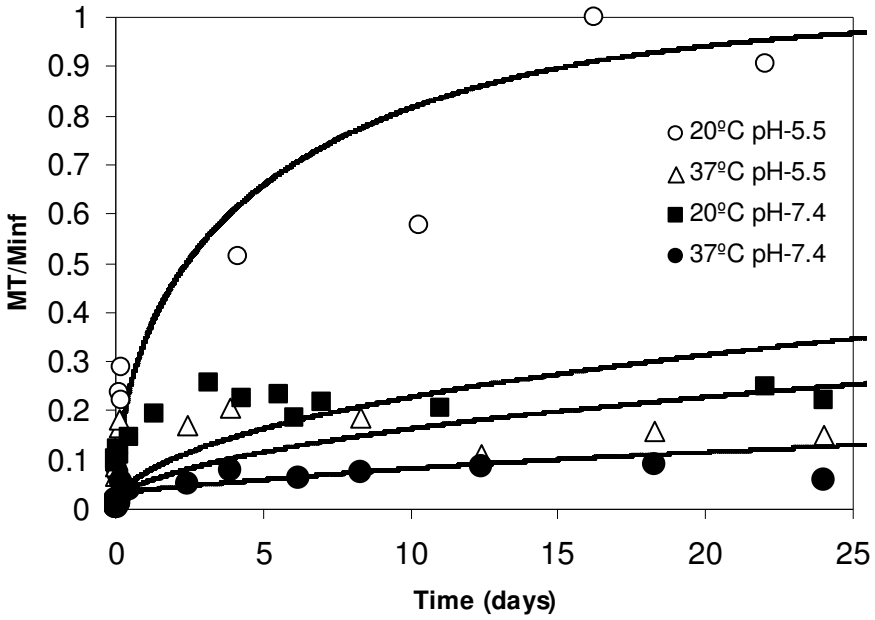

Figure 4.7 - Release of BSA from PNIPAAm coated CHT scaffolds.

We can observe that for such relatively large molecule as BSA the PNIPAAm layer is able to control the amount of protein that is released to the medium. At 20 ºC and pH 5.5 the scaffold presents the maximum swelling and the PNIPAAm chains are in the hydrophilic state interacting predominantly with water. In this case, the surface of unit cells become less crowded and the PNIPAAm chains extend outside the unit cell allowing enough space for the protein to cross the thermoresponsive layer and be released to the surrounding environment. In contrats, when the "smart" scaffolds are placed at 37 ºC and pH 7.4 the protein is retained. In these conditions the PNIPAAm chains are tangled interacting with their one blocking the protein passage through scaffold walls. When compared with the overall data it is possible to attain the following order of drug release: (20 ºC, pH5.5) > (20 ºC, pH7.4) > (37 ºC, pH5.5) > (37 ºC, pH7.4). The adjusted diffusion coefficients (Table 4.1) perfectly agree with these conclusions. Nevertheless the adjustment of the Fick's diffusion law can not explain all the results and a possible explanation to

the poor fitting is the existence of other factors that were not taken into account in the simplified model proposed, such as protein adsorption in the surface walls of the scaffolds.

It is interesting to notice that the isoelectric point of BSA is reported to be between 4.5 and 5 meaning that at a pH of 5.5 chitosan is positively charged and BSA is negatively charged, even so despite the strong interactions between protein and polymer the drug diffuses much faster than in the other cases due to the inexistence of the PNIPAAm barrier.

This means that PNIPAAm barrier is the predominant mechanism to drug release, nevertheless the swelling, the adsorption of active molecules, and the electrostatic charges of the different species involved have to be considered.

4.1.3 Conclusions

In summary, we have developed a novel, simple and green method to produce smart devices with possible applications as switchable release devices for molecules or scaffolds for tissue engineering applications. The coating was efficiently achieved without compromising the porosity and the biodegradability of the materials.

The results, demonstrate that we are able to control the swelling with external stimulus as pH and/or temperature. For large molecules such as proteins a thermoresponsive layer can be used as barrier to retain drugs until the exact stimulus is applied.

4.2 Thermoresponsive membranes

4.2.1 Introduction

Stimuli-responsive polymeric-based membranes received large interest during the last decade from various scientific fields because their permeation properties can be controlled or adjusted according to the external chemical and physical *stimulus*, such as pH [26], temperature [27], electric field [28], concentration of chemical species, light [29], or ionic strength [30] of their environments. They have found a broad range of applications, as controlled drug delivery devices [31], in bioseparation processes [32] chemical separation, water treatment, chemical sensors [33] and tissue engineering applications [34, 35].

A special interest has been given to thermoresponsive membranes since, in many cases, environmental temperature fluctuations occur naturally and because temperature stimulus can be easily designed and artificially controlled. Several techniques were used to prepare temperature sensitive polymeric-based membranes such as the vacuum filtration method [36], the adsorption method [37], the coating method [38], by the introduction of nanosized thermoresponsive particles into the membranes [39] or by simply grafting thermoresponsive polymers onto porous membranes substrates by different grafting techniques [40]. An advantage of such membranes is that the porous substrate acts as a dimensionally stable matrix for mechanical support, while the conformational changes of the graft thermoresponsive polymer induced by environmental *stimuli* lead to permeability changes. Temperature-[41,42,43] or pH-[41] polymers have been grafted onto porous substrates. The grafted polymers may be located mainly on the external membrane surface or be homogeneously distributed inside the pores. In some reports of plasma-induced graft polymerization active species are generated mainly near the membrane surface [44].

In chapter 3.1 and 4.1 it was proposed new strategy for the solvent-free impregnation/coating of polymeric surfaces and porous structures with thermoresponsive polymers. It was proved that

supercritical carbon dioxide ($scCO_2$) can be used as a carrier to homogeneously distribute the monomer, initiator and cross-linker within the micropores of a polymeric substrate and act as reaction medium for the polymerization reaction using the pores as microreactors. We strongly believe that this technique can be used to prepare membranes with high response performance to environment stimulus for advanced purification/ separation applications or systems for switchable release of molecules.

The phase behaviour of PNIPAAm in aqueous solutions was studied with several techniques, including turbidity [45, 46], light scattering [47] and IR spectroscopy [48]. The vast majority of these studies confirmed that free PNIPAM chains have its hydrophilic-hydrophobic phase transition (LCST in water at 32ºC) and that this transition is a very sharp transition (about 5 °C). Grafted chains of PNIPAM have shown promise for creating responsive surfaces. Conformational changes of the polymer are likely to play a role in some of these applications, in addition to changes in local interactions. However, the conformational change of the grafted PNIPAM brushes varies greatly with molecular weight and grafting density. The maximum conformational change was observed for PNIPAM brushes with high molecular weight and intermediate grafting density [49]. This trend was also predicted with a self-consistent-field calculation by Mendez and coworkers [50]. More recent experimental findings show that, under some grafting conditions, end-anchored PNIPAAm does not become insoluble and does not collapse above 32ºC.

In order to address the issue of temperature-responsive behaviour in PNIPAAM coated microporous substrates, we explored the ability of supercritical CO_2-assisted technology to produce “smart” polysulfone membranes. Our focus was to evaluate the temperature response performance of membranes that were coated /impregnated with PNIPAAm chains produced by *in situ* polymerisation in comparison to the PNIPAAm chains grafted to membranes in advanced

purification/ separation applications. The procedure developed is schematically represented in Figure 4.8.

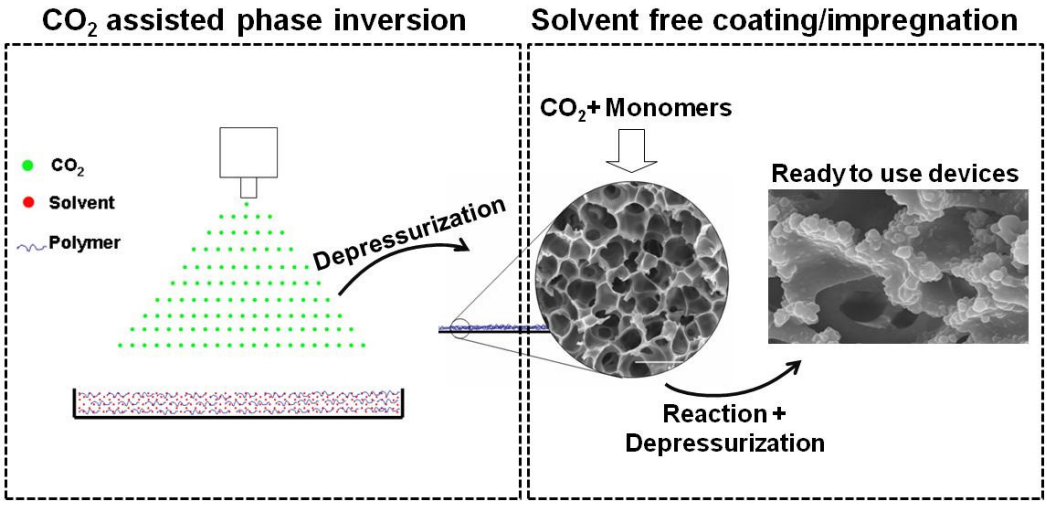

Figure 4.8 - Schematic description of thermoresponsive membranes preparation methodology

In a first step, the matrixes, porous membranes of polysulfone (PS), were prepared using the methodology developed in chapter 2 [51]. Secondly, the PS membranes with well defined pores in the micrometer range are coated/impregnated by *in situ* N-isopropylacrylamide (NIPAAm) polymerisation in $scCO_2$. To avoid compromising the integrity of the "smart" surface coating, PNIPAAm synthesis can be done in the presence of a cross-linking agent, N,N-methylenebisacrylamide (MBAM) [52], to allow the system to swell in aqueous media and to open and close the pores, without dissolving the thermoresponsive polymer. The use of $scCO_2$ as polymerisation medium offers many advantages when compared with conventional polymerisation since there is no need for an intensive drying action before further processing or characterization steps and it is possible to easily separate the solvent from the engineered matrix, leading to highly pure materials. In addition, permeation of bovine serum albumin (a model protein) through the thermoresponsive porous PS membranes is investigated.

Protein diffusion was selected as a case study because of its applications in biotechnology and food industries with unlimited business opportunities [53]. This is also a demanding process due to the complexity of proteins themselves and their biological environments.

4.2.2 Experimental

4.2.2.1 Materials

Polysulfone (PS) (Mw 67,000) in pellet form, N-isopropylacrylamide (NIPAAm, purity ≥ 97%), N,N-methylenebisacrylamide (MBAm, purity ≥ 98 %) and N, N-dimethylacetamide (purity ≥ 98 %) and bovine serum albumin (BSA) (MW=66kDa, purity ≥ 98 %) were obtained from Sigma-Aldrich. CO_2 was obtained from Air Liquide with purity higher than 99.998 %.

4.2.2.2 Membrane production

Polysulfone membranes were prepared following the procedure described in detail in chapter 2 [51, 54]. A supporting disk for the casting solution with 1 mm of thickness was used. The casting solution was prepared by solubilising a certain amount of polymer into a specific solvent (dimethylformamide, dimethylacetamide or dimethyl propionamide) in order to prepare a 15% w/w solution. In a typical procedure CO_2 is added until the desired pressure, with an exact flow, using a Gilson 305 piston pump. After reaching the normal operational pressure, the supercritical solution passes through a back pressure regulator (Jasco 880-81) which separates the CO_2 from the solvent.

All the experiments were performed at 18.6 ± 0.7 MPa with a CO_2 flow of 9.8 g/min for 2 hours. At the end the system is depressurized (1min) and a thin homogeneous membrane is obtained.

4.2.2.3 In situ polymerization inside polysulfone membrane.

In a typical procedure, the *in situ* polymerization of PNIPAAm within the membrane pores is performed by loading the membranes and reactants, monomer, cross-linking agent (1 wt%) and initiator (2 wt%), into the high-pressure cell. The reactor is then sealed and nitrogen is added to purge the cell and test the leaks. The nitrogen is slowly released and liquid carbon dioxide is loaded into the cell using a high-pressure compressor. The cell is immersed in the water bath and temperature and pressure are allowed to rise to the required experimental conditions. Additional CO_2 may be added to reach the exact desired pressure. The reaction were performed at 65 ºC and 20 MPa, as reported in the previous chapter and proceeded for 24 hours under stirring.

4.2.2.4 Membranes characterization

Scanning Electron Microscopy (SEM) was performed in a Hitachi S-2400, with an accelerating voltage set to 15 kV. For cross-section analysis the membrane samples were frozen and fractured in liquid nitrogen. All samples were coated with gold before analysis.

X-ray photoelectron spectroscopy (XPS) analyses were performed on a XSAM800 X-ray spectrometer, operated in the fixed analyser transmission (FAT) mode, with a pass energy of 20 eV, a power of 130 W and using a non-monochromatic radiation from Mg anode ($h\upsilon$ = 1253.6 eV). Spectra were collected with a step of 0.1 eV, and 60 s of acquisition by sweep, using a Sun SPARC Station 4 with Vision software (Kratos). The curve fitting for component peaks was carried out with a non-linear least-squares algorithm using a mixture of Gaussian and Lorentzian peak shapes. Sensitivity factors used were: C 1s - 0.25, O 1s 0.66, N1s - 0.44 and S2p – 0.54.

Membrane porosity and pore size distribution was determined by mercury porosimetry (micromeritics, autopore IV). Membrane hydrophobicity was evaluated through the measurement of the contact angle of water droplets in a KSV Goniometer model CAM 100 at two different temperatures 20 and 40 ºC.

The permeability to pure water, of the membrane, was determined by measuring the water flux trough the membranes using a 10 ml filtration unit (Amicon Corp., model 8010) with an effective area of 4.1 cm^2. All the experiments were carried out varying the applied hydrostatic pressure from 0 to 0.5 MPa.

4.2.2.5 Protein diffusion

A stirred cell consisting of two identical cylindrical chambers, with 50 cm^3, was used (Figure 4.9). A thermoresponsive membrane with 4.1 cm^2 was placed between the chambers and temperature was controlled by means of a thermostated water bath. In a typical procedure, one of the chambers is filled with a protein in phosphate buffer solution (PBS) (3mg/mL), at a certain temperature. The receptor chamber was filled with PBS at the beginning of the experiment. 1 mL aliquots were withdrawn periodically from the solutions and collected in Eppendorfs tubes.

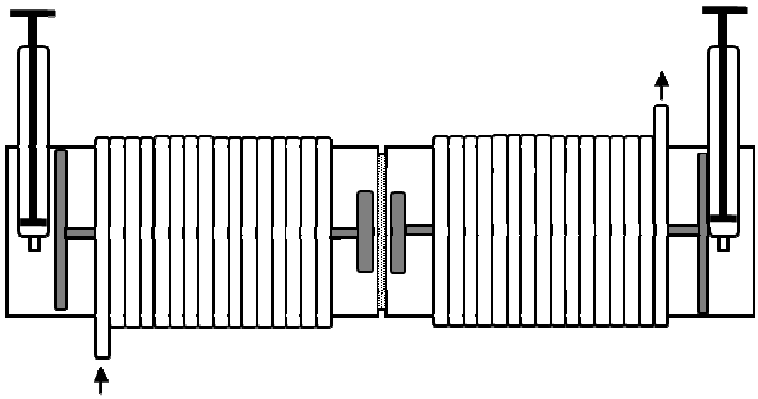

Figure 4.9 - Schematic representation of the filtration cell.

Vigorous stirring of each cell compartment was carried out to eliminate the thermo convective effect on permeation. BSA was quantified by UV spectroscopy (Helios Alpha Double-Beam UV / VIS Spectrophotometer) at a wavelength of 280 nm. To relate the absorbency to the concentration of the BSA, calibration measurements were performed.

4.2.2.6 Modelling experiments

To predict the diffusion of BSA through the pores at two different temperatures (above and below the LCST) a simple model was developed.

The protein flux through the membrane is the result of two different types of transport: diffusion and convection. The first one corresponds to the diffusion flow and can be calculated from the first Fick's law (Eq. (1)) while the contribution of convection J_s (solute flow) is assumed to be the protein that is transported due to the osmotic pressure difference,

$$J_{diff} = -D \frac{\partial c_{mx}}{\partial x} \tag{1}$$

where J_{diff} is the diffusion flux (kg.m^{-2}.s^{-1}), D is the diffusion coefficient (m^2.s^{-1}), $c_{mx)}$ is the concentration across the membrane (in kg.m^{-3}) and x is perpendicular to the membrane surface (m).

The flux of water (Jw) and solute (Js) are given by:

$$Jw = -Lp \cdot (\sigma \cdot \Delta\pi)$$

$$Js = -(1-\sigma) \cdot Jw \tag{3}$$

where Lp(m^3/m^2.s.Pa), $\Delta\pi$ (Pa) and σ are the pure water permeability, osmotic pressure, and selectivity, respectively. The osmotic pressure of BSA was obtained from the following correlation [55]:

$$\Delta\pi = 204.78 \times \frac{\partial c_{mx}}{\partial x} + 2 \times \frac{\partial c_{mx}}{\partial x}^2 + 8.44 \times 10^{-3} \times \frac{\partial c_{mx}}{\partial x}^3 \tag{4}$$

In many protein filtration processes the protein adsorption is not negligible. This equilibrium can be represented by the Langmuir equation:

$$q_x = q_m \cdot \frac{K.C_{mx}}{1 + K.C_{mx}} \tag{5}$$

where q_m (kg/m^2) is the monolayer adsorption capacity and K (m^3/kg) is the Langmuir constant or association constant, which is a measure of the apparent affinity of the protein with the surface.

The total protein permeation can be estimated using the following equation derived from eq. 1 to 5:

$$\frac{\partial c_{mx}}{\partial t} = D \ \frac{\partial^2 c_{mx}}{\partial x^2} + \frac{J_S \cdot A_{CP}}{V_{CP}} + \frac{\partial q_x}{\partial t} \cdot \frac{A_{Pore}}{V_{pore}} \tag{6}$$

with

$$\frac{\partial q_x}{\partial t} = \frac{q_m \cdot \left[K \cdot (1 + K \cdot C_{mx}) - K \cdot (K \cdot C_{mx})\right]}{\left[1 + K \cdot C_{mx}\right]^2} \tag{7}$$

where A_{CP} (m^2) and V_{CP} (m^3) are the cross section area and volume of a hypothetical cylindrical pore [56, 57] that crosses the membrane and A_{Pore} and V_{Pore} are the volume and internal area of a pore. From mercury intrusion porosimetry (MIP) data it was obtained a median pore diameter of 0.0119μm.

The material balance to the amount of protein is defined by:

$$C_{bi} \cdot V_{solution} = \\ = C_b \cdot V_{solution} + C_p \cdot V_{solution} + \sum_0^x C_{mx} \cdot V + \sum_0^x q_x \cdot A \tag{8}$$

with C_{bi} (kg/m^3), C_{b}, and C_{p}, the bulk initial concentration, the permeate concentration and the bulk concentration, respectively, at the different time points. V_{solution} and V are the volumes of the solution in contact with the membrane and the volume of solution inside the pores with a thickness x and A is the area where the protein is adsorbed, obtained from the MIP (14.1 m^2/mg).

The following boundary conditions were used:

$$C_{m0} = C_b \tag{9}$$

$$C_{mx} = C_p \tag{10}$$

The system of partial differential equations of the model was solved by uncoupling the spatial and time discretisation; the original partial differential equations of the model were converted into a system of ordinary differential equations (ODEs) using the control volume method, as used elsewhere [58], to which an efficient stiff-integrator was subsequently applied for time integration. The ODE system obtained after spatial discretisation was integrated in time using the commercial process simulation software package gPROMS [59].

4.2.3 Results and discussion

In this study, we have applied our group background on the preparation of porous structures and synthesis of temperature responsive polymers to fabricate smart membranes. The thermoresponsive PS membranes were prepared according to Figure 4.8: i) preparation of PS membranes from commercial polysulfone casted in different solutions by $scCO_2$ induced phase inversion method; ii) the impregnation/coating of porous PS matrixes by *in situ* synthesis of PNIPAAm in supercritical media.

Polysulfone membranes were prepared fixing all the main parameters that influence membrane morphology: depressurization time (1 min); temperature (45 ºC) and pressure (18.6 MPa). Three casting solutions were prepared, using the following solvents: dimethylformamide (DMF), dimethylacetamide (DMA) and dimethylpropionamide (DMPA) in order to prove our ability to control membrane morphology. In chapter 2.1 [51] we have presented the tuning of the water permeability by simply modifying the solvent in the casting solution. The water permeability and the pores increased with the molecular size of the solvents (DMF < DMA < DMPA). Due to the intermediate behaviour observed for the membranes prepared with DMA, they were selected in the case study of protein permeation control; nevertheless the results of water permeability will

be compared to verify if the pore size diameter is a paramount in the control of the coating/impregnation process.

Microscale manipulation of polysulfone membranes structure was achieved by coating/impregnating membrane pores and surface with PNIPAAm.

4.2.3.1 Morphological and chemical characterization

Figure 4.10 shows the membranes surface and cross-section SEM images before and after the *in-situ* PNIPAAM polymerization.

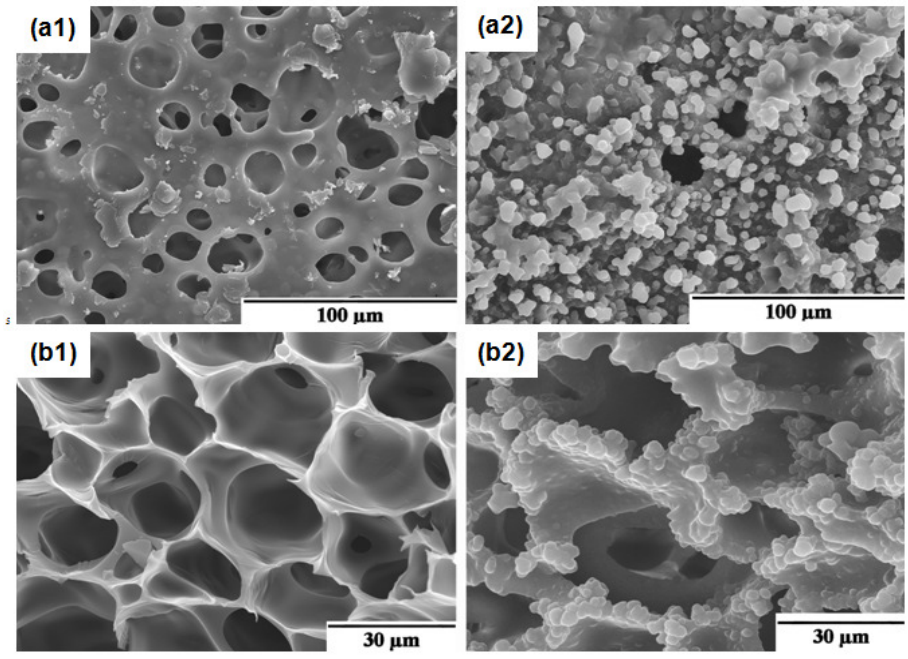

Figure 4.10 - Scanning electron micrographs of: (a) membranes surface morphology and (b) membranes cross section morphology. (1) unmodified polysulfone membranes and (2) PNIPAAm-coated membrane.

The results showed that the membranes internal and surface microstructures suffered modifications due to the pores and surface filling with PNIPAAm network. Mercury intrusion porosimetry (Figure 4.11) confirmed these observations. For the polysulfone membranes it was observed an average pore diameter of 23 μm and a porosity of 72% while for the thermoresponsive membranes these values decreased for 0.36 μm and 57% respectively.

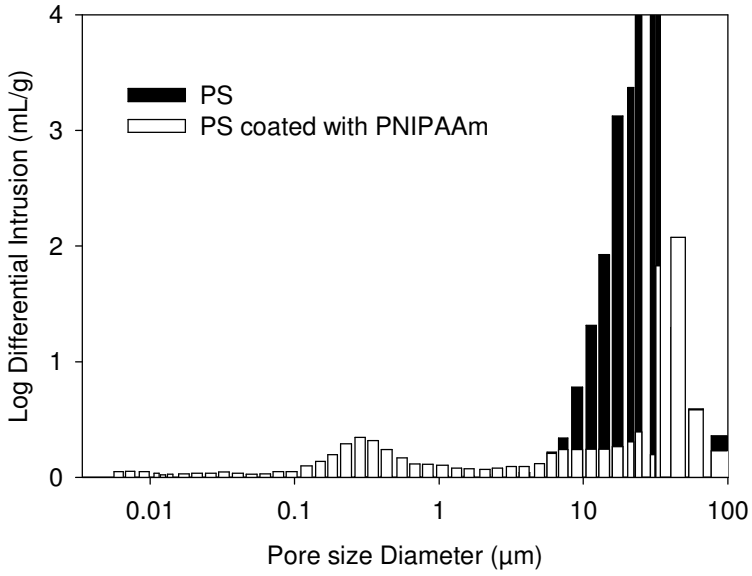

Figure 4.11 - Pore size distribution of membranes before and after coating with PNIPAAm.

The effectiveness of the supercritical assisted polymerization procedure for coating the pores on membrane surface was also evaluated by XPS analysis.

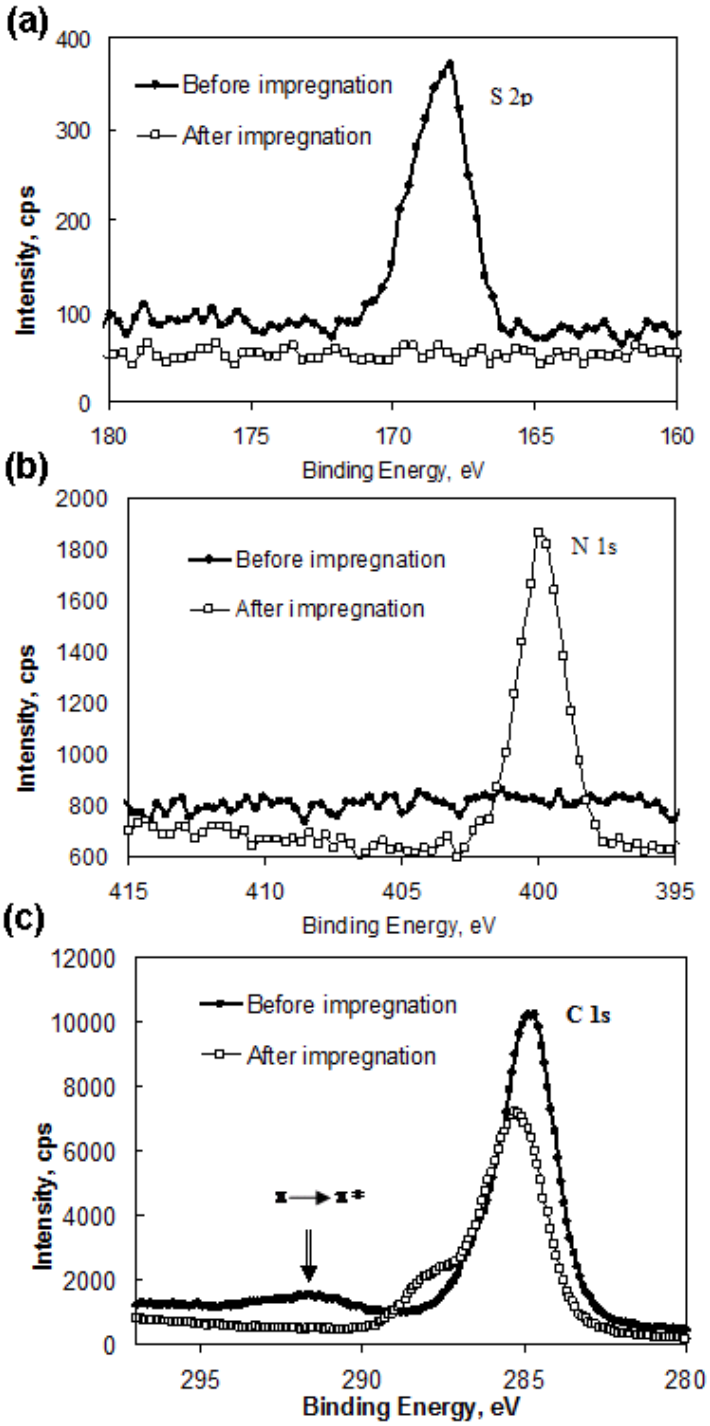

Figure 4.12 - XPS spectrum of unmodified polysulfone membrane and polysulfone membrane coated with PNIPAAm; (a) Sulphur (S 2p) peak, (b) Nitrogen (N 1s) peak, (c) Carbon (C 1s) peak and $\pi \rightarrow \pi$ transition.

XPS is a technique able to identify and quantify the elemental composition at the surface region with an analysis depth of the order of 3-10 nm. In Figure 4.12 (a) we could notice the absence of sulphur after PNIPAAm synthesis, although being present in polysulfone back bone chain, confirming that the surface was completely coated with the temperature sensitive polymer. The relative amount of nitrogen and carbon existing in the surface of the coated membranes was quantified for different sliced membrane samples. It was detected in the surface of the coated membranes an amount such that the atomic ratio N/C=0.137 is in accordance to PNIPAAm composition. These results are consistent with the nitrogen spectra (N 1s) presented in Figure 4.12 (b). Moreover, as expected, differences were observed in the carbon (C 1s) spectra in Figure 4.12 (a) and (b). For a carbon bonded with electron attractive groups such as the amide group from NIPAAm, a shoulder peak with a higher binding energy would appear besides the position corresponding to C-C and C-H bonds, which was visible in the spectrum of the coated membranes. Simultaneously, the typical π–π^* transition from the aromatic rings of polysulfone disappeared. Another important consideration is the fact that these results revealed that we were able to prepare porous structures without any residues of organic solvents. No contaminations from dimethylacetamide were observed.

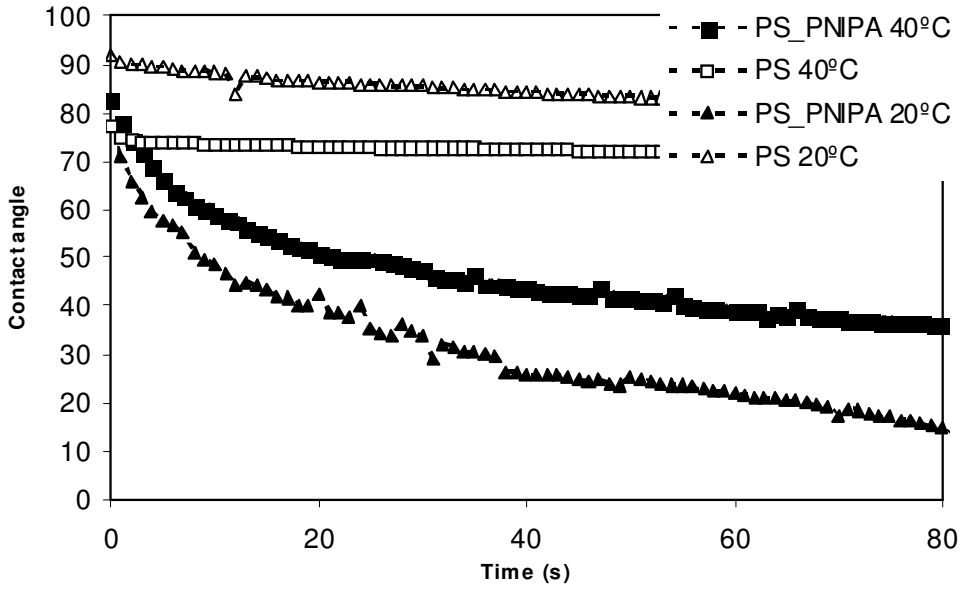

Figure 4.13 - Temperature dependence for dynamic contact angle changes on polysulfone membrane unmodified and coated with PNIPAAm.

Membrane hydrophobicity can also be assessed with contact angle measurements. Figure 4.13 presents the contact angles variations with temperature for the membranes before and after coating. Unmodified membranes had a constant behaviour at 20º and 40 ºC with contact angles of 74-70º and 90-80º respectively. This slight membrane hydrophobic behaviour when prepared by the CO_2 assisted phase inversion method was observed in chapter 2 [60]. These values, somewhat smaller than the ones obtained in other publications [61], are related with the different interactions solvent-non/solvent during the phase-inversion process and as a consequence different chemical groups appear in the surface of the membrane. The addition of PNIPAAm to the membranes increased their hydrophilic character and revealed that the thermoresponsive membranes present different behaviour when the temperature is above or below the LCST. The contact angles presented at 20 ºC were slightly smaller than the ones at 40 ºC which reflects the interactions with water that occur below the LCST. The decrease in the contact angle is due to the

hydrogel nature of PNIPAAm which will allow it to absorb more water and as a consequence the contact angle decreases.

4.2.3.2 Temperature dependent water permeability

The incorporation of the thermoresponsive polymer should provide other possibilities to polysulfone membranes including improved or switchable release control of bioactive molecules (protein) through membrane pores.

The pure water flux, which is defined as the volumetric flow rate divided by the membrane area and the pressure difference, is an important parameter to characterize. The flux of aqueous solutions through PNIPAAm-coated PS membranes was investigated as a function of temperature (in the range of 25−40ºC).

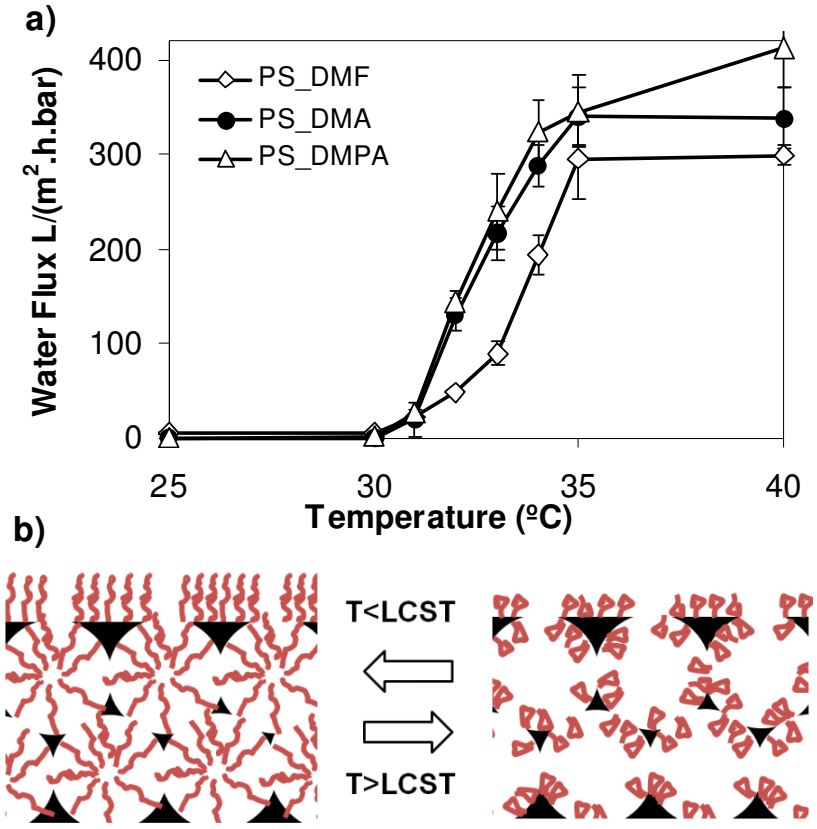

Figure 4.14 - (a) Phosphate buffer solution flux variation with temperature; (b) a schematic representation of stimuli-responsive porous membrane to control pore size, at temperatures below the lower critical solution temperature, T < LCST, expanded polymer chains

The results obtained for membranes prepared from three different casting solutions (DMF, DMA, and DMPA) are shown in Figure 4.14 (a). The temperature-dependent permeability is the direct regulatory effect of the PNIPAAm chains on the membranes and pore surfaces. In all examples when the temperature is below the LCST only a small amount of water is able to cross the membrane (water permeability ~ 0 L/(m^2.h.bar)), in contradiction with the results observed for temperatures above the LCST (water permeability > 300 L/(m^2.h.bar)). To the best of our knowledge this increase of several orders of magnitude was the biggest on-off ratio for water permeability data upon temperature changes reported in the literature. Meaning that at the surface

densities and molecular weight used in this study, the hydrophilic PNIPAAm chains assume a highly extended conformation below 32 ºC, leading to a remarkable reduction of the effective pore size. On the other hand, above LCST, the chains become less hydrophilic on the membrane and pore surface, assuming a much collapsed conformation resulting in the opening of the pores and hence the observed increase in the permeation rate. The mechanism of on-off valve pore aperture is schematically explained in Figure 4.14 (b).

These results demonstrate that the supercritical PNIPAAm coating method albeit leading to a low molecular weight polymer network produced a thermoresponsive matrix with a very sharp hydrophilic-hydrophobic phase transition (LCST in water at 32º±5ºC). Recent experimental findings [49] showed that, grafted PNIPAAm coatings only show temperature-triggered conformational changes depending on the grafting density and molecular weight. Indeed, it is known that the transition might be suppressed for low molecular weight (M_w < 75 000) end-grafted PNIPAAm. These chains therefore remain swollen above the LCST rather than attract.

It is also interesting to notice the correlation between the mean pore size diameter, the water permeabilities previously reported[28] and the tuning in the permeability after coating/impregnation with PNIPAAm. The membranes that presented higher permeability before coating continued to present this behaviour after impregnation.

4.2.3.3 Protein permeation

Permeation studies were carried out in a two compartment diffusion cell. Two chambers are separated by a circular thermoresponsive membrane having a diameter and thickness of 11 mm and 700 μm, respectively. For the monitoring of the smart PS membrane stimuli-responsive nature the bovine serum albumin (BSA) was the permeate studied.. Figure 4.15(a) shows the concentration profile of BSA through the coated membrane at two different temperatures: 20 ºC

and 40 ºC, below and above the transition temperature of PNIPAAm, respectively. It is evident that below the LCST the transport is much smaller in opposition to a high rate above the LCST.

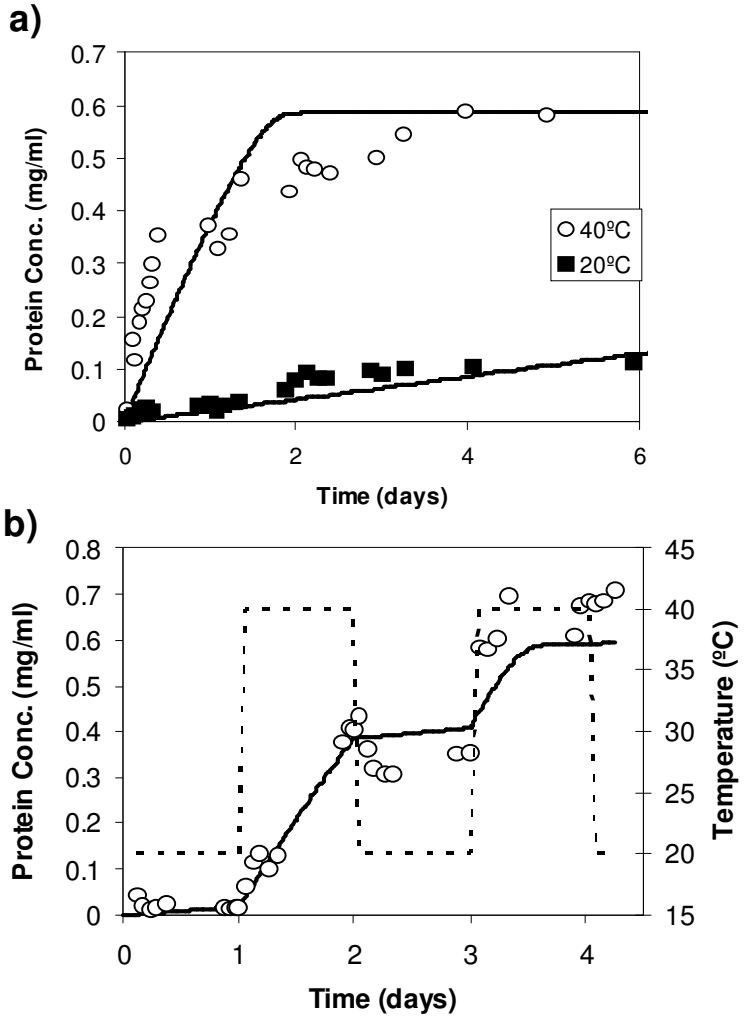

Figure 4.15 - (a) Diffusion cell experiment with 3 mg/ml BSA, pH 7.4 and 0.1M PBS at 20 and 40 ºC. (b) Effect of step temperature gradient on protein filtration. The curve fitting was performed according to the mathematical model developed in this work.

This is also a dynamic mechanism as we can observe in Figure 4.15 (b). As the temperature of the solutions surrounding the clamped smart PS membrane was changed, the permeability changed drastically. Inducing temperature pulses from 20-40 ºC it is possible to close and open the pores of the membrane for several days. Protein adsorption is also an important factor to have

in account. At 20 ºC when the PNIPAAm chains are more hydrophilic they will have a higher adsorption capability due to the fact that they are untangled. At 40 ºC, due to the more favourable interactions between the polymers chains they will be mostly tangled decreasing the adsorption capability [62].

To understand this process a simple mathematical model was developed. The bulk initial concentration, C_{bi} , the monolayer adsorption capacity, q_m, and the Langmuir constant or association constant, K, listed in Table 4.2 constitute the model input parameters along with median pore diameter and total pore area obtained from MIP data.

Table 4.2 - Bulk initial concentration, Cbi, monolayer adsorption capacity, qm, and Langmuir constant or association constant, K, used in the model.

	C_{bi} (mg/ml)	q_m(ng/m^2)	K (ml/mg)	X (μm)
20 ºC	3	220	1.36	700
40 ºC	3	150 [a)]	27.57	700
Ref.	-	62	62	[b)]

[a)] In ref. [62] this value is 188±22.
[b)] Measured from the SEM images

It was assumed that the protein concentration in the boundary layer next to the membrane was the same as the bulk concentration in both sides of the membrane and that $C_{m(x)}$ was in equilibrium with q_x. To adjust the model to the experimental data it was necessary to use higher water permeability (Table 2) than the ones that were obtained for the pure water system (Figure 4.14 a). This is related with the introduction of a third compound (BSA) that interferes in the hydrophilic-hydrophobic equilibrium established between water and PNIPAAm. It would be interesting to extend this strategy towards the study of using the smart membranes with surface properties that could change with temperature in the separation of different high value bioactive molecules.

Table 4.3 summarizes the parameters that were optimized in order to adjust the mathematical model to experimental protein diffusion.

Table 4.3 - Estimated values for protein diffusion coefficient, D, pure water permeability, Lp, and selectivity, σ, in this work.

	D (m^2.s)	L_p (m^3/m^2.s.Pa)	σ
20 ºC	$1x10^{-11}$	$7.3x10^{-12}$	0.9927
40 ºC	$7.7x10^{-10}$	$7.3x10^{-10}$	

The transport mechanism for these membranes is a consequence of two different types of transport: protein diffusion - which is the predominant mechanism when the pores are close below the LCST- and bulk transport of the protein by the solvent, predominant when the pores are open above the LCST. To test the stability of the PNIPAAm-coated membranes, the water and protein permeability measurements were repeated after 2 months and the on-off ratios were reproduced.

4.2.4 Conclusions

This work represents a new "green" alternative for the production of high-tech porous structures namely thermoresponsive membranes without any solvent residues. Besides these advantages the membranes prepared in this work exhibited a good performance in terms of valve mechanism in the pores with a complete on-off control of water permeability. The transport of a model protein was used as a proof of concept and the mathematical model was developed, based on the Fick's law and in Langmuir adsorption. Protein diffusion at temperatures below and above LCST showed sharp variation but the on-off control is different from pure water fluxes. This behaviour

is due to the PNIPAAm chain conformational changes caused by protein presence in the media introducing different water-protein-PNIPAAm interactions.

The approach used in this work is not merely limited to temperature responsive hydrogels. This concept can also be used to develop smart membranes whose pores can open and close by electronically induced external triggers such as pH, light or electrical field.

4.3 PMMA loaded membranes for drug delivery

In the last decade there has been an intensive research on polymeric delivery systems such as spherical particles and polymeric films, with the goal of improving efficacy and control of *in vivo* drug release [63]. One of the objectives of a controlled drug delivery system is to maintain a desirable concentration of drug in tissues and blood as long as possible. This concentration must be above a certain value, the therapeutic limit, and also be lower than the upper limit of toxicity. Therefore in order to be effective, the drug release must be between these two limits for an extended period of time, avoiding large fluctuations and reducing the need of several administrations [64]. The most common mechanisms by which a drug releases from a polymeric system are dissolution, diffusion and erosion. Each one of these mechanisms can be dominant but not exclusive, thus making the release of the drug a complex process to control. Depending on the matrix, type of drug and incorporated drug dose, preparation technique, geometry etc, many phenomena can be involved in the control of drug release processes such as wetting of the system`s surface, water penetration into the device through pores, drug and matrix solubility and degradation among many others [65]. Problems in controlling drug release from polymeric matrixes are common, such as, burst release of the drug, lack of drug solubility in the release medium, drug distribution within the carrier, etc. The incorporation of cyclodextrins into the polymeric matrixes can influence the mechanism of drug release and overcome this kind of problems. Cyclodextrins and their derivatives have been frequently incorporated into polymeric drug delivery devices with the purpose of controlling drug release [66].

Cyclodextrins are cyclic oligosaccharides able to accommodate drug molecules in their cone-shaped cavity forming inclusion complexes which are stabilised by intermolecular forces such as hydrophobic interactions, van der Waals forces and hydrogen bonding. Inclusion can occur when the cyclodextrin partially or fully entraps a guest compound in its cavity [67]. Physically

entrapped cyclodextrins in polymeric matrixes can modify drug solubility, promote erosion of the matrix or increase hydration. Bibby *et al.* [63] published a good review on how cyclodextrins can modify the drug release from these matrixes. Depending on the system, type of cyclodextrin and drug, the incorporation of cyclodextrins can result either in the increase of the release rate or in the decrease, being a complex process and with many variables able to interfere. Moreover, cyclodextrins are known to improve blood compatibility of polymeric biomaterials since they lead to an increase of the material hydrophilicity [68].

Membranes are of major importance in medical applications such as in drug delivery, tissue regeneration, artificial organs, diagnostic devices, coatings for biomedical devices and bioseparation [69]. Leprête *et al*. developed polyvinylidene difluoride membranes with fixed cyclodextrins for several applications, such as, guided tissue regeneration, and antiseptic delivery for periodontal applications [70].

Polymethylmethacrylate (PMMA) is a nonbiodegradable, biocompatible, hydrophobic and highly biostable polymer thus presenting a great variety of applications in biomedicine such as in dentures, cranioplasties, orthopaedic prostheses, etc. Temporary antibiotic loaded-PMMA spacers are commonly used for the treatment of bacterial infection, the major complication that can occur in total hip replacement [71]. PMMA is also used as part of polyphasic materials used in bone filling implants [72]. The controlled release of an anti-inflammatory drug from the implanted polymeric materials is an alternative to attain an effective drug concentration to fight the inflammatory response that often occur after the implantation.

As proven before $scCO_2$ is an important solvent in the processing of polymers for biomedical application. This technology has also shown to be a greener alternative to form drug-cyclodextrin inclusion complexes [73]. Natural cyclodextrins and some substituted ones such as HP-β-CDs are insoluble in $scCO_2$ [74]. Ibuprofen is a very common nonsteroidal anti-inflammatory drug

(NSAID), and known to form efficient inclusion complexes with HP-β-CDs [75]. Ibuprofen is very soluble in $scCO_2$ compared to other drugs [76] and thus suitable to be impregnated into a polymer using supercritical fluid technology without the need of co-solvents. Moreover, PMMA as the majority of polymers is able to absorb CO_2 and swell in $scCO_2$ [77].

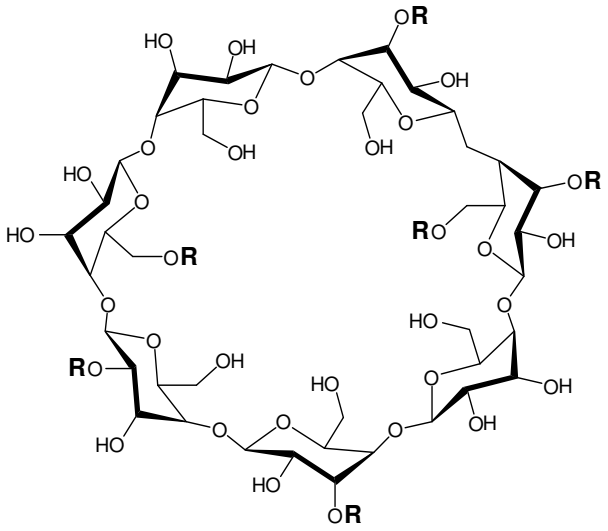

Figure 4.16 - Hydroxypropyl-beta-cyclodextrin chemical structure. R=$CH_2CHOHCH_3$ and H

In this work, PMMA membranes functionalized with different contents of HP-β-CDs were produced using a $scCO_2$-assisted phase inversion method. The polymeric membranes were further impregnated with ibuprofen using $scCO_2$ in batch mode. The membranes were then tested as controlled drug delivery devices by performing *in vitro* tests in a buffer solution at pH 7.4. The drug release data was modelled using a mathematical theory based on Fick's second law of diffusion.

4.3.1 Materials and methods

4.3.1.1 Materials

Poly(methyl methacrylate) (PMMA) (molecular weight 120,000), acetone (purity ≥ 99.5%) were purchased from Sigma-Aldrich. Hydroxypropyl-β-cyclodextrin (HP-β-CD) was obtained from Janssen Biotech with average molar substitution of 0.4. Methanol-d4 and water-d_2 were purchased from Fluka and acetonitrile from Scharlau Chemie (both purity ≥ 99.8%). Carbon dioxide was obtained from Air Liquide with purity better than 99.998 %. All materials were used as received without further purification.

4.3.1.2 Membrane preparation

Membranes were produced as already described in Chapter 2. Different contents of HP-β-CD, up to 9.2 wt%, are added to the casting solution. This solution is then loaded into a stainless steel cap (68 mm diameter and 1 mm height) and placed inside the high pressure vessel. The cell is then immersed in a visual water bath thermostatted by means of a temperature controller (Hart Scientific, Model 2200) within ±0.01 °C. The CO_2 is added up to the desired pressure using a Gilson 305 piston pump. After reaching the desired experimental conditions, the process starts running in continuous. The supercritical solution passes through a back pressure regulator (Jasco 880-81) which separates the CO_2 from the casting solvent. The pressure inside the system is monitored with a pressure transducer (Setra Systems Inc., Model 204) with a precision of ± 100 Pa.

All the experiments were performed at 20 MPa and 40 ºC, with a CO_2 flow of 9.8 g/min for 2 hours. At the end the system is slowly depressurized during 30 minutes and a thin homogeneous membrane is obtained, as shown in Figure 4.17.

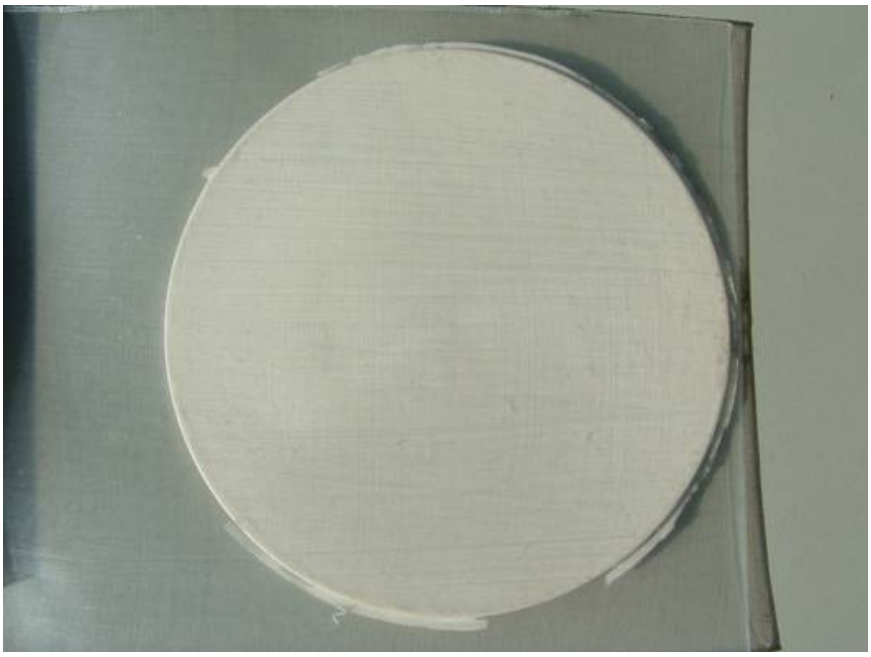

Figure 4.17- Appearance of a PMMA membrane prepared with the CO_2-assisted phase inversion method.

4.3.1.3 Impregnation experiments

The membranes produced were impregnated with ibuprofen using the same apparatus as for membrane production. The cell has a porous support which divides it in two compartments. Ibuprofen was placed under the porous support with a magnetic stirrer bar, in quantity enough to obtain a saturated solution at the *p,T* impregnation conditions [76]. The membrane is placed over the support. The cell is then closed and immersed in the thermostatted water bath at 40 ºC. CO_2 is loaded at the desired pressure of 20 MPa. The impregnation is undertaken in a batch mode for 4 hours. At the end, the cell is rapidly depressurized within approximately 1 min. Impregnated ibuprofen was calculated gravimetrically by weighting the membranes in a Sartorious balance (precision ± 0.00001g) prior and after the impregnation.

The cyclodextrin content as well as the impregnated ibuprofen in the final membranes was confirmed by ^{1}H-NMR spectroscopy using a Bruker Avance II 400 equipment (400.15 MHz). ^{1}H-NMR spectra were acquired with 256 scans over a 8000 Hz spectral window with a 30 degree flip

angle excitation pulse, the time between each repetition was set to 10 s to allow full relaxation of the proton magnetization. Solutions of the impregnated membranes were prepared in deuterated methanol using acetonitrile (4.92×10^{-7} M) as internal standard at 298 K. The quantification was done by integration of the peaks corresponding to the protons of the methyl group of acetonitrile (singlet at δ 2.04), the hydroxypropyl groups of HP-β-CD (multiplet at δ 1.14) and the methyl groups of the ibuprofen isopropyl moiety (doublet at δ 0.90). The peak corresponding to HP-β-CD has the contribution of an average of 8.4 protons (0.4 of degree of substitution). NMR results confirm the cyclodextrin content in the membrane and the impregnated ibuprofen mass determined gravimetrically (deviation lower than 5% and 11% respectively) being reasonable to say that no significant cyclodextrin is leached out during the membrane preparation by CO_2 inversion method neither during the impregnation step.

4.3.1.4 Membranes characterization

The surfaces and cross-sections of the membranes were characterized using Scanning Electron Microscopy (SEM) in a Hitachi S-2400 equipment, with an accelerating voltage set to 15 kV. For cross-section analysis the membrane samples were frozen in liquid nitrogen and fractured. Samples were mounted on aluminium stubs using carbon tape and were gold coated.

Pore size diameters and porosity were obtained by image analysis using SigmaScan Pro (Systat Software Inc.). EasyFit (MathWave Technologies) was used to fit statistical distributions to experimental data (Weibull, Lognormal) and to perform the Kolmogorov-Smirnov [78] and Anderson-Darling [79] tests to select the more adequate distribution function to each system.

Differential scanning calorimetry (DSC) measurements of the produced membranes were carried out at the REQUIMTE associated laboratory using a Setaram (Model DSC 131) equipment. The analyses were performed from 0 to 350ºC at 5ºC/min under dry nitrogen atmosphere.

4.3.1.5 *In vitro* controlled drug release

Small square pieces of each membrane (200 mg) were placed inside 200 ml phosphate buffer solutions (pH 7.4). Solutions were kept at 37 ºC for 40 days. 500µL aliquots were withdrawn periodically from the solutions and collected in *Eppendorf* tubes. In each sampling procedure the same volume of fresh buffer solution was added to the solution. Quantification of the released drug takes into account the dilution of the solution by adding the fresh buffer solution. Ibuprofen was quantified by UV spectroscopy at the maximum absorbance around 220 nm.

4.3.1.6 Modelling of ibuprofen release

The release of ibuprofen was modelled using a mathematical model based on Fick's second law of diffusion.

The diffusion of a drug from a thin film with negligible edge effects (high surface area: thickness ratio) is given by equation 1 [65].

$$\frac{M_t}{M_\infty} = 1 - \frac{8}{\pi^2}\sum_{n=0}^{\infty}\frac{1}{(2n+1)^2}\exp\left(\frac{-D(2n+1)^2\pi^2 t}{L^2}\right) \qquad (1)$$

Where M_t is the drug release at time t, M_∞ is the drug release at equilibrium and M_t/M_∞ is the fraction of drug released at time t. D is the diffusion coefficient of the drug through the membrane and L the half-thickness of the film. In order to avoid the use of infinitive series of exponential functions, an approximation for this equation, described in eq.(2), (Ritger and Peppas, 1987) can be used for $M_t/M_\infty \leq 0.6$.

$$\frac{M_t}{M_\infty} = 4\left(\frac{Dt}{\pi L^2}\right)^{0.5} \qquad (2)$$

No significant porosity and swelling changes in the matrix are considered during drug release, drug release is primarily controlled by diffusion through the carrier matrix and perfect sink conditions are maintained over the release period.

4.3.2 Results and discussion

Membranes were produced with different HP-β-CD contents according toTable 4.4.

Table 4.4- HP-β-CD content in the casting solution and in the produced membranes and corresponding glass transition temperatures of PMMA.

	wt% HP-β-CD, casting solution [a]	wt% HP-β-CD [b]	Tg/ºC [c]
Entry 1	0.0	0.0	102.07
Entry 2	1.5	5.1	102.73
Entry 3	2.6	8.7	111.72
Entry 4	4.0	13.7	114.21
Entry 5	9.2	33.4	*

[a] weight of HP-β-CD / total weight (Solvent+PMMA+ HP-β-CD). Ratio solvent/PMMA kept constant.

[b] weight percentage of HP-β-CD with respect to PMMA.

[c] not possible to measure due to a more pronounced dehydration peak of HP-β-CD compared to the other membranes. Tg of PMMA used in the casting solution: 102.48ºC.

Figure 4.18 shows SEM images of the surface and cross-section of a PMMA membrane.

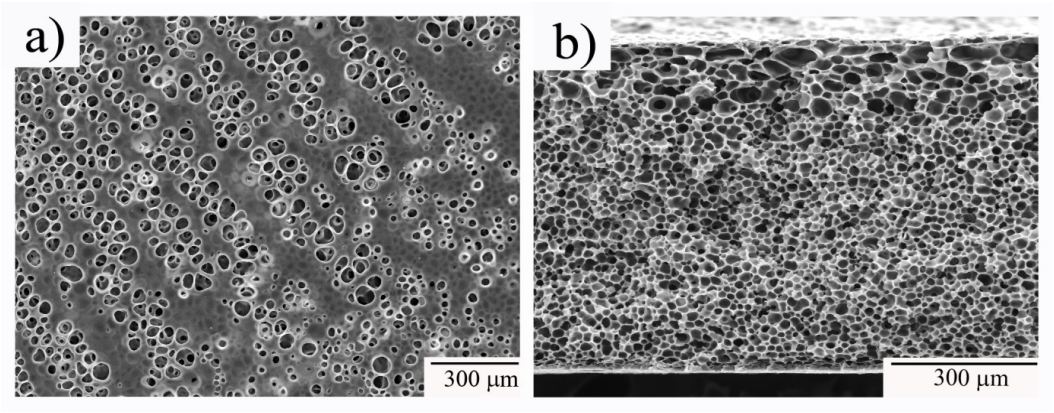

Figure 4.18 - Scanning electron micrographs of a PMMA membrane produced: a) surface top view; b) cross-section.

All membranes show analogous highly uniform porous structures. Pore size distributions of the membranes produced are shown in Figure 4.19. Similar pore size distributions were obtained, nevertheless an increase in the mean pore size diameter was observed, from around 14.9 μm to 18.4 μm, while increasing the content of HP-β-CDs in the casting solution up to 9.2 wt%. This increase, in the mean pore size diameter, could be explained by the interference of the cyclodextrin in the nucleation process of the polymer during the membrane formation as was also observed by other authors [80]. There is an obvious compositional dependence of PMMA's *T*g with the cyclodextrin content in the membrane as it is shown in

Table 4.4, suggesting that there is a good miscibility of PMMA with the cyclodextrin. *T*g increases with increasing cyclodextrin content meaning that there is an increase in the hardness of the membranes. Another possible explanation is the formation of inclusion complexes between cyclodextrins and PMMA [8182].

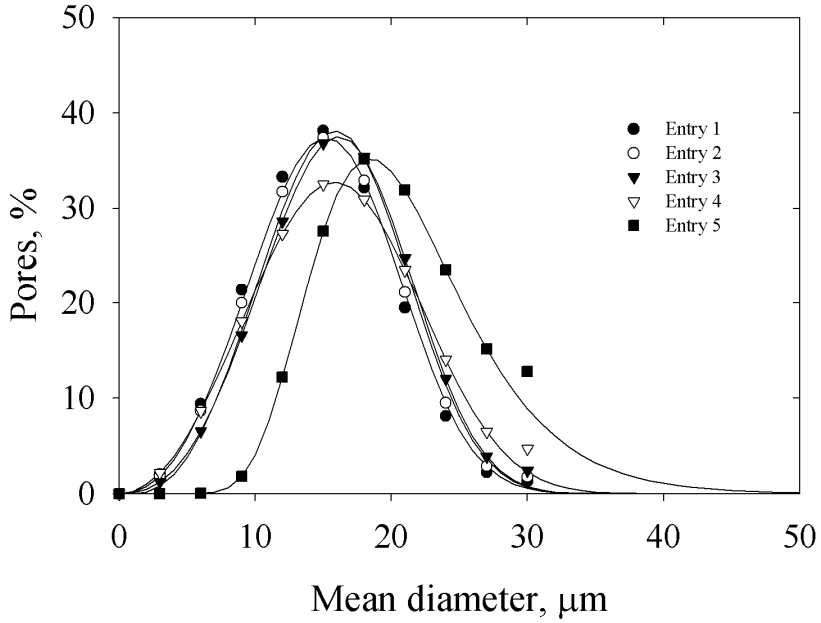

Figure 4.19 - Pore size distribution of PMMA membranes produced using different amounts of HP-β-CDs. Entries correspond to table 4.4.

The morphology of the membranes is not altered during the impregnation process as it can be seen from SEM images of the membranes before and after impregnation, presented in Figure 4.20. Just a slight pore elongation is observed, which could be a result of the plasticization and swelling of the polymeric matrix followed by rapid decompression at the end of impregnation, as it was also reported elsewhere for fast depressurizations from polysulfone membranes in chapter 2 [51]. The percentage of impregnated ibuprofen was analogous for all membranes, around 3 wt%, therefore the cyclodextrin content does not seem to influence the impregnation step. This can be explained by the high diffusivity of $scCO_2$ into the polymer matrix including the cyclodextrin cavities. $ScCO_2$ has already shown to be very effective in impregnating drugs into polymers and a good medium to include ibuprofen into cyclodextrins [83].

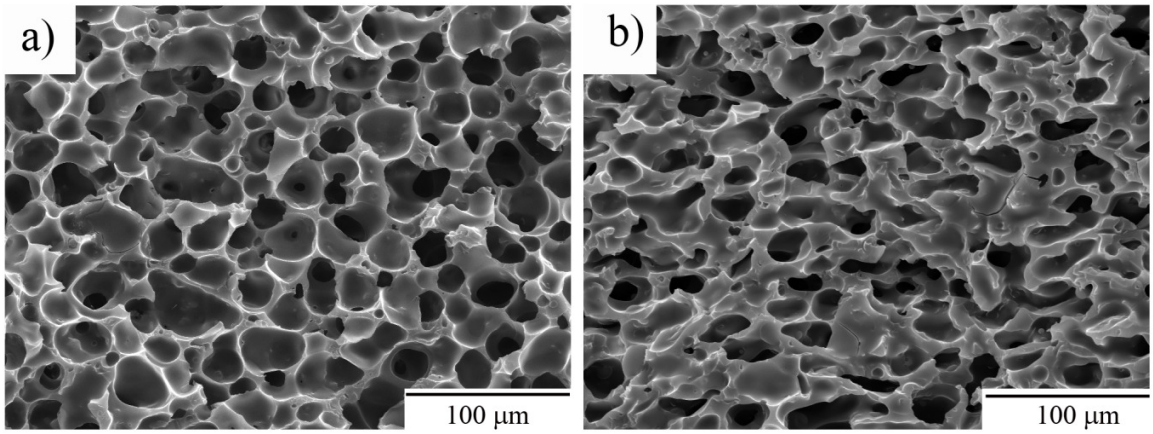

Figure 4.20- Scanning electron micrographs of PMMA membranes produced with 9.2 wt% of HP-β-CDs in the casting solution: a) before; b) after impregnation.

In order to study the influence of the PMMA membrane functionalization with the cyclodextrins, the release profile of the ibuprofen from the films was investigated towards the content of cyclodextrin.

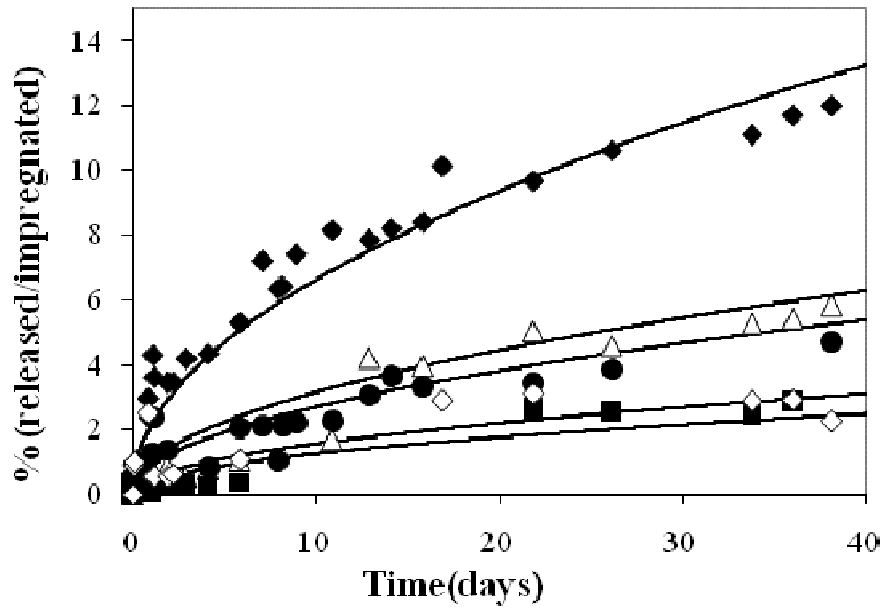

Figure 4.21- Ibuprofen release profile from the different membranes into buffer solution pH 7.4. ♦: 33.4 wt% of HP-β-CD; Δ: 13.7 wt%; ●: 8.7 wt%; ■: 5.1 wt%; ◊: 0 wt%.

Figure 4.21 shows *in vitro* release rates of ibuprofen from the membrane samples over time, into a 7.4 pH phosphate buffer solution at 37ºC. For all the membranes studied no burst release was observed. The initial slopes decrease rapidly and then monotonically which clearly indicates that the membranes are able to release the ibuprofen in a very controlled way including the one that does not contain cyclodextrin. The membrane with the highest content of cyclodextrin reached about 12 wt% of drug release in 40 days, six times more than the one with the lowest content, corresponding to 3.6×10^{-3} mg of ibuprofen released/mg of membrane compared to 6.7×10^{-4} mg ibuprofen/mg membrane. Figure 4.21 also shows the fitting of Equation 2 to the experimental drug release data, which follows the experimental trend and agree reasonably. As it can be seen release rates increase with increasing HP-β-CD content. Table 4.5 shows the diffusion coefficients that were optimized to fit the experimental data.

Table 4.5- Optimized diffusion coefficients to adjust the mathematical model to drug release data.

wt% HP-β-CD[a]	D/m^2s^{-1}
0.0	6.01×10^{-18}
5.1	2.88×10^{-18}
8.7	1.10×10^{-17}
13.7	2.08×10^{-17}
33.4	1.30×10^{-16}

[a] weight percentage of HP-β-CD with respect to PMMA in the membranes.

Comparing the release profiles of the membranes with and without cyclodextrin we can see that the increase in drug delivery is directly related with the increase of CD content. However all membranes were impregnated with the same percentage of ibuprofen (~3wt%) what means that there are no preferable impregnation/inclusion of drug in the CD cavities due to the increase of cyclodextrin content. As it was mentioned above the entire matrix is likely to be uniformly

impregnated due the high diffusivity of CO_2 within the matrix and consequent swelling of the PMMA.

On the other hand when the membranes are put into the buffer solution no swelling or degradability of the PMMA membranes is observed as it was expected since this polymer is hydrophobic and highly biostable, as it was pointed out in the introduction.

The release of the drug from the membrane without cyclodextrins is mainly due to the high porosity of the matrix as observed in the SEM images, which allow the wetting within the matrix promoting the dissolution and diffusion of the drug from the membrane.

By adding cyclodextrins there is a significant increase in the drug release, which can be tuned by varying the cyclodextrin content. We believe that this might have two main contributions: i) the ability of the cyclodextrin to act as a hydrating agent, due to their hydroxyl groups, promoting diffusion of water into the matrix. HP-β-CDs are able to form hydrogen bonding, and thus interfere in the conformation of the polymeric chains during the membrane formation, turning the matrix less hydrophobic. The presence of the cyclodextrin restrains the degrees of freedom in the organization/conformation of the polymeric chains, and a less random organization is obtained, which also explains the increment of *T*g temperature while increasing cyclodextrin concentration; ii) the release of ibuprofen from the cyclodextrin cavities, which are more accessible to the release medium than the PMMA itself.

Our NMR studies confirmed that no leaching of the HP-β-CD occurred upon the process of membrane formation nor during impregnation as it was expected since this cyclodextrin derivative is completely insoluble in $scCO_2$. However as HP-β-CDs are hydrophilic one could expect that they would be also released to the medium alone or by forming ibuprofen-(HP-β-CD) inclusion complexes. ^{1}H-NMR experiments of drug release from the membranes were performed in deuterated water at 37ºC. Although cyclodextrins are soluble in water, ^{1}H-NMR spectra do not

show any traces of cyclodextrin even after several weeks, which confirms that no cyclodextrin leaching from the membranes occurs. This means that the cyclodextrin is entrapped physically within the matrix.

Our results demonstrate that the drug release from the membrane is increased by incorporating cyclodextrins and that it can be further tuned by varying the cyclodextrin content, which could have potential applications as implant materials and as drug release devices.

4.3.3 Conclusions

By varying the content of HP-β-CDs in the casting solution during the $scCO_2$-assisted membrane production process, it is possible to obtain PMMA membranes functionalized with different cyclodextrin contents. The introduction of cyclodextrins physically entrapped in the PMMA matrix, leads to an increase of drug release to the buffer solution at pH 7.4 when compared to the neat PMMA membrane. Also by controlling the amount of cyclodextrin entrapped in the membrane, the ibuprofen release rate from the membranes can be tuned. Therefore we demonstrate that the supercritical fluid-assisted membrane formation is a greener alternative to produce porous polymeric matrixes containing cyclodextrins, with controlled drug release ability, which might have promising biomedical applications.

4.4 References

[1] C.S. Brazel, N. A. Peppas, Pulsatile local delivery of thrombolytic and antithrombotic agents using poly(N-isopropylacrylamide-co-methacrylic acid) hydrogels, Journal of *Controlled Release* 39 (**1996**) 57-64.

[2] J. Kost, R. Langer, Responsive polymeric delivery systems, *Advanced Drug Delivery Reviews* 46 (**2001**) 125-148.

[3] P. Gupta, K. Vermani, S. Garg, Hydrogels: from controlled release to pH-responsive drug delivery, *Drug Discovery Today* 7 (**2002**) 569-579.

[4] Y. Bae, N. Nishiyama, S. Fukushima, H. Koyama, M. Yasuhiro, K. Kataoka, Preparation and biological characterization of polymeric micelle drug carriers with intracellular pH-triggered drug release property: Tumor permeability, controlled subcellular drug distribution, and enhanced *in vivo* antitumor efficacy. *Bioconjugate Chem.* 16 (**2005**) 122-130.

[5] V. Pillay, R. Fassihi. In vitro release modulation from crosslinked pellets for site-specific drug delivery to the gastrointestinal tract - I. Comparison of pH-responsive drug release and associated kinetics, *Journal of Controlled Releas*e 59 (**1999**) 229–242.

[6] M. Nakayama, T. Okano, T. Miyazaki, F. Kohori, K. Sakai, M. Yokoyama, Molecular design of biodegradable polymeric micelles for temperature-responsive drug release. *Journal of Controlled Release* 115 (**2006**) 46–56.

[7] Y. Shin, J. Liu, J. H. Chang, G. J. Exarhos. Sustained drug release on temperature-responsive poly(N-isopropylacrylamide)-integrated hydroxyapatite. *Chem. Commun*., (**2002**) 1718–1719.

[8] S.-H. Hu, T.-Y. Liu, H.-Y. Huang, D.-M Liu, S.-Y. Chen. Magnetic-Sensitive Silica Nanospheres for Controlled Drug Release. *Langmuir* 24 (**2008**) 239-244.

[9] T.-Y. Liu, S.-H. Hu, T.-Y. Liu, D.-M. Liu and S.-Y. Chen, Magnetic-sensitive behavior of intelligent ferrogels for controlled release of drug, *Langmuir*, 22 (**2006**) 5974-5978.

[10] I.C. Kwon, Y.H. Bae, T. Okano, S.W. Kim, Drug release from electric current sensitive polymers, *Journal of Controlled Release*, 17 (**1991**) 149-156.

[11] M. Temtem, T. Casimiro, J. F. Mano, A. Aguiar-Ricardo, Green Synthesis of a temperature sensitive hydrogel, *Green Chemistry*, 9 (**2007**) 75-79.

[12] S. V. Madihally, H.W.T. Matthew. Porous chitosan scafolds for tissue engineering. *Biomaterials* 20 (**1999**) 1133-1142.

[13] T. Casimiro, A. M. Banet-Osuna, A. M. Ramos, M. Nunes da Ponte and A. Aguiar-Ricardo, Synthesis of highly cross-linked poly(diethylene glycol dimethacrylate) microparticles in supercritical carbon dioxide, *Eur. Polym. J,* 41 (**2005**) 1947-1953.

[14] T. Freier, H. S. Koh, K. Kazanian, M. S. Shoichet, Controlling cell adhesion and degradation of chitosan films by N-acetylation, *Biomaterials* 26 (**2005**) 5872-5878.

[15] T.C. Sampaio and S. Barreiros, in Methods in Biotechnology, Supercritical Fluid Methods and Protocols, edited by J. R. Williams and A. A. Clifford (Humana-Press Inc., Totowa, N.J., **2000**).

[16] S.-X. Cheng, J.-T. Zhang and R.-X. Zhuo, Macroporous poly(N-isopropylacrylamide) hydrogels with fast response rates and improved protein release properties, *J. Biomed. Mater. Res.* 67A (**2003**) 96-103.

[17] S. Gunasekaran, T. Wang, C. Chai, Swelling of pH-Sensitive Chitosan–Poly(vinyl alcohol) Hydrogels. *J. Appl. Polym. Sci*., 102 (**2006**) 4665-4671.

[18] X. Qu, A.Wirsén, A.-C. Albertsson, Synthesis and Characterization of pH-Sensitive Hydrogels Based on Chitosan and D,L-Lactic Acid. *J. Appl. Polym. Sci*., 74 (**1999**) 3193- 3202.

[19] X. Qu, A. Wirsén, A.-C. Albertsson, Novel pH-sensitive chitosan hydrogels: swelling behavior and states of water. *Polymer*, 41 (**2000**) 4589- 4598.

[20] K.Tomihata, Y. Ikada, *In vitro* and *in vivo* degradation of films of chitin and its deacetylated derivatives. *Biomaterials* 18 (**1997**) 567-575.

[21] S.D. Yeo, E. Kiran, Formation of polymer particles with supercritical fluids: A review, *J. Supercrit. Fluids* 34 (**2005**) 287–308.

[22] S.G. Kazarian, G.G. Martirosyan, Spectroscopy of polymer/drug formulations processed with supercritical fluids: in situ ATR–IR and Raman study of impregnation of ibuprofen into PVP, *Int. J. Pharm*. 232 (**2002**) 81–90

[23] M. Muntó, N. Ventosa, S. Sala, J. Veciana, Solubility behaviors of ibuprofen and naproxen drugs in liquid "CO2–organic solvent" mixtures. *J. of Supercritical Fluids* 47 (**2008**) 147–153.

[24] J.M. Vergnaud, Controlled Drug Release of Oral Dosage Forms. Ellis Horwood, (**1993**) New York.

[25] J. Siepmann, F. Siepmann, Mathematical modeling of drug delivery, *Int. J. Pharma*. 364 (**2008**) 328–343.

[26] D. Lee, A.J. Nolte, A.L. Kunz, M.F. Rubner and R.E. Cohen, pH-Induced Hysteretic Gating of Track-Etched Polycarbonate Membranes: Swelling/Deswelling Behavior of Polyelectrolyte Multilayers in Confined Geometry, *J. Am. Chem. Soc*., 128 (**2006**) 8521-8529.

[27] Y.S. Park, Y. Ito and Y. Imanishi, Permeation Control through Porous Membranes Immobilized with Thermosensitive Polymer, *Langmuir*, 14 (**1998**) 910-914.

[28] G. Brisson, M. Britten and Y. Pouliot, Electrically-enhanced crossflow microfiltration for separation of lactoferrin from whey protein mixtures, *J. Membr. Sci*., 297 (**2007**) 206-216.

[29] Y. S. Park, Y. Ito and Y. Imanishi, Photocontrolled Gating by Polymer Brushes Grafted on Porous Glass Filter, *Macromolecules*, 31 (**1998**) 2606-2610.

[30] Y. Ito, M. Inaba, D.-J. Chung and Y. Imanishi, Control of water permeation by pH and ionic strength through a porous membrane having poly(carboxylic acid) surface-grafted *Macromolecules*, 25 (**1992**) 7313-7316.

[31] C.C. Ng, Y.-L. Cheng and B.A. Saville, Thermoresponsive polymer. membrane for the local delivery of drugs, *J. Sex. Reprod. Med*., 1 (**2001**) 21-27.

[32] P. Maharjan, B.W. Woonton, L.E. Bennett, G.W. Smithers, K. DeSilva, M.T.W. Hearn, Novel chromatographic separation — The potential of smart polymers, *Innov. Food Sci. Emerg. Technol.,* 9 (**2008**) 232-242.

[33] A. Baldi, Y. Gu, P. S. Lofness, R. A. Seigel and B. Ziaie, A hydrogel-actuated environmentally sensitive microvalve for active flow control, *J. Microelectromech. Syst*., 12 (**2003**) 613-621.

[34] N. Yamada, T. Okano, H. Sakai, F. Karikusa, Y. Sawasaki and Y. Sakurai, Thermo-responsive polymeric surfaces; control of attachment and detachment of cultured cells, *Makromol. Chem. Rapid. Commun*. 11 (**1990**) 571-573.

[35] T. Okano, N. Yamada, H. Sakai, Y. Sakurai, A novel recovery system for cultured cells using plasma-treated polystyrene dishes grafted with poly(N-isopropylacrylamide) *J. Biomd. Mat. Res*. 27 (**1993**) 1243-1251.

[36] S.-Y. Lin, C.-J. Ho and M.-J. Li, Precision and reproducibility of temperature response of a thermo-responsive membrane embedded by binary liquid crystals for drug delivery, *J. Control. Release*, 73 (**2001**) 293-301.

[37] S.-Y. Lin, H.-L. Lin and M.-J. Li, Reproducibility of temperature response and long-term stability of thermo-responsive membrane prepared by adsorption of binary liquid crystals, J. Membr. *Sci*., 225 (**2003**) 135-143.

[38] J.-P. Chen, Y.-M. Sun and D.-H. Chu, Immobilization of α-amylase to a composite temperature-sensitive membrane for starch hydrolysis, *Biotechnol. Prog*., 14 (**1998**) 473-478.

[39] K K. Zhang and X.Y. Wu, Temperature and pH-responsive polymeric composite membranes for controlled delivery of proteins and peptides, *Biomaterials*, 25 (**2004**) 5281-5291.

[40] L.-Y. Chu, Y. Li, J.-H. Zhu and W.-M. Chen, Negatively Thermoresponsive Membranes with Functional Gates Driven by Zipper-Type Hydrogen-Bonding Interactions, *Angew. Chem. Int. Ed*., 44 (**2005**) 2124-2127.

[41] J. Xue, L. Chen, H.L. Wang, Z.B. Zhang, X.L. Zhu, E.T. Kang, K.G. Neoh, Stimuli-Responsive Multifunctional Membranes of Controllable Morphology from Poly(vinylidene fluoride)-graft-Poly[2-(N,N-dimethylamino)ethyl methacrylate] Prepared via Atom Transfer Radical Polymerization, *Langmuir*, 24 (**2008**) 14151-14158.

[42] S. J. Lue, J.-J. Hsu, C.-H. Chen, B.-C. Chen, Thermally on-off switching membranes of poly (N-isopropylacrylamide) immobilized in track-etched polycarbonate films, *J. Membr. Sci*., 301 (**2007**) 142-150.

[43] A. Kikuchi, T. Okano, Intelligent thermoresponsive polymeric stationary phases for aqueous chromatography of biological compounds, *Prog. Polym. Sci*., 27 (**2002**) 1165-1193.

[44] M. Yang, L.-Y. Chu, Hai-Dong Wang, Rui Xie, Hang Song, and Catherine Hui Niu, A Thermoresponsive Membrane for Chiral Resolution, *Adv. Func. Materials* 28 (**2008**) 652-663

[45] S. Fujishige, K. Kubota, I. Ando, Phase transition of aqueous solutions of poly(N-isopropylacrylamide) and poly(N-isopropylmethacrylamide), *J Phys. Chem*., 93 (**1989**) 3311-3313.

[46] P. Stayton, T. Shimoboji, C. Long, A. Chilkoti, G.H. Chen, J.M. Harris, A.S. Hoffman, Control of protein-ligand recognition using a stimuli-responsive polymer, *Nature*, 378 (**1995)** 472-474.

[47] X. Wang, X. Qiu, C. Wu, Comparison of the Coil-to-Globule and the Globule-to-Coil Transitions of a Single Poly(N-isopropylacrylamide) Homopolymer Chain in Water, *Macromolecules*, 31 (**1998**) 2972-2976.

[48] Y. Katsumoto, T. Tanaka, H. Sato, Y. Ozaki, Conformational Change of Poly(N-isopropylacrylamide) during the Coil–Globule Transition Investigated by Attenuated Total Reflection/Infrared Spectroscopy and Density Functional Theory Calculation, *J Phys. Chem*., 106 (**2002**) 3429-3435..

[49] H. Yim, M.S.Kent, S. Mendez, G.P. Lopez, S. Satija and Y. Seo, Effects of Grafting Density and Molecular Weight on the Temperature-Dependent Conformational Change of Poly(N-isopropylacrylamide) Grafted Chains in Water, *Macromolecules*, 39 (**2006**) 3420-3426.

[50] S. Mendez, J. G. Curro, J. D. McCoy, G. P. Lopez, Computational Modeling of the Temperature-Induced Structural Changes of Tethered Poly(N-isopropylacrylamide) with Self-Consistent Field Theory, *Macromolecules* 38 (**2005**) 174-181.

[51] M. Temtem, T. Casimiro, A. Aguiar-Ricardo, Solvent power and depressurization rate effects in the formation of polysulfone membranes with CO2-assisted phase inversion method. *J. Membrane Sci*. 283 (**2006**) 244-252.

[52] R.H. Pelton and P. Chibante, Preparation of aqueous latices with N-isopropylacrylamide, *Colloids Surf.* 20 (**1986**) 247-256.

[53] A. Shah, Separation systems for commercial biotechnology, BCC Research, **2007**.

[54] M. Temtem, L.M.C. Silva, P.Z. Andrade, F. Santos, C. Lobato da Silva, J.M.S. Cabral, M.M. Abecasis and A. Aguiar-Ricardo, Supercritical CO2 generating chitosan devices with controlled morphology. Potential application for drug delivery and mesenchymal stem cell culture, J. Supercrit. Fluids, in press, (doi:10.1016/j.supflu.2008.10.020).

[55] V.L. Vilker, C.K. Colton, K.A. Smith, The osmotic pressure of concentrated protein solutions: Effect of concentration and ph in saline solutions of bovine serum albumin, *J. Coll. Interf. Sci*., 79 (**1981**) 548-566.

[56] S.J. Lue, J.-J. Hsu, T.-C.Wei, Drug permeation modeling through the thermo-sensitive membranes of poly(N-isopropylacrylamide) brushes grafted onto micro-porous films, *J. Membr. Sci*., 321 (**2008**) 146-154.

[57]S. J. Lue, J.-J. Hsu, C.-H. Chen, B.-C.Chen, Thermally on–off switching membranes of poly(N-isopropylacrylamide) immobilized in track-etched polycarbonate films, *J. Membr. Sci.,* 301 (**2007**) 142-150.

[58] P. C. Simões, J. Fernandes, J. P. B. Mota, Dynamic model of a supercritical carbon dioxide heat exchanger, *J. Supercrit. Fluids*, 35 (**2005**) 167-173.

[59] Process Systems Enterprise, gPROMS v2.0 Introductory User Guide, Process Systems Enterprise Ltd, London, **2001**.

[60] M. Temtem, T. Casimiro, J.F. Mano and A. Aguiar-Ricardo, Preparation of membranes with polysulfone/polycaprolactone blends using a high pressure cell specially designed for a CO2-assisted phase inversion, *J. Supercrit. Fluids*, 43 (**2008**) 542-548.

[61] D.S. Wavhal and E.R. Fisher, Modification of polysulfone ultrafiltration membranes by CO2 plasma treatment, *Desalination*, 172 (**2005**) 189-205.

[62] X. Cheng, H.E. Canavan, D.J. Graham, D.G. Castner, B.D. Ratner, Temperature dependent activity and structure of adsorbed proteins on plasma polymerized N-isopropyl acrylamide, *Biointerphases*, 1 (**2006**) 61-72.

[63] D.C. Bibby, N.M. Davies, I.G. Tucker, Mechanisms by which cyclodextrins modify drug release from polymeric drug delivery systems*, Int. J. Pharm*. 197 (**2000**) 1-11.

[64] A.R.C. Duarte, T. Casimiro, A. Aguiar-Ricardo, A.L Simplício, C.M.M Duarte, Supercritical fluid polymerisation and impregnation of molecularly imprinted polymers for drug delivery. *J. Supercrit. Fluids* 39 (**2006**) 102-106.

[65] J. Siepmann, F. Siepmann, Mathematical modelling of drug delivery. *Int. J. Pharm*. 364 (**2008**) 328-343.

[66] F. Hirayama, K. Uekama, Cyclodextrin-based controlled release system. *Adv. Drug Delivery Rev*. 36 (**1999**) 125-141.

[67] S. Junco, T. Casimiro, N. Ribeiro, M. Nunes da Ponte, H.M. Cabral Marques, A comparative study of naproxen-beta-cyclodextrin complexes prepared by conventional methods and using supercritical carbon dioxide. *J. Incl. Phenom. Macro*. 44 (**2002**) 117-121.

[68] X. Zhao, J. M. Courtney, Surface modification of polymeric biomaterials: utilization of cyclodextrins for blood compatibility improvement, *J. Biomed Mater Res A*, 80 A (**2007**) 539-553.

[69] D.F. Stamatialis, B.J. Papenburg, M. Gironés, S. Saiful, S.N.M. Bettahalli, S. Schmitmeier, M. Wessling, Medical applications of membranes: Drug delivery, artificial organs and tissue engineering. *J. Membrane Sci*. 308 (**2008**) 1-34.

[70] S. Leprêtre, F. Boschin, N. Tabary, M. Bria, B. Martel, N. Blanchemain, H.F. Hildebrand, M. Morcellet, E. Delcourt-Debruyne, Guided tissue regeneration membranes with controlled delivery properties of chlorhexidine by their functionalization with cyclodextrins. *J. Incl. Phenom. and Mac. Chem*. 57 (**2007**) 297-302.

[71] E.B. Minelli, A. Benini, B. Magnan, P. Bartolozzi, Release of gentamicin and vancomycin from temporary human hip spacers in two-stage revision of infected artoplasty. *J. Antimicrob. Chemoth*. 53 (**2004**) 329-334.

[72] S. Ladrón de Guevara-Fernández, C.V. Ragel, M. Vallet-Regí, Bioactive glass-polymer materials for controlled release of ibuprofen. *Biomaterials* 24 (**2003**) 4037-4043.

[73] T.V. Hees, V. Barillaro, G. Piel, P. Bertholet, S.H. De Hassonville, B. Evrard, L. Delattre, Application of Supercritical carbon dioxide for the preparation of drug-cyclodextrin inclusion compounds. *J. Incl. Phenom. Macro*. 44 (**2002**) 271-274.

[74] S. Junco, T. Casimiro, N. Ribeiro, M. Nunes da Ponte, H.M. Cabral Marques, Optimisation of supercritical carbon dioxide systems for complexation of naproxen: beta-cyclodextrin. *J. Incl. Phenom. Macro*. 44 (**2002**) 69-73.

[75] Y. Tozura, T. Fujito, K. Moribe, K. Yamamoto, Ibuprofen-cyclodextrin inclusion complex formation using supercritical carbon dioxide, *J. Incl. Phenom. Macro*., 56 (**2006**) 33-37.

[76] D. Suleiman, L.A. Estévez, J.C. Pulido, J.E. Garcia, C. Mojica, Solubility of anti-inflammatory, anti-cancer, and anti-HIV drugs in supercritical carbon dioxide. *J. Chem. Eng. Data* 50 (**2005**) 1234-1241.

[77] A. Rajendran, B. Bonavoglia, N. Forrer, G. Storti, M. Mazzotti, M. Morbidelli, Simultaneous measurements of swelling and sorption in a supercritical CO_2-poly(methylmethacrylate) system. *Ind.& Eng. Chem. Res*. 44 (**2005**) 2549-2560.

[78] I.M. Chakravarti, R.C Laha, J. Roy, Handbook of Methods of Applied Statistics, Volume I, (**1967**) John Wiley and Sons.

[79] M.A. Stephens, EDF Statistics for Goodness of Fit and Some Comparisons, *J. Amer. Stat. Assoc*. 69 (**1974**) 730-737.

[80] E. Fontananova, A. Basile, A. Cassano, E. Drioli, Preparation of polymeric membranes entrapping β-cyclodextrins and their molecular recognition of naringin. *J. Inc. Ph. Macroc. Chem*. 47 (**2003**) 33-37.

[81] M. Wei, A. E. Tonelli, Compatiblization of Polymers via Coalescence from Their Common Cyclodextrin Inclusion Compounds. Macromolecules, 34 (2001) 4061-4065.

[82] J.F. Mano, Thermal Behaviour and Glass Transition Dynamics of Inclusion Complexes of a-Cyclodextrin with Poly(D,L-lactic acid). *Macromol. Rapid Commun*. 29 (**2008**) 1341–1345.

[83] R. Mammucari, N.R. Foster, Dense gas technology and cyclodextrins: state of the art and potential. *Cur. Org. Chem*. 12 (**2008**) 476-491.

Chapter 5

CONCLUSIONS AND PROSPECTS

5. Conclusions and Prospects

5.1 General conclusions

New technologies and approaches are needed to manufacture devices capable to deliver drugs at the right time in a safe and reproducible manner to a specific target at the required level. The use of carbon dioxide as a solvent presents a range of interesting opportunities in this field. In addition to reducing the need for toxic volatile organic solvents, CO_2 allows the synthesis and processing of a broad range of polymeric materials with well defined structures and properties. It is not certainly the answer to all the problems, neither the solution to all the environmental issues but it is an alternative that should be always considered.

The formation of well defined porous structures for controlled drug release or tissue engineering applications has been an important area of research as it is evidenced by the number of different technologies that were developed (foaming, emulsion, phase inversion) and the growing number of scientific papers and patents. Even with a better knowledge of the many fundamental principles underlying these techniques the number of industrial successes is to date still very low. As mentioned by Val Krukonis, one of the supercritical fluid mentors, in the First International Symposium on Supercritical Fluids in 1988 "There is no point in doing something in a supercritical fluid just because it`s neat. Using the fluids must have some real advantages."

The purpose of this thesis was to study the possibility to use $scCO_2$ to process and prepare "smart" systems with applicability in the medical field. A new high pressure apparatus for the preparation of non residue membranes was developed and different materials, for different applications were successfully processed. Polysulfone membranes for filtration purposes,

chitosan membranes for cell expansion and poly methyl methacrylate membranes for drug release are examples of these structures.

The bigger advantage of CO_2 assisted phase inversion is the introduction of additional parameters to control the morphology of the membrane, particularly due to the fact that CO_2 properties can be easily adjusted by simply tuning temperature and pressure conditions. Depressurization rate, solvent-non solvent affinity and incorporation of a blowing agent were efficiently used in this work to modify the structure of the membranes. There are not many solvents with this capability.

The second advantage is the ability to remove undesirable residues (process solvents in the case of polysulfone membranes or acetic acid vestiges in the case of chitosan membranes) which is particularly important if we consider the safety requirements of medical products, for example addressed in the International Conference on Harmonisation of Technical Requirements for Registration of Pharmaceuticals for Human Use (ICH) guidelines restrictions [1]. This was confirmed in chapter 4 where the membranes that were analyzed by XPS (a highly sensitive technique) revealed no solvent residues.

Similarly, it was proved the potential use of $scCO_2$ in the coating/impregnation of small pores either with thermo or pH responsive polymers or with active molecules such as drugs or peptides. There are not many solvents that present low viscosities and high diffusivities associate a good and tunable solvent power and that are able to transport molecules into the interior of small pores without collapsing them. The “smart” porous structures, membranes and scaffolds that were successfully prepared in this work are a proof of the advantages of supercritical fluids and how pH and temperature response can be used to control the diffusion/release of model proteins and model drugs.

Nevertheless due to the high costs associated, only the processing of high valuable materials for very specific applications is economically viable and may lead to future industrial applications.

5.2 Future perspectives

Science is in a continuous mutation where it is always possible to improve. In order to "exploit" the whole potential of CO_2 phase inversion it is necessary to obtain more thermodynamic data for the construction of reliable ternary diagrams that could be used to predict and improve the morphology of the porous structures. This is of great importance to improve porosity and pore interconnectivity, which are crucial aspects, when we are dealing with porous structures for tissue engineering applications.

The preparation of asymmetric membranes with applications in filtration field should become a subject of research because this structure could improve the mass transfer properties. A lot of knowledge from the traditional technologies can be applied for the preparation of this type of structures with a broad range of success. An example is surface modification by graft polymerization or plasma technology.

Finally, in terms of coating/impregnation of the porous structures there is still a lot of work to be performed in order to control the whole process, particularly the morphology and thickness of the stimuli responsive material layer that are paramount when these structures are used in tissue engineering applications (e.g. cell sheet technology).

5.3 References

[1] http://www.ich.org/

ANNEXES

Annexes

A- Gproms Model applied in chapter 4.2

PARAMETER

x AS REAL DEFAULT 700e-6 # membrane tickness; m

DISTRIBUTION_DOMAIN

axialf AS [0: x]

VARIABLE

Cb AS Conc # concentration in bulk (first reservoir) - this concentration will decrease with time as part of the BSA permeates through the membrane or is absorbed by the membrane; kg/m^3.

Cbi AS Conc # initial concentration of BSA in the first reservoir; kg/m^3.

Cp AS Conc # concentration in permeate (second reservoir); kg/m^3.

Cm AS Distribution(AxialF) of Conc # concentration throughout the membrane; kg/m^3.

Lp AS Coefs # water permeability coefficient; $kg.m^{-2}.h^{-1}.bar^{-1}$

Diff AS Coefs # diffusion coefficient (to be estimated)

Jv AS Distribution(AxialF) of Flux

Js AS Distribution(AxialF) of Flux

Temp AS Temperature # temperature; ºC.

Select AS Coefs # Membrane selectivity

DeltaPI AS Distribution(AxialF) of Conc # osmotic pressure; bar

K AS Coefs # mass transfer coefficient in the membrane interface with the bulk liquid

Annexes

A AS Coefs # membrane total surface area; m^2.

q AS DISTRIBUTION(AxialF) OF conc # protein adsorbed; (kg/m^2).

qm AS Coefs # maximal monolayer adsorption; (kg/m^2).

Kd AS Coefs # Langmuir constant; m^3/kg.

V AS Coefs # Volume of each cut through the membrane; m^3

DeltaQ AS Distribution (AxialF) OF conc # variation of the amount of protein that it is adsorbed; $Kg.m^{-2}$

EQUATION

V = 2 * 3.1416 * (1/2 * 1.103013E-2) * x / 12; ## Volume of each cut on the membrane length ##

A = 150E-3 * 14.108 / 12; # mass. Mercury porosimetry area

FOR y := 0|+ TO x DO

$Cm(y)=Diff*PARTIAL(Cm(y),AxialF,AxialF)+Js(y)*3.14*((0.0000000119/2)^2)/(3.14*((0.00000000119/2)^2 * x /12)) - DeltaQ(y) * 0.013933069;

END

FOR y := 0 TO x DO

DeltaQ(y) = qm * (Kd * (1+ Kd * Cm(y)) - Kd * (Kd * Cm(y)))/((1 + Kd * Cm(y))^2) ;

Jv(y) = Lp * (Select * DeltaPI(y)) ;

Js(y) = (1-Select) * Jv(y) ;

DeltaPI(y) = (204.78 * PARTIAL(Cm(y),AxialF) + 2 * (PARTIAL(Cm(y),AxialF))^2 + 8.44E-3 * (PARTIAL(Cm(y),AxialF))^3) ;

q(y) = qm * Kd * Cm(y) / (1 - Kd * Cm(y)) ;

END

Cbi * 40E-6 = cb * 40E-6 + Cp * 40E-6 + Sigma(Cm(0:x) * V) + (Sigma(q(0:x) * A)) ;

Kd = exp(-13807.182 / (temp + 273.15) + 47.4081289) ;   # m3/kg

Cm(0) = K * Cb ;

Cm(x) = K * Cp ;